UNIVERSITY OF SOUTHAMPTON

FACULTY OF MEDICINE

Human Development and Health

Bone and Joint Research Group

The Role of the Vasculature in Skeletal Development and Repair–Clues to Improved Regenerative Strategies

by

Stefanie Inglis

Thesis for the degree of Doctor of Philosophy

June 2017

UNIVERSITY OF SOUTHAMPTON

ABSTRACT

FACULTY OF MEDICINE, HUMAN HEALTH AND DISEASE

Bone and Joint Research Group

Doctor of Philosophy

The Role of the Vasculature in Skeletal Development and Repair- Clues to Improved Regenerative Strategies

By Stefanie Inglis

A functional vasculature has a central role during tissue development and repair. It is essential in bone development and is often the major limiting factor in the successful healing of bone fractures particularly in critical sized defects. To date, engineering a functional vasculature remains a major challenge in the field of regenerative medicine. In this study, the potential of human vascular (endothelial) cells to drive osteogenic and angiogenic differentiation in direct co-cultures with human skeletal stem cells, was established. In addition, the role of the potent mitogen vascular endothelial growth factor (VEGF) to this system was examined and observed to potentiate a modulation of the osteo- and angiogenic process by stimulating the endothelial cell population.

In 2D co-culture studies, human fetal femur-derived stem cells (FFDSCs) and human adult bone marrow stromal cells (HBMSCs) were co-cultured with human umbilical vein endothelial cells (HUVECs) over 7 days, supplemented with or without VEGF. A significant enhancement of the enzyme activity of the early bone marker alkaline phosphatase (ALP) in the co-cultures was observed. Additionally, an increase of *type I collagen* (*COL-1*) gene expression as well as substantial modulation of the VEGF receptor genes 1 (*FLT-1*) and 2 (*KDR*) was found. In marked contrast, VEGF supplementation to the co-cultures invoked a differential response on osteogenesis but enhanced VEGF receptor gene expression.

In the 3D co-culture studies HBMSC/HUVEC pellets were placed into a drill defect created in E18 chick femurs and cultured organotypically at the air-liquid interface over a period of 10 days. Micro-CT image analysis demonstrated significant bone formation for all cell pellet treatment groups, but more so for the HUVEC implanted group, and demonstrated strong protein expression of angiogenic markers von Willebrand Factor (vWF) and CD31 (PECAM-1).

In subsequent investigations, decellularised human placental vessel sleeves were employed around the cell pellet-implanted femoral defects as a structural ECM dressing, to enhance cell biochemical signalling and to act as a substrate for cell and tissue conductive processes during bone healing. Superior bone formation in femurs containing the sleeve dressing was measured by an increase in bone volume over the organotypic culture period, demonstrated by micro-CT imaging. Reduction in femoral defect size and periosteal integration with cellular invasion of the decellularised vessel sleeves was observed, together with expression of COL-2- and HIF-1α within cartilaginous bands connecting the bone periosteum with the decellularised vascular sleeve.

These studies have demonstrated that endothelial cells drive osteogenic and angiogenic modulations when co-cultured with fetal/adult skeletal cells. This research has highlighted the variability in the effect of VEGF supplementation *in vitro*. Furthermore, these studies have underlined the importance of the intricate temporal coordination of osteo- and angiogenic processes during bone formation and the implications this may have for effective approaches using cell-based bone regenerative therapies.

Harnessing the findings from both culture systems will ultimately underpin our understanding of the temporal cascade of fracture repair and this knowledge will be utilised in refining regenerative therapies.

Contents

List of tables

List of figures

DECLARATION OF AUTHORSHIP

I, Stefanie Inglis declare that the thesis entitled

The Role of the Vasculature in Skeletal Development and Repair–Clues to Improved Regenerative Strategies

and the work presented in the thesis are both my own, and have been generated by me as the result of my own original research. I confirm that:

- this work was done wholly or mainly while in candidature for a research degree at this University;
- where any part of this thesis has previously been submitted for a degree or any other qualification at this University or any other institution, this has been clearly stated;
- where I have consulted the published work of others, this is always clearly attributed;
- where I have quoted from the work of others, the source is always given. With the exception of such quotations, this thesis is entirely my own work;
- I have acknowledged all main sources of help;
- where the thesis is based on work done by myself jointly with others, I have made clear exactly what was done by others and what I have contributed myself;
- none of this work has been published before submission, or [delete as appropriate] parts of this work have been published as: [please list references]

Signed: Stefanie Inglis

Date: 30/06/2017

Acknowledgements

I am extremely grateful to my supervisor Dr. Janos Kanczler for his help and support throughout my PhD and for always having an open ear. I particularly enjoyed our creative discussions and appreciated his skilfully deflection of my unnecessary qualms.

I am also extremely grateful to my supervisor and the chief, Professor Richard Oreffo, without whom this PhD would not have been possible and who always provided just the right amount of pressure to make me move forward.

I would like to thank the whole Bone and Joint Research group for their encouragement and support and for being such a fabulous and versatile bunch of people. I am grateful to my family for their support throughout this PhD and particularly my brother Georg Johnen, who came to my unsolicited financial rescue.

I would like to thank Dr Karl Schneider, previously at the Ludwig Boltzmann Institute for Experimental and Clinical Traumatology in Vienna, Austria, for kindly providing the decellularised vessel sleeve used for the work in chapter 5.

List of abstracts and publications

Publications

- **Inglis S**, Christensen D, Wilson DI, Kanczler JM, Oreffo RO. Human endothelial and foetal femur-derived stem cell co-cultures modulate osteogenesis and angiogenesis. Stem Cell Res Ther. 2016 Jan 18;7(1):13. doi: 10.1186/s13287-015-0270-3.

Book chapter

- Kanczler J, Hulsart Billstrom G, **Inglis S**, Moreno I, Oreffo RO. Bridging the gap: organotypic and CAM models in biomaterials & tissue engineering research. Book Chapter: Comprehensive Biomaterials II. 2017.

Abstracts with oral presentation

- **S Inglis**, JM Kanczler, ROC Oreffo
  The effect of 2D and 3D co-cultures of foetal skeletal and endothelial cells on osteogenic induction
  Firm symposium 2013, Girona, Spain as part of Biodesign – Future investigators of regenerative medicine

- **S Inglis**, D Christensen, DI Wilson, JM Kanczler, ROC Oreffo Human endothelial and foetal femur-derived stem cell co-cultures modulate osteogenesis and angiogenesis European Cells and Materials Vol. 29. Suppl. 3, 2015 (page 16) ISSN 1473-2262

Poster presentations

- **S Inglis**, JM Kanczler, ROC Oreffo
  The effect of 2D and 3D co-cultures of foetal skeletal and endothelial cells on osteogenic induction
  Firm symposium 2013, Girona, Spain as part of Biodesign – Future investigators of regenerative medicine

- G Hulsart Billström, **S Inglis**, ROC Oreffo
  Development of μCT and *ex vivo* Techniques to reduce Animal Use in Screening of Biomaterials for Regenerative Medicine

Bruker annual microCT User Meeting 2015, Bruges, Belgium

- G Hulsart Billström, **S Inglis**, ROC Oreffo
  Development of μCT and *ex vivo* Techniques to reduce Animal Use in Screening of Biomaterials for Regenerative Medicine
  Faculty of Medicine Research Conference, 2015, Southampton, UK

- **S Inglis**, JM Kanczler, SG Hulsart Billström, ROC Oreffo 3D Human bone marrow and endothelial cell pellets induce osseointegration and differentiation in organ cultures of E18 chick femur drill defects. European Cells and Materials Vol. 29. Suppl. 3, 2015 (page 97) ISSN 1473-2262

- SG Hulsart Billström, **S Inglis**, ROC Oreffo Screening growth factor loading capacity of distinct biomaterials using a high throughput *ex vivo* avian model. European Cells and Materials Vol. 29. Suppl. 3, 2015 (page 67) ISSN 1473-2262

Definitions and Abbreviations

2D	Two-dimensional
3D	Three-dimensional
α-MEM	Minimum essential medium Eagle, alpha modification
Akt	Protein kinase B (PKB)
AEC	3-amino-9-ethyl-carbozole
ALP	Alkaline phosphatase
ANOVA	Analysis of variation
A/S	Alcian blue/Sirius red
BMdC	Bone marrow derived cells
BMP	Bone morphogenetic protein
BMSC	Bone marrow stromal cells
BSA	Bovine serum albumin
CAM	Chorioallantoic Membrane
CD31	Cluster of differentiation 31 (PECAM-1)
cDNA	Complementary DNA
CMFDA	5-chloromethylfluorescein diacetate
CTG	Cell tracker green
DAPI	4',6—diamidino-2-phenylindole
dH_2O	Distilled water
DMEM	Dulbecco's modified Eagle's medium
DNA	Deoxyribonucleic acid
Dpc	Days post-conception

DPX	Distyrene plasticizer xylene
dsDNA	Double stranded DNA
EC	Endothelial cell
ECGS	Endothelial cell growth supplement
ECM	Extracellular matrix
EDTA	Ethylene-diaminetetraacetic acid
EGF	epidermal growth factor
EH-1	Ethidium homodimer 1
ERK	Extracellular signal-regulated kinase
FCS	Fetal calf serum
FFDSC	Fetal femur-derived stem cells
FGF	Fibroblastic growth factor
FGFR	Fibroblast growth factor receptor
FLT-1	Fms-like tyrosine kinase 1 (VEGF receptor 1)
FLK	Fetal liver kinase
GAG	Glycosaminoglycan
H_2O_2	Hydrogen peroxide
HBMSC	Human bone marrow stromal cell
HUVEC	Human umbilical vein endothelial cell
IHC	Immunohistochemistry
ICC	Immunocytochemistry
IGF	Insulin-like growth factor
IMG	Intussusceptive micro-vascular growth

KDR	Kinase-insert domain receptor (VEGF receptor 2)
micro-CT	Micro-computed tomography
MAPK	Mitogen activated protein
MMP	Matrix metalloproteinase
MSC	Marrow stromal cell
MSC	Mesenchymal stem cell
OA	Osteoarthritis
OB	Osteoblast
OC	Osteocalcin
OPGL	Osteoprotegerin ligand
PBS	Phosphate buffered saline
PCL	Porous polycaprolactone
PCR	Polymerase chain reaction
PDGF	Platelet derived growth factor
PECAM-1	Platelet endothelial cell adhesion molecule
PGLA	Poly(DL-lactide-co-glycolide)
PI3K	Phosphoinositide 3-kinase
P/S	Penicillin/Streptomycin
PTH	Parathyroid hormone
qPCR	Quantitative polymerase chain reaction
RANK(L)	Receptor activator of nuclear factor k B (ligand)
RNA	Ribonucleic acid
Ras	Rat sarcoma

SD	Standard deviation
SC	Skeletal cells
SMAD	Small body size (SMA); mothers against decapentaplegic (MAD)
TCP	Tri-calcium phosphate
TGF	Transforming growth factor
TIE	tunica interna endothelial cell kinase
TNF	Tissue necrosis factor
Tor	Target of rapamycin
UV	Ultra violet
VEGF	Vascular endothelial growth factor
VEGFR	Vascular endothelial growth factor receptor
vWF	Von Willebrand factor

CHAPTER 1

Introduction

1.1 Overview

Blood vessel formation is one of the earliest processes in embryonic development. Vasculogenesis (de novo blood vessel formation) and angiogenesis (sprouting from existing blood vessels) are the two essential processes by which blood vessels are formed in the developing organism and throughout the life of an organism (Figure 1.1). Once the embryo has grown to and surpassed the critical size of approximately 200µm passive diffusion ceases to supply sufficient oxygen and nutrients for tissue homeostasis and survival (Carmeliet *et al.*, 2000) (Buchwald, 2009). Therefore, a functional blood supply has to fulfil this role which continues throughout the life of the organism. Blood vessels thus have to constantly adapt to the ever changing requirements of the organism. The distinct lineages of the embryonic mass, from which these tissues originate, provide insights into the complexity of development and the possible malformations of blood vessels during embryogenesis. In adulthood these malformations can result in debilitating conditions, chronic pain and failure of organ function (Chung *et al.*, 2011).

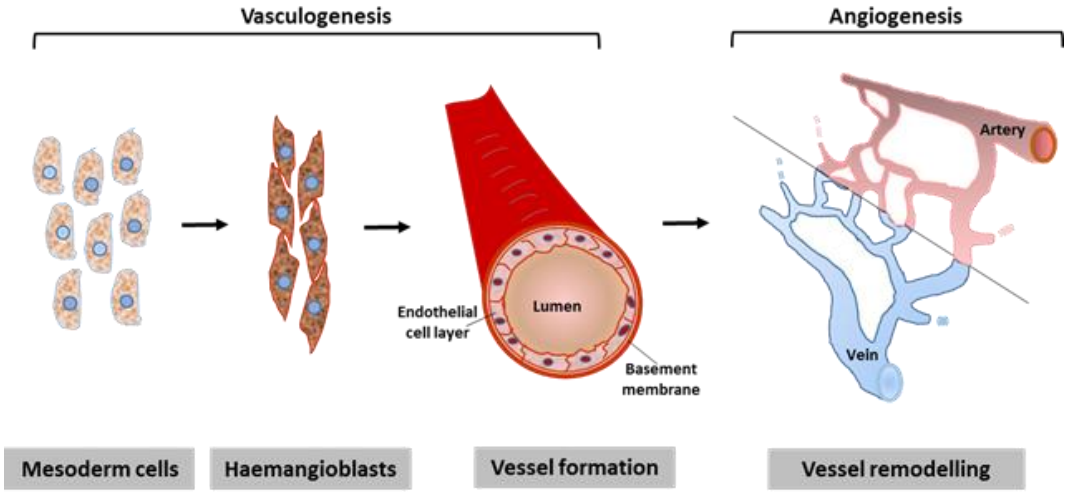

Figure 1.1 **Blood Vessel Development**. Vasculogenesis produces initial blood vessels from mesodermal cells differentiating into angioblasts. Angiogenesis extends vasculature by sprouting of endothelial cells from existing vessels; adapted from (Oliver, 2004).

Blood vessels are responsible for the delivery of nutrients and oxygen to the cells and tissue of the human body and subsequent removal of waste product via an intricate hierarchical and tightly regulated network (Chung and Ferrara,

2011). Endothelial cells, which line the internal surface of blood vessels, function as a barrier as well as a conduit for communication and exchange of growth factors, nutrients and cytokines between the tissue and blood. Blood vessels display significant heterogeneity depending on tissue type and developmental stage (Garlanda *et al.*, 1997).

In 1763, Albrecht von Haller first documented the importance of blood vessels in the formation of the skeleton proposing the theory that arteries were responsible for osteogenesis. This opposed the popular periosteal theory of bone formation at that time (von Haller, 1763; Hernigou, 2015). During the 19th century the osteoblast became a popular candidate as the main instigator of osteogenesis and the role of blood vessels was somewhat overlooked. During the early part of the 20th century interest in bone formation waned but published data by Trueta, in 1963, proposing a vascular stimulating factor (VSF) released at the fracture site of bones, revived the interest in the role of vasculature in osteogenesis (Trueta, 1963).

Osteogenesis and blood vessel formation are two closely linked events that are governed by processes involving distinct cell populations, tissues, cytokines and growth factors. The blood supply during skeletal development and fracture repair is crucial for viable bone formation and healing (Horner *et al.*, 2001; Kanczler *et al.*, 2008). Annually, over 2.5 million allo- and autograft procedures for orthopaedic repair are performed worldwide (Giannoudis *et al.*, 2005), resulting in a significant socio-economic burden, exacerbated with an increasingly ageing population. These surgical procedures can also hold major limitations, such as tissue rejection, infections and importantly, a lack of vascular supply to and from the site of repair, leading to the subsequent necrosis of the tissue or the implanted graft. The central limitation in bone tissue engineering for large skeletal regeneration and repair of non-union fractures remains the re-creation of a functional vascular network around the regenerative site or graft. In both skeletal development and fracture repair, the tissue is infiltrated by the vasculature as it develops and differentiates; this becomes critical during development when the tissue spans a distance in excess of 100-200μm (Lovett *et al.*, 2009) and during bone healing when a critical gap/lesion fails to be bridged by the blood vessels (Xue *et al.*, 2013).

During fracture repair, non-union fractures are categorised as fractures that do not heal autonomously after six to eight months of injury (Tseng *et al.*, 2008). The inevitable result is a pseudoarthrosis with subsequent hypoxia and necrosis of the tissue due to the lack of; i) nutrient and oxygen supply, ii) waste product removal and, iii) recruitment of new cells to populate the bone defect region. Angiogenesis, the development of new blood vessels is augmented by numerous factors. One of the key modulators in angiogenesis is the secreted mitogen, vascular endothelial growth factor (VEGF), a 40kDa dimeric glycoprotein (Olsson *et al.*, 2006) with the potential to attract endothelial cells and stimulate osteoblast differentiation. Furthermore VEGF receptors have been shown to be expressed in both fetal and adult bone tissue and are believed to couple angiogenesis and osteogenesis during endochondral bone formation (Deckers *et al.*, 2002; Ferrara *et al.*, 2003).

Although the understanding of the mechanisms of blood vessel formation is increasingly detailed and the design of bioengineered components has become progressively intricate, an optimal model that can combine the different areas of bioengineering and functional translation into a working model remains elusive. The goal remains to mimic the extracellular matrices of the human body to initiate a blood supply and prevent ischemia in the repair and regeneration of bone in large skeletal defects.

1.2 Blood vessels

1.2.1 Endothelial cells

Endothelial cells (ECs) line the inner surface of blood vessels are specialist squamous cells that secrete/express matrix proteins (fibronectin, laminin, collagens, proteoglycans and proteases), growth factors (FGF, PDGF, EDGF, IGF, TGF-β), antithrombotic factors, pro-coagulants, inflammatory mediators and vasomotor factors (Sumpio *et al.*, 2002).The function of ECs is multifactorial and essential for building and maintaining blood vessels by regulating thrombosis, anticoagulation, platelet adherence inflammation, immune responses, vascular tone and blood flow. EC dysfunction plays a critical role in various pathologies including artherosclerosis, allograft vasculopathy and

hypertension (Sumpio *et al.*, 2002). ECs also function as a selectively semi-permeable barrier within blood vessels controlling the transfer of molecules and the secretion of paracrine and endocrine factors to affect the underlying smooth muscle cells and blood cells (Sumpio *et al.*, 2002). ECs are important in the inflammatory response cascade to infection and blood vessel damage by releasing factors such as vWF. ECs are stimulated during injury or inflammation by thrombin or histamine and switch to an increasing thrombotic proliferative and vasoconstrictive action (Kim *et al.*, 2010).

The endothelium covers the surface of the entire human vasculature and depending on the type of vessel, is exposed to varying degrees of shear force (van Hinsbergh, 2012). The luminal surface of endothelial cells lining the blood vessels has an essential role in blood haemostasis by regulating blood clotting, the activation of platelets and subsequent repair (van Hinsbergh, 2012). Thus, in addition to thrombotic processes during injury, thrombo-resistant and anticoagulating processes are active to maintain the flow of blood and prevent platelet adhesion (Yau *et al.*, 2015).

The luminal surface of endothelial cells is covered by a network of glycoproteins known as the glycocalyx, producing a layer ranging between 20-3000 nm of thickness. The glycocalyx has a protein core with negatively charged GAG sidechains that contribute to the endothelial barrier function by selectively attracting and repelling blood plasma components by means of electrostatic charge (Kolarova *et al.*, 2014).

The glycocalyx backbone consists of proteoglycans including syndecans and membrane glycoproteins such as PECAM-1 (CD31) and ICAM-1 (CD54) anchoring the glycocalyx to the endothelial cell plasma membrane and providing structural support. Endothelial cells secrete soluble proteoglycans (decorin, versican, biglycan, perlecan) integrated within the matrix containing hyaluronic acid and interwoven with glycosaminoglycan side chains composed of largely heparan sulphate and chondroitin sulphate (Reitsma *et al.*, 2007). Changes in expression of adhesion molecules can alter glycocalyx structure regulating endothelium attachment and barrier function. The glycocalyx plays an important role in the antithrombotic maintenance of the endothelium by binding anticoagulants including antithrombin III to heparan sulphate GAGs. Thrombomodulin, produced by endothelial cells, is a cofactor for thrombin and

binds chondroitin sulphate, activating the anticoagulating protein C pathway (Alphonsus *et al.*, 2014). Damage or destruction of the glycocalyx can impair barrier and anticoagulating mechanisms leading to pathological changes in the vasculature such as platelet aggregation, inflammation and oedema as well as capillary leakage (Alphonsus and Rodseth, 2014).

During vascular lesions endothelial cells become activated and platelets will aggregate to form a thrombus as the sub-endothelium, the basal lamina is exposed and coagulation factors such as thrombin and von Willebrand factor are released, promoting the clotting of platelets and red blood cells to aggregate at the site of injury (Yau *et al.*, 2015). In the intact lining and during blood clot attenuation, endothelial cells counteract thrombotic action and inhibit platelet aggregation by releasing prostaglandin, exonucleotidases and nitric oxide. Coagulation factors are cleaved and disintegrated by ADAMTSs (a disintegrin and metalloproteinase with a thrombospondin type 1 motif), disrupting platelet aggregates and adhesion (van Hinsbergh, 2012).

1.2.2 Blood vessel formation

Endothelial cells (ECs) are bi-directional communicators in the tissue (Brandi *et al.*, 2006) and are instrumental as activators or barriers in the unfolding of blood vessel formation (Gerber *et al.*, 1999) (Colnot, 2005). During embryonic development, blood island cells proliferate and differentiate into angioblasts, the precursor cells of blood vessels. Central in the processes by which the vascular networks are formed is vasculogenesis, the formation of new blood vessels from progenitor cells during embryonic development and angiogenesis, the subsequent formation and sprouting of blood vessels from endothelial cells of existing vessels (Drake *et al.*, 1998) (Figure 1.1 and Figure 1.2). Whereas vasculogenesis is restricted to developmental processes, angiogenesis continues throughout life during remodelling (Risau, 1997), in wound healing or pathological angiogenesis (Coultas *et al.*, 2005).

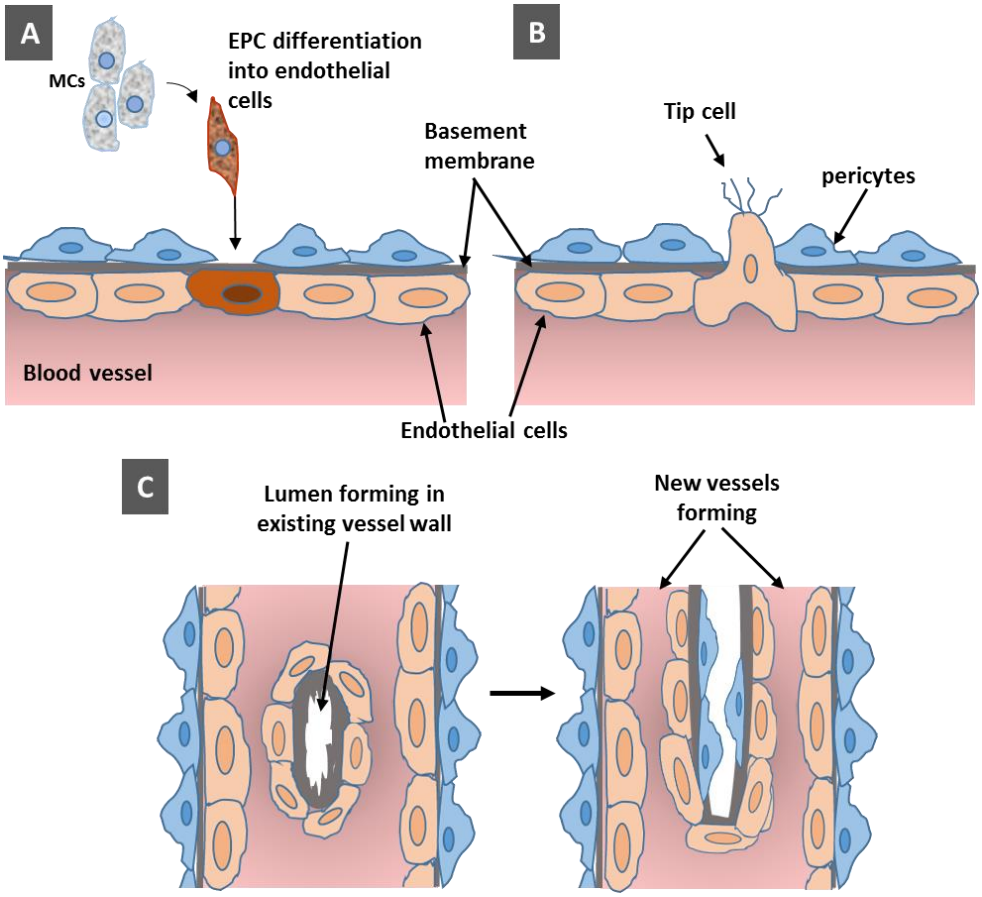

Figure 1.2. **Schematic of blood vessel formation**. **A** Vasculogenesis: Endothelial progenitor cells (EPCs) differentiate from mesodermal cells (MCs) into endothelial cells forming the walls of new vessels. **B** Sprouting angiogenesis: endothelial tip cells loosens from the basement membrane of existing vessels and extend outwards from the vessel wall. **C** Intussusceptive microvascular growth (IMG): luminal endothelial cells of existing vessels fold inwards sub-dividing the lumen and extending to form further vessels; adapted from (Carmeliet *et al.*, 2011).

During de novo blood vessel formation, haemangioblasts (angioblast-hematopoietic precursor cells) emerge from the mesodermal condensations in the extra-embryonic yolk to form blood islands (Garlanda *et al.*, 1997; Patan, 2000). These early endothelial and hematopoietic cells subsequently undergo differentiation *in situ* with the outer cells forming a tubular structure and the inner cells forming blood cells. The resulting angioblasts, together with the blood precursor cells in the lumen, fuse to form the primary capillary plexus (Risau, 1997). The primary plexus is part of a primitive network that comprises major vessels such as the dorsal aorta and the major veins (Gale *et al.*, 1999) (Yancopoulos *et al.*, 2000) (Jain, 2003).

Both the endo- and mesoderm induce vasculogenesis in the embryo. In mice, VEGF is strongly expressed by endodermal cells, as early as day 8.5 (Patan,

2000), during formation of the vascular plexus, however expression is less pronounced in mesodermal cells. ECs express tyrosine kinase receptors for VEGF, which are activated during the earliest stages of vasculogenesis, in particular VEGF-R2/FLK-1/*KDR* and VEGF-R1/Flt-1, a high affinity receptor for VEGF-A (Shibuya, 2001). The angiopoietin protein ligands of the Tie-2 tyrosine kinase receptors, specific for endothelial cells are also important angiogenic factors, promoting cell migration, proliferation, maintenance of vascular integrity and prevention of apoptosis in endothelial cells (Brindle *et al.*, 2006).

Angiogenesis commences once the primitive vasculature is in place resulting in sprouting and remodelling of existing vessels that further develop and extend the vascular network. Angiogenesis is facilitated by hypoxia, which stimulates gene expression of factors such as VEGF and Ang-2 (Schipani *et al.*, 2001; Jain, 2003). During vascular development, blood vessel walls undergo maturation as ECs are firmly joined together with supporting smooth muscle cells and pericytes (Yancopoulos *et al.*, 2000). Pericytes are contractile structural support cells present around small blood vessels. Pericytes are typically embedded in the EC basement membrane of capillaries and venules, and communicate directly and *via* paracrine action with endothelial cells (Cleaver *et al.*, 2003), monitoring EC maturation. Pericytes have been shown to express α-smooth muscle actin (α-SMA) (Gushi *et al.*, 2008; Mogensen *et al.*, 2011), CD146, CD133 and NG2 (Crisan *et al.*, 2008), ALP and platelet derived growth factor receptor β (PDGFR-β) (Mogensen *et al.*, 2011) (Crisan *et al.*, 2008).

Angiogenesis can be sub-divided into endothelial sprouting from existing vessels and intussusceptive micro-vascular growth (IMG) (Figure 1.2A, C) (Patan *et al.*, 1996; Burri *et al.*, 2002; Carmeliet and Jain, 2011) from the dividing vessel-lumen of existing vessels. In essence, the endothelial cell layer forms an intraluminal tissue pillar and the vessel divides, splitting the lumen. Endothelial sprouting involves a high level of communication between ECs and the extracellular matrix (ECM), via growth factors such as VEGF, FGF, TGF-β and the angiopoietins (Ucuzian *et al.*, 2007). New vessel segments are added and pruned to the optimal size (Patan, 2000). The pool of freed ECs from the basement membrane of existing vessels is increased by enzymatic degradation of matrix metalloproteinases (MMPs). This releases endothelial cells,

endothelial matrix and signalling proteins further propagating the process by proliferation, migration, reformation of vessel lumen that are subdivided by splicing through IMG, forming more vessel networks (Carmeliet and Jain, 2011).

Notch signalling has been implicated in the initial arterial/venous blood vessel division during blood vessel maturation (Lawson *et al.*, 2001). Suppression of downstream activation of Notch resulted in reduced ephrin B2 protein (involved in venous development) and an increase in ectopic venous markers on the dorsal aorta of zebrafish. Conversely, the downstream activation of the Notch pathway increased ectopic arterial markers on the posterior cardinal vein, indicating the activation requirement of the Notch signalling pathway to suppress venous differentiation and hence allowing arterial differentiation (Lawson *et al.*, 2001).

In 1971, Judah Folkman proposed that angiogenic factors could regulate the growth of tumours and that removal of this factor could be an effective treatment for cancer (Folkman, 1971). Subsequently, Ferrara successfully isolated and cloned VEGF and was able to demonstrate that inhibiting VEGF activity aided tumour suppression and offered a possible treatment of wet age-related macular degeneration (AMD) (Leung *et al.*, 1989) (Ribatti, 2011).

1.3 Bone

1.3.1 Long bone anatomy

There are two major types of bone in the adult human skeleton, cortical bone (80%) is of a dense and solid consistency and trabecular bone (20%), which is softer has a honey comb-like structure (20%). The ratio of cortical/trabecular bone varies depending on the site of bone throughout the skeleton (Clarke, 2008).

Mature long bones typically comprise a tubular shaft called the diaphysis consisting of compact bone with a highly vascularised central marrow cavity. At either end are the proximal and distal epiphysis containing the growth plate, consisting of spongy bone covered by articular cartilage. The epiphysis is

separated from the diaphysis by the metaphyseal region, a bone-cartilage intermediate part of the growth plate (Figure 1.3).

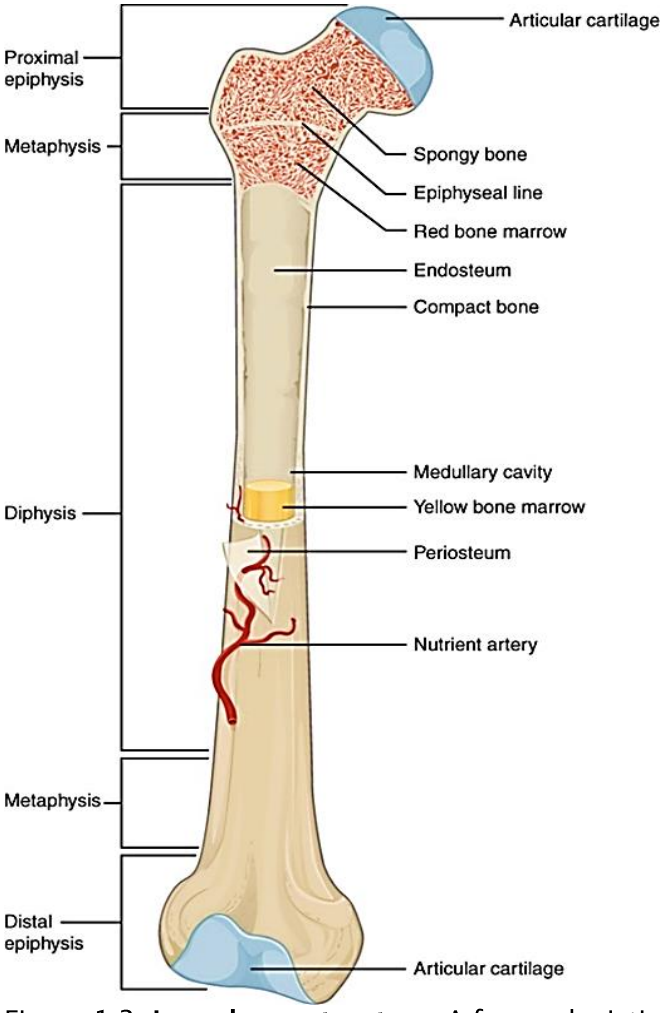

Figure 1.3. **Long bone structure.** A femur depicting the diaphysis, the midshaft of the bone and the proximal and distal end called the epiphysis. The layer of connective tissue surrounding the bone shaft is the periosteum with compact bone beneath it. The metaphysis separates the diaphysis and epiphyses. The epiphysis which is predominantly made up of spongy bone is covered by articular cartilage. The most inner chore of the diaphysis is called the medullary cavity and this contains the bone marrow. (Image from: http://cnx.org/content/m46281/latest/); (accessed: 06/01/17).

Surrounding the diaphysis and attached to the underlying cortical bone by collagenous fibre bundles (Sharpey fibres), is a band of connective tissue known as the periosteum. The underside of the periosteum is lined with osteoblasts on top of the cortical bone (Summerlee, 2013). Within the cortical bone, along the length of the diaphysis, are cylindrical osteons surrounded by a boundary layer of organic matrix. Osteons consist of concentric layers of lamellar bone with a central canal (Haversian canal) containing blood vessels, lymphatic vessels and nerves (Buckwalter *et al.*, 1995). Within the lamellae of

the osteons are lacunae containing osteocytes radially interconnecting through canaliculi.

1.3.2 Bone cell biology

1.3.2.1 Bone matrix

The organic portion of bone matrix consists predominantly (90%) of collagen (type I) protein and 10–15% of non-collagenous proteins such as osteonectin, osteopontin, BMPs and osteocalcin (Clarke, 2008). The arrangement of the collagen fibres determines the resulting bone structure and density (Clarke, 2008). The inorganic portion of bone matrix consists predominantly of calcium and phosphate ions that form hydroxyapatite (HA) crystals and reside within the collagen fibres, contributing to the strength of the bone tissue (Florencio-Silva *et al.*, 2015). The inorganic bone matrix constitutes the body's reservoir of bone minerals such as calcium, magnesium, potassium, sodium and iron (Florencio-Silva *et al.*, 2015).

1.3.2.2 Bone cells

1.3.2.2.1 Osteoprogenitors

Osteoprogenitor (stromal) cells are present within the heterogeneous cell population in the bone marrow alongside haematopoietic cells residing within the red marrow. Osteoprogenitor stromal cells are able to differentiate into skeletal cell lineages including, osteogenic, adipogenic and chondrogenic and have been identified to express the cell surface marker STRO-1 (Simmons *et al.*, 1991). Osteoprogenitor cells differentiating towards the osteoblastic lineage express RUNX-2 (runt-related transcription factor) also known as CBF-α1 (core-binding factor alpha 1) and Osterix (osteoblast-specific transcription factor) (Ducy *et al.*, 1997; Pérez-Campo *et al.*, 2016).

1.3.2.2.2 Osteoblasts

Osteoblasts are immature bone cells that reside within the marrow cavity of long bones within trabeculae as well as lining the outer marrow cavity (endosteum) and the periphery of bones (periosteum) (Buckwalter *et al.*, 1995). Osteoblasts differentiate from mesenchymal cells and actively deposit osteoid, organic bone matrix consisting of type I collagen, osteopontin, bone

sialoprotein, gla protein, alkaline phosphatase and osteocalcin (Kini *et al.*, 2012). Osteoblasts also secrete growth factors including TGF-β (transforming growth factor beta) and BMPs (bone morphogenetic protein) (Kini and Nandeesh, 2012). Osteoblast function is essential in bone matrix production, bone homeostasis and bone mineralisation (Buckwalter *et al.*, 1995)

1.3.2.2.3 Osteocytes

Osteocytes arise through terminally differentiated osteoblasts within the bone matrix. While osteoblasts have a more rounded morphology, once entrapped within the bone matrix osteoblast osteoid protein secretion decreases and the cells develop a more flat morphology with cytoplasmic extensions protruding as the surrounding matrix becomes calcified. Mature osteocytes located within the calcified bone matrix lacunae exhibit reduced expression of previous osteoblastic markers such as osteocalcin, collagen type 1 and ALP (Florencio-Silva *et al.*, 2015). Protruding cytoplasmic processes of osteocytes connect through canaliculi with neighbouring osteocytes and with osteoblasts of the periosteum, via gap junctions (Donahue, 2000). Facilitated by osteocyte morphology, connections and location, these cells are said to transduce mechanical stimulation and sense and affect changes in bone physiology (Pajevic, 2009).

1.3.2.2.4 Osteoclasts

Osteoclasts are bone resorbing cells and differentiate from macrophage progenitor cells of the hematopoietic cell lineage. Osteoclasts reside within the inner lining of the marrow cavity (endosteum) and the perichondrium of joints (Clarke, 2008). Osteoclast proliferation and differentiation is activated through osteoblast secretion of macrophage colony stimulating factor (M-CSF) and receptor activator of nuclear factor kappa-B ligand (RANKL) binding RANK receptors on osteoclasts (Caetano-Lopes *et al.*, 2007) (Figure 1.4). Upon activation osteoclasts initiate bone resorption by secretion of hydrogen ions dissolving bone matrix minerals and cathepsin K enzyme, digesting bone matrix proteins (Cohen Jr, 2006). Osteoclast mediated bone resorption is regulated by the RANKL antagonist osteoprotegerin (OPG), produced by cells including osteoblasts and stromal cells, by binding RANKL and preventing osteoclastogenesis (Cohen Jr, 2006).

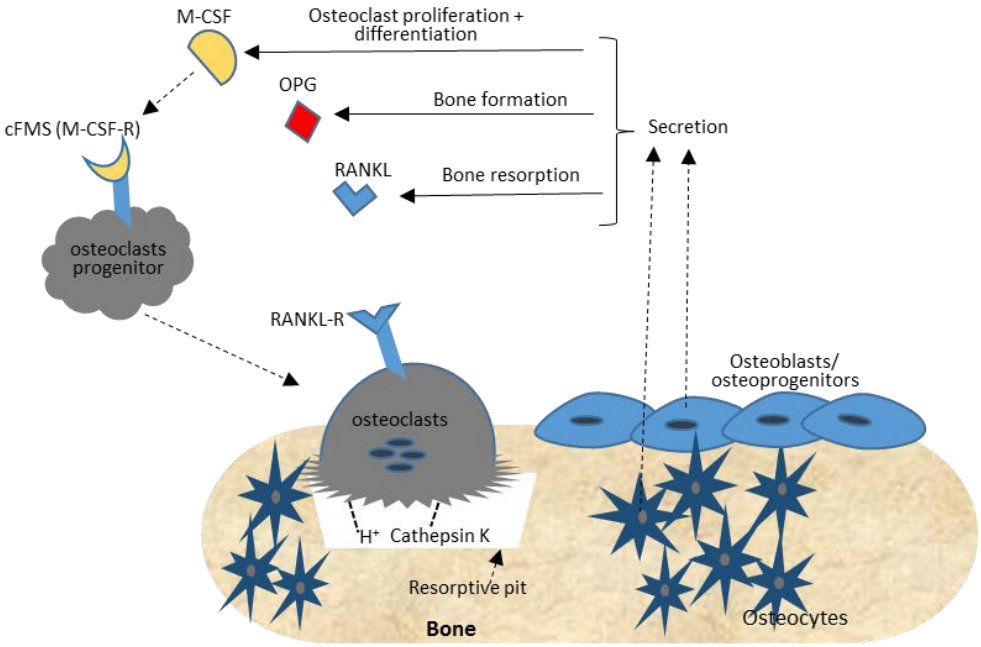

Figure 1.4. **Schematic of osteoclast bone resorption** mediated by osteoblast and osteocyte secretion of ligands OPG (osteoprotegerin), RANKL (receptor activator of nuclear factor kappa B ligand) and M-CSF (macrophage colony stimulating factor).

1.3.3 Bone development

The two main processes for vertebrate bone formation are intramembranous and endochondral ossification. Both bone forming processes require a functioning vasculature. Intramembranous ossification (Figure 1.5) is the process by which flat bones are formed, such as those of the cranio-facial region, scapula, sternum, coccyx, pelvis and ribs and the lateral part of the clavicle (Kini and Nandeesh, 2012).

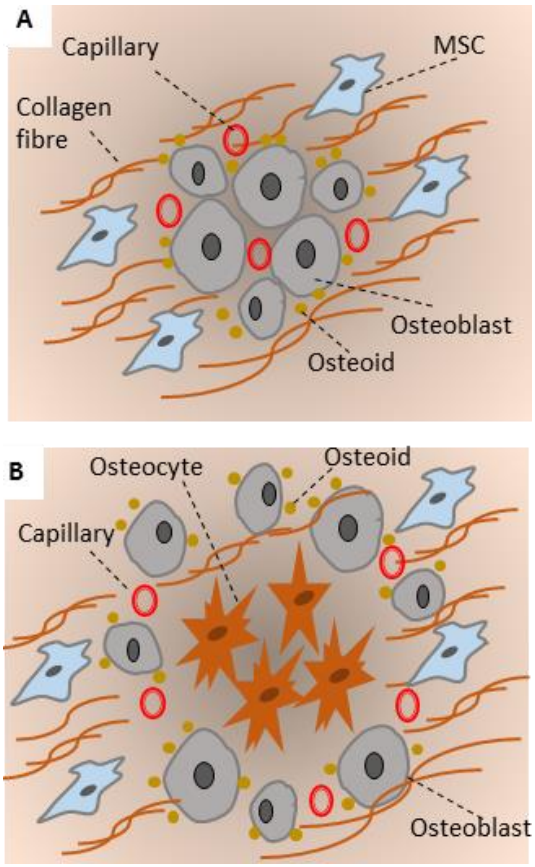

Figure 1.5. **Intramembranous Ossification. A.** Mesenchymal cells adhere to form a condensation and differentiate into osteoblasts that secrete osteoid **B.** Osteoblasts secrete osteoid and become trapped in the mineralised matrix differentiating into osteocytes.

During Intramembranous ossification, embryonic bone is formed from mesenchymal stem cell condensations (Figure 1.5A) (Nowlan *et al.*, 2007; Kini and Nandeesh, 2012) around invading capillaries. MSC condensations differentiate into pre-osteoblasts and secrete a bone matrix consisting of collagen and proteoglycans. Early osteoblasts settle on the deposited matrix, mature and either become osteoblast lining cells or incorporated into the bone and become osteocytes (Florencio-Silva *et al.*, 2015) (Figure 1.5B). The matrix spindles eventually fuse to form bone trabeculae, which in turn become interconnected with woven bone created through mineralisation. The woven bone is later replaced by lamellar bone (Yang *et al.*, 2012).

The most common process of bone formation in vertebrates is endochondral ossification (Figure 1.6) (White *et al.*, 2001; Ortega *et al.*, 2004; Mackie *et al.*, 2008), which forms the long bones such as those of the limbs and vertebrae associated with load-bearing functions. The distinct difference to

intramembranous bone formation is that the bone is formed from a cartilage template.

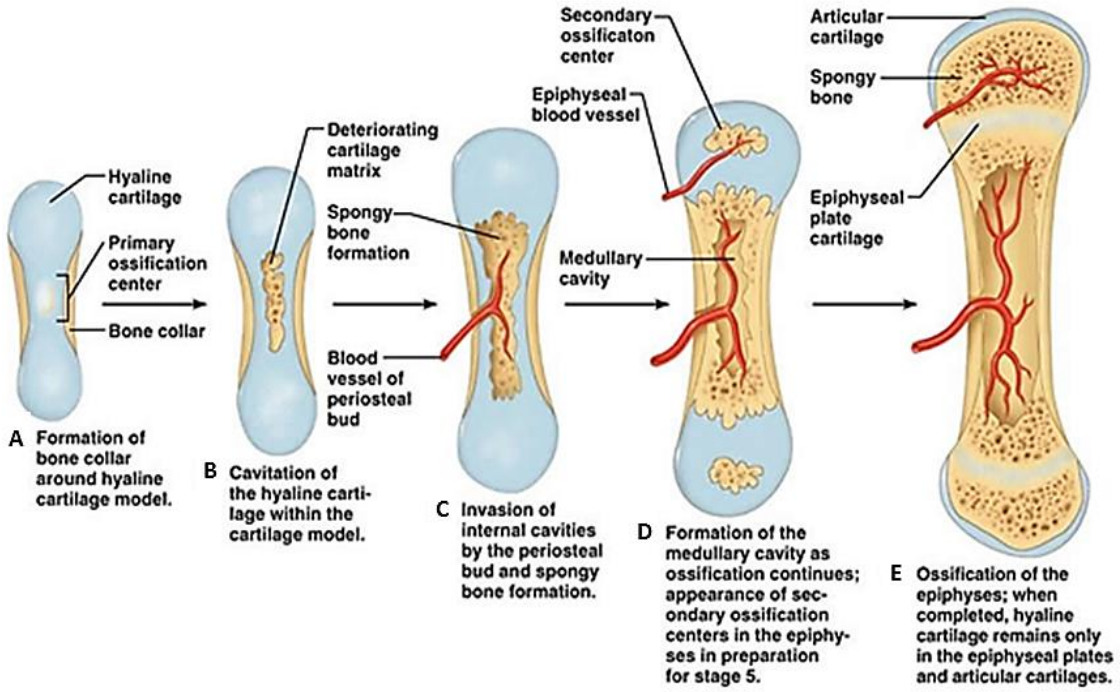

Figure 1.6. **Endochondral ossification.** A schematic diagram demonstrating the stages of Endochondral Ossification. Progression from a cartilaginous template to formation of the primary and secondary ossification centres to a mature mineralised bone with epiphyseal growth plates (Image from: http://classes.midlandstech.edu/carterp/Courses/ bio210 /chap06/ lecture1.html); (accessed: 06/01/17).

During early development, mesenchymal condensations within the skeletal blastema give rise to cartilage cells under the influence of surrounding tissue; reviewed by (Hidaka *et al.*, 2008). In endochondral ossification the cartilage anlage matches the morphology of the limb subsequently formed (Figure 1.6A). The cartilage template develops ossification centres that maintain bone turnover to ensure longitudinal growth of the bone.

The primary ossification centre develops in the centre of the diaphysis (Figure 1.6 A/B) where the matrix becomes calcified and the central marrow cavity is formed (Gerber *et al.*, 2000).The secondary ossification (Figure 1.6D) centres develop at the distal ends in the metaphysis between the diaphysis and epiphysis of the bone. The early cartilage produces anti-angiogenic factors that inhibit the vasculature prior to invasion. Later in the development process, vascularisation is initiated (Figure 1.6C) and endothelial cells forming primitive blood vessels invade from the perichondrium into the cartilage, stimulated by VEGF during what is termed quiescent angiogenesis (Gerber and Ferrara, 2000)

(Figure 1.6C/D), bringing with them a range of stromal cells such as endothelial cells, osteoblasts and chondroblasts (Ortega *et al.*, 2004).

The cartilage subsequently matures and differentiates along the hypertrophic zone and over time is resorbed and replaced with bone tissue. It is essential for both intramembranous and endochondral bone formation that the balance between bone formation and resorption and the blood flow is appropriately maintained (Mackie *et al.*, 2008). The balance between chondrogenesis and osteogenesis is dependent on the blood flow to and from the tissue and through this temporal and spatial coupling of processes, the rate of ossification and growth of bone is ensured (Kanczler and Oreffo, 2008).

1.3.4 Chondrogenesis during bone development

In the process of chondrogenesis, mesenchymal cells migrate to areas of future bone and form condensations that become the cartilage anlage of the limbs (DeLise *et al.*, 2000). ECM enriched with collagen I, hyaluronan and fibronectin is subsequently produced. In the transition to chondrocytes the makeup of the ECM changes with the disappearance of type I collagen and production of collagen type II, IX and XI, proteoglycans and aggrecan (DeLise *et al.*, 2000). Figure 1.7 provides an overview of the main stages of chondrogenesis and protein interactions therein. The cartilage precursor cells form nodules within the centre of the blastema and cells of the periphery elongate and flatten to subsequently form the periosteum. The chondrocytes then proliferate and differentiate forming the long bone, further differentiating and maturing into hypertrophic chondrocytes expressing type X collagen and a decreased expression of type II collagen (COL-2) and fibronectin (Dessau *et al.*, 1980).

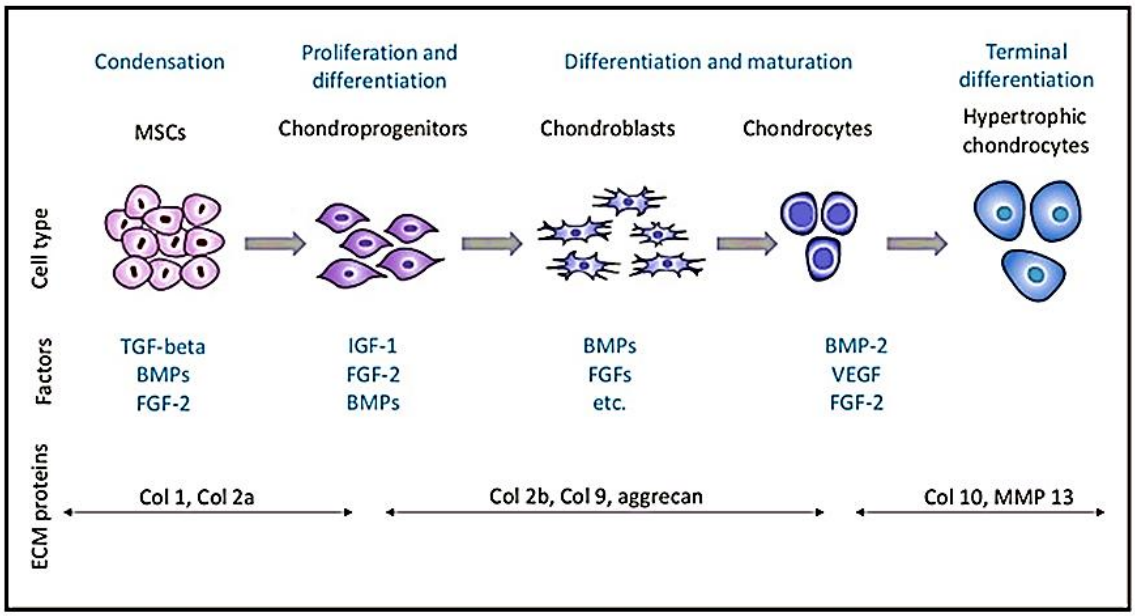

Figure 1.7. **Chondrogenesis:** Schematic diagram of the differentiation of mesenchymal cells to chondrocytes. Chondroblasts emerge from mesenchymal condensations producing a matrix rich in collagens and proteoglycans. Growth factors of the TGFβ superfamily, FGFs VEGF and transcription factors act during differentiation to mature chondrocytes. (Image source: http://www.intechopen.com/books/current-issues-in-sports-and-exercise-medicine/novel-therapies-for-the-management-of-sports-injuries); (accessed: 06/01/17).

The cartilage of the secondary ossification centres of forming long bones are arranged in pre-hypertrophic and hypertrophic zones (Figure 1.8). At the distal end of the growth zone chondrocytes are in a resting state, while in the pre-hypertrophic zones, chondrocytes continue to proliferate. FGFR-3 (fibroblast growth factor receptor 3) has been shown to act as a major inhibitor of chondrocyte proliferation, with FGF-18 serving as its ligand (Liu *et al.*, 2002). Mice lacking a functional FGF-18 gene show an increase in proliferation and differentiation of chondrocytes in the epiphyses with an expanded proliferative and hypertrophic zone comparable to that shown in FGFR-3 deficient mice (Liu *et al.*, 2002). Differentiating chondrocytes secrete an extracellular matrix comprised of proteoglycans and collagens. At the metaphysis, capillaries from the perichondral plexus invade the growth zone, a process regulated by VEGF isoforms and receptors Flk expressed on ECs (Liu *et al.*, 2002). Additionally, Gerber and colleagues postulated that for the directional growth of the bone and vascular invasion to occur, a gradient of VEGF expressed by hypertrophic chondrocytes is needed, given that blocking VEGF receptors resulted in impaired trabecular bone formation in mice and primate models (Gerber *et al.*, 1999). This resulted in specific inhibition of resorption of hypertrophic

chondrocytes leading to a marked expansion of the hypertrophic zone (Gerber *et al.*, 1999).

With the influx of the early vasculature, chondrocytes undergo maturation, becoming increasingly hypertrophic and form column-like structures alongside vascular channels (Figure 1.8), before undergoing apoptotic cell death. At the stage of hypertrophy, high levels of ALP, Collagen type X and VEGF are expressed and secreted by these chondrocytes (Gerber and Ferrara, 2000). Apoptotic chondrocytes are resorbed by osteoclasts and replaced by osteoblasts, which secrete an osteoid-like matrix. The arrangement and organisation of chondrocytes in distinct columns progressing from proliferation to maturation and resorption allow the directional growth of the bone (Hidaka and Goldring, 2008).

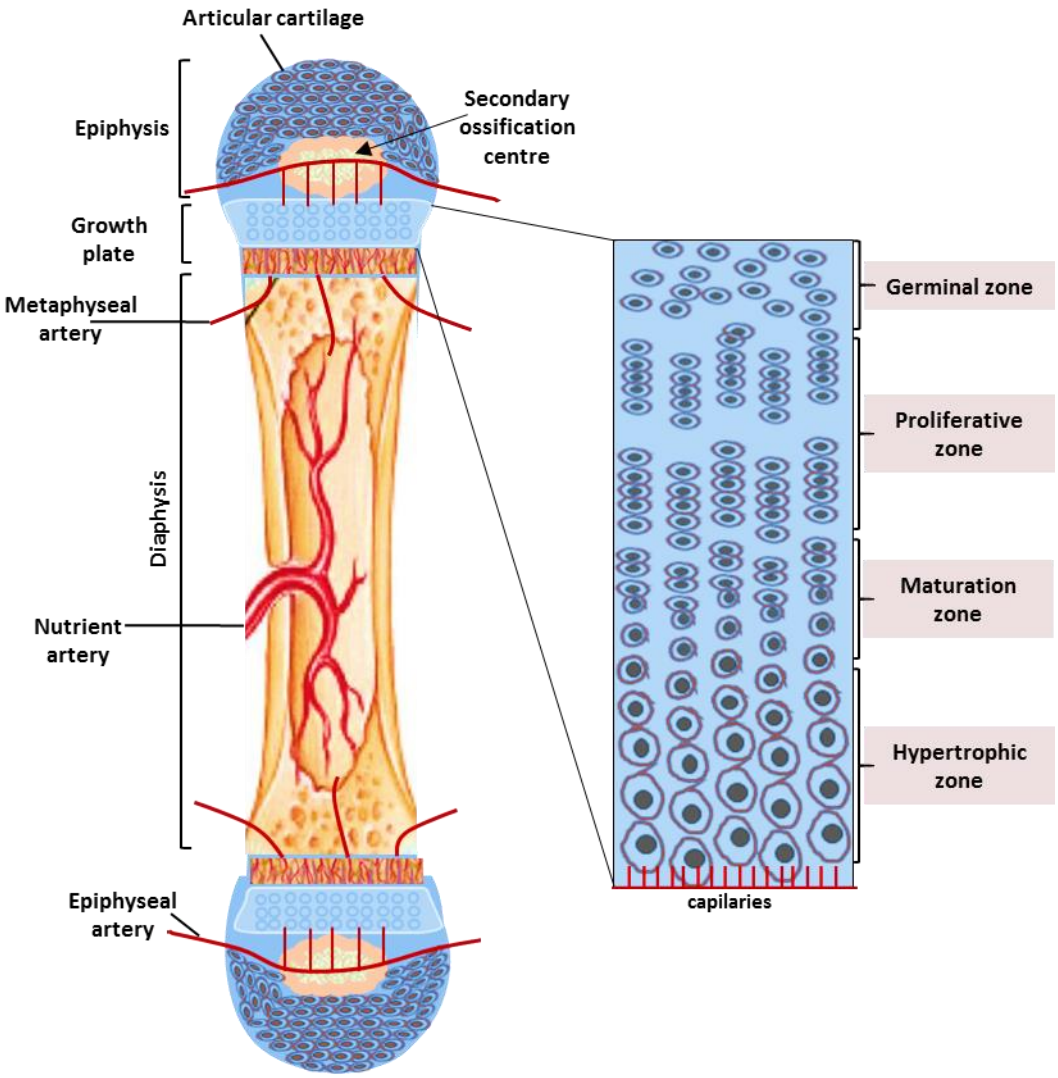

Figure 1.8. **The growth plate during long bone growth.** Columnar arrangement of chondrocytes progressing from the germinal/resting zone *via* proliferation and maturation to the hypertrophic zone, prior to chondrocyte apoptosis, mineralisation and vascularisation; adapted from (Wallis, 1996).

1.4 Angiogenesis during bone development

The mesenchymal precursor cells of the embryonic limb bud differentiate into chondrocytes and immature blood vessels invade from the peripheral perichondrium during late embryonic development. Hypoxia is thought to be one of the main triggers for blood vessel invasion *via* activation of the hypoxia-inducible factor α (HIFα) pathway (Ceradini *et al.*, 2005; Dery *et al.*, 2005; Wang *et al.*, 2007; Kashiwagi *et al.*, 2010). In response to low oxygen levels, gene expression of angiogenic growth factors such as VEGF is elicited by osteoblast signalling via the HIF-1α pathway (Wang *et al.*, 2007). During post-natal development the skeleton undergoes a rapid growth spurt during

which vascular structures invade the bone from the metaphysis, at the base of the secondary ossification centres, channelling their way through terminal hypertrophic chondrocytes (Gerber and Ferrara, 2000). The invasion of the bone by vascular capillaries is triggered by the cellular release of pro-angiogenic factors, such as VEGF (Petersen *et al.*, 2002) in response to hypoxia, a decrease in pH, hypocalcaemia and physical tension. In addition further recruitment of stem cells for the differentiation into chondro- and osteoprogenitor cells necessary for bone synthesis occurs (Hall *et al.*, 2006).

The endothelial cells further expand the vascular network by angiogenesis and recruit osteoclast precursors that develop into mature osteoclasts that resorb cartilage, which is subsequently replaced with bone tissue (Brandi and Collin-Osdoby, 2006). Thus, angiogenesis ensures the function of the blood supply is adapted to the newly formed tissue and requisite function. Chondrocytes proliferate at the apical end of the forming bone and bone is generated in the centre, slowly pushing the ossification centre towards the epiphysis.

Osteoblasts in contact with endothelial cells display a marked increase in proliferation over 7 days in culture and an up-regulation of ALP and collagen type 1 (Leszczynska *et al.*, 2013). Several growth factor families have been implicated in the induction of these processes beyond VEGF (Tammela *et al.*, 2005), including FGF, Platelet derived Growth Factor (PDGF), various Transforming Growth Factors (TGFs) (Coultas *et al.*, 2005), Interleukins, such as Il-8 and Hypoxia-inducible factor (HIF) (Wang *et al.*, 2007), together with the tyrosine kinase receptors systems Tie/angiopoietin and Eph-B/Ephrin-B (Patan, 2000).

VEGF activation is believed to occur by an ability of chondroblasts and osteoblasts to sense oxygen depletion during the process of ossification, thereby triggering the hypoxia-inducible factor alpha (HIF-α) pathway (Wang *et al.*, 2007). HIF is a central regulator of hypoxia adaptation in vertebrates. In normoxic (normal oxygen levels) conditions HIF displays no activity; however in hypoxic conditions HIF activates hypoxia-responsive genes, such as VEGF and is therefore one of the major inducers of VEGF (Dery *et al.*, 2005). This relationship of blood vessels and their immediate surroundings is of high importance in maintaining the tissue homeostasis when developmental growth

ceases and the implications of a disturbance of this balance can lead to conditions such as osteonecrosis and osteoporosis (Coultas *et al.*, 2005).

1.4.1 VEGF – vascular endothelial growth factor

In humans VEGF-A has various spliced isoforms: VEGF-121, VEGF-165, VEGF-189 and VEGF-206 (Petersen *et al.*, 2002), named after the number of amino acids they are composed of (Ferrara *et al.*, 2003). VEGF has been identified as a key mediator during developmental and adult angiogenesis (Table 1.1). VEGF acts as a mitogen and anti-apoptotic factor on endothelial cells during development and in wound healing *via* its Tyrosine-Kinase Receptors 1 and 2 (*FLT-1* and *KDR*/FLK-1). The high affinity tyrosine-kinase receptor 1 (*FLT-1*) is implicated in having an inhibitory effect on VEGF whereas most of the VEGF activity is believed to be modulated through receptor 2 (*KDR*) (Horner *et al.*, 2001) (Ferrara, 2004) (Ferrara *et al.*, 2005). VEGF's inhibitory actions in the physiological mechanism of angiogenesis appear to have a key role in pathological angiogenesis. VEGF has the ability to induce vascular leakage, therefore having an important part in the diffusion of inflammatory cytokines that can cause oedema and swelling (Carano, 2003).

Ligands	Receptor	Function
VEGF A	R1 (FLT-1), R2 (KDR/FLK-1), Nrp-1	Vasculo-/ angiogenesis: migration & proliferation of endothelial cells; creates blood vessel lumen. Homeostasis; permeability; recruitment HBMSC, chemotactic for macrophage/granulocytes
VEGF B	R2	Embryonic (myocardial tissue) angiogenesis; monocyte migration, up-regulation VEGF-A, recruitment HBMSC
VEGF C	R2, R3 (FLT-4)	Lymph angiogenesis; recruitment of HBMSC
VEGF D	R2, R4	Lymphatic vasculogenesis (lung bronchioles)
PIGF	R2	Vasculogenesis, angiogenesis ischemia, wound healing/inflamation

Table 1.1. **Main VEGF ligands / receptors and their functions.** (Ferrara, 2001)

VEGF is secreted by various cell types, such as osteoblasts, hypertrophic chondrocytes, fibroblasts and smooth muscle cells. VEGF secretion *in vivo* is induced by various stimuli including hypoxia, other growth factors such as insulin-like growth factor 1 (IGF-1), transforming growth factor alpha (TGF-α), epidermal growth factor (EGF) and steroids such as vitamin D (Cardus *et al.*, 2009; Rui *et al.*, 2012).

1.4.2 FGF – fibroblast growth factor

Fibroblast growth factor family is a large group of signalling molecules involved in embryonic development, angiogenesis and wound healing (Liebermann *et al.*, 2002). FGF-1 and FGF-2 regulate cell proliferation and differentiation of mesenchymal cells. FGF-1 promotes chondrocyte proliferation and FGF-2 is associated with and expressed by osteoblasts. FGF is a heparin-binding protein that signals *via* cell surface heparan sulphate proteoglycans that activate receptors FGFR1-4 (Ornitz *et al.*, 2001). Proliferating chondrocytes express FGFR-3 and it has been suggested that FGF-18 binding to FGFR-3 decreases chondrocyte proliferation and regulates hypertrophic differentiation during the ossification process (Liu *et al.*, 2002; Minina *et al.*, 2002). FGF-2 has also been implicated in the up-regulation of TGF-β, VEGF and BMP-2 in BMSC (bone marrow stromal cells) *in vitro* (Farhadi *et al.*, 2005).

1.4.3 TGF – transforming growth factor

The transforming growth factor β (TFG-β) superfamily, of which the bone morphogenetic proteins (BMPs) are members, are a group of paracrine factors that induce bone formation, bone growth, differentiation and ECM synthesis (Liebermann *et al.*, 2002). TGF-β1 is released in response to osteoclast activity and is said to regulate bone formation and resorption via the SMAD-signalling pathway (Tang *et al.*, 2009), critical for skeletogenesis. TGF-β1 is enhanced during endochondral ossification and both chondrocytes and osteoblasts express receptors for TGF-β1 (Liebermann *et al.*, 2002).

1.4.4 PDGF – platelet derived growth factor

Platelet derived growth factor, similar to VEGF, plays an important role in the regulation of skeletogenesis. PDGF functions as a mitogen for cells of mesenchymal origin thus promoting proliferation and migration (Shinbrot *et al.*, 1994). PDGF receptor, PDGFRβ, has been found to be highly expressed in the small blood vessel and vascular structure endothelium during mouse organogenesis at E9.5-16.5 (Shinbrot *et al.*, 1994). PDGF consists of four ligands, PDGFA-D interacting with two cell surface receptor kinases PDGFRα and PDGFRβ, expressed on mesenchymal cells, activating signalling pathways such as Ras-MAPK and PI3K (Andrae *et al.*, 2008). PDGF is synthesised and stored mainly by the alpha granules of platelets but is also secreted by various cells, such as endothelial cells, macrophages and smooth muscles cells (Tennant *et al.*, 1991).

1.4.5 IGF-1 – Insulin like growth factor

IGF-1 is a hormone that has a similar molecular structure to insulin. Growth hormone is secreted by the pituitary gland. Following hepatic receptor binding of growth hormone, IGF-1 is released by the liver. IGF-1 has pro-angiogenic properties and is said to stimulate endothelial cells during blood vessel differentiation once release from the extracellular matrix of the basement membrane. IGF has two ligands IGF-1 and IGF-2 that interact with two surface receptors IGF1R and IGF2R. In osteoblasts, IGF-1 can induce VEGF activation and HIF-1 synthesis via the PI3K/AKT/TOR signalling pathway (Schipani *et al.*, 2009).

1.4.6 Osterix – osteoblast-specific transcription factor

Osterix (OSX) is a transcription factor for osteoblast differentiation during bone formation. Osterix is essential during the coupling of osteogenesis and angiogenesis (Tang *et al.*, 2012). Tang *et al.*, 2012, demonstrated that osterix controls VEGF expression *via* VEGF promoter activation. Silencing *OSX* by siRNA led to repression of VEGF transcription and to the absence of osteocalcin (OC) expression in osteoblasts. Conversely, overexpression of OSX resulted in an up-regulation of both VEGF and OC (Tang *et al.*, 2012).

1.4.7 Angiopoietins

The main angiopoietins, Ang-1 and Ang-2 are ligands for the cell surface receptors Tie-1 and Tie-2, part of the Tie receptor tyrosine kinase family. Angiopoietins act during the later stages of vasculogenesis; they are modulators of angiogenesis and maintain blood vessel integrity. The Tie receptors are selectively expressed on endothelial cells and early haemopoietic cells (Yancopoulos *et al.*, 2000; Ucuzian and Greisler, 2007). Angiopoietin 1 (Ang-1) suppresses plasma leakage and thereby blocking inflammatory factors leaking into the vasculature (Brindle *et al.*, 2006) and is thought to be involved in vessel branching, remodelling, maturation and stabilisation (Gale and Yancopoulos, 1999). Ang-1/tie2 is also thought to promote IMG vessel growth (Patan, 2000). Angiopoietin 2 (Ang-2) blocks Ang-1 activity via Tie-2 receptor. Ang-2 in cooperation with VEGF promotes endothelial sprouting and vessel elongation. In the absence of VEGF it is linked to vessel regression (Patan, 2000). The function of Tie-1 receptor is not well understood. When overexpressed *in vitro* Tie-1 upregulated expression of endothelial adhesion molecules and is said to have pro-inflammatory properties (Chan *et al.*, 2008).

1.5 The blood supply in adult bone

There are three main arterial networks that supply blood, nutrients and stem cells to the distal and proximal regions of the fully developed adult bone 1) the nutrient arteries 2) the metaphyseal and epiphyseal arteries and, 3) the periosteal arteries (Trueta, 1963). Figure 1.9 depicts arterial and venous blood vessels to and from a fully grown femur respectively. The medullary/nutrient artery enters from the periosteum through the foramen and runs through the cortex, dividing into descending and ascending branches in the medullary cavity. There are arterioles extending into capillaries pervading the corresponding regions and sinusoids in the bone marrow, which are highly permeable. Sinusoids excrete CXCL12 (SDF-1, stromal cell-derived factor 1), a chemokine required for the maintenance of stem cells (Sugiyama *et al.*, 2006) (Kanczler and Oreffo, 2008). The capillaries return back into the perichondral plexus *via* a venule.

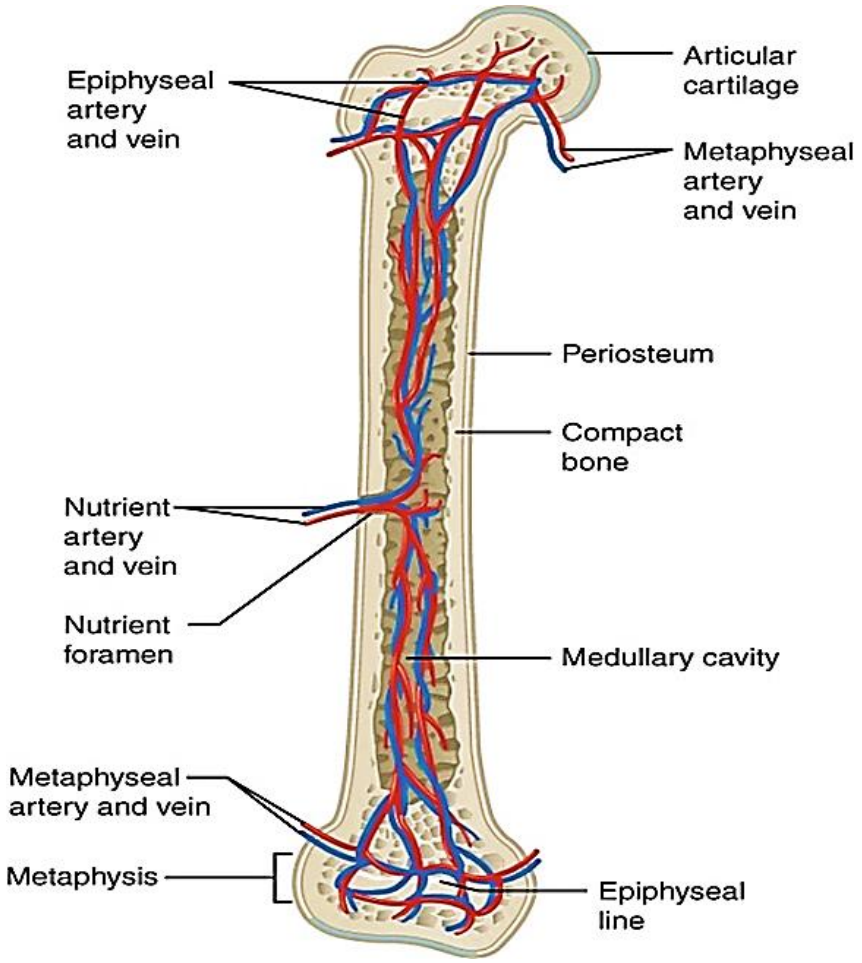

Figure 1.9. **Blood supply of the femur.** Schematic diagram depicting the major blood vessel network to and from the femur. (Image source: http://cnx.org/content/m46281/latest/); (accessed: 06/01/17)

This microvasculature is particularly important for the maintenance and integrity of the bone. The underlying communication between osteoblast precursor cells and endothelial cells offers clues for skeletal tissue engineering. Xue and colleagues reported that contact co-cultures of marrow stromal cells (MSC) and ECs over 5 and 15 days of culture, analysed by micro-array, showed an up-regulation of several genes associated with angiogenesis and osteogenesis. These include von Willebrand factor (*vWF*), cadherin 5 (*CDH-5*), platelet/endothelial cell adhesion molecule-1 (*PECAM1*) and angiopoietin-related gene 4 (*ANGPTL4*), *ALP* and Bone Morphogenetic Protein (*BMP*) respectively (Xue *et al.*, 2013). Leszczynska and colleagues demonstrated an increase in ALP activity in contact co-cultures EC/HMDC associated with the gap junction protein connexin 43 (Cx43), which was expressed by both ECs and HMDCs separately and in co-cultures at contact areas between the two cell types (Leszczynska *et al.*, 2013).

During long bone development the metaphysis is separated from the epiphysis by the growth plate. At the end of growth and after closure of the physis, some epiphyseal vessels penetrate the physeal scar and the epiphyseal and metaphyseal vessels anastomose and connect with branches of the nutrient artery (Trueta, 1963). The mature epiphysis is prone to necrosis after injury due to the reduced blood supply in this part of the bone. Furthermore, the epiphyseal artery passes across the femoral head making the upper epiphysis more vulnerable to loss of blood supply through injury by hip dislocation or femoral neck fracture (Buckwalter *et al.*, 1995)

Disruption of the blood supply can lead to an imbalance in both bone formation and bone resorption. Factors such as Angiopoietin-1 and VEGF along with mesenchymal stem cell recruitment are expressed by osteoblasts (Liu *et al.*, 2012) (Kasama *et al.*, 2007). The over-expression of Angiopoietin-1 in transgenic mice leads to increased bone formation and an elevation in CD31 positive ECs, together with an increase in ALP expression (Suzuki *et al.*, 2007) (Mi *et al.*, 2012). Hence, bone fractures not only lead to a displacement of bone but also to the disruption of the underlying vascular network. This emphasises the importance of the concomitant re-forming of bone alongside the regeneration of a functional vascular network.

The periosteal blood supply plays a particularly important role after injury as the vascular plexus lying above the periosteum anastomoses with vessels of the skeletal muscles and penetrates the cambium (the inner cellular layer of the periosteum) to anastomose with the intraosseus vessels (Buckwalter *et al.*, 1995). During adulthood the periosteal plexus diminishes, however it is still important during some injuries, such as crush injuries, where the blood flow to the skeletal muscle has been disrupted but the connection between muscle and underlying periosteum is maintained and may hence prevent ischaemia (Buckwalter *et al.*, 1995).

1.6 The Role of the vasculature in bone disease and fracture repair

Avascular necrosis (Chan *et al.*, 2012), osteoporosis (Danilevicius *et al.*, 2007; Ding *et al.*, 2011) and multiple myeloma (Bruns *et al.*, 2012) have their origins in pathological changes in the normal vasculature altering bone formation. Rheumatoid arthritis and osteoarthritis are said to be affected by increased vasculature and inflammatory cytokines (Smith *et al.*, 2003; Mi *et al.*, 2012; Wang *et al.*, 2012). Thus an understanding of how the vasculature is formed and maintained offers valuable clues for the development of novel techniques and new strategies to inform tissue and bone engineering (Brandi and Collin-Osdoby, 2006).

In contrast to soft tissue, bone does not produce a fibrous scar which could compromise tissue strength post-healing (Carano, 2003). Following bone fracture, direct or indirect fracture healing can occur. Direct fracture healing follows the pattern of intramembranous bone formation by recruitment, proliferation and differentiation of mesenchymal stem cells (MSCs) directly into osteogenic cells for regeneration of lamellar bone without the added bone remodelling bone step. Direct fracture healing can only occur when conditions are stable and often requires a reduction of fracture ends first (Marsell *et al.*, 2011). In the majority of cases, rigidity cannot be maintained and the healing process follows a multi-phase repair process, much like the process of bone development during embryogenesis (Marsell and Einhorn, 2011). However, in some instances the trauma is so severe that healing cannot proceed unaided resulting in a non-union, where fusion at the fracture site does not occur over a period of three months or longer (Wan *et al.*, 2012). A bone fracture with direct damage to the blood supply and surrounding soft tissue can lead to acute necrosis and hypoxia (Glowacki, 1998). In this respect bone fracture healing typically follows four stages (Figure 1.10):

1) Inflammation: Initially, the disruption of blood vessels in and around bone a fracture will form a haematoma together with coagulants supplied to the site of injury while angiogenic growth factors trigger and increase angiogenesis. Additionally two predominant Interleukins, TNF-α (tumour necrosis factor alpha) and INF-γ (Interferon gamma) are elevated at the fracture site

(Mountziaris *et al.*, 2008). This leads to the recruitment of inflammatory cells together with, fibroblasts and stem cells, which in turn triggers swelling, heat and pain.

2) Soft callus formation: A soft callus comprising of cartilage and fibrocartilage is formed over a period of 3–4 weeks. In preparation for bone repair and angiogenesis, cytokines and growth factors such as VEGF, PDGF and TGF-β1 are released from the surrounding tissue. Capillaries then invade the haematoma, supplying phagocytic cells, thereafter a coordinated action of fibro- and osteoblasts migrate into the repair site in preparation for bone reconstruction (Mountziaris and Mikos, 2008), (Barnes *et al.*, 1999).

3) Hard callus formation: Over 2–3 months the soft callus is ossified. At the base of the wound, granulation tissue produces cartilage in the absence of inflammatory cytokines. The periosteum initially forms an external cartilage callus by stem cells; these stem cells subsequently differentiate into osteoblasts. Matrix containing hydroxyapatite synthesised by osteoblasts gradually mineralises the callus, initially forming woven bone (Street *et al.*, 2002), (Carano, 2003).

4) Remodelling: The callus of woven bone is remodelled and replaced by the harder lamellar bone. Osteoclasts, promoted by the release of RANKL resorb parts of the callus to a size fitting the initial fracture gap. During this final phase, anti-angiogenic factors then reduce angiogenesis and return to a normal homeostatic supply.

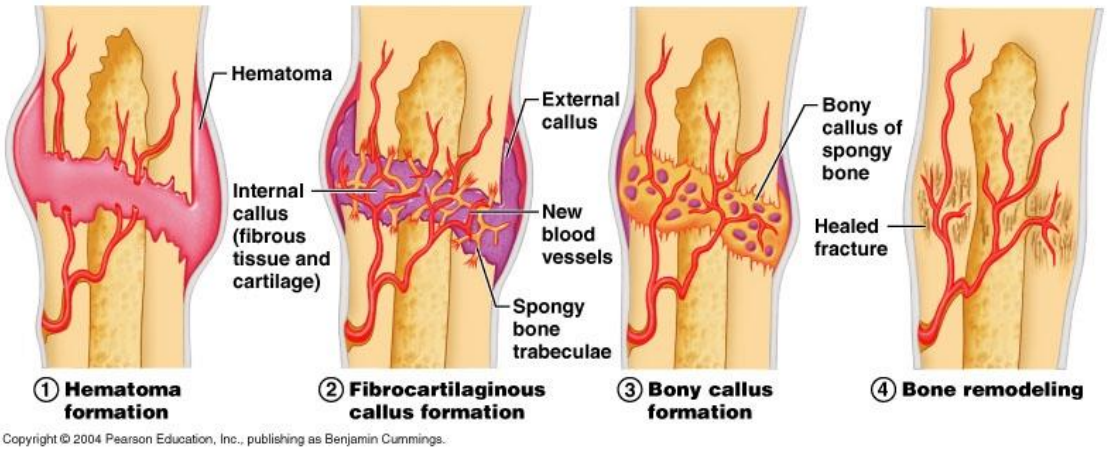

Figure 1.10. **The four stages of bone fracture healing.** 1. Inflammation 2. Soft callus formation 3. Hard callus formation and 4. Remodelling. (Image from: http://www.apsubiology.org/anatomy/2010/2010_Exam_Reviews/Exam_2_Review/Ch_6_Bone_Fractures.htm); (accessed: 06/01/17)

The process of bone repair and regeneration in fracture healing occurs by endochondral ossification, relying on the close relationship between bone and blood vessel or, endothelial cells and osteoblasts (Ortega *et al.*, 2010). A lack of blood supply during bone repair can cause a lack of bone-forming tissue and therefore inadequate development of bone mass. In fractures a lack of a blood supply can cause impaired healing and, as a consequence, causes pain and disability or deformities due to the subsequent non-union (Carano, 2003).

Unlike during skeletal development, the healing process employs various inflammatory cytokines throughout the repair but like the developing bone, the bone forming process is aided by signalling of the different cell types that are supplied by the vasculature and those present at the fracture site. During callus resorption in fracture repair, osteoclasts produce heparinase, an enzyme that releases heparin bound VEGF and thus contributes to further local angiogenesis and osteoclast formation (Brandi and Collin-Osdoby, 2006). Street *et al.*, in 2002 demonstrated that VEGF is required for endochondral bone repair. Street and colleagues found that neutralising VEGF activity decreased angiogenesis, osteogenesis and callus mineralisation in femoral fractures of mice; and further showed in a separate model that the addition of exogenous VEGF had the opposite effect (Street *et al.*, 2002).

An imbalance in the breakdown of ECM by matrix metalloproteinases (MMPs) can lead to pathological loss of cartilage, which plays a role in osteoarthritis (Lambert *et al.*, 2012). Cells from the marrow space secrete MMP-2, MMP-9

and MMP-13 to break down non-calcified matrix, while hypertrophic chondrocytes express type X collagen (COL X) and ALP and deposit mineral matrix prior to apoptosis. The activation of osteoclasts and their differentiation is regulated through osteoblast-derived factors like osteoprotegerin ligand (RANKL), which binds to receptor activator of nuclear factor kappa B (RANK). RANK is present on the cell membranes of pre-osteoclasts. An imbalance between osteoblasts and osteoclasts can cause a pathological increase in bone resorption (osteoporosis) or an increase in bone mass (osteopetrosis) resulting in skeletal tissue abnormalities (Gerber and Ferrara, 2000).

Osteoporotic bone displays increased bone fragility with defects in the microarchitecture and low bone density linked to the lack of blood supply to the bone. Ding *et al.* 2011 demonstrated reduced blood perfusion of the proximal femur, with a marked reduction of microvasculature and abnormal microarchitecture, in osteoporotic, ovariectomised mice. These alterations caused an imbalance of bone-turnover, i.e. osteogenesis and bone resorption, due to low oestrogen levels in the postmenopausal mice (Ding *et al.*, 2011). More recently, Liu *et al.* confirmed a role for VEGF in the differentiation of osteoblasts during osteogenesis, where VEGF acted as a stimulator and played a role in cell fate determination during bone formation (Liu *et al.*, 2012). VEGF was conditionally inhibited in mice *via* the Osterix pathway, resulting in osteoblast precursor cells with reduced osteoblastic differentiation. These mice exhibited an osteoporotic phenotype with increased bone marrow fat and decreased bone density. The exogenous addition of VEGF did not affect this outcome but retroviral restoration of VEGF reduced adipocyte differentiation, suggesting intracrine mechanisms of VEGF, separate from the secreted VEGF/receptor function (Liu *et al.*, 2012).

1.7 Angiogenesis and bone tissue engineering – strategies for regenerative therapies

Approximately 65,000 hip fractures occur annually in the UK, at a cost of approximately £1 billion per annum (NHFD, 2016). Morbidity is high (one third of people die within a year of injury) but is frequently due to conditions associated with the fracture, not the fracture itself (NHFD, 2016). Additionally, many patients will require further treatment as a consequence of bone loss, infection and ischaemia. Common surgical interventions for non-union fractures such as allo- and autografts also hold associated risks, reviewed in (Ohba *et al.*, 2009). Such risk factors arise owing to tissue rejection and poor tissue/implant integration due to problems with biocompatibility causing infections and/or tissue necrosis in allo- and autograft repairs (Yasuda *et al.*, 2012). For this reason, there has been a drive for the development of biopolymers (Chen *et al.*, 2012), metals and ceramics (Yuan *et al.*, 2010) for surgical implants, scaffolding and stem cell based strategies.

Metal on metal hip implants are particularly prone to corrosion and the subsequent elevation of serum metal ion levels as a consequence of metal debris, into the surrounding tissue and the blood circulation, can have profound health consequences (Bosker *et al.*, 2012; Smith *et al.*, 2012; Goriainov *et al.*, 2014). Bosker *et al.* performed a prospective cohort study in which a significantly high incident of peri-articular pseudo-tumour formation and follow up revisions, was observed in patients with large-diameter metal-on-metal (MoM) total hip replacement (THR); these patients also displayed high metal ion serum levels together with physical symptoms of discomfort and pain (Bosker *et al.*, 2012).

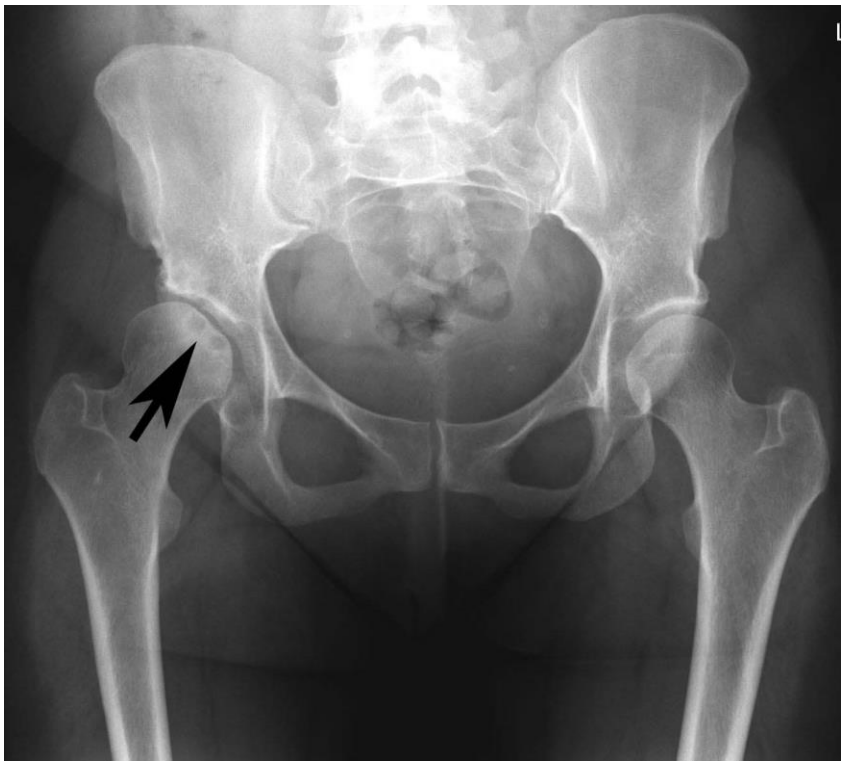

Figure 1.11. **Necrosis of the femur.** X-ray image of avascular necrosis (AVN) of the right femoral head (arrow). Picture obtained from http://manishdvd.blogspot.co.uk/ (06/01/17)

Figure 1.11 shows an x-ray image depicting necrosis of the left femoral head with two necrotic centres (darker circles) surrounded by an ischaemic zone (arrow). Tissue necrosis occurs most commonly in the hip joint. Whereas necrosis of the hip is more prevalent in the elderly population, necrosis of other bones is not restricted to age/gender, but is more common in males aged between 30-60 years. Ischaemic fractures lead to tissue necrosis, which delays healing or can result in non-union. A number of tissue engineering strategies have attempted to stimulate fracture repair in ischaemic tissue. Lu *et al.* injected bone morphogenetic protein 7 (BMP7) directly into the fracture site in mice and an increase in vascularisation as well as cartilage and bone formation over a period of 28 days was observed (Lu *et al.*, 2010).

Generating a functional blood supply in larger bone defects thus represents a significant challenge but could offer therapeutic avenues in human regenerative medicine. A study performed by Rozen *et al.,* 2009, demonstrated regeneration of bone tissue in sheep bone defects, with formation of bone tissue throughout. This was achieved by transplanting blood-derived endothelial progenitor cells (EPC) into the defect. Initially, mineralisation at the

defect site was evident by 2 weeks and complete bridging of the facture was observed at 8-12 weeks. Controls showed predominantly fibrous tissue, whereas sheep defects with EPC showed dense woven bone throughout the defect (Rozen *et al.*, 2009). This poses the questions, whether to: i) generate bone and vasculature de novo using progenitor cells, or ii) to generate bone from skeletal stem cells and graft an established/engineered blood supply into the defect, or iii) to combine all within an engineered construct (Figure 1.12).

1.7.1 Arteriovenous loop-grafts for large bone defects

A popular model for tissue engineering of complex bone defects is the arteriovenous loop-graft-model (AVL). In order to overcome problems associated with autologous grafts, in a study by Boos *et al.* independent axial vascularised bio-artificial constructs were engineered, by auto- transplanting mesenchymal stem cells combined with hydroxyapatite granules into sheep. Dense vascularisation extending from an arteriovenous loop (AVL) and significant formation of vascularised transplantable bone tissue occurred over 12 weeks (Boos *et al.*, 2012).

In 2012, Dong *et al.* investigated pre-vascularisation of larger scaffolds, prior to implantation. An arteriovenous fistula was surgically engineered by anastomosing the proximal ends of the femoral artery and vein of a rabbit femur (Figure 1.12A). This loop was then incorporated into a coral block of dimension 6x8x10mm, pore size was 100-200µm and covered by an expanded-polytetrafluoroethylene (ePTFE) membrane (Figure 1.12B).

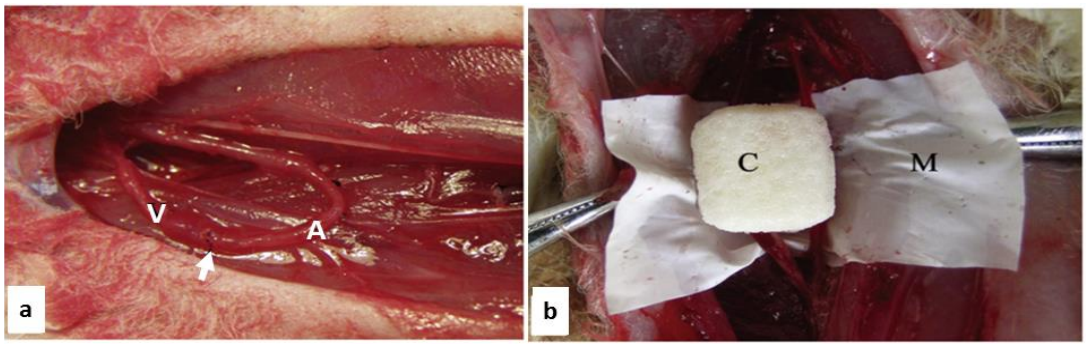

Figure 1.12. **Arterio-venous loop (AVL) model for bone tissue engineering. A)**: Anastomosed loop (arrow) of popliteal artery (A) and femoral vein (V). **B).** Arteriovenous bundles placed at side of coral (C) to be wrapped with ePTFE membrane (M), (Dong *et al.*, 2012) ©Image-Reprint-copyright (2017), with permission from Elsevier.

The vascularised scaffold was subcutaneously implanted into the rabbit groin. Between weeks 4 and 8, considerable invasion and increased sprouting of the vasculature throughout the coral scaffold was evident by histological analysis of Indian ink perfusion and scanning electron microscopy, compared to control (Dong *et al.*, 2012).

Increasingly, researchers have attempted to reduce the burden on large animal studies for preclinical testing and have instead pursued the refinement of *in vitro* based techniques and testing in small animal models. However, it remains far from clear, how well the outcome of *in vitro* models can predict *in vivo* or clinical success, reviewed in (Hulsart-Billstrom *et al.*, 2016).

1.7.2 Growth-factor-releasing scaffolds and hydrogels

Many of the current strategies use biodegradable scaffolds made from biocompatible polymers in an attempt to induce angiogenesis whilst serving as a matrix for the newly formed tissue reviewed in (Stratton *et al.*, 2016). The release of growth factors from scaffolds attempts to simulate the physiological microenvironment of the cells during growth, attachment and proliferation. However, a major problem remains the lack of control over the release and possible over-exposure following growth factor delivery, leading to toxicity or tumour formation as well as the lack of stability of the scaffolds causing deformations or fractures (Nguyen *et al.*, 2012).

Other studies have attempted to stimulate angiogenesis *in vitro*, using VEGF-releasing polymers, coated with bioactive glass (Leach *et al.*, 2006) and

protein-hydrogel scaffold for the delivery of growth factors in a three-dimensional setting as reviewed by (Zustiak *et al.*, 2012). Hydrogels are of particular interest in delivering growth factors such as VEGF and cells to repair sites, given their biocompatibility and permeability. Clay gels such as Laponite are also able to self-assemble *in situ* and due to their charged surface, are excellent vehicles for molecule-delivery. However due to their hydrophilic characteristics, the challenge is to refine the clay to remain *in situ* for a sufficient period of time to fulfil the potential therein (Dawson *et al.*, 2011).

Singh *et al.* used VEGF loaded collagen-coating over a porous polycaprolactone (PCL) scaffolds and implanted these subcutaneously into mice. Increased vascularisation at the scaffold perimeter sites at day 7 compared to scaffolds without VEGF was observed. Furthermore, at day 14 blood vessel density was comparable to that of the surrounding tissue, demonstrating that the absorbed VEGF on these scaffolds significantly stimulated angiogenesis (Singh *et al.*, 2012).

1.7.3 Combining cell biology with tissue engineering

Biomaterial-based approaches in tissue engineering increasingly recognise the importance of the cellular components in bioengineered scaffold or grafts, in order to recreate cytokine induced neovascularisation; a schematic of cell-based tissue engineering strategies for bone is depicted in Figure 1.13. In an attempt to alter the cell phenotype of stem cells within a scaffold towards the angiogenic lineage, Zonari *et al.,* 2012, used human adipose tissue-derived stem cells (hASCs) to demonstrate a novel strategy in differentiating adipose stem cells toward the endothelial lineage. HASCs were seeded onto electrospun fibre meshes, composed of biodegradable, non-toxic, biocompatible polyester glass polymer, and cultured in endothelial medium with added VEGF and bFGF after which the cells began to express vascular markers such as vWF and VE-Cadherin (Zonari *et al.*, 2012).

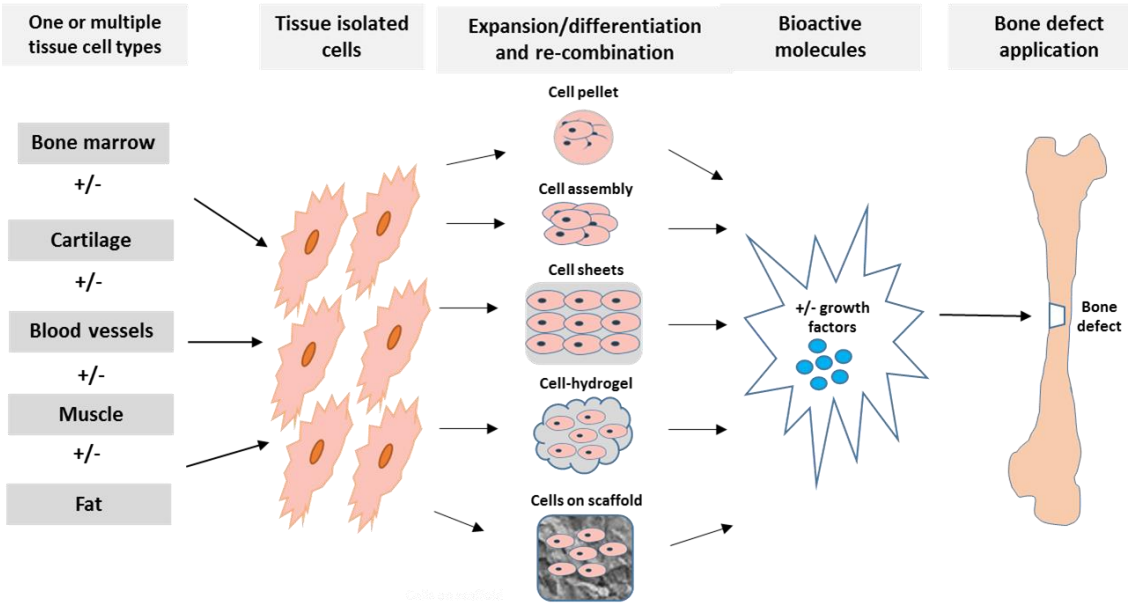

Figure 1.13 **Schematic of cell-based tissue engineering strategies for bone defect regeneration and repair.** Primary cells are extracted from various tissues. One or multiple primary cell types are expanded in vitro and re-combined as cell pellets, cell assemblies/micromass, cell sheets, suspended in or applied onto hydrogel or scaffold with or without the addition of growth factors and subsequently applied to a bone defect.

Using skeletal and endothelial cells in combination with growth factors, Tsigkou *et al., 2010*, developed a two stage protocol to generate vascular bone grafts, seeded with MSCs and HUVECs on a porous scaffold of poly(DL-lactide-co-glycolide) (PGLA) in mice. Labelled endothelial and mesenchymal cells were mixed in a collagen fibronectin gel and applied to the scaffold. Prior to seeding, HMSCs were pre-cultured with TGF-β to induce a smooth muscle or pericyte-like phenotype. The formation of a vascular plexus-like network was observed throughout the scaffolds *in vitro* and *in vivo*. The vessels were stable for over one month *in vitro* compared to controls omitting TGF-β induction treatment, emphasising that the interaction of endothelial cells with the smooth muscle-induced HMSCs played a crucial part in the development of stable vessels (Tsigkou *et al.*, 2010).

Mendes and colleagues designed a triple co-culture model of combined cell sheets. Co-cultures consisted of perivascular-like HBMSC, induced by TGFβ1, directly cultured with HUVECs and separated by poly(vinylidene difluoride) (PVDF) membrane from osteo-induced HBMSCs. Mendes and colleagues demonstrated the distinct organisation of the different cell types over the osteogenic cell sheet and pronounced elongation of perivascular-like cells

expressing CD146 after 14 days. Further *in vivo* assessments of the cell constructs in mice revealed integration of HUVECs with the host vasculature, where CD31 was shown to be expressed along with the presence of osteogenic markers such as osteocalcin and COL-1 (Mendes *et al.*, 2012).

1.7.4 3D printing

An increasingly promising area of tissue engineering is computer assisted 3D printing of scaffolds, reviewed in (Tang *et al.*, 2016). For example, scaffolds of Hydroxyapatite (HAP) and tri-calcium phosphate (TCP) are created by sintering from powder and customised in 3D with highly distinct characteristics such as pore sizes using Computer Assisted Design (CAD). The tailored scaffolds can be designed to precisely fit the defect, and can be pre-seeded with cells (Shafiee *et al.*, 2016). The pore channels can facilitate vascular and nerve ingrowth (Shafiee and Atala, 2016). Virtually any shape or size of scaffold can be created in this way and seeded with the patient's own cells.

The goal is to recreated functional tissues, maintained by a microfluidic network to produce 'organs-on-chip'. A series of steps are involved in the process of bioprinting: 1. Imaging, 2. CAD, 3. Material selection, 4. Cell selection, 5. Bioprinting and 6. Application. The inkjet bioprinter (Figure 1.14) can employ multiple cartridges containing the constituting elements, such as cells, hydrogel and polymer/thermoplastic biomaterial (hybrid 3D constructs) that are forced through a nozzle onto a substrate. A transducer along the printer nozzle applies heat or alternatively, an acoustic wave alters the shape of the ink (e.g. cells) into precise droplets, expelled by the nozzle in a specific programed pattern of cells-hydrogel and polymer layers. The three main categories of bioprinting are: 1. Droplet inkjet bioprinting, employs a thermal resistor or piezoelectric actuator to form cell droplets, 2. Laser bioprinting employs a pulsating laser beam with a laser-absorbing interlayer and, 3. Extrusion bioprinting, applies mechanical force by pistons, screw or pneumatic force to extrude the liquid material from the nozzle (Murphy *et al.*, 2014).

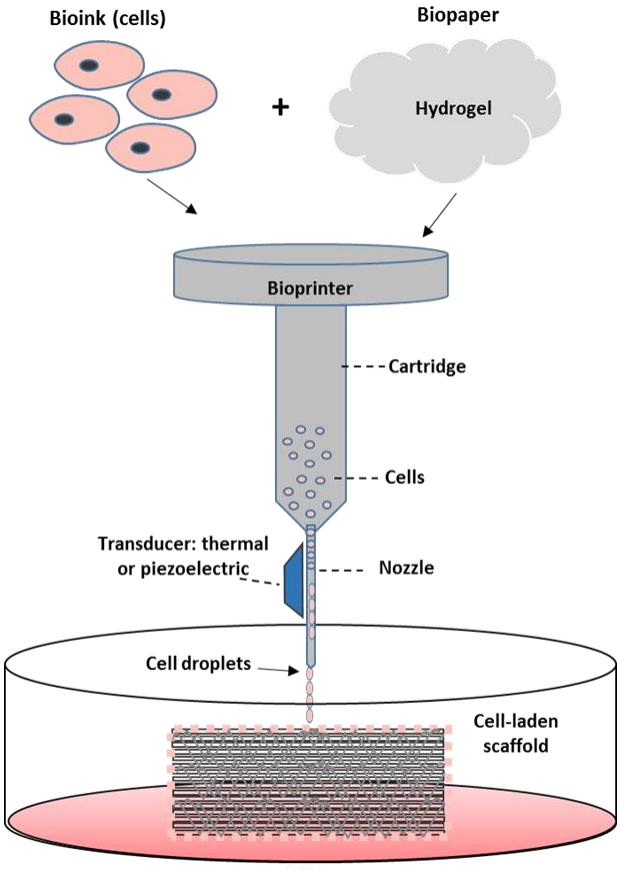

Figure 1.14. **Schematic of 3D inkjet-bioprinting of cells mixed with hydrogel onto a scaffold.** The single cartridge mode of inject-bioprinting combines the cells with a hydrogel, resembling the printer ink and paper, respectively. Heat or a voltage is applied to the flow-through within the nozzle by a transducer to produce either cell droplets or filaments onto a scaffold.

There are, however, limitations in the use of bioprinting techniques as it requires chemical modifications of the biological material to facilitate the use with the printer. Chemical modifications can be toxic to cells or heat can alter the biological properties of the ECM, thus affecting cell viability and leading to inconsistencies in cell droplets or, clogging of the printer nozzle (Murphy and Atala, 2014). In addition, for bio printing, cell densities must be low to reduce shear stress on cells and to facilitate crosslinking of hydrogels. Inkjet bioprinters using piezoelectric crystals that create uniform droplets in response to voltage avoid some of the associated flaws of heat and mechanical forces, however, the concern remains that the frequencies used to create the droplet may damage the cell membranes. (Murphy and Atala, 2014). Bioprinting is a rapidly evolving area of 3D printing offering a particularly rapid, cost-effective and precise way of creating a 3-dimensional anatomical structure with intricate detail, combining scaffold, graft and nanotopography.

Nonetheless, fabrication of large tissue or bone substitutes or even smaller bone scaffolds using 3D bioprinting is still elusive in clinical use, due to limitations in recreating a functional vasculature and maintaining mechanical stability within the printed graft. Neovascularisation of bone grafts is delayed and capillaries regress within weeks. This is exacerbated with an increased size of the implant leading to lack of vascular penetration in order to avoid bone necrosis and structural/mechanical instability (Tang *et al.*, 2016).

More recently engineers have addressed the limitation of size and stability of 3D implants by creating specialised cell-laden hydrogel polymer scaffolds as whole tissue replicates using 3D bioprinting (Kang *et al.*, 2016). The group devised a system of bioprinting, termed ITOP (integrated tissue-organ printer) that employed multiple microscale nozzles capable of 2μm tissue resolution and 50μm cell resolution printing driven by air pressure, producing cell-laden hydrogels hybridised with PCL polymer (Kang *et al.*, 2016). The 3D printing template and motion program was obtained by scanning human samples and processing CT or MRI imaging data using CAD, commanding a 3-axis stage connected to a multiple cartridge module (cells, hydrogel PCL) that combined produced the 3D printed construct (Kang *et al.*, 2016). Kang *et al.* optimised the hydrogel composition of fibrinogen, hyaluronic acid and high glucose DMEM to obtain a finite printing medium resembling the tissue type constructs printed, such as muscle, cartilage and bone. Mechanical strength and porosity (microchannels) of the constructs was conferred by a variation in PCL placement and layering pattern between the construct tissue-types produced. Cell viability was determined to be high (>90%) and increased cell proliferation within the gel was observed. 3D printed calvaria bone construct produced excellent integration into rat calvaria defects over 5 months with new bone and vascularisation evident. Similarly implantation of 3D printed ear cartilage constructs demonstrated cartilage morphology and phenotype together with mechanical properties after 1-2 months of mice subcutaneous implantation. Key improvements Kant *et al.* achieved included mechanical stability, nutrient/oxygen diffusion and vascularisation observed with in vivo implantations of printed constructs. Furthermore, the thermo-polymer used, PCL, has a low melting temperature beneficial to cell survival and a slow degradation rate, prolonging structural integrity. This study has produced promising improvements for future clinical use of 3D printed tissue.

In summary, smart engineering is at the forefront of biomaterial technology. The ultimate aim is to design biomaterials that show sustainability in a designed environment, or extracellular matrix, which mimics the function and responses of the natural environment of the host (Dawson *et al.*, 2008). Ideally this will have the ability to stimulate cellular invasion, proliferation and differentiation and at the same time trigger blood vessel formation. Additionally, these constructs require to be biodegradable over time whilst having the functional characteristics in maintaining a healthy non-inflammatory or destructive environment.

1.7.5 Organotypic cultures

With the plethora of smart engineered biomaterials, there are increasing ethical concerns around animal experimentation and a growing demand for efficient *in vitro* and *ex vivo* models to reduce and replace existing pre-clinical animal studies (Kilkenny *et al.*, 2010). The organotypic culture models have gained popularity as an intermediate model between *in vitro* and *in vivo* culture techniques. The origins of organotypic model systems date as far back as 1929, where the organ culture was described as a relatively simplistic design of embryonic rudiments cultured on top of a plasma clot in a watch glass; in later models replaced by a semi-permeable membrane (Fell *et al.*, 1929; Roach, 1990). To date, the principle of this culture method has been preserved as growing an organ or tissue on a semi permeable membrane, at an air liquid (culture medium) interface to emulate *in vivo* conditions and maintain tissue integrity (Figure 1.15). Thus, the organ culture allows for the tissue to be handled easily as well as processed and analysed, post-culture. During culture, the tissue/organ may be exposed to various conditions and factors. The subsequent processing can be performed without major damage or disruption of the tissue.

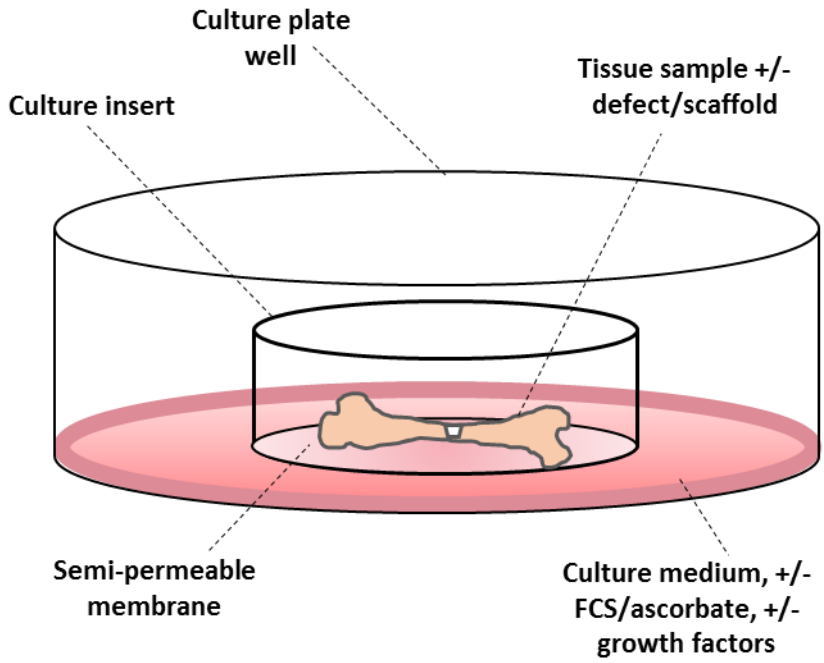

Figure 1.15 **Organotypic culture of a bone organ sample on top of a semi-permeable membrane of a culture well insert**. The well insert is placed into a tissue culture plate well on top of culture medium (1ml), exposed to air at the top. Culture medium can be supplemented with ascorbic acid replacing FCS, +/- factors.

The organ culture can be controlled more rigidly compared to *in vivo* experiments and the culturing of an organ, compared to *in vitro* cell culture, will give an improved insight into the life-like conditions and improved correlations can be drawn to the *in vivo* processes (Fell and Robison, 1929). In 1990, Roach *et al.*, replaced serum in the culture medium with ascorbic acid to encourage collagen formation in bone samples whilst minimising tissue growth by cell proliferation in order to streamline observed tissue changes due to treatments applied (Roach, 1990).

An array of applications using different organ culture setups have been employed to study the temporal development of various tissues such as the myocardium (Brandenburger *et al.*, 2012), lungs (Hofmann *et al.*, 2015), brain (Stoppini *et al.*, 1991) and bone (Kanczler *et al.*, 2012; Hoffmann *et al.*, 2015; Smith *et al.*, 2015). The common denominator of this culture method, however, is preserving the tissue architecture (Vaira *et al.*, 2010). To overcome morphological restriction of tissue, various studies have employed the deconstruction of tissue into smaller constituent; for example, tissue slice organ cultures of brain tissue to study tumour formation (Hickman *et al.*, 2014; Chadwick *et al.*, 2015) or neurological treatments (Ren *et al.*, 2015;

O'Sullivan *et al.*, 2016); alternatively the re-assembly of tissue constituents into constructs may be employed (Lopatina *et al.*, 2015; Pinto *et al.*, 2015).

The addition of biochemicals and biomaterials to the organ culture have also been advanced in the screening of drugs (Nickerson *et al.*, 2007), wound healing and tissue regeneration (Shamir *et al.*, 2014). In bone regenerative studies, chick femora have been observed throughout developmental stages exposed to chondrogenic and osteogenic differentiation conditions (Kanczler *et al.*, 2012). More comprehensively, Smith *et al.*, tested the effect of multifactorial exposure of cells embedded in ECM hydrogels to microparticles loaded with bone enhancing factors such BMP-2, and TGF-β3 and VEGF. Enhanced cartilage and bone formation was reported (Smith *et al.*, 2014; Smith *et al.*, 2014). Other organotypic chick bone defect culture models have reported enhanced bone forming parameters with application of vitamin D3 and TGF-β3 (Smith *et al.*, 2015) and VEGF (Inglis *et al.*, 2016).

Typically, the organ is incubated statically (Roach, 1990), however more recently, researchers have employed perfusion techniques during culture (Stannard *et al.*, 2016) such as bioreactors to mimic mechanical stimulation and perfusion. Stannard *et al.* employed a rotating wall vessel bioreactor organ culture for the comparative study of healthy and injured vertebral discs of whole rat invertebrate explant. The rat explant organs were exposed to 50 rpm rotations in culture medium supplemented with ascorbic acid over 14 days. While *in vitro* whole organ intervertebral disc models are typically associated with low cell viability, Stannard *et al.* demonstrated good tissue architectural integrity and viable compression properties as well as high cell viability in the healthy intervertebral discs (Stannard *et al.*, 2016).

The use of bioreactors has added a critical element to organotypic studies of recent years, such as mechanical forces, crucial in bone development. Significantly enhanced bone growth and mineralisation were reported in embryonic chick femurs cultured over 14 days in a cyclic hydrostatic pressure bioreactor (Henstock *et al.*, 2013). The hydrostatic forces created by mechanical stimulation encourages osteo- and chondrogenesis via hydrostatic pressure within the bone canaliculi and joints (Henstock *et al.*, 2013). Bioreactor studies to date, have been limited by the size of the organ or tissue

being studied. Other limitations of the organ culture include the lack of a physiological response of the whole organism such as an immune or inflammatory system and the lack of a functional blood supply. Furthermore, due to limited availability of human tissue, the source of the tissue tested is often restricted to tissue of animal origin. These factors cumulatively limit the translatability of results obtained using *in vitro* organotypic cultures to *in vivo* human studies. However, further refinement and innovation of culture techniques have made the organ culture a useful preclinical model that continues to evolve with some successful applications in humans such as the culture of human cornea tissue for graft transplantations (Armitage *et al.*, 2014). An innovative way to overcome the lack of vasculature in organ cultures was demonstrated by Warnke *et al.*, 2004, when using a patient's own body as a human bioreactors by implanting an engineered mandible resection graft into the latissimus dorsi for 7 weeks, which was subsequently successfully transplanted back into the patient's mandible (Warnke *et al.*, 2004; Warnke, 2006). While the implant eventually failed, partly due to the patient's life-style choices, it offered an alternative approach of overcoming some of the limitation of the organ culture that may in the future be explored.

1.7.6 Chorioallantoic membrane culture

The chorioallantoic membrane assay (CAM) is (similar to the organotypic culture model), a valuable *ex vivo* model allowing the investigation of several treatment groups simultaneously but, with the unique advantage of utilising the existing vasculature of the chick embryo within the chorioallantoic membrane (Figure 1.16). The chick embryo remains *in situ*, whilst samples are placed through an opening in the shell onto the highly vascularised membrane surrounding the chick embryo. The eggs are incubated allowing the samples to be integrated into the chick embryonic blood supply within the membrane. The CAM assay is an *ex vivo* technique used to assess development, cancer activity, and angiogenesis and the CAM also gives an insight into toxicity of biomaterials (Leng *et al.*, 2004). Limitations of this model include the absence of physical forces acting on the organ within the organism, which is particularly important in bone formation.

Similar to the organ culture, the CAM culture has gained popularity as a useful research-intermediated between *ex vivo* and *in vivo* research. It has added a vascular component, lacking in the organotypic culture but is equally inexpensive with the potential of high sample turnover, although, still requiring the culling of embryos. In the 1970s, the model was used by Folkman and colleagues, in experiments characterising the vascular stimulating properties of tumour angiogenic factor (TAF) by inducing neovascularisation in the CAM.

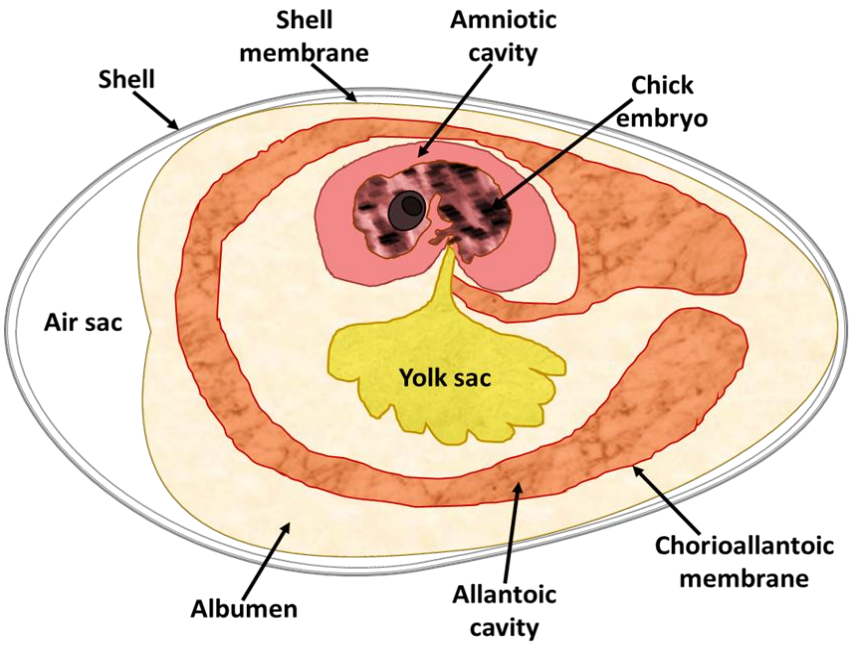

Figure 1.16. **Schematic of the developing chick embryo.** Image depicts the chorioallantoic membrane surrounding the chick embryo within the amnion.

More recently, the CAM has been a crucial research tool in studies of tumour metastasis demonstrating vessel sprouting and screening of angiogenic and anti-angiogenic factors, such as VEGF, FGF-2, as well as anti-angiogenic factors such as avastin (Yildiz *et al.*, 2013). In bone studies, anti-angiogenic properties of cartilage have been investigated in a osteoarthritis (OA); CAM OA and non-OA explants were exposed to VEGF and MMP-9 of which 72% of OA samples demonstrated vascular invasion, compared to 5% of non-OA samples (Smith *et al.*, 2003). Successful repair progression over a 9-day CAM culture of chick femoral osteotomy was performed, with complete bone union at day 9 of the culture. Observations included vascular invasion of the fracture site and

fibrous ingrowth without callus or cartilage transitional stage (Takahash *et al.*, 1991).

The densely vascularised chorioallantoic membrane allows for close gas and nutrient exchange with the rapidly developing chick embryo, particularly during E3-E10 (Patan *et al.*, 1996; Nowak-Sliwinska *et al.*, 2014). Developing chick embryos possess low immune competence until E10, which reduces rejection of the sample implants or material tested; at E18 the embryo has reached full immune-competence (Ribatti, 2008). During the culture period, the vascular supply of the chorioallantoic membrane provides oxygen and nutrients to the implant. The CAM, however, has a limited culture period since egg gestation ends at day 21 with hatching of the chick; therefore, the culture must be terminated prior to hatching, at day 18.

Two main culture methods can be employed using the CAM (Figure 1.17), termed *in ovo* (A) and *ex ovo* (B), which refer to the placement of the sample within the egg. During *in ovo* CAM culture, a small window is created in the eggshell at day 10; the sample is placed through the window on top of the CAM. Culture duration using the *in ovo* method is also determined by the type of sample. For instance, an E18 chick femur, typically used for bone defect studies, cannot be supported on the CAM prior to E10 due to the size and weight, therefore creating an 8 day culture limit. Due to the lack of visibility of the CAM through the small shell opening, inconsistencies or failure to place the sample correctly can lead to non-integration of sample or can cause perforation of the chick membrane. Candling of the egg prior to creating the shell opening, can aid in locating the embryo contained within the chorioallantoic membrane and thus improve correct placement of the implant. Integration of the sample into the CAM and survival are typically indicators for a successful setup.

The second culture method termed *ex ovo* (Figure 1.17B), refers to the transference of the entire embryonic content from the egg to a sterile culture dish at E3. The test sample is placed on top of the CAM and cultured under sterile conditions for up to 15 days. The culture time for *ex ovo* culture is extended since the sample placement occurs at an earlier time point of development. The sample can be observed during placement and culture on the CAM; however, there is a risk of infection due to the exposed culture

method. Furthermore, there is a risk of rupture of the embryonic tissue during transfer to the culture dish. Sterility and tissue integrity of the egg are crucial for the survival of the chick embryo.

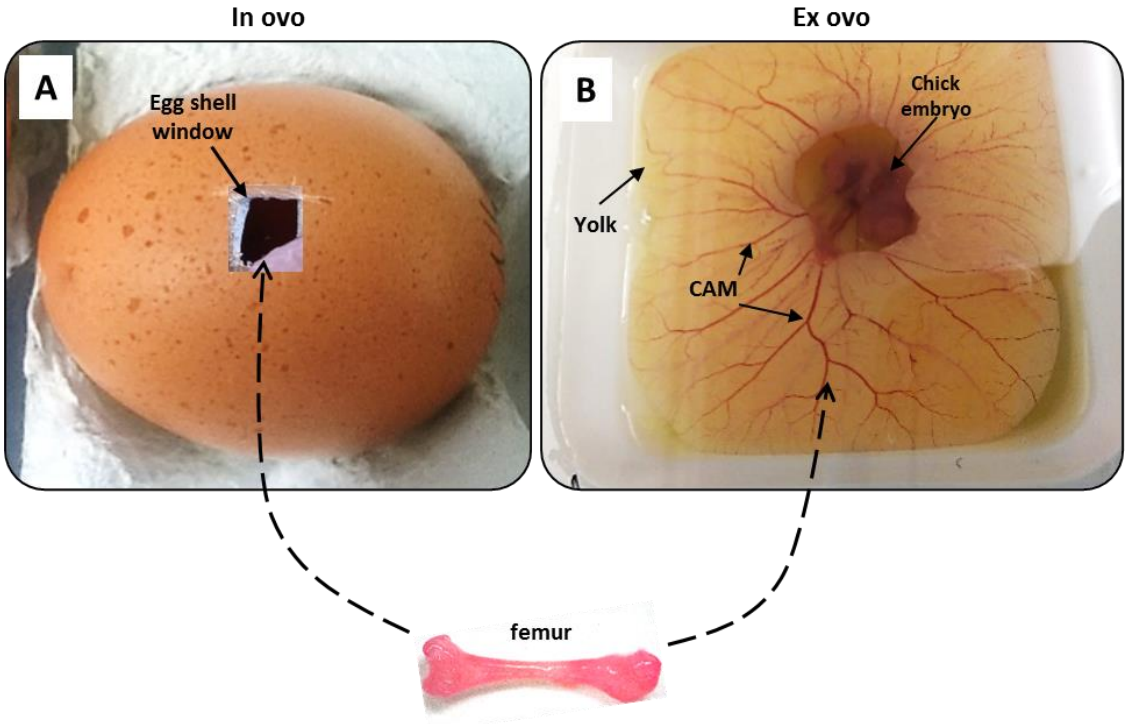

Figure 1.17. **Culture methods of the CAM:** A. *In ovo* placement through a small egg shell window onto the chorioallantoic membrane (not visible); B. *Ex ovo* placement on top of exposed chorioallantoic membrane overlaying egg the yolk.

For nearly half a century, the CAM assay has been implemented effectively for pre-assessment of tissue, biomaterials, drugs and growth factors, evolving into an interdisciplinary technique in assessing development and angiogenesis. Advancements in screening and analysis techniques have contributed to its popularity in research to date.

As well as the benefit of the CAM assay in utilising a blood supply, both techniques, the organ culture and the CAM assay are significantly less invasive than *in vivo* techniques, reducing the need for larger animal surgeries, thus underpinning the guiding principles of the three Rs: Replacement, Reduction and Refinement (Schuppli *et al*., 2005). The challenge will be to translate these techniques into a functional design for use in human physiology and to produce a comparable responses in the multiplicity of the human tissue as has been demonstrated *in vitro*.

1.8 Hypothesis

Vascular and skeletal progenitor cells cooperatively enhance bone formation when combined in contact-culture or in constructs.

1.8.1 Aims and Objectives

The aim of this thesis is to establish the potential of endothelial cells to drive osteogenesis and angiogenesis in combination with fetal or adult skeletal cells. Furthermore, this project sets out to understand the underlying mechanisms and processes in the coupling of osteogenesis and angiogenesis in order to improve cell tissue engineering therapies for bone repair.

1.8.2 Objectives:

1. To investigate the potential osteogenic differentiation and activity of fetal femur-derived stem cells (FFDSCs) or adult human bone marrow stromal cells (HBMSCs) in 2D co-cultures with human umbilical vein endothelial cells (HUVECs). This will involve the characterisation of vascular and osteogenic gene expression as well as the examination of the early bone functional marker, alkaline phosphatase.

2. To investigate the effect of vascular endothelial growth factor (VEGF) on osteogenesis in 2D co-cultures of FFDSCs or HBMSCs with HUVECs. This will involve the analysis of osteogenic and angiogenic gene expression in response to different concentrations of VEGF on fetal and adult human bone stromal cells in co-culture with endothelial cells.

3. To engineer a 3D skeletal cell-pellet culture constructs and assess the potential to drive osteogenesis and angiogenesis using an *ex vivo* chick femur drill defect organ culture model.

To assess levels of bone formation in the chick femora, micro-CT imaging will be used. In addition histological and immunohistochemical assessment will be performed using bone tissue staining and antibodies indicative of osteogenesis and angiogenesis respectively.

4. To test if human placental decellularised vessels can be re-seeded with HUVECs and the ability of the recellularised human placental vessels to integrate into an *in vivo* vascular bed model.

5. To examine the potential of human placental decellularised vessels to improve bone repair in a bone defect when employed as a protective sleeve around the femur.

Bone volume and structure will be assessed using micro-CT imaging and tissue architecture will be assessed by histological and immunohistochemical analysis.

CHAPTER 2

Materials and methods

2.1 Reagents and materials

Tissue Culture, histological and molecular reagents were purchased from the following suppliers: FCS (Fetal Calf Serum 10270106), Cell Tracker™ Green CMFDA (5-chloromethylfluorescein diacetate, C7025), Ethidium Homodimer-1 (EthD-1, E1169), Vybrant® CFDA SE Cell Tracer Kit V12883 and Vybrant™ Dil cell labelling solution V22885, were purchased from Molecular Probes®, Life Technologies Ltd., Paisley, UK. Alpha-MEM (minimum essential medium α-modification, BE02-002F), Trypsin/EDTA (ethylenediamine tetra-acetic acid, BE02-007E), Penicillin/streptomycin (DE17-602E), PBS (Phosphate buffered saline, BE17-512F) and Medium 199 (BE12-117E) were purchased from Lonza Group Ltd., Switzerland, through Scientific Laboratory Supplies, Nottingham, UK. Culture plate inserts (Millicell-CM, 10412511), cell strainers (Fisherbrand, 11597522), syringe filters (Millipore, 10268401) and histological consumables/reagents were procured from Fisher Scientific, Leics., UK. Bovine Serum Albumin (BSA, A3294), alkaline buffer solution (A9226), alkaline phosphatase substrate (P4744), alkaline phosphatase standard (AP standard, 104-1), Naphthol AS-MX phosphate 0.25% (855) and Fast Violet B salts (F1631) were purchased from Sigma-Aldrich Ltd., UK. ECGS/H (Endothelial cell growth Supplement/Heparin, bovine hypothalamic extract, C-30120) was procured from Promocell GmbH, Germany. Collagenase B was purchased from Roche Diagnostics Ltd. UK (11088815001). VEGF (Vascular endothelial growth factor 165, human recombinant, 100-20) was purchased from PeproTech EC Ltd. London, UK. The RNA purification kit RNeasy Plus Mini Kit (74134) was obtained from Qiagen Ltd., Sussex, UK. SuperScript® Vilo cDNA Synthesis kit and Power SYBR Green PCR master mix (4368708) were purchased from Invitrogen Life Technologies UK.

2.1.1 Antibodies:

Antibodies were purchased from the following suppliers:

Primary Antibody	Host/Type/Target	Dilution	Manufacturer	Product #
VEGF-165	Rabbit polyclonal anti-human	1/50	ThermoScientific, Loughborough, UK	12663367
VEGF-R1 (FLT-1)	Rabbit polyclonal anti-human	1/100	Abcam, Cambridge, UK	ab32152
VEGF-R2 (KDR)	Rabbit polyclonal anti-human	1/50	R&D Systems, Oxon UK	AF357
CD31 (PECAM-1)	Rabbit polyclonal anti-human	1/100	ProteinTech, Manchester UK	11265-1-AP
von Willebrand Factor (VWF)	Rabbit polyclonal anti-human	1/100	Dako, Cambridgeshire UK	A0082
Type I Collagen (COL-1)	Rabbit polyclonal anti-human	1/1000	Dr. Larry Fisher (NIH, Bethesda USA)	LF68
Type II Collagen (COL-2)	Rabbit polyclonal anti-human	1/500	Calbiochem, Merck-Millipore, Watford, UK	234188
Tie-2	Rabbit polyclonal anti-human	1/50	Santa Cruz Biotechnology, Heidelberg, Germany	SC324
Angiopoietin 1	Goat polyclonal anti-human	1/50	R&D Systems, Oxon UK	AF923
Angiopoietin 2	Rabbit polyclonal anti-human	1/200	Abcam, Cambridge UK	ab8452
Stro-1	Mouse IgM hybridoma, anti-human	none	Bone & Joint Research Group, Southampton UK	
Hif-1α	Rabbit polyclonal anti-human	1/200	GeneTex Inc., CA, USA	GTX127309
Secondary Antibodies	Goat anti-Rabbit IgG, biotin-linked	1/100	Sigma-Aldrich Ltd., UK	B7389
	Goat anti-Mouse IgG, biotin-linked	1/100	Sigma-Aldrich Ltd., UK	B7264
	Goat anti-Mouse IgM, biotin-linked	1/100	Sigma-Aldrich Ltd., UK	B9265
	Rabbit anti-goat IgG, HRP conjugate	1/100	Dako, Cambridgeshire UK	P0449
Alexa Fluor 488	Goat anti-Mouse IgG	1/200	Life Technologies, Paisley, UK	A11008
DAPI nucleic stain	A-T rich regions in DNA	1/200	Life Technologies, Paisley, UK	D3571

Table 2.1 **List of Antibodies and dilutions used.**

2.2 Tissue culture

2.2.1 Human bone marrow stromal cell isolation

Human bone marrow samples were obtained from haematologically normal patients undergoing hip replacement surgery (Table 2.3). With approval of Southampton & South West Hampshire Local Research Ethics Committee (rec. number 194/99/1); only marrow that would have been discarded was used. Marrow samples containing spongy bone material were repeatedly washed by

adding plain α-MEM, shaking the tube briskly then pouring the liquid into a separate 50ml falcon tube. The cell suspension was centrifuged at 189g for 4 minutes at 18ºC. The supernatant was removed and the pellet was re-suspended in basal α-MEM (containing 10% FCS, 1% Penicillin/Streptomycin (P/S) and passed through a 70µm cell strainer. Bone marrow stromal cells (HBMSC) were cultured at 37°C, 5% CO_2/balanced air until confluent (Oreffo *et al.*, 1998).

2.2.2 Fetal femur dissection and cell isolation

Human fetal tissue was obtained from female patients undergoing termination of pregnancy in line with the Polkinghome Report guidelines. Informed consent was given in writing by the patients and ethical approval was obtained from Southampton & South West Hampshire Local Research Ethics Committee (LREC296/100). Femurs corresponding to 53-63 days (4mm-7mm) post-conception were isolated from foetuses (Table 2.2). The age of the foetus was ascertained by measuring foot-length (Table 7.1) of the foetus and were described as days post-conception (dpc). The surrounding skeletal connective and muscle tissues were removed from the fetal femur sample and the epiphyses at both ends were separated from the diaphysis by micro-dissection (Figure 2.1).

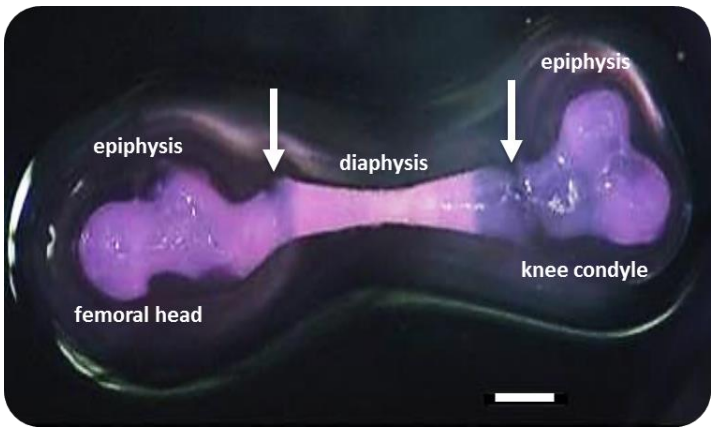

Figure 2.1**. Dissected human fetal femur.** Human Fetal Femur (8.5mm/70dpc) post-dissection. Arrows depicting dissection points for diaphysis/epiphysis. Scale bar: 100µm.

The dissected femur parts were submerged in Collagenase B solution (Roche, Germany) (5mg/ml dissolved in plain alpha MEM) in a 6-well plate and incubated overnight at 37ºC, 5% CO_2/balanced air. The cell suspension was

centrifuged at 156g for 4 minutes and re-suspended in α-MEM, supplemented with 10% FCS and 1% P/S. The fetal femur-derived cells (FFDSC) were monolayer cultured under standard conditions (37°C, 5% CO_2/balanced air) until 95% confluency was reached.

Co-cultures suppl with 100ng/ml VEGF			
Foetal Sample	**Foot length mm**	**days post conception**	**P (Passage)**
H1481	5.5	56	2
H1728	5	55	2
H1740	5	55	1
Co-cultures suppl with 50ng/ml VEGF			
Foetal Sample	**Foot length mm**	**days post conception**	**P**
H1604	7	63	2
H1540	7	63	3
H1704	7	63	3
Co-cultures suppl with 100ng/ml VEGF			
HBMSC	**Age yrs**	**Gender**	**P**
M62	62	M	2
F87	87	F	2
F66	66	F	0

Table 2.2 **Human fetal and adult samples used.** Details of the age and culture passage number of Human Fetal femur and human bone marrow samples used for co-culture studies. M=male; F=female; H=human; P=Passage of culture

2.2.3 Human umbilical vein endothelial cell (HUVEC) isolation and culture

Human umbilical cords were obtained, following signed consent, from healthy mothers after normal, full-term deliveries from the Princess Anne Hospital, Southampton, under ethical approval from Southampton & South West Hampshire Local Research Ethics Committee (LREC 05/Q1702/102). HUVEC were isolated and cultured as described by (Jaffe *et al.*, 1973) with minor modifications. The umbilical cord was cleaned and checked for needle insertion and clamp marks to prevent any leakage. The umbilical cord vein was flushed with 1x PBS (Phosphate buffered saline) to remove cord blood and then drained of any excess fluid. Cords were then infused with a 5mg/ml solution (in plain Medium 199) Collagenase B (Roche Diagnostics UK) and incubated for 1 hour at room temperature to detach the endothelial lining cells (Figure 2.2).

The Collagenase solution was drained from the umbilical cord using a 20ml syringe and collected in a sterile 50ml conical tube. The cell suspension was diluted by adding equal amounts of 1x PBS and then centrifuged at 156g for 5min.

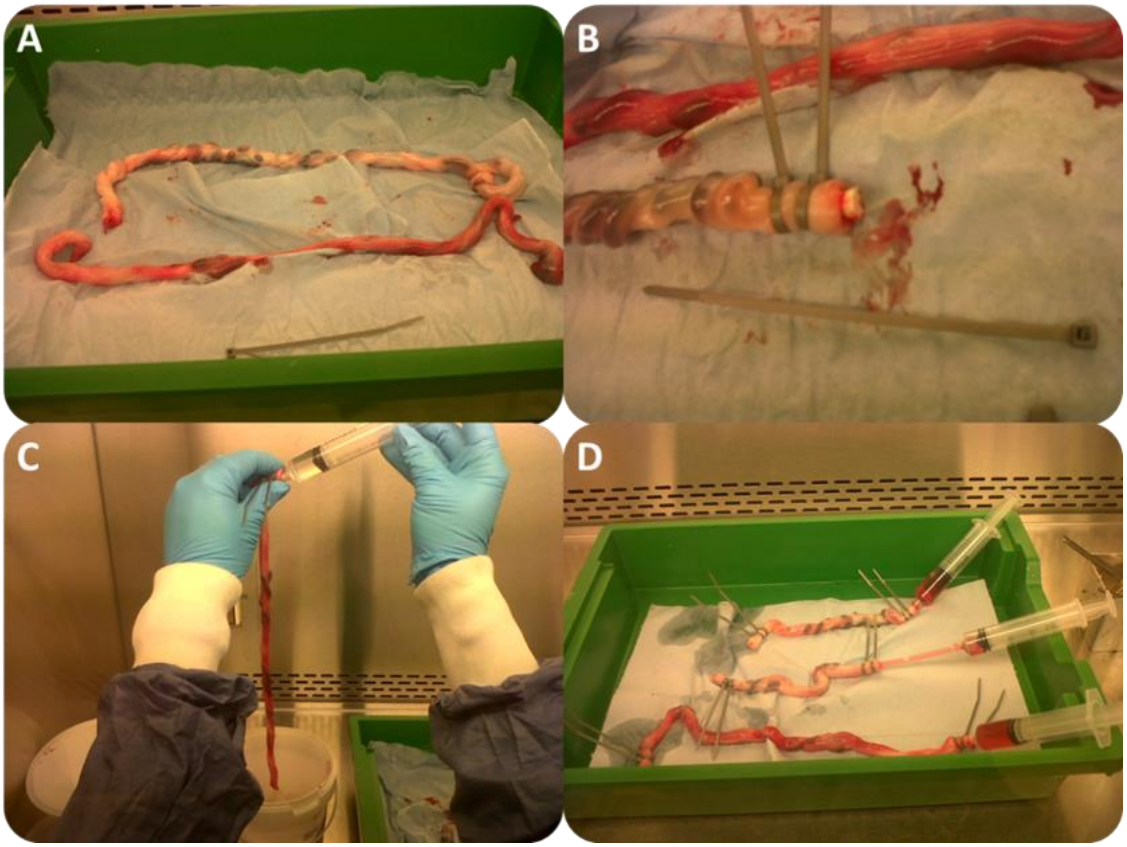

Figure 2.2. **Human Umbilical Cord (UC) endothelial cell isolation. A)** Full term UCs **B)** A cannula is inserted into umbilical cord vein and tied into place. **C)** UC is flushed with1x PBS using a 20ml syringe; one end of the UC is constricted using cable ties **D)** The UC is infused with Collagenase B solution (5mg/ml) and incubated for 1hr at room temperature.

The HUVEC pellets were re-suspended and cultured in endothelial cell culture medium (Medium 199, Lonza) (Table 2.4), supplemented with 1% P/S, 10% FCS, Endothelial Cell Growth Supplement/Heparin (ECGS/H) 0.4% (v/v) (Promocell, Germany). Endothelial cell phenotype of the HUVECs was confirmed using CD31 immunostaining. Cells were cultured at 37°C, 5% CO^2/balanced air; cell culture media was replenished every 3-4 days.

2.2.4 2D co-cultures of HUVEC with FFDSCs/HBMSCs, supplemented with and without VEGF-165 to assess ALP activity and molecular gene expression analysis

At around 90% sub-confluency the endothelial (passage 1-4) and skeletal cells were trypsinised (1x Trypsin/EDTA), washed in 1x PBS and re-suspended in a 1:1 ratio of each $5x10^4$ diaphyseal cells/HUVECs, epiphyseal cells/HUVECs and HBMSCs/HUVECs and cultured in a 6-well tissue culture plate at 37°C, 5% CO_2 for 7 days. Co-culture experiments of HUVECs/FFDSCs and HUVECs/HBMSCs were run separately. The culture medium consisted of a 1/1 mixture of endothelial culture medium (supplemented with ECGS) and α-medium, both supplemented with 10% FCS, 1% Pen/Strep (Table 2.4). Control monocultures of $5x10^4$ cells of each fetal diaphyseal, fetal epiphyseal, HBMSCs and HUVECs were plated in a 6-well tissue culture plate and grown alongside the co-cultures. Co-cultures and monocultures of FFDSC and HUVEC were supplemented with or without either 100ng/ml or 50ng/ml VEGF-165. Co-cultures and monocultures of HBMSCs and HUVECs were supplemented with or without 100ng/ml VEGF-165.

2.2.5 Preparation of pellets and co-culture pellets for organotypic cultures of E18 chick femur drill defects for micro-CT and histological analysis

Cell monolayers were harvested by trypsinisation (1x Trypsin/EDTA) and centrifuged at 189g for 4 minutes at 18°C. Cells were resuspended and for mono-cell pellets 2.5 x 10^5 cells were transferred to a 15ml conical tube; for the co-culture cell pellets 1.25x 10^5 cells of each HUVEC/HBMSCs were transferred to 15ml conical tubes. Cell suspensions were pelleted by centrifugation at 156g for 5 minutes. Pellets were incubated in the tubes, leaving the lid slightly loose to maintain oxygenation at 37°C, 5% CO_2/balanced air for 2 days.

Pellet Co-cultures Constructs			
HBMSC	**Age**	**Gender**	**P**
M71	71	M	2
F66	66	F	3
F63	63	F	3
M57	57	M	3
M69	69	M	1
F45	45	F	2

Table 2.3 **Human bone marrow samples used for cell pellet constructs.** Details of the age and culture passage number of human bone marrow stromal samples used for co-culture cell construct studies. M=male; F=female; H=human; P=Passage of culture.

2.2.7 Fluorescent cell labelling of HBMSC and HUVECs

Cell monolayers were harvested by trypsinisation (1x Trypsin/EDTA) and centrifuged at 189g for 4 minutes at 18°C. HBMSCs were incubated in 10μM CFDA (Vybrant® Cell Tracer Kit V12883) in 1ml of 1x PBS for 15min. at 37°C. HBMSCs were re-pelleted and then re-suspended in culture medium. The cell suspension was incubated for 30 minutes at 37°C, while CFDA underwent acetate hydrolysis. After incubation the cells were washed 2x prior to transfer to 15ml conical tubes. HUVECs were incubated in 5μl/ml of 10^6cells in Vybrant™ Dil cell labelling solution (V22885) for 20 minutes at 37C, centrifuged at 352g for 5 minutes and re-suspended in culture medium. Cells were washed a further 2x and a cell count was performed. 2.5x 10^5 cells each of HUVECs and HBMSC in 1ml of either ECM or alpha MEM respectively, for monoculture pellets or 1.25x 10^5 cells each HUVECs/HBMSCs in 1ml of co-culture medium (Table 2.4) for co-culture pellets were transferred to 15ml conical tubes. The cells were then pelleted by centrifugation at 156g for 5 minutes. Pellets were incubated in the tube, leaving the lid slightly loose to maintain oxygenation at 37°C, 5% CO_2 for 2 days.

2.2.8 Cell viability staining

To demonstrate cell/tissue viability 10μg/ml Cell Tracker Green™ CMFDA (5-Chloromethylfluorescein Diacetate) and 5μg/ml Ethidium Homodimer-1

(CTG/EH-1) (Life Technologies UK) was used to label viable and necrotic cells respectively. Cells were incubated in cell culture medium containing CTG/EH-1 at 37°C for 1 hour. Samples were washed twice with phosphate buffered saline (1x PBS) solution and then incubated for 1 hour at 37°C in cell culture medium. Samples were then washed twice in 1x PBS before imaging under fluorescent microscopy.

2.2.9 Isolation of E18 embryonic chick femurs, application of drill defects and organotypic culture

E18 chick embryos were culled by a schedule 1 method. The femora were dissected free of soft tissue (adherent muscles and ligament) while preserving the periosteum.

A 0.5mm metal pin was initially used to make a small insertion in the mid-shaft region of the femur. Then a 0.9mm drill bit was inserted into the defect and using the thumb and index finger twisted left and right to create the drill hole through the depth of the femur. The cell pellets (described in 2.2.4) were removed from the 15ml conical tubes using a 1ml pipette tip and placed on top of the drill hole, while visualising under a stereo microscope. Forceps were used to gently push the pellet into the drill-hole region. Femurs were transferred to culture inserts (Millicell-CM, 0.4µm pore size, 30mm diameter, Fisher Scientific 10412511) in a 6-well tissue culture plate (2 femurs/insert) with 1ml α-medium supplemented with 2µl/ml Ascorbate-2-phospate, 1% pen/strep (without the addition of FCS) (Table 2.4). Femurs were cultured at 37°C, 5% CO_2/balanced air for 10 days at the air-liquid interface. Media was replaced daily (Figure 2.3).

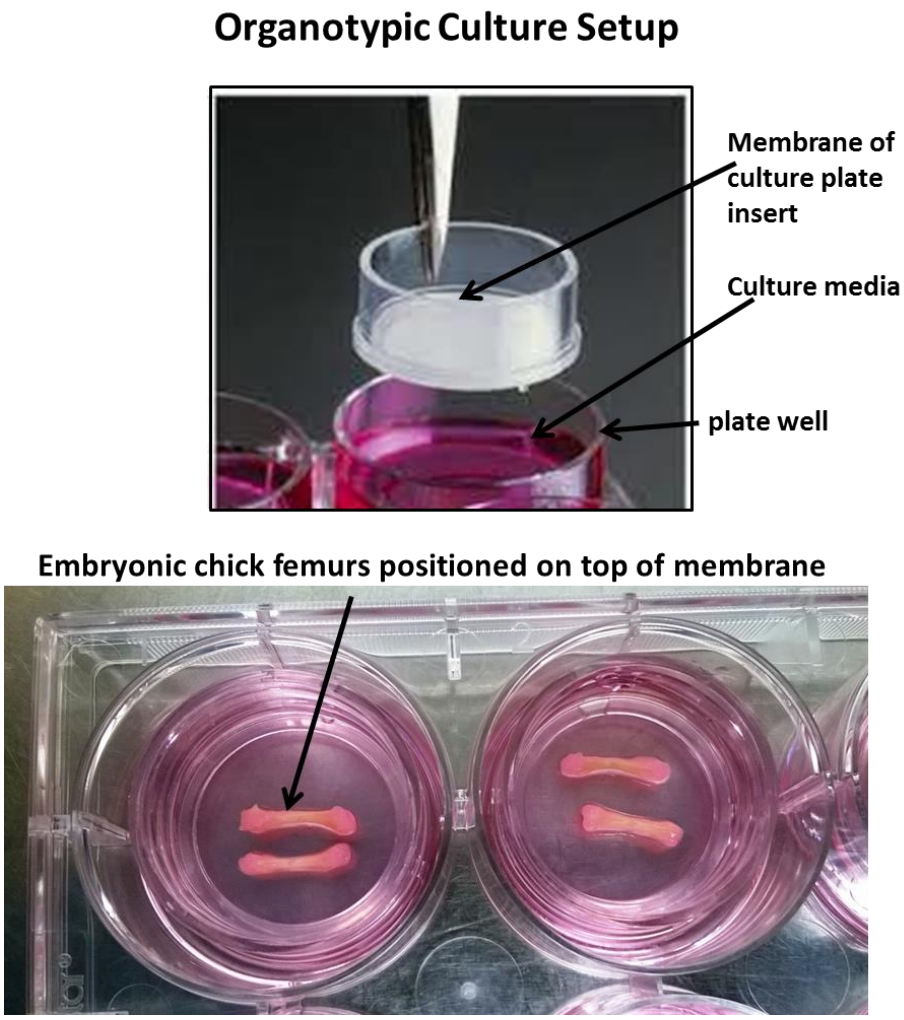

Figure 2.3. **Organotypic culture setup.** Organotypic culture insert with E18 chick femurs on top of a membrane (Polyethylene Terephthalate (PET) with a 0.4µm pore size placed in a 6 well tissue culture plate.

Name	Acronym	Media	FCS	Supplements
Alpha-MEM (minimum essential medium α-modification)	α-MEM	α-MEM	10%	1% of 10.000 UI/ml Penicillin/Streptomycin (P/S)
Endothelial cell Medium	ECM	Medium 199	10%	0.4% (v/v) ECGS/H (Endothelial cell growth Supplement/Heparin); 1% P/S
Co-culture Medium	Co-culture Medium	50% α-MEM/50% ECM	10%	As above
Organotypic Medium	OTM	α-MEM	0%	µ% (v/v) L-ascorbic acid 2-phosphate, P/S
Plain alpha-MEM	Plain TCM (tissue culture medium)	α-MEM	0%	P/S
Plain endothelial cell medium	Plain ECM (endothelial culture medium)	Medium 199	0%	ECGS/H, PS

Table 2.4. **A table of the various culture media used in the experiments**

2.3 Histological analysis

2.3.1 Tissue processing, embedding and sectioning

Unless specified otherwise tissue samples were fixed in 4% PFA-1x PBS (w/v) overnight at 4°C and then dehydrated through increasing concentrations of

ethanol 50%, 90% and 100%. Tissue samples were then taken through histoclear (National Diagnostics, Fisher Scientific, UK) prior to immersing in liquid paraffin wax (Fisher Scientific UK, 12624077, with added polymers 57°C to 58°C) at 60°C for 1hr to ensure full penetration by the wax. The samples were embedded in paraffin blocks for sectioning. Sections were cut at 7µm on a Microm330 microtome (Optec UK) and transferred to glass slides, pre-heated at 37°C for approximately 2 hours. When dried, slides were stored at 4°C, wrapped in aluminium foil.

2.3.2 Alcian blue/Sirius red staining

Prior to staining, the tissue slide sections were brought to room temperature, rehydrated through Histoclear (2x 7min.) and decreasing concentrations of ethanol solution: 2x in 100% ethanol for 2min.; 90% ethanol for 2min and in 50% ethanol for 2min; slides were subsequently immersed in water. Weigert's Haematoxylin (Fisher Scientific UK, 10181710) was applied for 10min. to stain the cell nuclei. Any excess stain was removed by immersing the slides into acid/alcohol and washing in H_2O. Slides were immersed in 0.5% Alcian blue 8GX (Fisher Scientific UK, 40046-0100) in 1% acetic acid to stain for proteoglycan expression. Slides were treated in 1% molybdophosphoric acid (Sigma-Aldrich UK, 221856) prior to staining with 1% Sirius red F3B (Direct Red 80, Sigma 365548) to visualise collagen. Any excess stain was rinsed off with H_2O and slides were dehydrated in increasing concentrations of ethanol and histoclear, before mounting with dibutyl phthalate xylene (DPX) (Fisher Scientific UK, 10050080) and imaging on Zeiss Axiovert200 digital imaging system.

2.3.3 Von Kossa staining

The tissue slides were rehydrated as described in 2.3.2. Following rehydration, slides were incubated with silver nitrate under UV light, for 20 minutes. Slides were then washed in H_2O and incubated with sodium (Na) thiosulfate for 8 minutes, washed and counterstained with Alcian blue (proteoglycans) for 1minute. Following another wash in H_2O, van Gieson stain (collagen fibres) was applied to sections for 5 minutes. After this, slides were blotted and dehydrated through decreasing ethanols starting with 90% and histoclear for

30 seconds each. Slides were then mounted with DPX and imaged on the Zeiss Axiovert200 digital imaging system.

2.3.4 Immunohistochemistry/immunocytochemistry

Reactivity of antibodies was assessed on fetal femur sections after rehydration in histoclear, decreasing ethanol concentration solutions and finally water. 3% H_2O_2 (hydrogen peroxide, Sigma-Aldrich UK, H1009) was applied to slides for 5min. to block endogenous peroxidase in the tissue section. After washing in water, slides were incubated in citrate buffer (0.003g/ml sodium citrate, pH 6.0) for 20min. at 70°C to retrieve the antigens from the tissue, where appropriate. Slides were washed in 1x PBS and water before blocking with 1% BSA in 1x PBS. The primary antibody (Table 2.1) against specified antigens was applied at an appropriate dilution in 1% BSA-PBS and incubated overnight at 4°C. The primary antibody was washed off in water for 1-2min., slides were then washed in 0.5% TWEEN-1xPBS for 10-15min. before incubating the slides with the appropriate corresponding biotinylated secondary antibody against the primary antibody for 1hr at room temperature. Extravidin Peroxidase (1:50) was applied to the slides for 30min to form an avidin-biotin complex. The slides were washed in tap water and 0.5% TWEEN-1x PBS and the antibody complex/colour was developed by incubation with 3-amino-9-ethylcarbazole (AEC) in acetate buffer with 0.015% hydrogen peroxide. The sections were then covered with Hydromount (Fisher Scientific UK, 12964910) dried and images were taken of the slide sections using a Zeiss Axiovert 200 digital imaging system.

2.3.5 Immunofluorescent staining

Samples were prepared as described in 2.3.4. Following the primary Antibody incubation step overnight, the appropriate secondary Alexa Fluor 488-conjugated antibody was diluted 1/100 with 1% BSA in 1x PBS (Table 2.1). Sections were covered and incubated for 1 hour at room temperature. Slides were washed in water and subsequently with 0.5% TWEEN-1x PBS for 10-15min. In order to visualise cell nuclei DAPI nuclear stain was diluted 1/100 with 1x PBS and applied to the slide sections for 5 minutes. Slides were washed

in water for approximately 1-2min. to remove any excess stain and mounted with Fluoromount™ (Sigma F4680).

2.3.6 Alkaline phosphatase staining

At day 7, mono- and co-cultured cells in 6-well tissue culture plates (Corning UK) were washed in 1x PBS and then fixed in 90% ethanol with further washes in 1x PBS. Alkaline phosphatase activity was measured by the addition of 600µl of 4% (v/v) Naphthol AS-MX phosphate (Sigma) and 0.0024% (w/v) Fast Violet B-salt (Sigma) mixed in distilled water. Cells were incubated in the dark at 37°C for 40min. The staining solution was neutralised with distilled water. An increase in red colour of the fixed cells was an indication of alkaline phosphatase activity.

2.4 Image capture

Slide and tissue samples were captured and processed using a Zeiss Axiovert 200 inverted microscope, Axiovision software - version 4.7. (Carl Zeiss Ltd., Cambridge, UK). Other images were captured using a Canon Powershot G2 digital camera. Confocal images were kindly captured by Dr. David Johnston in the Biomedical imaging unit, Southampton General Hospital, using a confocal laser scanning platform Leica TCS SP8.

2.5 Biochemical analysis

2.5.1 Alkaline phosphatase activity

After 7 days of culture, cells were washed 3 times in 1x PBS and fixed in 90% ethanol. 600µl Triton-X detergent (0.05%) was added to each well of a 6-well cell culture plate. The cells were lysed by freeze-thawing 3 times at -20°C. Alkaline phosphatase activity was measured using a colorimetric assay measuring absorbance at 410nm on a Biotech UK, ELx800 spectrophotometer. P-nitrophenol phosphate (pNPP) (Sigma-Aldrich UK, N7660) turnover was measured against standards. Absorbance indicates de-phosphorylation of pNPP. 10µl of cell lysate was transferred to a 96-well clear assay plate and made up to 100µl with 90µl substrate, consisting of phosphatase substrate

(Sigma UK, P4744) in 1.5M alkaline buffer solution (Sigma UK, A9226). Cell lysate was incubated at 37°C for up to 40min and the reaction was terminated with 100µl of 1M sodium hydroxide solution prior to reading on the spectrophotometer. Results were expressed as nmol pNPP/ml hr^{-1}.

2.6 Molecular analysis

2.6.1 RNA isolation

RNA isolation was performed according to the manufacturer's instructions using Qiagen RNeasy Plus Mini Kit (Qiagen UK, 74134) (Figure 2.4). Cultured cells were washed twice in 1x PBS and then lysed using RLT buffer (component of Qiagen kit). The sample was snap-frozen and stored in 1.5ml RNase-free Eppendorf tubes at -80°C. Prior to isolation, tubes containing RNA were thawed at room temperature. The lysate was transferred to a gDNA spin column and centrifuged for 15 seconds at 8000g to remove any genomic DNA (gDNA). The spin column was discarded and one volume of 70% Ethanol was added to the flow-through and mixed to precipitate the RNA. The lysate was transferred to an RNeasy spin column and centrifuged to separate the RNA. The spin column was washed two times and dried. RNA was eluted from the spin column with RNase-free H_2O. RNA concentration of 1µl of sample was determined using the Nanodrop 2000 spectrophotometer.

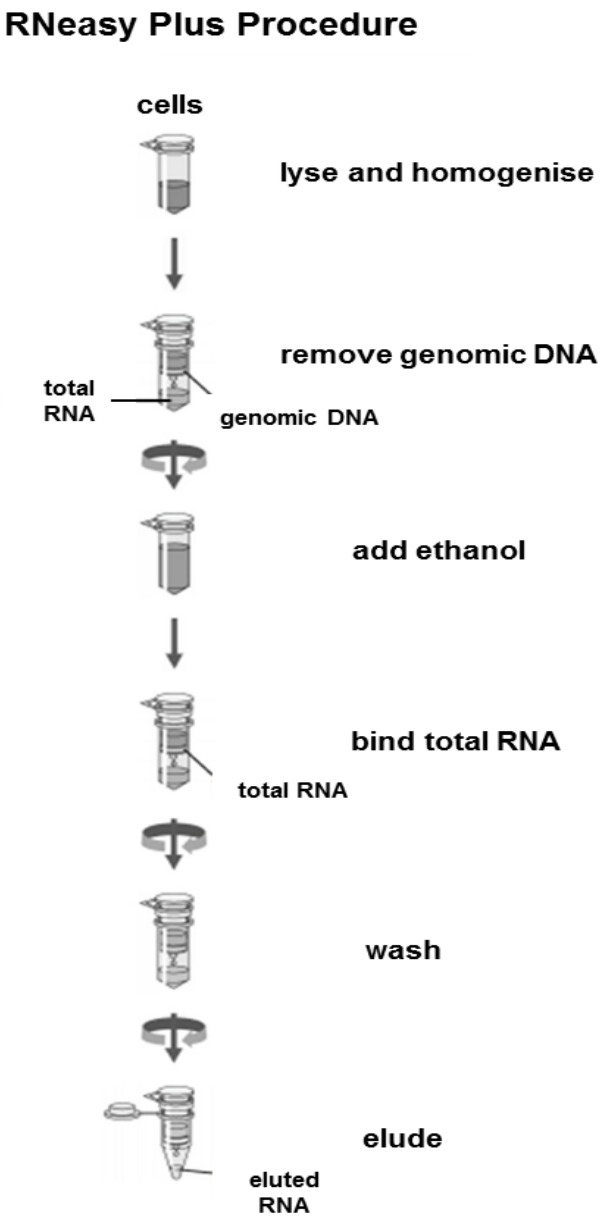

Figure 2.4. **Schematic process of RNA isolation.** The various steps in using the RNeasy Plus Mini Kit to isolate RNA (source: Qiagen UK, 74134, RNeasy Plus Mini Handbook 12/2014).

2.6.2 cDNA synthesis

SuperScript® VILO™ (Life Technologies UK, 11754050) cDNA Synthesis Kit was used for cDNA synthesis according to the manufacturers protocol. 5x VILO™ reaction mix and 10 x SuperScript© enzyme were added to the appropriate amount of RNA and incubated at 25°C for 10 minutes in a 0.2ml PCR reaction tube, followed by 2 hours at 42°C. The reaction was terminated at 85°C for

5minutes. The cDNA sample was diluted 1:2 with RNase free H_2O and stored at -20°C or used immediately for quantitative RT-PCR analysis.

2.6.3 Quantitative polymerase chain reaction (qPCR)

Quantitative PCR was performed using Power SYBR-Green PCR master mix (Life Technologies UK, 4368708). The 25µl reaction was made up with 1µl of cDNA sample, 12.5 µl of SYBR-Green master mix, 6.5 µl RNase free H_2O and 2.5µl each of reverse and forward primers for the gene of interest (Table 2.5). The final reaction mix was transferred to a 96-well plate, centrifuged briefly and analysed using Applied Biosystems 7500 Real Time PCR system (LifeTechnologies). The resulting data was analysed using AB7500 SDS Software, version 2.0.5 program. Ct values for each sample were normalised to the housekeeping gene β-Actin. Fold-expression levels of each target gene were calculated using the ΔΔ Ct (cycle threshold) method. The basal epiphyseal mono-cell culture group was used as an internal relative reference. In order to overcome sample variability between patients samples, repeat data of relative expression of 3 individual patients were analysed (in triplicates or quadruplicates as stated) for all genes investigated.

Gene	Abbreviations	Forward Primer	Reverse Primer
HOUSEKEEPING GENE			
Human β-Actin	Actin	ggcatcctcaccctgaagta	aggtgtggtgccagattttc
OSTEOGENIC GENES			
Human Alkaline Phosphatase	ALP	ggaactcctgacccttgacc	tcctgttcagctcgtactgc
Human Type I Collagen (COL1A1)	COL-1	gagtgctgtcccgtctgc	tttcttggtcggtgggtg
ANGIOGENESIS-RELATED GENES			
Human von Willebrand Factor	VWF	cccctgaagcccctcctccta	acgaacgccacatccagaacc
Human VEGF-A (165)	VEGF	tatgcggatcaaacctcacca	cacagggatttttcttgtcttgct
Human FLT-1 (VEGF-R1)	FLT-1	aaaggcacccagcacatcat	ttccccccctgcattgga
Human KDR (VEGF-R2)	KDR	attcctcccccgcatca	gctcgttggcgcactctt

Table 2.5 **List of human primers used in qPCR.** A list of the primer sequences of osteogenic and angiogenic genes; with housekeeping gene β-Actin. VEGF-165 primer sequence (Grellier *et al.*, 2009); all other primers were designed in house by members of the Bone and Joint Research Group.

2.7 Micro-computed tomography

Quantitative 3D bone structural analysis of the chick femurs was performed using a SkyScan 1176 scanning system (Bruker μCT, Kontich, Belgium). The X-ray source was set to the following parameters: no filter, voltage 50kV, current 500μA, 35μm pixel size and 496ms exposure time. Samples were scanned at time intervals D0 and D10 at 35μm resolution to preserve maximum cell viability. At D0 prior and post to the organotypic culture, samples were transferred under sterile conditions to 0.5ml Eppendorf tubes and numbered. Post-scanning, femur samples were transferred under sterile conditions to 6

well culture plates containing 0.4μm filter well inserts. The sequence of the femurs was maintained in order of the initial scan. At D10, sample femurs were again transferred to Eppendorf tubes preserving the same order as at D0 scans. Post-scan raw data was reconstructed using NRecon software interface (v.1.6.10.4, Bruker μCT) with corrections for misalignment, ring artefacts and beam hardening (30%), an artefact created by low energy x-ray beam attenuation. Reconstructed image data was analysed using CT Analyser (CTAn v.1.16.4.1+, Bruker μCT). In order to analyse the same area of interest for each femur at D0 and D10, a dataset comprising the same volume of interest was selected over the same area. Images were binarised within a grey scale threshold to determine bone against background and bone volume (BV), bone volume / tissue volume ratio (BV/TV) was determined for each femur pre- and post-culture. The change in bone volume was derived relative to the initial micro CT scan.

2.8 Statistical analysis

Data from at least three replicates of at least 3 experiments was analysed using one-way analysis of variance (ANOVA) with either Sidak's or Dunnett's multiple comparison posthoc test on GraphPad Prism 6 software version 6.07. *P* values ≤0.05 were considered significant. Graphical representation of significance: *p≤0.05, **p≤0.01, ***p≤0.001. All data presented as mean ± standard deviation (SD). Specific statistical analyses are stated in individual chapter methods.

CHAPTER 3

Examination of cell phenotype modulation following co-cultures of human endothelial with human skeletal cells.

Part of the work undertaken in this chapter was published in Stem Cell Research and Therapy in 2016 (Inglis *et al.*, 2016).

(Inglis S, Christensen D, Wilson DI, Kanczler JM, Oreffo ROC. Human endothelial and fetal femur-derived stem cell co-cultures modulate osteogenesis and angiogenesis. Stem Cell Res Ther. 2016 Jan 18;7:13. doi: 10.1186/s13287-015-0270-3).

3.1 Introduction

Long bone formation during development and repair occurs by the process of endochondral bone formation (reviewed in 1.3). This is a highly orchestrated and coordinated process involving mechanical, biochemical, molecular and cellular factors (Colnot, 2005). The developing femur arises from a cartilaginous anlage, which matures and is remodelled with the sequential influx of an evolving vasculature, giving rise to bone (Colnot, 2005). As the femur grows and differentiates, the appearance of blood vessels marks an important stage in development, driving differentiation of various cell types. There is substantial evidence for an interplay between the cells involved in bone formation and the development of a functional vasculature and cells responsible for the maintenance of skeletal homeostasis (Chen *et al.*, 2012).

The vasculature provides a supply of oxygen, nutrients, cells as well as serving as a conduit for the removal of waste (Brandi and Collin-Osdoby, 2006). Various studies have demonstrated that a close interaction between Human Umbilical Vein Endothelial Cells (HUVECs) in co-culture with human bone marrow stromal cells (HBMSCs) results in an enhancement of osteogenic markers upon direct contact (Xue *et al.*, 2009; Zhang *et al.*, 2010). Up-regulation of osteogenic markers such as ALP (Villars *et al.*, 2000; Guillotin *et al.*, 2008) and COL-1 have been well documented (Villars *et al.*, 2002; Leszczynska *et al.*, 2013). Recent studies by Leszcynska and colleagues demonstrated that direct co-cultures of HBMSCs and HUVECs at distinct ratios (50:50, 80:20 and 20:80) significantly enhanced ALP activity, *ALP* and *COL-1* gene expression and cell proliferation over a 7 day culture period (Leszczynska *et al.*, 2013). Moreover, Zhang *et al.* reported that HUVECs in contact co-culture with the osteosarcoma osteoblast-like cell line MG-63, initially stimulated the proliferation of MG-63 cells. A significant increase in COL-1 and ALP expression was reported, although a decrease in osteocalcin, a late marker of osteogenesis, close to the mineralisation-stage, was also observed (Zhang *et al.*, 2010). Furthermore, Villars and colleagues demonstrated that the addition of VEGF to contact co-cultures had no significant effect but showed a negative effect on ALP activity in HBMSCs compared to HBMSC monocultures.

(Villars *et al.*, 2000). Kaigler *et al., 2005,* showed that EC-mediated BMP-2 signalling enhanced HBMSC's osteogenic differentiation in co-culture *in vitro*, with a significant increase in ALP activity reported. Transplantation of co-cultured cells on to polymer scaffolds increased bone formation *in vivo*, however there was no significant angiogenic response compared to monoculture controls (Kaigler *et al.*, 2005).

VEGF-A (Vascular endothelial growth factor A) is a key modulator of endothelial cells (see chapter 1.4.1 & Table 1.1). VEGF and the various isoforms of VEGF are involved in regulating blood vessel growth and permeability as well as endothelial cell proliferation, maturation and survival (Ferrara *et al.*, 2003). VEGF activity is modulated mainly through VEGF receptors 1 (*FLT-1*) and 2 (*KDR*) (Ferrara *et al.*, 2003). VEGF and its receptors have been linked with the onset of bone development and with a role in fracture repair (Reumann *et al.*, 2010). In a mouse rib fracture model, Reumann and colleagues demonstrated that VEGF receptor activity was increased during endochondral bone repair. Interestingly, during the inflammatory response both receptors and VEGF were detected. Indeed, VEGF receptor 1 maintained similar mRNA levels throughout the bone healing process, whereas VEGF receptor 2 showed significant mRNA level increases during callus formation and maturation (Reumann *et al.*, 2010).

To determine new approaches in the augmentation and induction of a vascular supply into fracture healing sites to enhance bone regeneration, the current study has examined the effects of the three key cell types present during development: endothelial cells (ECs), human fetal diaphyseal (D) and epiphyseal cells (E). To elucidate and understand the cell interactions involved in modulating osteogenesis and angiogenesis, human umbilical vein endothelial cells (HUVECs) with human fetal diaphyseal (CoD) and epiphyseal cells (CoE) were co-cultured with and without supplementation of VEGF-165 (described synonymously as VEGF herein). This entailed assessment of the ability of endothelial cells (HUVEC) and human fetal femur derived stromal cells (FFDSC) in contact co-culture to modulate osteogenesis and angiogenesis. Additionally for comparison, adult HBMSCs from human femoral marrow samples were co-cultured with HUVECs to determine if any similar regulatory mechanisms of osteo-and angiogenic markers that were found in the fetal co-culture investigations.

3.2 Hypothesis

Vascular and skeletal progenitor cells cooperatively enhance markers of bone formation when maintained and combined in contact-culture.

3.2.1 Aims and Objectives

1. To investigate the potential osteogenic differentiation and activity of fetal femur-derived stem cells (FFDSCs) or adult human bone marrow stromal cells (HBMSCs) in 2D co-cultures with human umbilical vein endothelial cells (HUVECs). This will involve the characterisation of vascular and osteogenic gene expression as well as the examination of alkaline phosphatase, an early bone functional marker.

2. To investigate the effect of vascular endothelial growth factor (VEGF) on osteogenesis, at different concentrations, in 2D co-cultures of FFDSCs or HBMSCs with HUVECs. This will involve the investigation into variations in osteogenic and angiogenic gene expression in response to different concentrations of VEGF on fetal and adult human bone stromal cells in co-culture with endothelial cells.

3.3 Methods

3.3.1 2D co-culture of fetal and adult skeletal and endothelial cells

HUVECs were isolated as described in chapter 2.2.3 from full-term UCs as shown in (Figure 2.2). Fetal femur cells (Table 2.2) were obtained as described in chapter 2.2.2. Cells were culture expanded to passage 2/3 then washed with 1x PBS and incubated in 1x Trypsin/EDTA solution to acquire a cell suspension.

Co-cultures of HUVEC/diaphyseal FFC and HUVEC/epiphyseal FFC and HBMSC/HUVEC and monoculture controls were established as described in chapter 2.2.4. Cells were cultured in a 6-well tissue culture plate +/- 100ng/ml VEGF-165 (Peprotech, UK) at 37°C, 5% CO_2 balanced air for 7 days in a 1:1 ratio of endothelial culture medium (supplemented with ECGS) and alpha-MEM-, both supplemented with 10% FCS, 1% Pen/Strep (Table 2.4). Basal or VEGF supplemented culture media was renewed at day 3/4 during the 7 day culture period. The same ratio of culture media was used for all mono-/co-cultures.

3.3.2 Quantitative polymerase chain reaction

Analysis of relative gene expression was performed as detailed in chapter 2.6, with the basal epiphyseal mono-cell culture group as an internal relative reference.

3.3.3 Statistical analysis

Data derived from at least 3 replicates per experiment (3 experiments run) was analysed using one-way analysis of variance (ANOVA) with Sidak's multiple comparison posthoc test on GraphPad Prism 6 software version 6.07. Data presented as mean ± SD and *P* values ≤0.05 were considered significant.

3.4 Results

3.4.1 Cell Characterisation

To visualise cell phenotypic characteristics, HUVECs and FFDSCs were cultured in 6-well TC plates for 7 days. Figure 3.1 shows a representative image of endothelial and skeletal cells at day 1 of culture. HUVECs displayed a heterogeneous morphology and FFDSCs displayed a fibroblast-like phenotype. Diaphyseal cells displayed a honeycomb-like structure at day 1 and an enhanced confluency in comparison to epiphyseal cells.

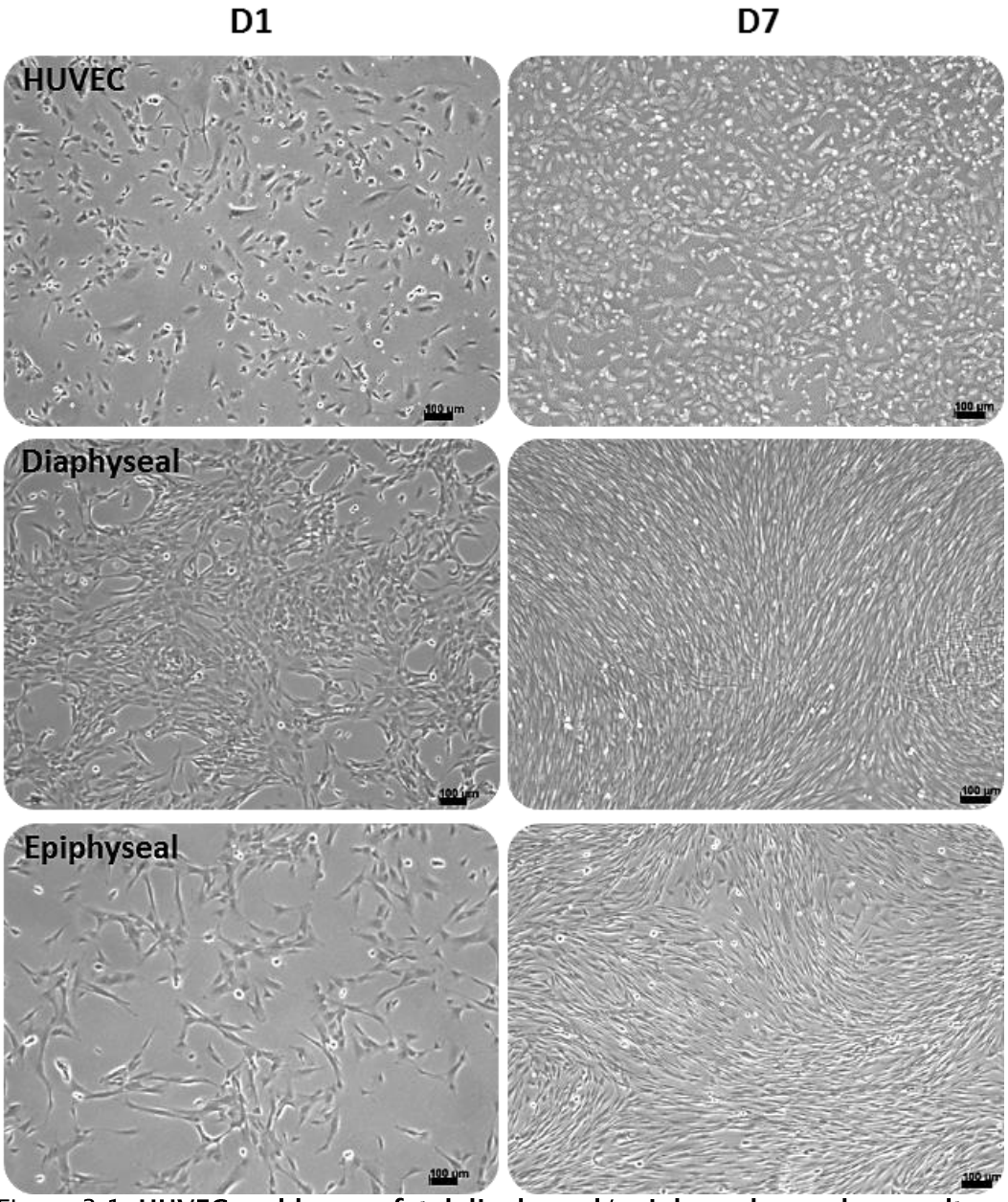

Figure 3.1. **HUVEC and human fetal diaphyseal/epiphyseal monolayer cultures.** Phase contrast images of cells cultured in basal media at day 1 and day 7 time points. HUVECs (passage 2), fetal femur diaphyseal and epiphyseal cells. Scale bar: 100μm.

HBMSCs are a heterogeneous population of adult skeletal cells derived from the bone marrow aspirates of patients undergoing hip replacement or hip revision surgery (Figure 3.2). As visible in the phase contrast image, the cells displayed a typical fibroblastic morphology comparable to that of fetal skeletal cells at similar time-points of culture. The adult cells appeared more elongated with extended filopodia in migrating cells and reduced confluency at D7 in comparison to fetal skeletal cells.

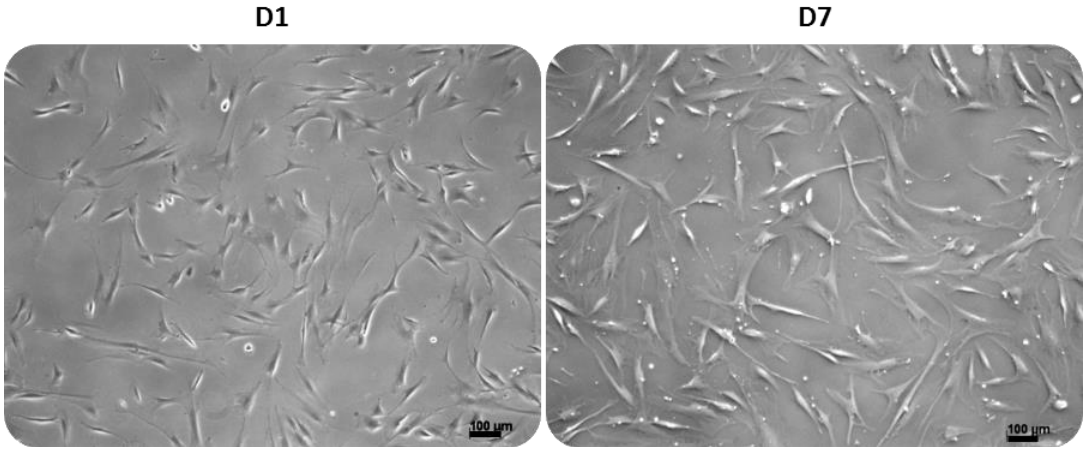

Figure 3.2. **Human bone marrow stromal cells in culture over 7 days.** Phase contrast image of human bone marrow stromal cells (HBMSCs) at D1 and D7 of basal culture. Female patient, 87 years old. Cells at passage 2 of culture. Scale bar: 100µm.

Protein expression was assessed using immunocytochemistry (ICC) (2.3.4) for markers characteristic for endothelial and skeletal cells to confirm cell phenotype (Figure 3.3 & Figure 3.4 and Figure 3.5). Immunohistochemistry (IHC) against a number of antigens and Alcian blue/Sirius red staining for the presence of collagen and proteoglycans was performed on whole fetal femurs of consecutive age/size in order to demonstrate the temporal expression of developmental angiogenic and osteogenic markers in human fetal femurs (Figure 3.6 & Figure 3.7).

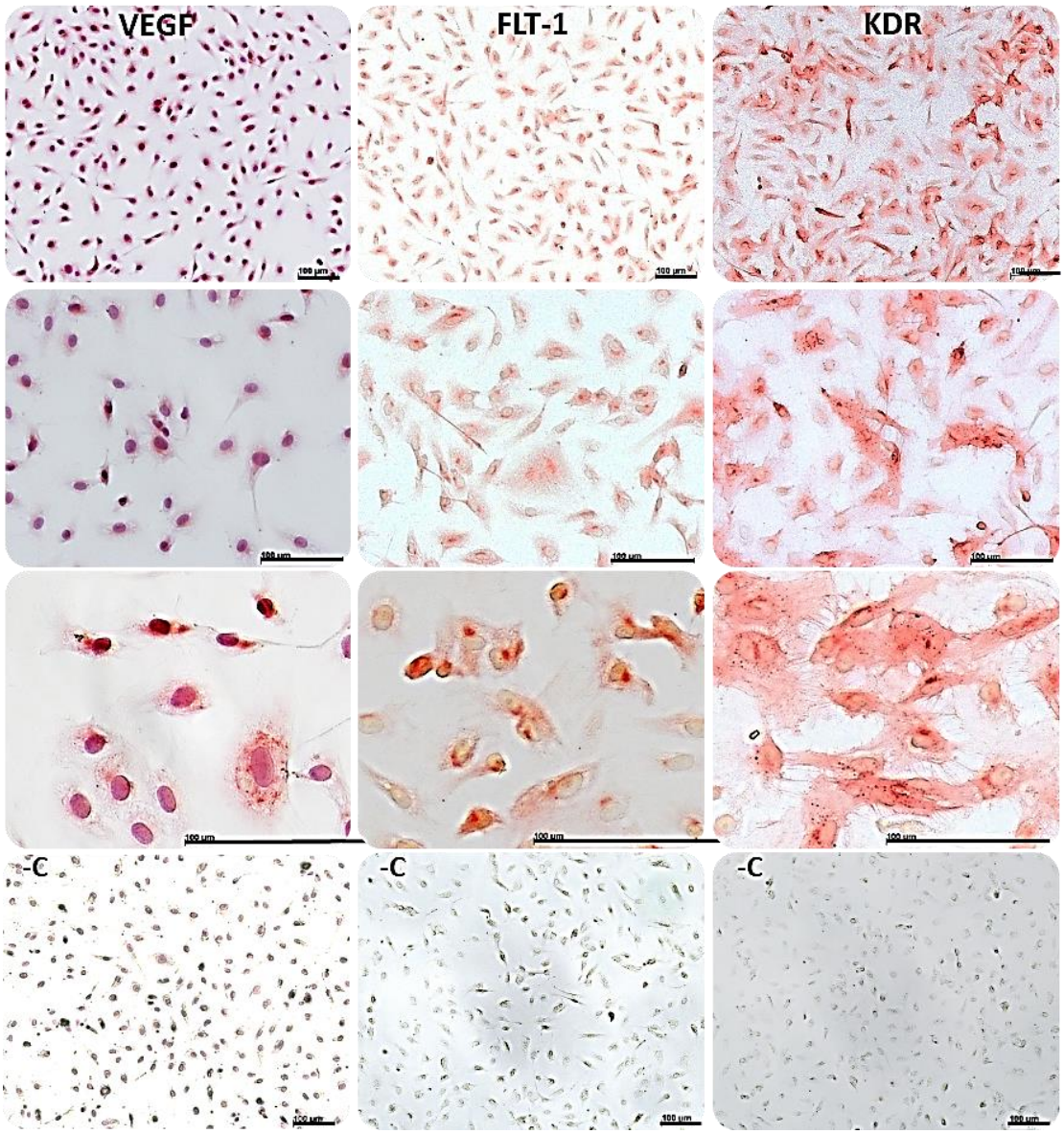

Figure 3.3. **Immunocytochemistry of HUVEC markers.** HUVEC (passage 4) protein expression of VEGF-165, VEGF-receptors FLT-1 (R1) and KDR (R2) antigen after day 7 in culture. Negative controls (-C) in the absence of respective primary antibodies. Scale bar: 100µm.

HUVECs strongly expressed VEGF and VEGF-receptors FLT-1 (R1) and KDR (R2) as shown in Figure 3.3. In addition, endothelial cells were observed to express the markers von Willebrand Factor (vWF), a large multi-meric adhesive glycoprotein involved in blood homeostasis and PECAM-1 (CD31), a cell surface adhesion molecule abundant on endothelial cells at the intercellular junctions (Figure 3.4).

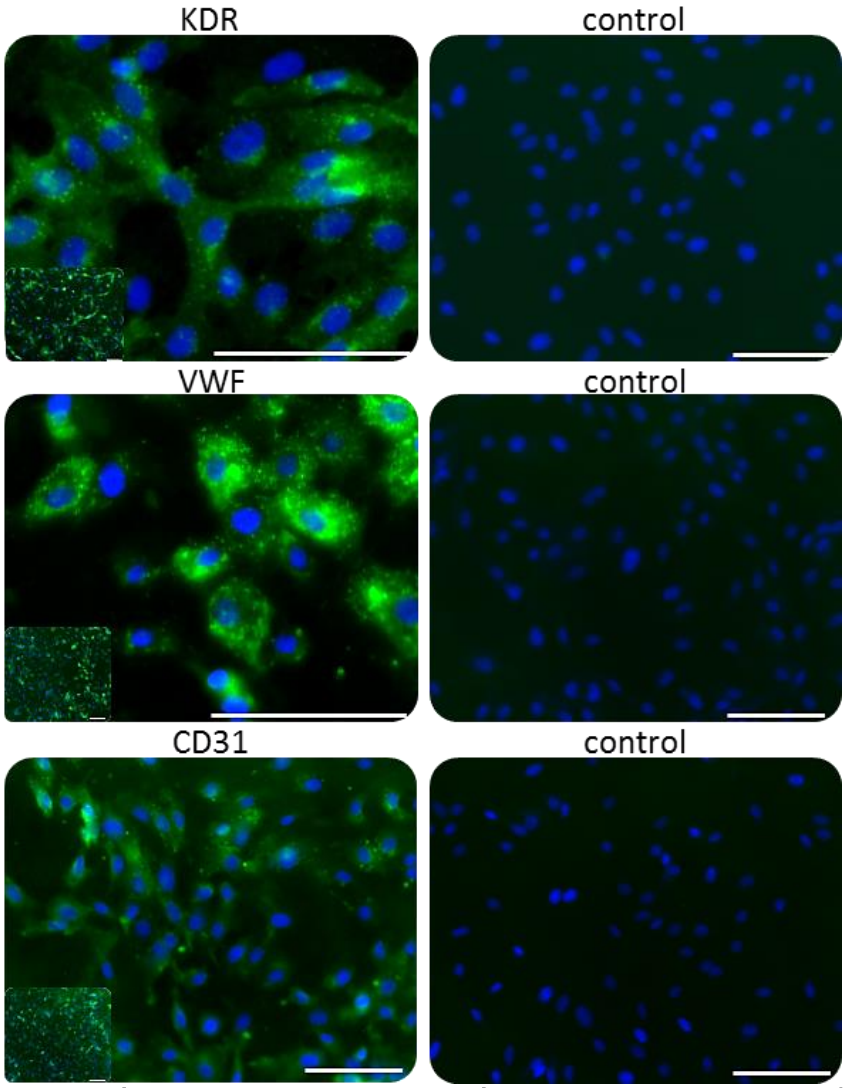

Figure 3.4. **Immunofluorescent examination of HUVEC markers.** Immunofluorescent staining for protein expression on HUVECs for KDR (VEGFR-2), vWF and CD31 at D7 in culture; negative controls with: primary antibodies omitted. Secondary Ab Alexa 488 and DAPI (blue) nucleic counterstain stain were employed. Inset pictures at lower magnification to demonstrate level of expression. Scale bar: 100μm.

Immunocytochemistry of fetal diaphyseal and epiphyseal cells revealed intense expression of OSX (Osterix), Ang-2 and TIE-2 protein in diaphyseal cells (Figure 3.5). Interestingly, the epiphyseal cells showed enhanced expression for VEGF antigen compared to diaphyseal cells. Angiopoietins and receptor TIE-2, together with OSX were expressed by epiphyseal cells but appeared less prominent compared to diaphyseal cell populations; however, this may have been a consequence of reduced confluency of epiphyseal cells in culture.

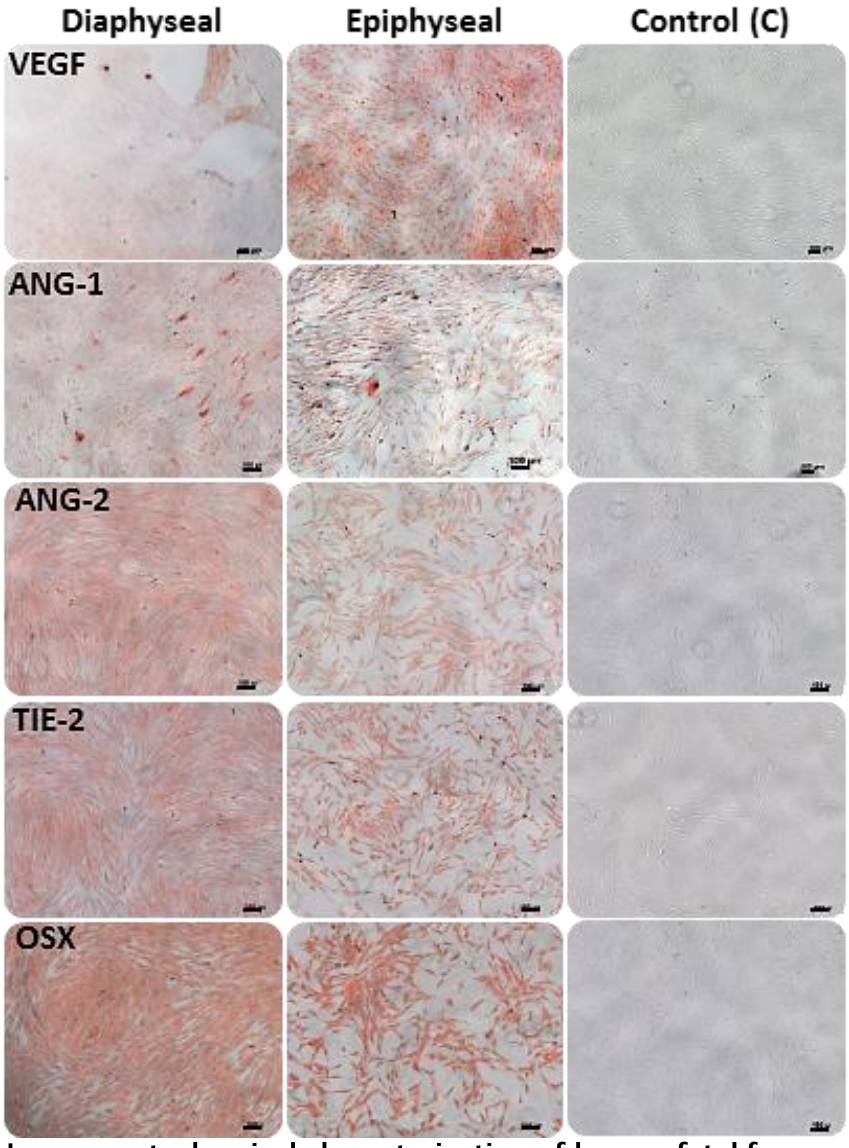

Figure 3.5. **Immunocytochemical characterisation of human fetal femur cells.** Fetal explant cells at passage1/day7 of cell culture. Diaphyseal and epiphyseal cells, stemming from the outgrowth of dissected diaphyseal and epiphyseal regions of the fetal femur respectively. **A.** VEGF Vascular endothelial growth factor. **B.** ANG-1 Angiopoietin 1. **C.** ANG-2 Angiopoietin 2. **D.** TIE-2. **E.** OSX Osterix. Controls (C) omitting primary antibody. Scale bar: 100μm.

3.4.1.1 Immunohistochemistry and A/S staining

To assess osteo- and angiogenic protein expression in the developing human fetal femur, we performed immunohistochemistry (2.3.4) on whole fetal femurs at consecutive sizes/ages post-conception: range 4mm to 8.5mm or 53 days to 70 days post-conception (dpc), respectively (Figure 3.6 and Figure 3.7).

Initially, Alcian blue/Sirius red staining (A/S) (2.3.2) revealed a clear demarcation between the early cartilaginous femur and the surrounding tissue

(Figure 3.6A). Robust staining of proteoglycans (blue) was visible within the cartilage regions and intense collagen (red) staining in the tissue surrounding the femur. From ~55dpc, a distinct band of collagen was visible surrounding the femur along the dense irregular connective tissue known as the perichondrium. Expression of STRO-1 (used in the enrichment of SSCs) was observed throughout the tissue and surrounding the early femurs (53dpc) (A). STRO-1 was more distinctly expressed within the diaphysis at 55dpc and the epiphysis of femurs at 59dpc. At 70dpc, STRO-1 was further evident along the diaphyseal periosteum of the femur (A).

Classical markers for endothelial cells, CD31 (PECAM-1) and vWF (von Willebrand Factor) (Figure 3.6A) were examined in the fetal femur samples. CD31 (PECAM-1) was found to be expressed at 55dpc predominantly within the surrounding tissue of the femur forming clusters of CD31 positive cells and more sparingly within the perichondrium of the epiphyseal region. CD31 expression was localised along the periosteum in the later staged femurs. In contrast, vWF could be distinctly detected in the outer regions of the femur throughout the developmental stages up to 70dpc, where vWF expression was associated in the periosteum and perichondrium (A).

VEGF was weakly expressed within the surrounding tissue of the early staged femurs and emerged in the epiphyseal region of the later staged femur from 59dpc (Figure 3.71B). By day 70 post conception, VEGF expression was observed within the periosteal region. Ang-1 was present in the tissue surrounding the femur at 53dpc (B) and discreetly expressed throughout the ages of the femurs examined, although increasingly localised at the interface of the cartilage and perichondrium. Conversely, Tie-2 (an angiopoietin 1 receptor) was weakly expressed in the surrounding tissue of the early femur and distinctly expressed from 59dpc and 70dpc in the epiphyseal chondrocytes and the perichondrium region (B). Moreover, the angiogenic marker Angiopoietin 2 (Ang-2) a factor regulating endothelial vascular remodelling, was distinctly present in the tissue adjacent to the early femur from ~53dpc, subsequently Ang-2 was more defined in the epiphyseal cartilage and the perichondrium at 59dpc but expression was diminished by 70dpc (8.5mm) (B).

Overall, antigens for early osteogenic and angiogenic markers tested, were shown to be distinctly expressed at 59dpc, either along the diaphyseal perichondrium, or, along the epiphyseal chondrocytes, indicating a heterogeneous expression pattern of the developing fetal femur, containing cells transitioning from chondrogenic to osteogenic phenotype in preparing for vascular invasion (summarised in Table 3.1.

During development of the human femur, formation of the periosteum by intramembranous ossification occurs at around 56dpc (Nowlan *et al*., 2007). This was reflected by the staining pattern of proteins displayed within the fetal femur of sequential ages confirming a culmination of expression of the angiogenic and osteogenic markers at 59dpc as well as collagen staining prominent in the periosteal regions of the femur.

Prior to 59dpc hypertrophy of the mid diaphyseal chondrocytes occurs, followed by capillary invasion through the perichondrium (Nowlan *et al*., 2007). This could explain the expression patterns of the angiogenic factors observed such as angiopoietins and angiopoietin receptors as well as CD31 and vWF. The presence of angiogenic factors was initially stronger in the tissue surrounding the femurs and subsequently became more prominent within the outer femoral regions. Presence of these proteins during the developmental stages observed, contribute to the differentiation of the femur lining cells towards the osteoblastic phenotype as well as the impending vascular invasion. Endochondral ossification and formation of the marrow cavity commences at around 77dpc (Nowlan *et al*., 2007), in line with VEGF staining observed at 70dpc along the periosteum of the femur, presence of KDR positive staining, as well as clusters of CD31 and vWF positive staining along the diaphysis and epiphysis respectively. It must be noted that variation between timing of developmental patters described in the literature and those observed in the current study may occur as a result of sample variation and subjectivity in the initial staging of the femurs

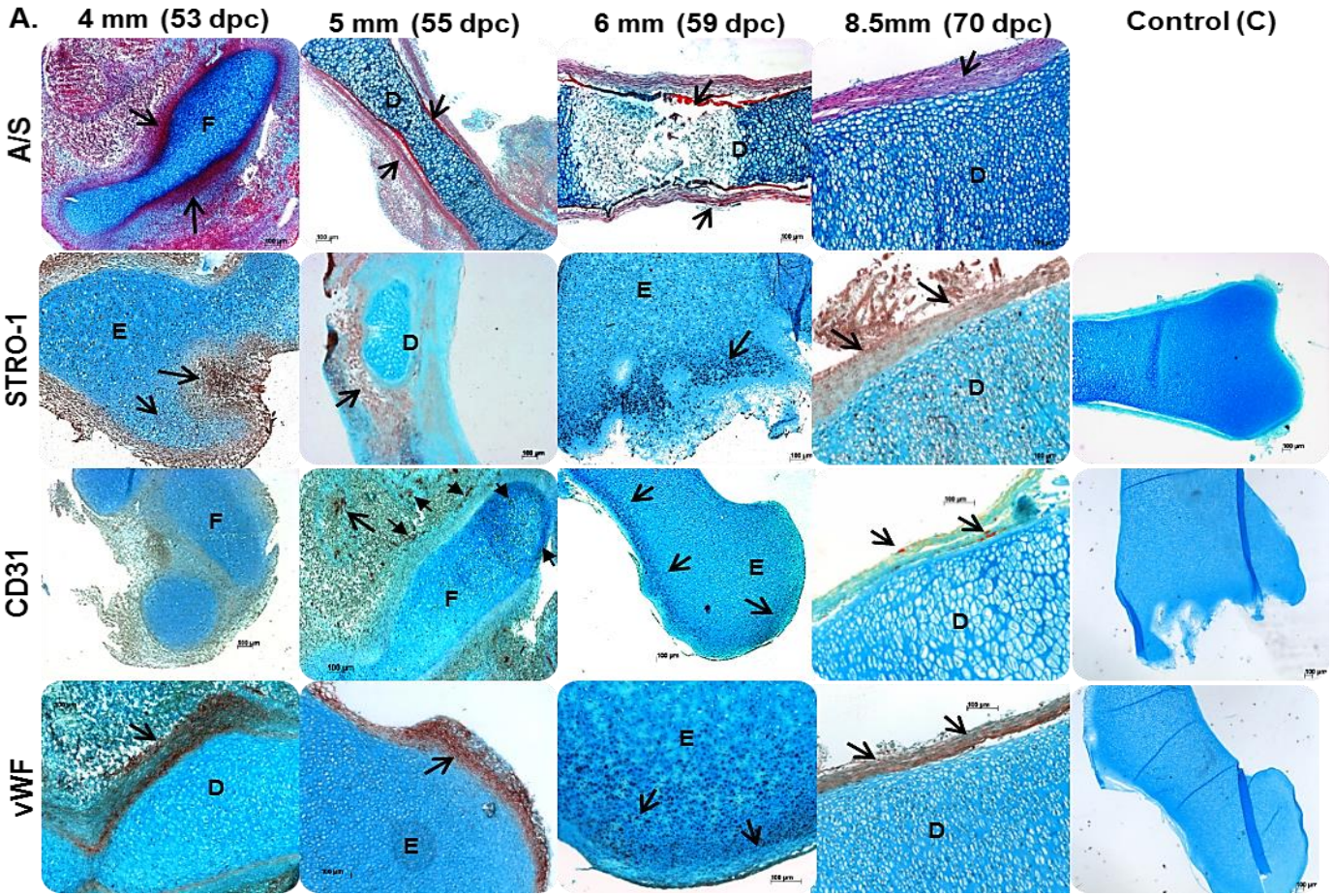

Figure 3.6. **A. Overview of the developmental staging of human fetal femurs** aged 53–70 days-post-conception (dpc) (4mm–8.5mm). Antibody markers: PECAM-1 (CD31), von Willebrand Factor. Negative controls (C), absence of primary antibody. D=Diaphysis, E=Epiphysis, F=femur. Arrows depict positive staining. Scale bar: 100μm

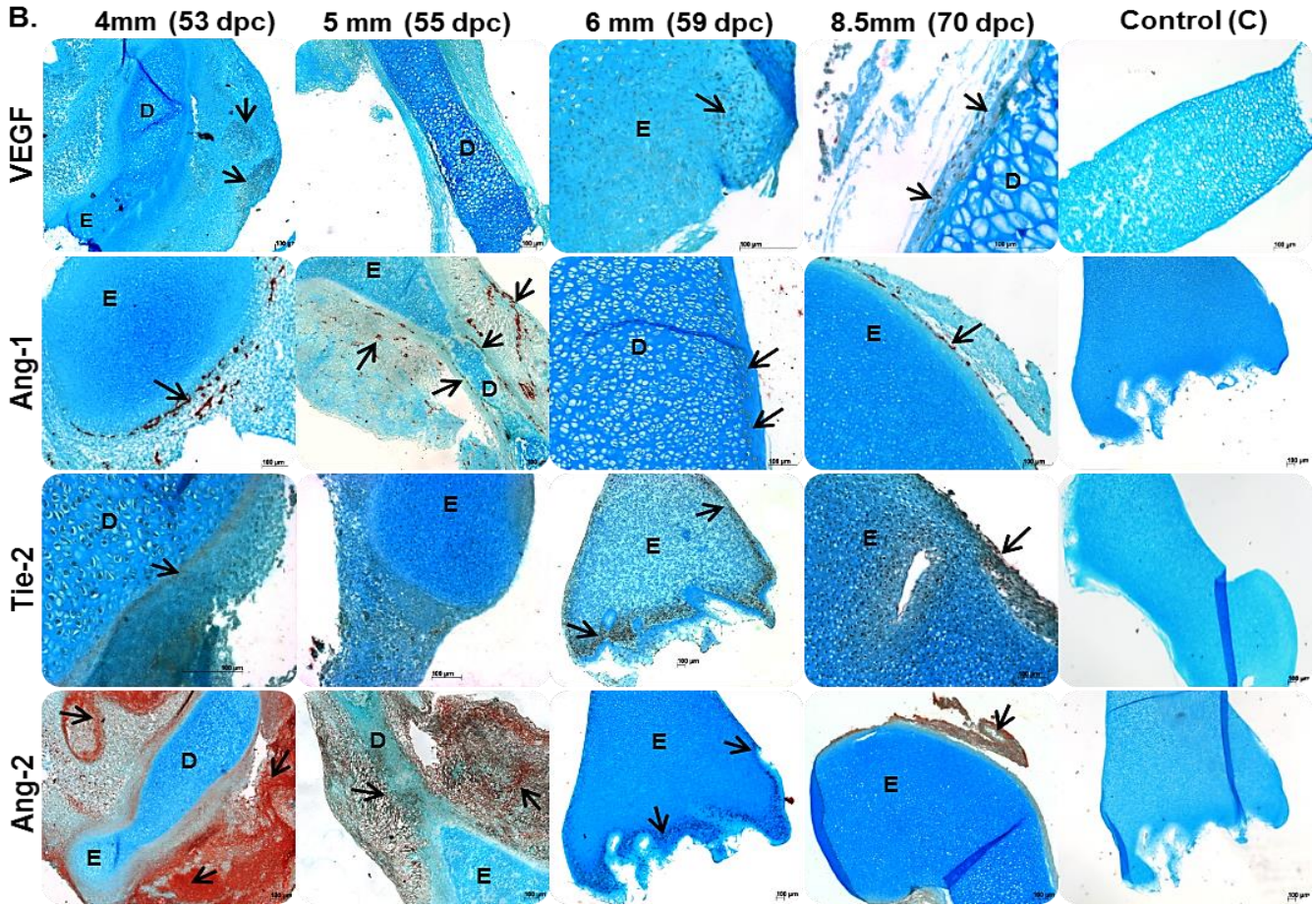

Figure 3.7.**B. Overview of the developmental staging of human fetal femurs** aged 53-70 days-post-conception (dpc) (4mm-8.5mm). Antibody markers: Vascular Endothelial Factor (VEGF), Angiopoietin 1 (Ang-1), Angiopoietin receptor (Tie-2), Angiopoietin 2 (Ang-2). Negative controls (-C) absence of primary antibody. D=Diaphysis, E=Epiphysis, F=femur. Arrows depict positive staining. Scale bar: 100μm.

Upon further analysis of the femurs, VEGFR-2 (KDR) protein was found to be weakly expressed in sections of fetal femurs (54dpc/4.5mm) but was strongly evident in cells within the cartilage at 59dpc (6mm) (Figure 3.8A) and within the connective tissue surrounding the femur (not shown). Negligible expression for VEGFR-1 (FLT-1) protein was evident on the sections of fetal femurs tested at either 54dpc (4.5mm) or 59dpc (6mm), using Immunohistochemistry (Figure 3.8B).

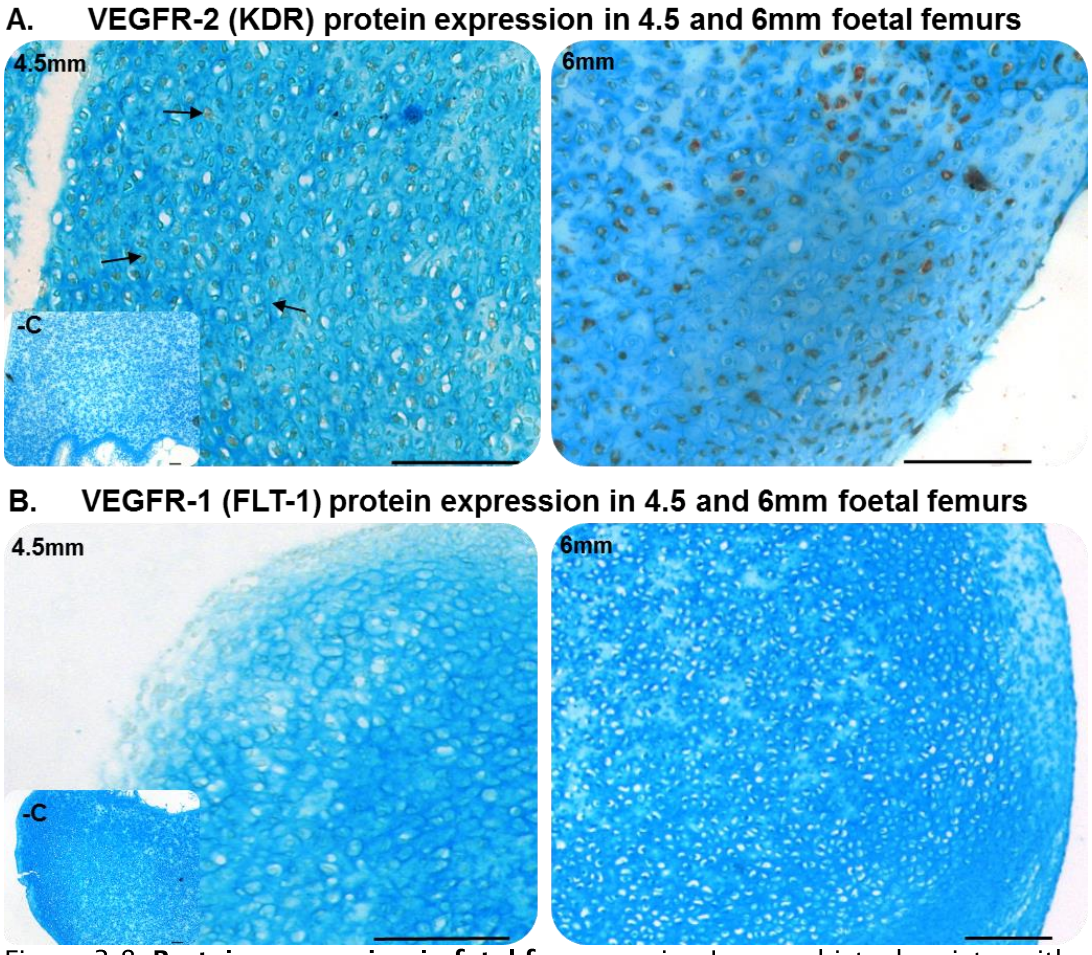

Figure 3.8. **Protein expression in fetal femurs** using Immunohistochemistry with antibodies against **A.** VEGFR-2 (*KDR*) (arrows) and **B.** VEGFR-1 (*FLT-1*). Fetal femurs at 54dpc (4.5mm) (A/C) and 59dpc (6mm) (B/D) were tested for presence of antigens. Scale bar: 100µm.

Table 3.1 represents an overall summary of the associated angiogenic proteins expressed in the fetal femurs of sequential size/age correlating to the images of immunohistochemistry in Figure 3.6 and Figure 3.7. ANG-1-, TIE-2- and

vWF proteins demonstrated presence within the femoral tissue (+) throughout the developmental stages examined compared to all other proteins.

Fetal femur size/age / Protein	4mm (53dpc)	5mm (55dpc)	6mm (59dpc)	8mm (70dpc)
STRO-1	-	+	+	+
CD31	-	-	+	+
VEGF	-	-	+	+
vWF	+	+	+	+
ANG-1	+	+	+	+
TIE-2	+	-	+	+
ANG-2	-	+	+	-

Table 3.1. **Expression pattern of proteins in fetal femurs.** +/- indicates positive/negative expression (respectively) of protein corresponding to age/size of the fetal femur as observed in Figure 3.7.

3.4.2 The effect of VEGF-165 on alkaline phosphatase protein expression and activity in D7 mono- and co-cultures of Fetal Femur-derived Cells/HUVECs

Cell cultures were assessed for ALP protein expression and enzyme activity after a 7 day culture period. Cell populations derived from the diaphysis of the fetal femur in monoculture demonstrated enhanced ALP activity in contrast to epiphyseal fetal femur-derived cells or HUVECs (Figure 3.9). Enhanced expression of ALP was observed in co-cultures of diaphyseal cells/HUVECs and epiphyseal cells/HUVECs in contrast to monoculture populations alone.

The supplementation of VEGF (100ng/ml) to the diaphyseal cultures reduced the levels of ALP expression in both, the mono and co-cultures with HUVECs. There were no observable changes in the epiphyseal mono and co-cultures upon VEGF supplementation. Interestingly, the HUVEC cultures displayed a

marked increase in cell proliferation visible upon addition of VEGF to the culture media (Figure 3.9A and D).

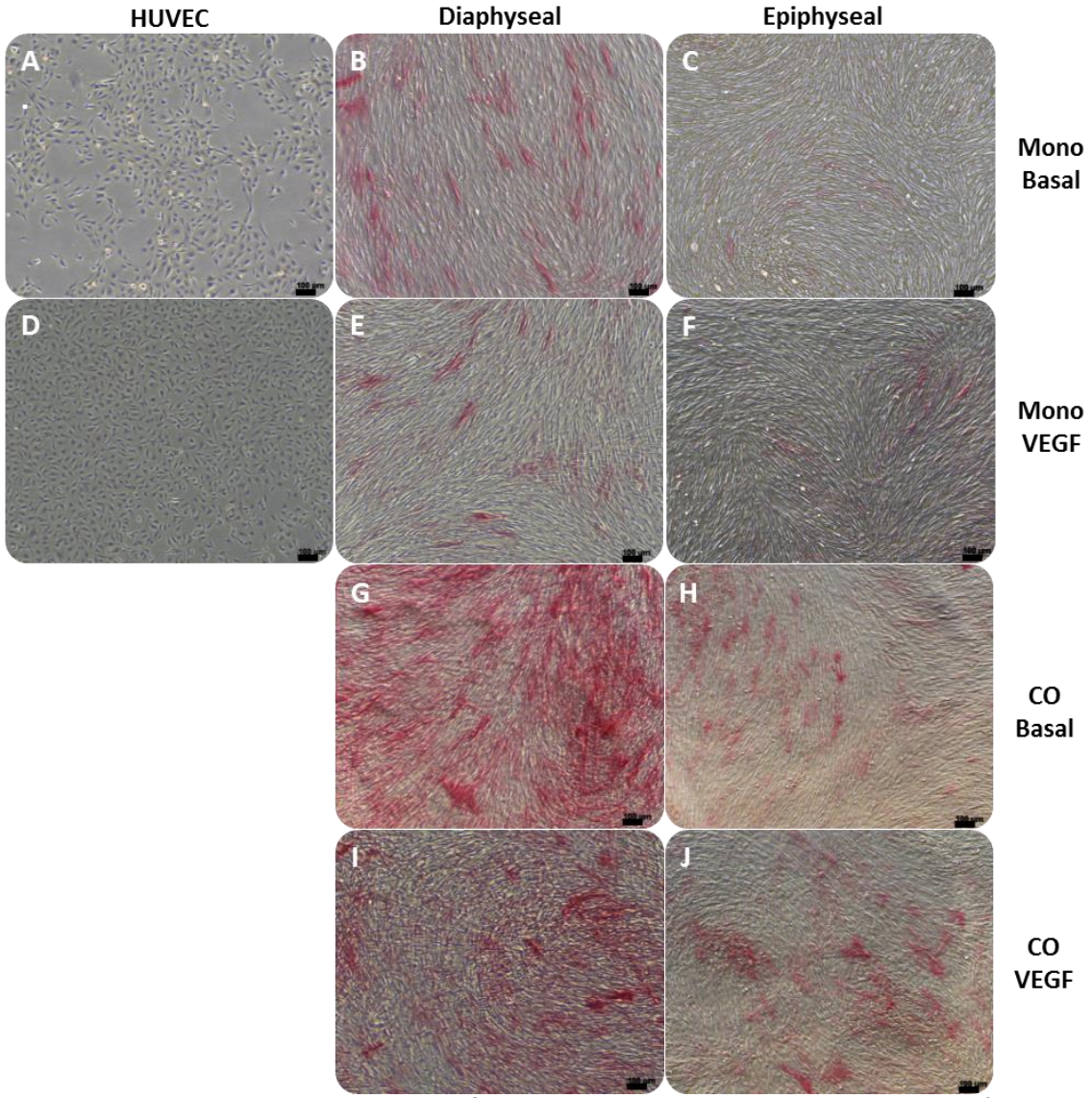

Figure 3.9. **Representative Images of alkaline phosphatase staining** at D7 of (A–C) basal monocultures; (D–F) monocultures supplemented with 100ng/ml VEGF; (G–H) basal co-cultures; (I–J) co-cultures (CO) supplemented with VEGF. Scale bar: 100µm

Following the observation of increased ALP protein expression in the mono and co-cultures by staining, ALP activity in these culture groups was assessed by biochemical analysis to quantify the actual levels of ALP enzyme activity. Figure 3.10 provides an overview of the combined ALP assays performed and highlights the variation in enzyme activity revealed between assays/samples.

For improved clarity of the results, Figure 3.11 depicts the deconstruction of graphs of individual experiments/patient samples.

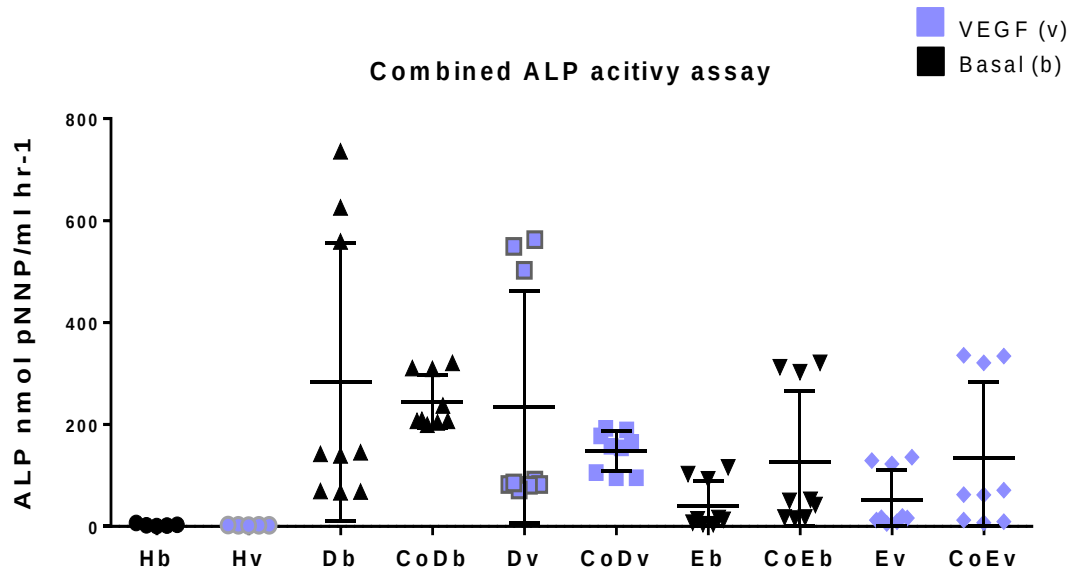

Figure 3.10. **The combined alkaline phosphatase assay data from 3 experiments**, showing overall change in levels of ALP activity of diaphyseal and epiphyseal mono- vs. co-cultures in basal media and supplemented with 100ng/ml VEGF. Basal/VEGF supplemented cultures denoted with **b** and **v** (purple) respectively. H= HUVEC, D= diaphyseal, E= epiphyseal. Co= co-cultures. Data presented as mean ± SD, n=3 replicates; *p≤0.05, **p≤0.01, ***p≤0.001.

Diaphyseal cells (D) in basal monocultures displayed enhanced ALP activity compared to epiphyseal cells (E) in basal monocultures, while HUVECs displayed negligible ALP activity (Figure 3.11). ALP activity was distinctly higher (640.3nmol±89.2) in the basal diaphyseal monoculture of patient 2 (Figure 3.11) relative to basal diaphyseal cultures of patient 1 and 3 (150nmol and 50nmol respectively), indicating a marked variation in initial ALP activity between patients. In basal epiphyseal co-cultures (CoE), ALP activity was significantly increased in two out of three patient samples, with a ~3fold (Table 3.2) increase in all three samples. In comparison, two out of three basal diaphyseal co-cultures (CoD) displayed a significant increase (~1-3fold) (Table 3.2), while there was a reduction in ALP activity in patient 2 (Figure 3.11).

Upon addition of VEGF to the diaphyseal co-cultures, a significant diminution in ALP activity was evident, compared to respective basal co-cultures. In the

epiphyseal co-cultures, a negligible response was observed upon VEGF supplementation (Figure 3.11 Patient 2).

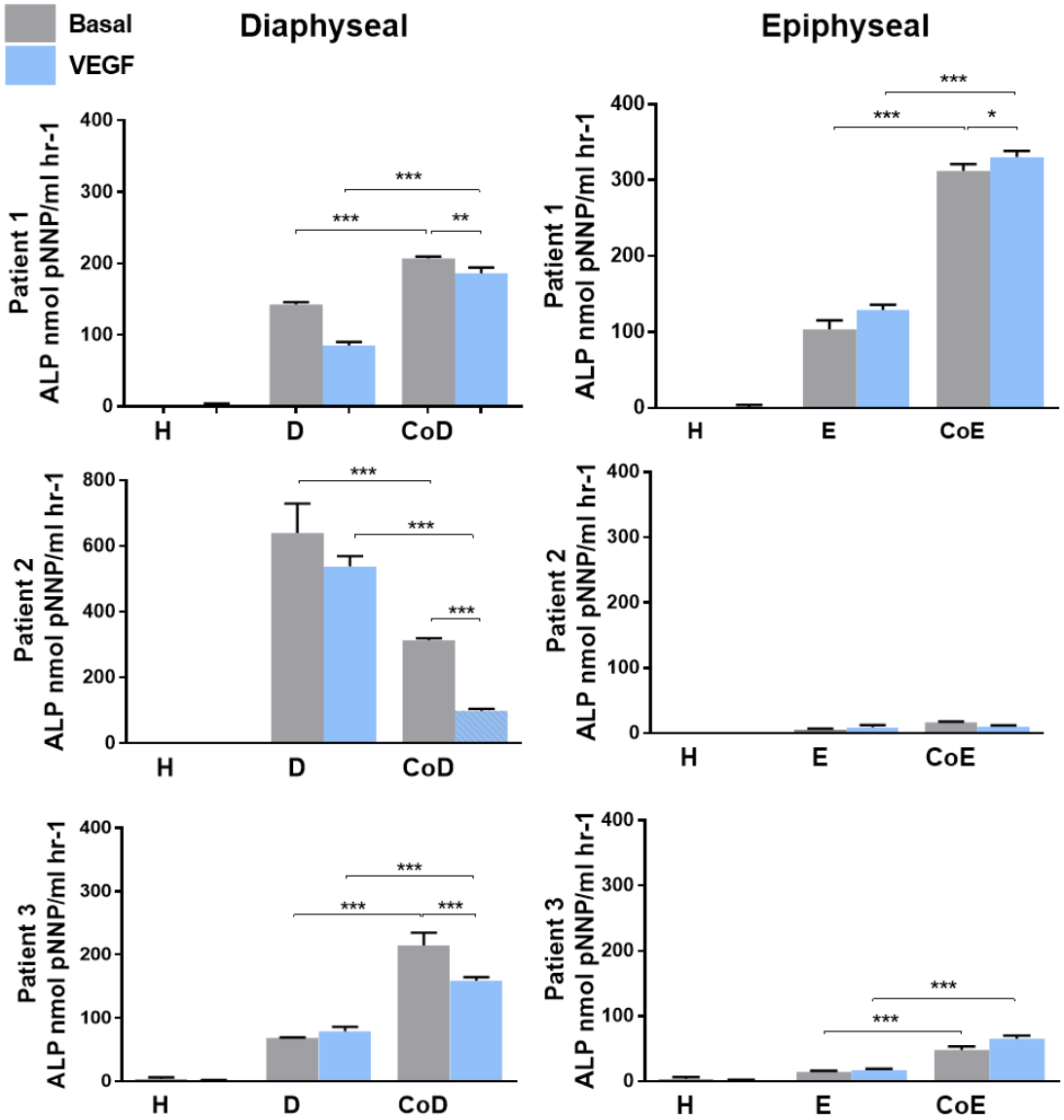

Figure 3.11. **Alkaline phosphatase activity in mono-/co-cultures**, supplemented with and without 100ng/ml VEGF. Graphs represent assays from 3 separate patients/experiments **Patient 1 – 3 Left**: Basal diaphyseal/HUVEC mono-/co-cultures in grey with addition of VEGF (in blue) and **Right**: Basal epiphyseal/HUVEC mono-/co-cultures (grey) with the addition of VEGF (blue). Results represent mean ± S.D; n=3 replicates; *p≤0.05, **p≤0.01, ***p≤0.001. H= HUVECs, E= epiphyseal cells, D= diaphyseal cells, CoD= diaphyseal/HUVEC co-culture, CoE= epiphyseal/HUVEC co-culture.

Basal Diaphyseal			
Patient	**D basal**	**CoD basal**	**Fold increase ALP activity in co-culture (basal)**
1	142.5	207.0	**1** ↑
2	640.3	313.6	**2** ↓
3	68.4	214.9	**3** ↑
VEGF Diaphyseal			
Patient	**D (vegf)**	**CoD (vegf)**	**Fold in-/decrease ALP activity in co-culture (vegf)**
1	85.3	186.4	**2** ↑
2	538.1	99.1	**5** ↓
3	79.3	158.9	**2** ↑

Basal Epiphyseal			
Patient	**E basal**	**CoE basal**	**Fold increase ALP activity in co-culture (basal)**
1	103.6	311.9	**3** ↑
2	5.3	16.9	**3** ↑
3	14.4	48.1	**3** ↑
VEGF Epiphyseal			
Patient	**E (vegf)**	**CoE (vegf)**	**Fold in-/decrease ALP activity in co-culture (vegf)**
1	129.2	330.3	**3** ↑
2	9.2	9.7	**1** ↑
3	17.6	65.1	**4** ↑

Table 3.2. **An overview of the fold change in alkaline phosphatase activity** in diaphyseal (top) basal and VEGF supplemented monocultures (D) and co-cultures (CoD) and epiphyseal (bottom) monocultures (E) and co-cultures (CoE) with HUVECs. VEGF concentration 100ng/ml. Average ALP activity (measured in nmol pNNP/ml hr^{-1}) presented.

3.4.3 Relative quantification of gene expression of osteogenic genes *ALP* and Collagen I in mono- and co-cultures using real-time quantitative polymerase chain reaction (qPCR)

Relative gene expression of *ALP* and *COL-1* in mono- and co-cultures was performed to assess similarities or differences to results obtained by the ALP enzyme assay and to measure the osteogenic potential of co-cultures supplemented with 50ng/ml VEGF. Gene expression of combined experiments, shown in Figure 3.12, demonstrated variable range of expression levels for both genes.

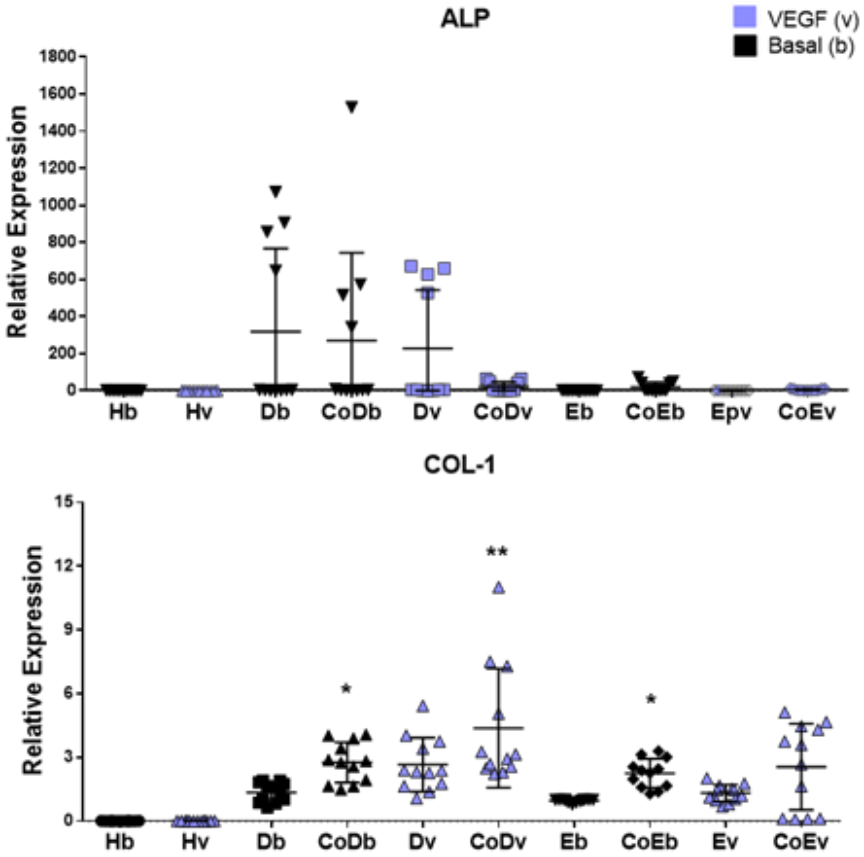

Figure 3.12. **The combined alkaline phosphatase (ALP) and Type I Collagen (COL-1) relative gene expression data** from 3 experiments; showing overall change in levels of *ALP* gene expression of diaphyseal and epiphyseal mono- vs. co-cultures in basal media and supplemented with 100ng/ml VEGF. Basal/VEGF supplemented cultures denoted with **b** and **v** (purple) respectively. Asterisks denotes significant difference between co-culture and respective skeletal mono-culture. H= HUVECs, D= diaphyseal, E= epiphyseal. Co= co-cultures. Data presented as mean ± SD, n=4 replicates; *p≤0.05, **p≤0.01, ***p≤0.001.

On closer inspection of individual graphs, *ALP* expression in basal diaphyseal co-cultures (CoD) displayed a varied response to co-culture conditions between patient samples (Figure 3.13). In contrast, basal epiphyseal co-cultures (CoE) displayed a more consistent significant increase of *ALP* gene expression in two out of three patients analysed (range ~3-40fold differences) (Figure 3.13). Corresponding to data for ALP activity (Figure 3.11), relative gene expression levels of *ALP* in basal diaphyseal monoculture ranged between ~1-750fold, with patient 2 displaying distinctly higher levels, compared to the remaining patient samples (Figure 3.13). Interestingly, *ALP* gene expression in the corresponding epiphyseal monoculture of patient 2 was negligible compared to that of the other two patient samples (Figure 3.13). The addition of VEGF to the cultures resulted in the suppression of *ALP* gene expression in diaphyseal co-cultures, but in the epiphyseal co-cultures, there was no effect on *ALP* expression apart from patient 2, where it was reduced (Figure 3.13).

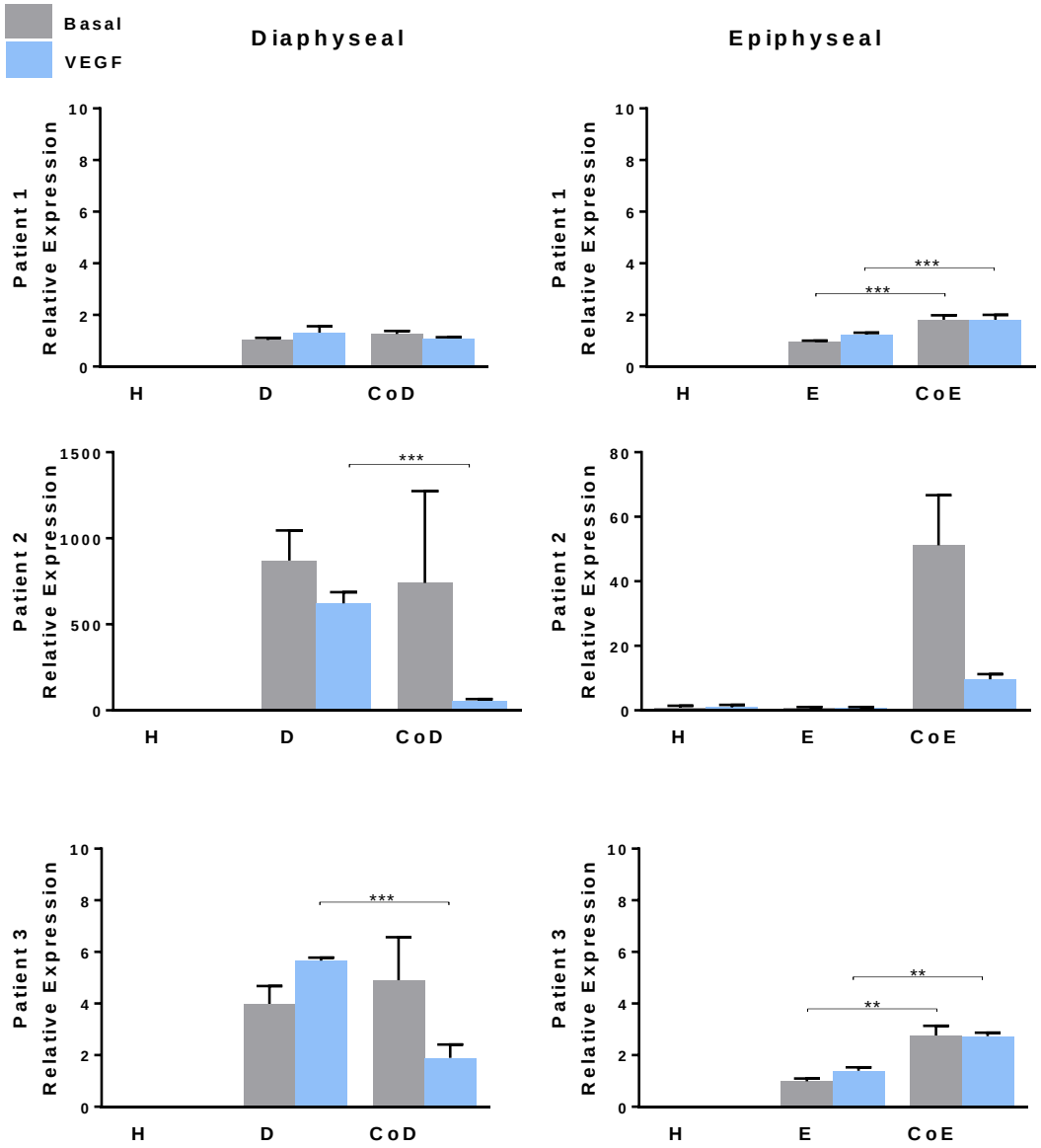

Figure 3.13. **The effect on alkaline phosphatase gene expression of mono-and co-cultures supplemented with or without 100ng/ml VEGF.** Graphs represent data from 3 separate patients/experiments **Patient 1 – 3 Left**: Basal diaphyseal/HUVEC mono-/co-cultures in grey with addition of VEGF (in blue) and **Right**: Basal epiphyseal/HUVEC mono-/co-cultures (grey) with the addition of VEGF (blue). Results represent mean ± S.D; n=4 *p≤0.05, **p≤0.01, ***p≤0.001. H= HUVECs, E= epiphyseal cells, D= diaphyseal cells, CoD= diaphyseal/HUVEC co-culture, CoE= epiphyseal/HUVEC co-culture.

The co-culture effects on the modulation of the osteogenic gene, *COL-1* indicated a significant increase in basal diaphyseal co-cultures of two patients (2/3) and in all epiphyseal co-cultures, compared to their respective basal monoculture groups (Figure 3.14), with a 2-4fold increase in expression levels.

The addition of VEGF to the epiphyseal and diaphyseal co cultures, produced a significant increase in expression of two out of three patients, but had a negative effect on the epiphyseal co-culture of patient 2 (Figure 3.14).

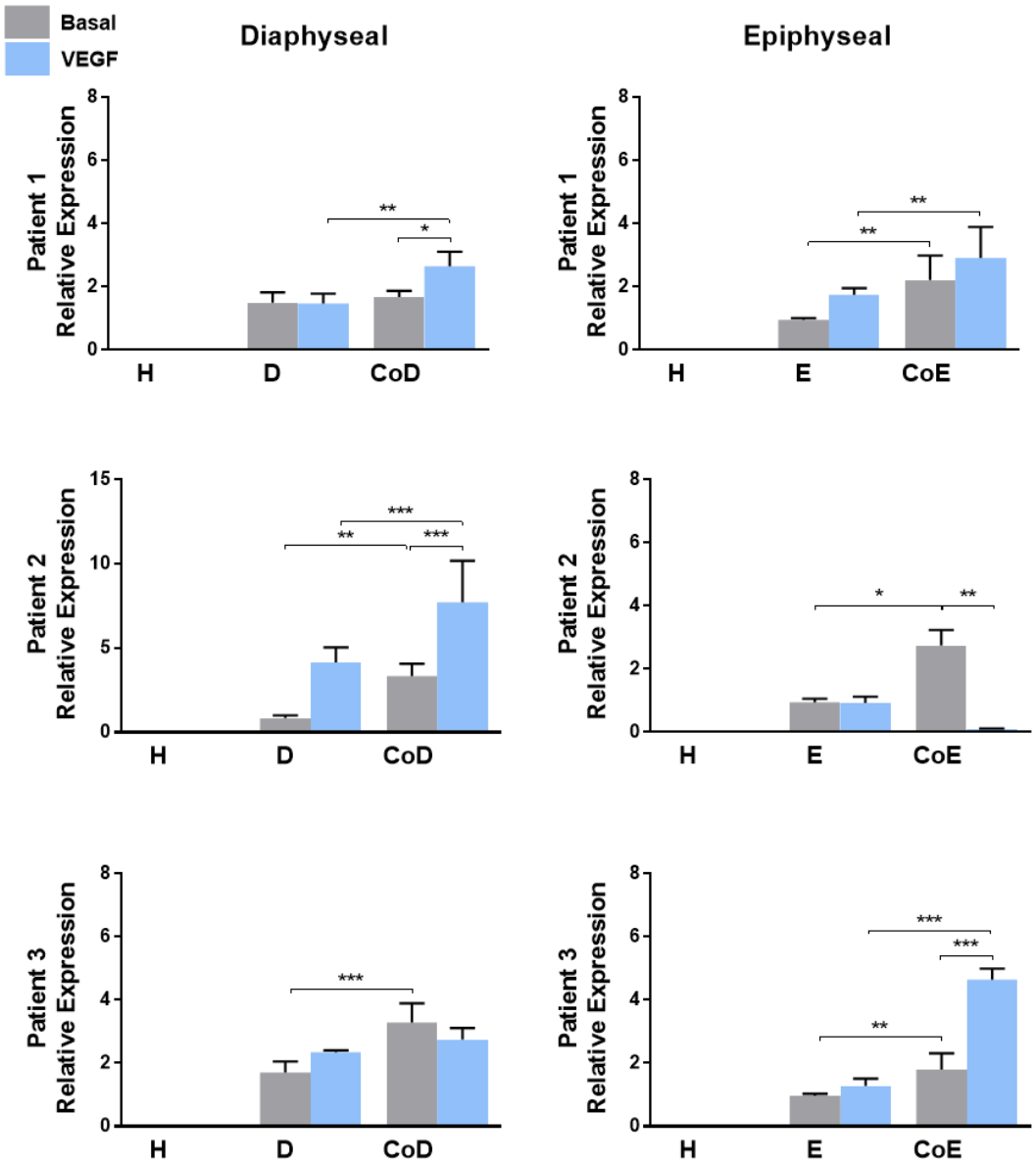

Figure 3.14. **The effect on *COL-1* gene expression of mono-and co-cultures supplemented with or without 100ng/ml VEGF**. Graphs represent assays from 3 separate patients/experiments **Patient 1 – 3 Left**: Basal diaphyseal/HUVEC mono-/co-cultures in grey with addition of VEGF (in blue) and **Right**: Basal epiphyseal/HUVEC mono-/co-cultures (grey) with the addition of VEGF (blue). Results represent mean ± S.D; n=4 replicates, *p≤0.05, **p≤0.01, ***p≤0.001. H= HUVECs, E= epiphyseal cells, D= diaphyseal cells, CoD= diaphyseal/HUVEC co-culture, CoE= epiphyseal/HUVEC co-culture.

3.4.4 Relative quantification of angiogenesis-related genes in mono- and co-cultures using qPCR

Following osteogenic gene expression analysis of mono- and co-cultures, the angiogenic potential of the cell cultures with and without VEGF supplementation was assessed. *VWF* and *VEGF* gene expression was, in general, low in most culture settings and no marked changes in expression were detected (Appendix 7.3.1-2). Addition of VEGF to the cultures had little effect on the epiphyseal mono- and co-cultures but did produce an increase in *vWF* and *VEGF* gene expression, in the HUVEC population and in the diaphyseal co-cultures of the same patient (patient 2).

In contrast to *vWF* and *VEGF* gene expression levels, HUVECs expressed distinctly high levels of the VEGF receptor gene *FLT-1* (R1) in basal and VEGF supplemented cultures, summarised in Figure 3.15.

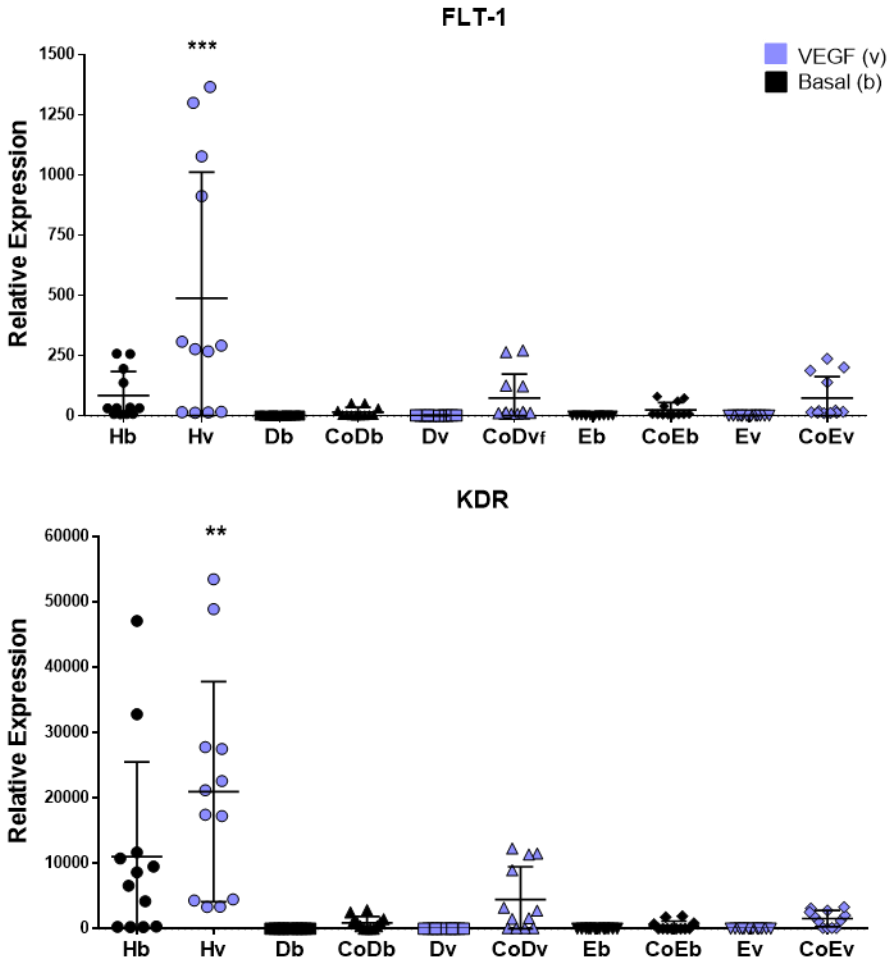

Figure 3.15. **The combined VEGF receptor 1 (FLT-1) and VEGF receptor 2 (KDR) relative gene expression data from 3 experiments**; showing overall change in levels of *ALP* gene expression of diaphyseal and epiphyseal mono- vs. co-cultures in basal media and supplemented with 100ng/ml VEGF. Basal/VEGF supplemented cultures denoted with **b** and **v** (purple) respectively. Asterisks denotes significant difference between HUVEC basal and VEGF supplemented monocultures. H= HUVECs, D= diaphyseal, E= epiphyseal. Co= co-cultures. Data presented as mean ± SD, n=4 replicates; *p≤0.05, **p≤0.01, ***p≤0.001.

On closer observation of individual patient samples, it was evident that the addition of VEGF to the HUVEC monocultures significantly increased relative gene expression levels of *FLT-1* (2-10fold) (Figure 3.16). In contrast, expression of *FLT-1* gene in basal skeletal cell monocultures (D/E) was negligible with or without VEGF supplementation. *FLT-1* gene expression in the basal co-cultures was observed (D/CoD= max ~80fold; E/CoE= max ~80fold) (patient 1/2), and a further ~3-5fold increase was evident with the addition of VEGF to diaphyseal and epiphyseal co-cultures compared to their respective basal co-cultures. There was no apparent pattern to distinguish whether

diaphyseal or epiphyseal co-cultures showed a greater response given sample variability.

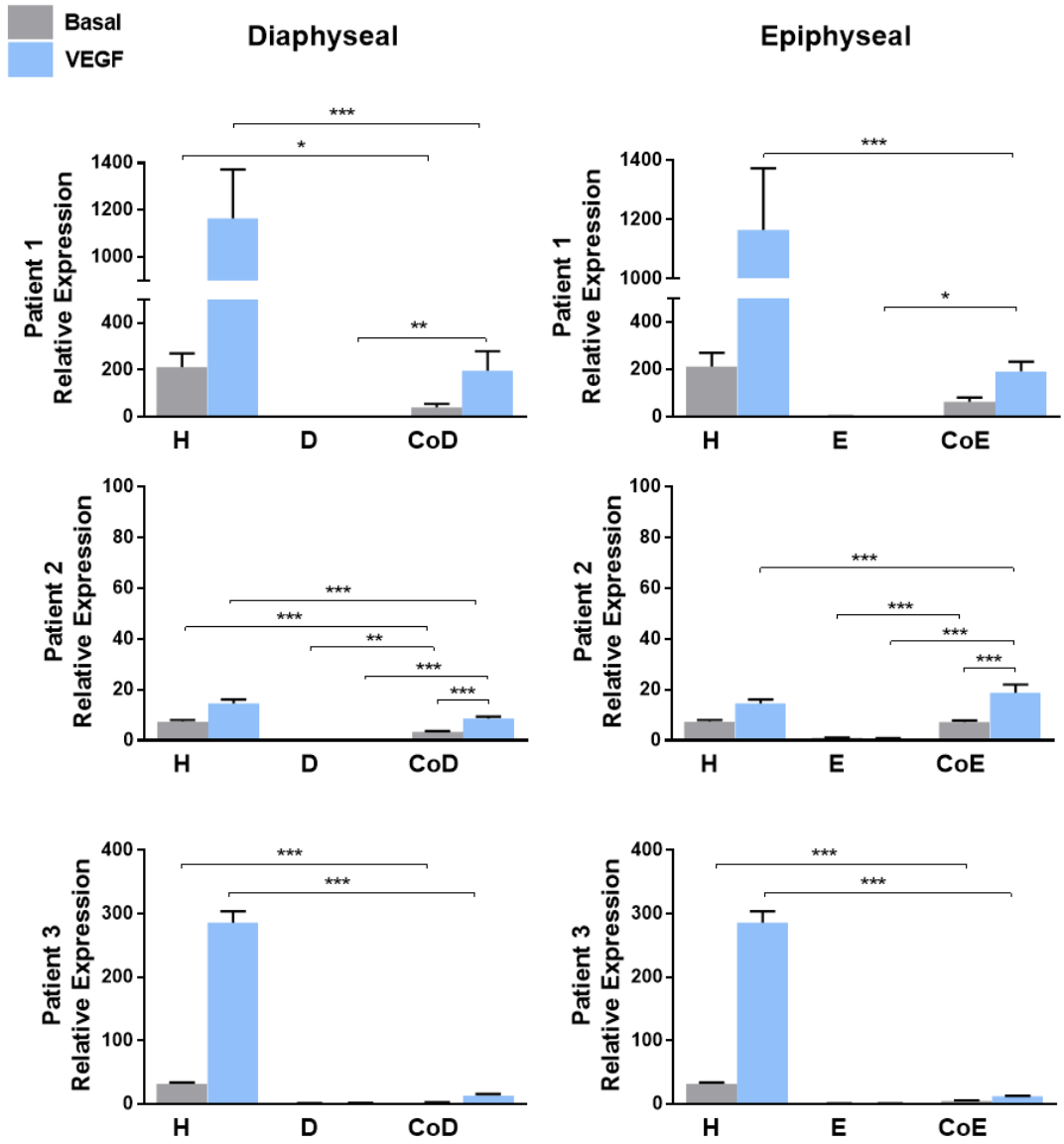

Figure 3.16. **The effect on *FLT-1*/VEGFR-1 gene expression of mono-and co-cultures supplemented with or without 100ng/ml VEGF**. Graphs represent data from 3 separate patients/experiments **Patient 1 – 3 Left**: Basal diaphyseal/HUVEC mono-/co-cultures in grey with addition of VEGF (in blue) and **Right**: Basal epiphyseal/HUVEC mono-/co-cultures (grey) with the addition of VEGF (blue). Results represent mean ± S.D; n=4 replicates; *p≤0.05, **p≤0.01, ***p≤0.001. H= HUVECs, E= epiphyseal cells, D= diaphyseal cells, CoD= diaphyseal/HUVEC co-culture, CoE= epiphyseal/HUVEC co-culture.

KDR (R2) gene expression in HUVECs was overall more enhanced compared to *FLT-1* (R1) gene expression. In the three HUVEC culture groups, expression

levels for *KDR* increased by 2-13fold, when VEGF was added to the culture media. *KDR* expression levels were found to be minimal in both diaphyseal and epiphyseal monocultures with or without VEGF supplementation (Figure 3.17). Furthermore, in diaphyseal co-cultures a 16-600fold (D/CoD) increase and in epiphyseal co-cultures, a 20-700fold (E/CoE) increase in *KDR* expression levels was observed in basal co-cultures. The addition of VEGF evoked a further 6fold increase in diaphyseal co-cultures and 17fold increase in epiphyseal co-cultures compared to respective basal co-cultures (Figure 3.17).

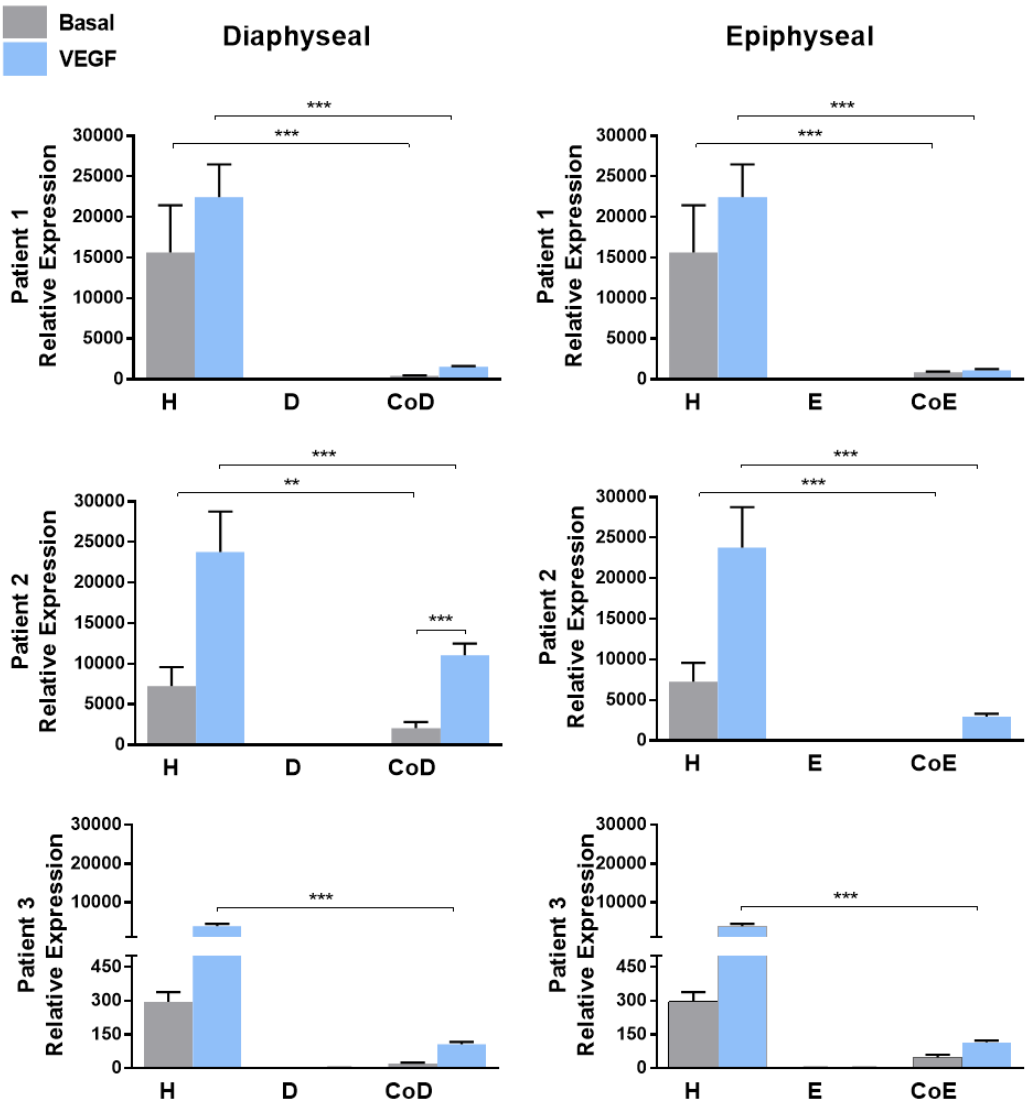

Figure 3.17. **The effect on *KDR*/VEGFR-2 gene expression of mono-and co-cultures supplemented with or without 100ng/ml VEGF.** Graphs represent data from 3 separate patients/experiments **Patient 1 – 3 Left**: Basal diaphyseal/HUVEC mono-/co-cultures in grey with addition of VEGF (in blue) and **Right**: Basal epiphyseal/HUVEC mono-/co-cultures (grey) with the addition of VEGF (blue). Results represent mean ± S.D; n=4 replicates; *p≤0.05, **p≤0.01, ***p≤0.001. H= HUVECs, E= epiphyseal cells, D= diaphyseal cells, CoD= diaphyseal/HUVEC co-culture, CoE= epiphyseal/HUVEC co-culture.

3.4.5 The effect of reduced concentration of VEGF-165 on alkaline phosphatase protein expression and activity in D7 mono- and co-cultures of FFDSCs/HUVECs

Previous results demonstrated the osteogenic modulating effect of HUVEC/SSDC co-cultures on ALP enzyme and *COL-1* and *ALP* gene expression. However, the studies also demonstrated a reductive effect of VEGF supplementation using 100ng/ml in the diaphyseal co-cultures. Subsequent studies used 50ng/ml VEGF supplementation to compare cultures with the higher dose and in order to determine, if differences in response of the cell co-cultures and monocultures, to this lower dose of VEGF, could be detected.

As shown by ALP staining (Figure 3.18), both co-cultures, diaphyseal/HUVEC and epiphyseal/HUVEC, demonstrated increased staining compared to their respective monocultures. ALP staining was most enhanced in diaphyseal co-cultures with VEGF supplementation. Overall VEGF supplementation of 50ng/ml resulted in a more stimulatory effect of ALP protein expression on diaphyseal cells compared to the epiphyseal cell cultures.

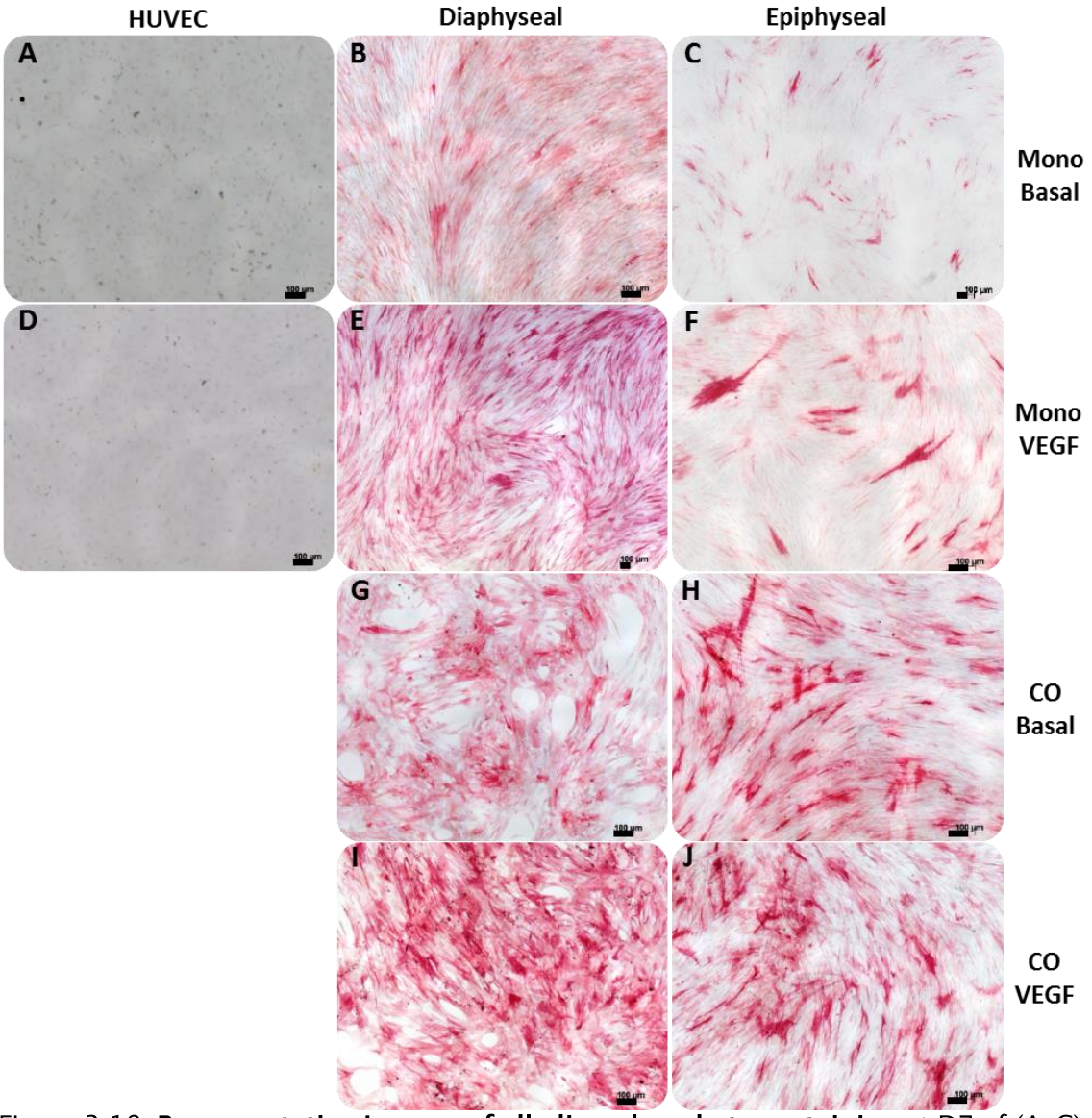

Figure 3.18. **Representative Images of alkaline phosphatase staining** at D7 of (A–C) basal monocultures; (D–F) monocultures supplemented with 50ng/ml VEGF; (G–H) basal co-cultures; (I–J) co-cultures supplemented with VEGF. Scale bar: 100µm.

In general, the ALP enzyme activity assays confirmed increased activity in the majority of basal co-cultures, compared to respective monocultures. Levels of ALP were overall lower in epiphyseal cultures. Figure 3.19 depicts a combined summary of changes in ALP activity between mono- and co-cultures of all three experiments.

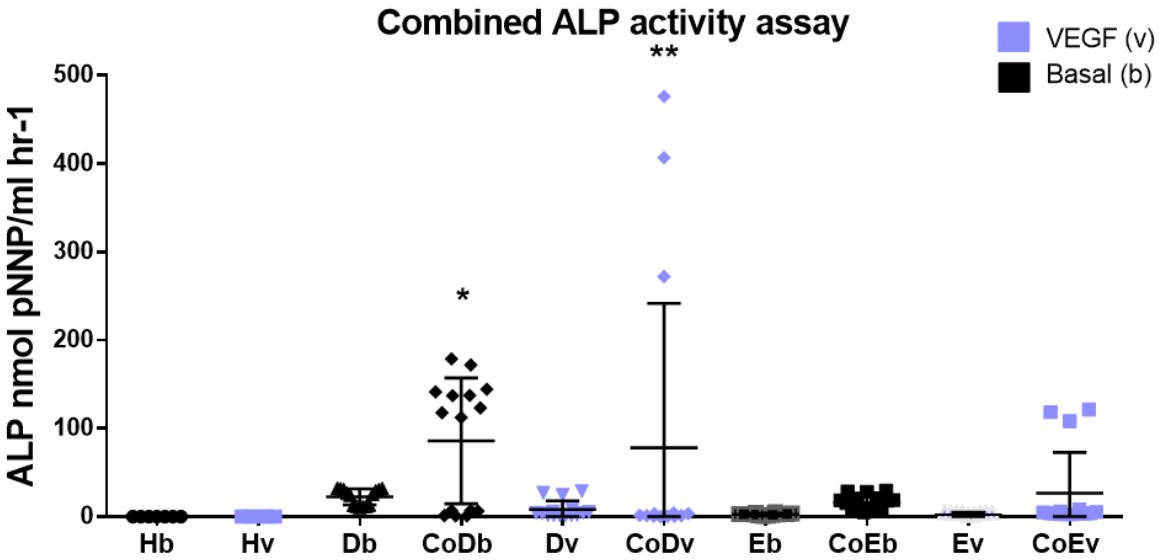

Figure 3.19. **The combined alkaline phosphatase assay data from 3 experiments**, showing overall change in levels of ALP activity of diaphyseal and epiphyseal mono- vs. co-cultures in basal media and supplemented with 50ng/ml VEGF. Basal/VEGF supplemented cultures denoted with **b** and **v** (purple) respectively. Asterisks denotes significant difference between co-culture and respective skeletal mono-culture. H= HUVECs, D= diaphyseal, E= epiphyseal. Co= co-cultures. Data presented as mean ± SD, n=3 replicates; *p≤0.05, **p≤0.01, ***p≤0.001.

A breakdown of the combined data graph into individual patients (Figure 3.20) gave a clearer picture of the variability that was observed between patients. A significant increase in ALP was evident in two basal diaphyseal co-cultures (patient 1/3) and in one basal epiphyseal co-culture (patient 3) (Figure 3.20). However, with supplementation of VEGF, a variable response was observed in diaphyseal co-cultures, with one co-culture displaying a significant increase in ALP activity (patient 1) and another co-culture displaying a significant reduction (patient 2), compared to respective basal co-cultures (Figure 3.20). With addition of 50ng VEGF, an increase observed in basal epiphyseal ALP activity of one patient was abolished (patient 3) but a significant increase of the other two patient samples was observed, which had previously not shown any significant changes.

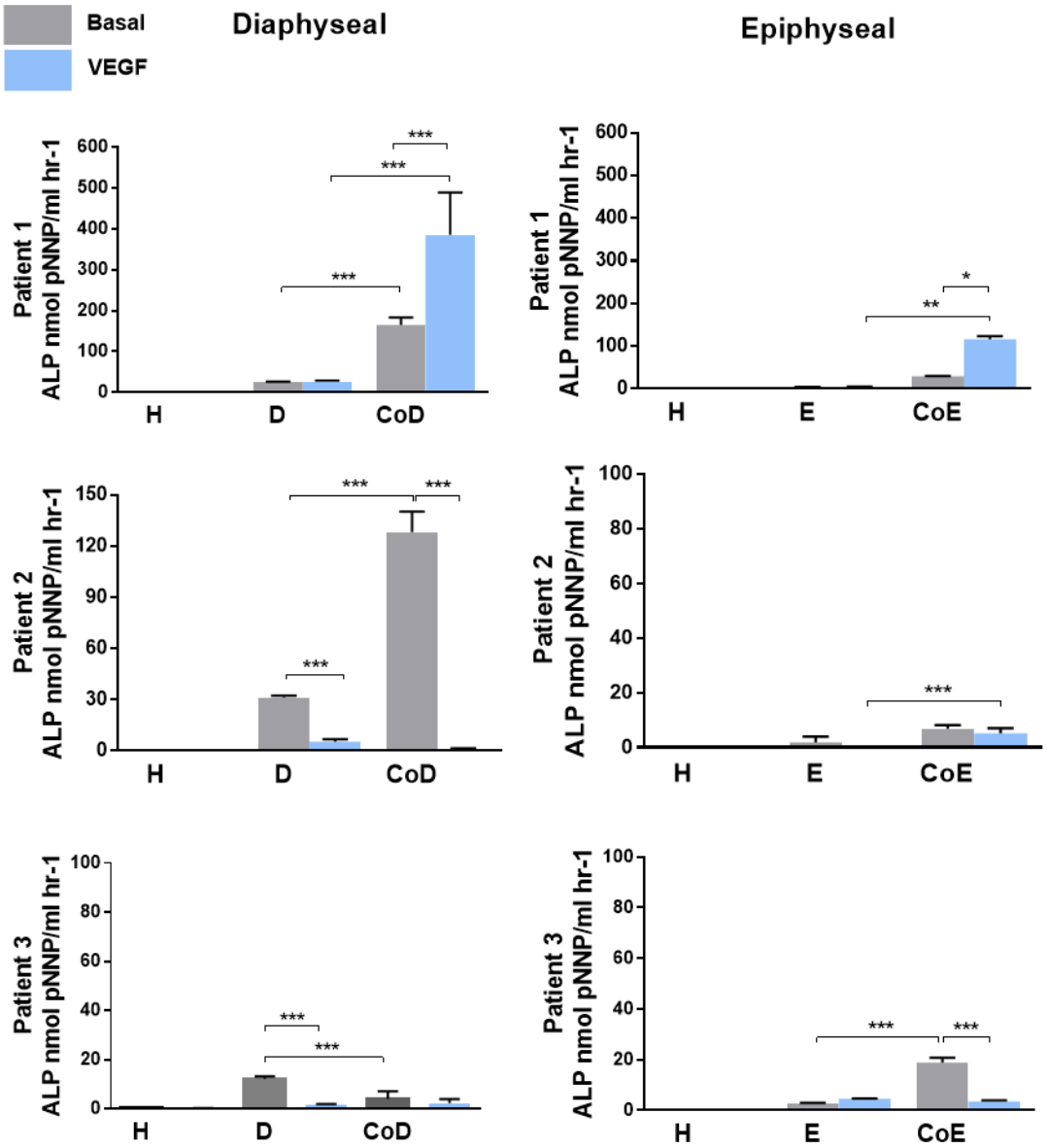

Figure 3.20. **Alkaline phosphatase activity in mono-/co-cultures**, supplemented with and without 50ng/ml VEGF. Graphs represent data from 3 separate patients/experiments **Patient 1 – 3 Left**: Basal diaphyseal/HUVEC mono-/co-cultures in grey with addition of VEGF (in blue) and **Right**: Basal epiphyseal/HUVEC mono-/co-cultures (grey) with the addition of VEGF (blue). Results represent mean ± S.D; n=3 replicates; *p≤0.05, **p≤0.01, ***p≤0.001. H= HUVECs, E= epiphyseal cells, D= diaphyseal cells, CoD= diaphyseal/HUVEC co-culture, CoE= epiphyseal/HUVEC co-culture.

Table 3.3 depicts fold-increase/-decrease in co-cultures of HUVECs/FFDSCs with and without VEGF supplementation. There was an increase in ALP activity in the majority of co-cultures of both fetal skeletal cell types in basal media

and this increase in activity was reversed in one of each diaphyseal and epiphyseal co-cultures, supplemented with VEGF.

Basal Diaphyseal			
Patient	**D basal**	**CoD basal**	**Fold increase ALP activity in co-culture (basal)**
1	25.6	165.1	**6** ↑
2	31.3	128.3	**4** ↑
3	12.1	4.0	**0.3** ↓
VEGF Diaphyseal			
Patient	**D (vegf)**	**CoD (vegf)**	**Fold in-/decrease ALP activity in co-culture (vegf)**
1	26.8	385	**14** ↑
2	5.4	0.3	**18** ↓
3	1.6	2.3	**1** ↑
Basal Epiphyseal			
Patient	**E basal**	**CoE basal**	**Fold increase ALP activity in co-culture (basal)**
1	3.8	28.8	**8** ↑
2	1.9	6.9	**4** ↑
3	2.8	18.9	**7** ↑
VEGF Epiphyseal			
Patient	**E (vegf)**	**CoE (vegf)**	**Fold in-/decrease ALP activity in co-culture (vegf)**
1	3.2	116.1	**37** ↑
2	1.4	5.2	**4** ↑
3	4.6	3.4	**1** ↓

Table 3.3. **An overview of the fold change in alkaline phosphatase activity** in diaphyseal (top) basal and VEGF supplemented monocultures (D) and co-cultures (CoD) and epiphyseal (bottom) monocultures (E) and co-cultures (CoE) with HUVECs. VEGF concentration 50ng/ml. Average ALP activity (measured in nmol pNNP/ml hr^{-1}) presented.

3.4.6 Relative quantification of gene expression of osteogenic genes *ALP* and *COL-1* in mono- and co-cultures using real-time quantitative polymerase chain reaction (qPCR)

Relative gene expression of *ALP* and *COL-1* was examined in basal and VEGF supplemented mono- and co-culture to determine any changes in gene expression of cultures in response to the lower VEGF dose (50ng/ml).

Similar to previous observations the graph depicting the combined *ALP* and *COL-1* gene expression data demonstrated a wide range of expression levels of the various culture conditions, making it difficult to correlate the individual data sets (Figure 3.21).

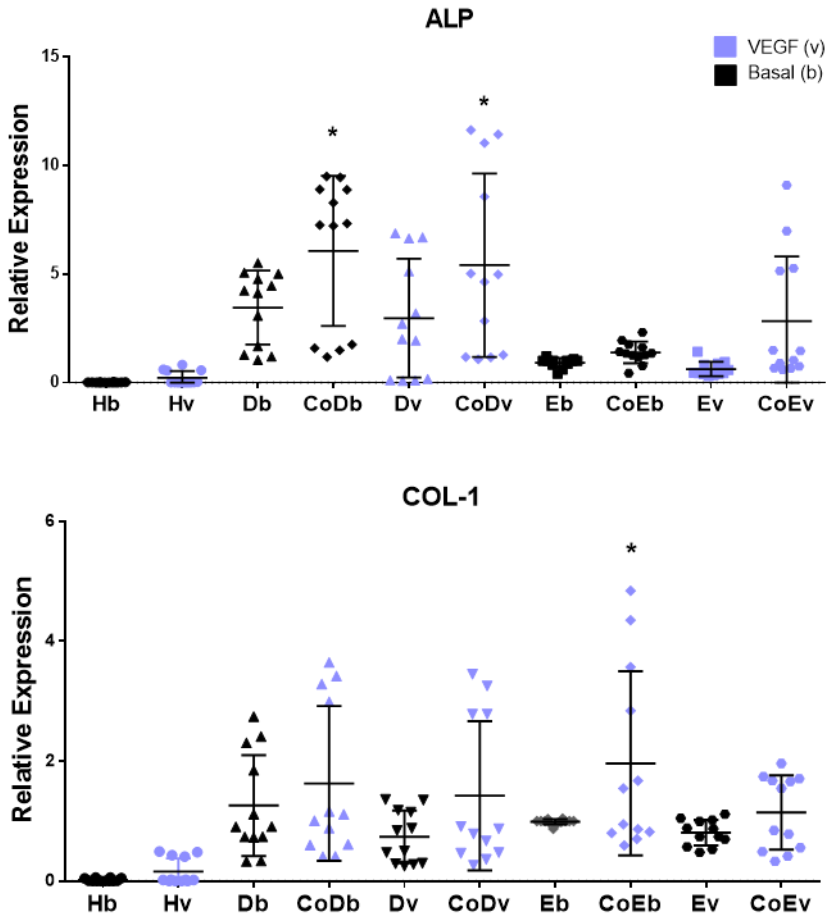

Figure 3.21.**The combined alkaline phosphatase (ALP) and Type I Collagen (COL-1) relative gene expression data from 3 experiments**; showing overall change in levels of *ALP* gene expression of diaphyseal and epiphyseal mono- vs. co-cultures in basal media and supplemented with 100ng/ml VEGF. Basal/VEGF supplemented cultures denoted with **b** and **v** (purple) respectively. Asterisks denotes significant difference between co-culture and respective skeletal mono-culture. H= HUVECs, D= diaphyseal, E= epiphyseal. Co= co-cultures. Data presented as mean ± SD, n=4 replicates; *p≤0.05, **p≤0.01, ***p≤0.001.

In individual graphs, it was demonstrated that in two out of three patients basal diaphyseal co-cultures showed a significant increase in *ALP* gene expression (Figure 3.22, patient 2/3). Results were also significantly higher in diaphyseal co-cultures of patients 1 and 2 following supplementation with VEGF. This, however, was partly due to a decrease in *ALP* expression in cell monoculture with VEGF rather than an increase in the co-cultures relative to basal diaphyseal co-cultures (Figure 3.22). *ALP* mRNA was significantly reduced in VEGF supplemented cocultures of patient 3. Epiphyseal cells showed a significant increase in basal epiphyseal co-cultures of patient 1 (Figure 3.22), similar to the increases observed in the biochemical assay

(Figure 3.20); similarly, one patient showed a significant up-regulation after addition of 50ng VEGF (Figure 3.22), with a maximum 16fold increase in *ALP* mRNA in the epiphyseal co-cultures.

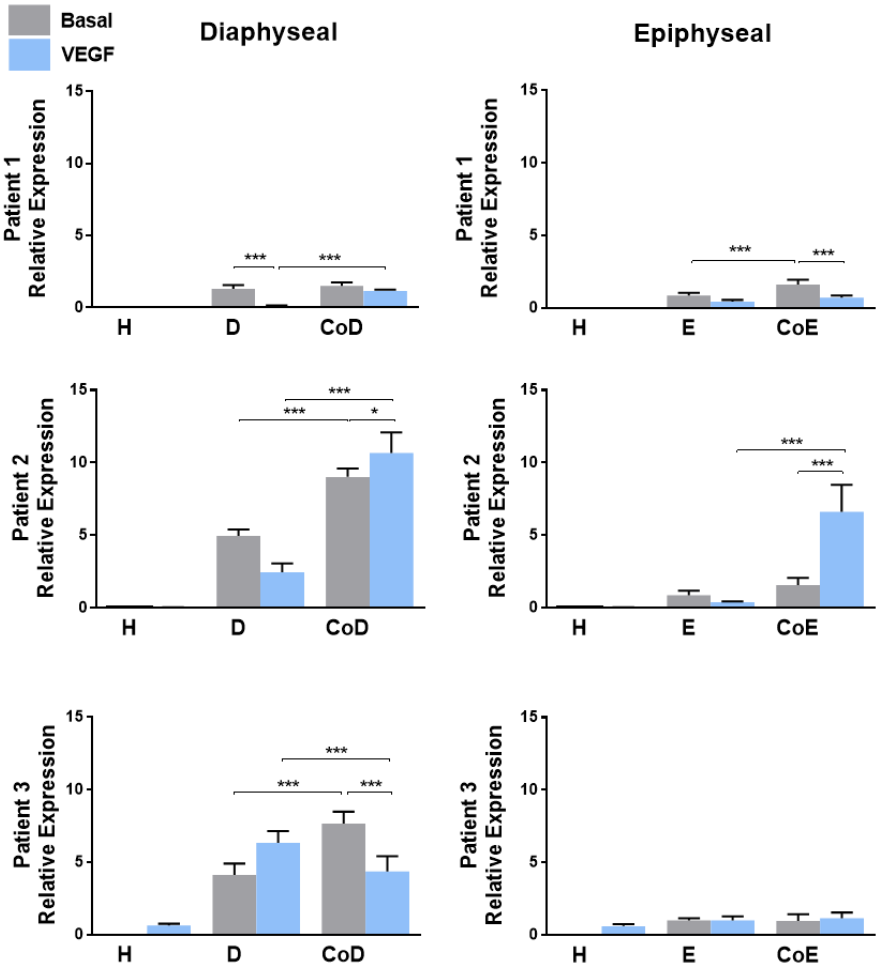

Figure 3.22. **The effect on *ALP* gene expression of mono-and co-cultures supplemented with or without 50ng/ml VEGF.** Graphs represent data from 3 separate patients/experiments **Patient 1 – 3 Left**: Basal diaphyseal/HUVEC mono-/co-cultures in grey with addition of VEGF (in blue) and **Right**: Basal epiphyseal/HUVEC mono-/co-cultures (grey) with the addition of VEGF (blue). Results represent mean ± S.D; n=4 replicates; *p≤0.05, **p≤0.01, ***p≤0.001. H= HUVECs, E= epiphyseal cells, D= diaphyseal cells, CoD= diaphyseal/HUVEC co-culture, CoE= epiphyseal/HUVEC co-culture.

There was variability in *COL-1* gene expression in basal and VEGF-supplemented diaphyseal co-cultures (Figure 3.23); only patient 2 showed significant elevation of mRNA in basal and in VEGF supplemented diaphyseal co-cultures. Equally, only one patient demonstrated a significant increase in

COL-1 mRNA levels of the basal epiphyseal co-cultures (Figure 3.23, patient 1), which was substantially decreased with the addition of VEGF. VEGF supplemented co-cultures of patient 2 demonstrated significant elevation of *COL-1* expression levels relative to respective basal co-cultures.

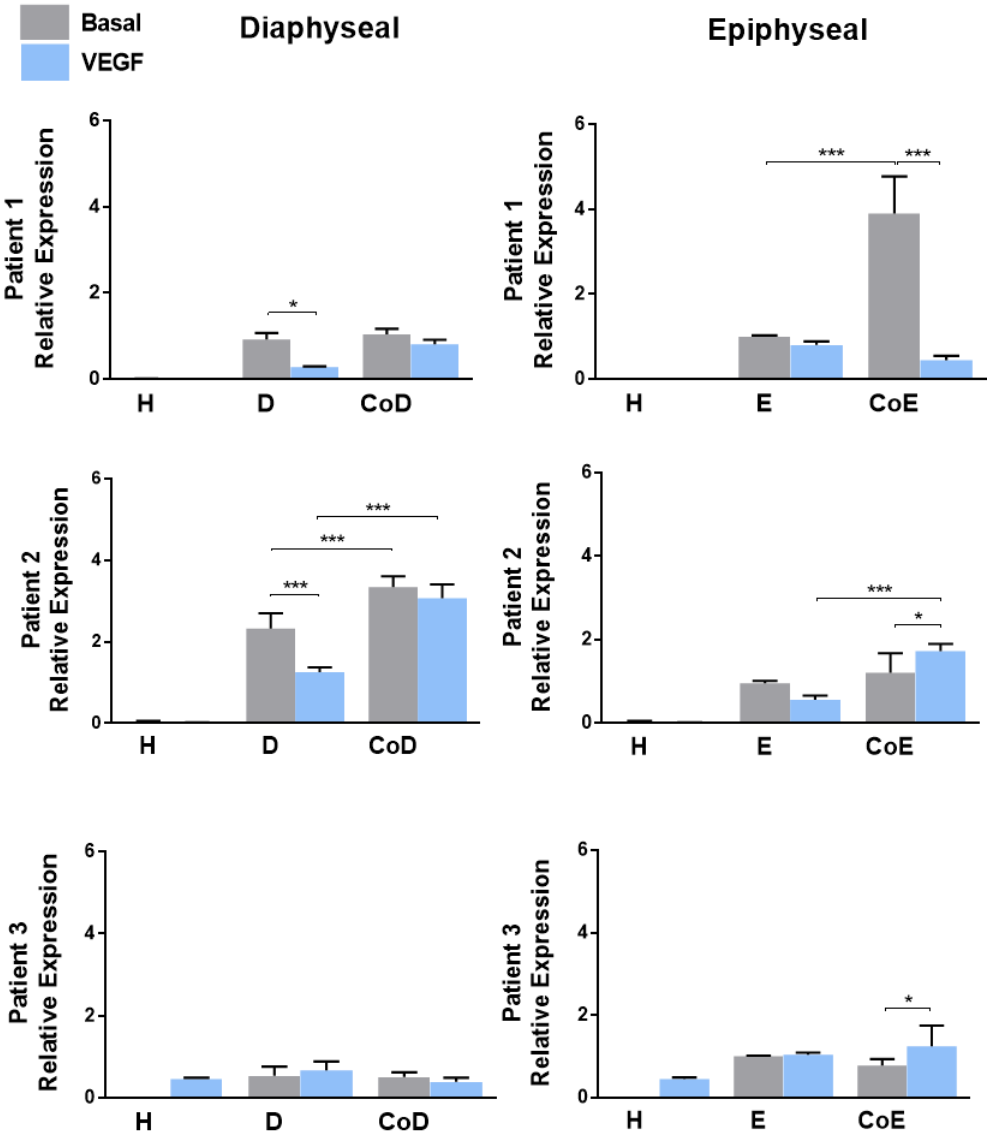

Figure 3.23. **The effect on *COL-1*gene expression of mono-and co-cultures supplemented with or without 50ng/ml VEGF.** Graphs represent data from 3 separate patients/experiments **Patient 1 – 3 Left**: Basal diaphyseal/HUVEC mono-/co-cultures in grey with addition of VEGF (in blue) and **Right**: Basal epiphyseal/HUVEC mono-/co-cultures (grey) with the addition of VEGF (blue). Results represent mean ± S.D; n=4 replicates; *p≤0.05, **p≤0.01, ***p≤0.001. H= HUVECs, E= epiphyseal cells, D= diaphyseal cells, CoD= diaphyseal/HUVEC co-culture, CoE= epiphyseal/HUVEC co-culture.

3.4.7 Relative quantification of angiogenesis-related genes during mono- and co-cultures using qPCR

Previous gene expression analysis of angiogenesis-related genes (3.4.4) using 100ng/ml VEGF supplementation demonstrated significant modulation of VEGF receptor genes but negligible changes in vWF and VEGF mRNA levels. Subsequent experiments were performed using a lower dose of VEGF (50ng/ml) to supplement fetal/HUVEC co-cultures in order to observe comparable differences in gene expression to the higher VEGF dose.

Similar to results earlier in this chapter (3.4.4), no significant effects on relative expression of the *vWF* or *VEGF* gene in co-culture were observed in either basal or VEGF supplemented groups. The addition of VEGF evoked a marginal increase in the HUVEC monocultures and a variable change in skeletal monocultures (Appendix 7.3.3-4).

Equally in line with findings reported in 3.4.4, expression levels of *FLT-1* (R1) and *KDR* (R2) genes were upregulated in all co-cultures and highly expressed in HUVECs (Figure 3.24). In basal HUVEC monocultures expression levels for *FLT-1* and *KDR* were observed to be between 50-8000fold higher respectively than in the skeletal monoculture controls (Figure 3.25).

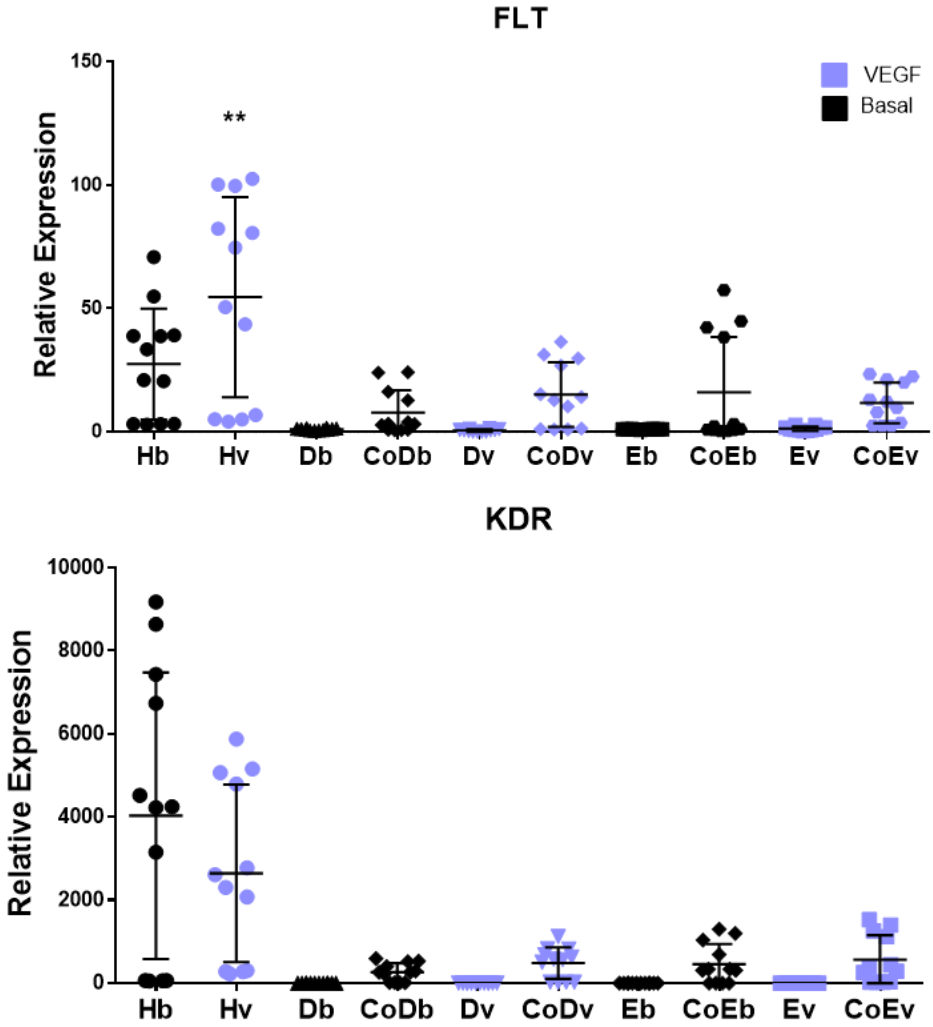

Figure 3.24.**The combined VEGF receptor 1 (FLT-1) and VEGF receptor 2 (KDR) relative gene expression data from 3 experiments**; showing overall change in levels of *ALP* gene expression of diaphyseal and epiphyseal mono- vs. co-cultures in basal media and supplemented with 50ng/ml VEGF. Basal/VEGF supplemented cultures denoted with **b** and **v** (purple) respectively. Asterisks denotes significant difference between HUVEC basal and VEGF supplemented monocultures. H=HUVECs, D= diaphyseal, E= epiphyseal. Co= co-cultures. Data presented as mean ± SD, n=4 replicates; *p≤0.05, **p≤0.01, ***p≤0.001.

FLT-1 gene expression in HUVEC monocultures increased 2-5fold with the addition of VEGF. Similar to previous results (Figure 3.16), both diaphyseal and epiphyseal skeletal monocultures showed negligible expression for *FLT-1*. In the basal co-cultures, expression of receptor mRNA increased significantly in diaphyseal and epiphyseal co-cultures of one patient compared to basal monoculture (Figure 3.25, patient 3). The addition of VEGF raised *FLT-1* expression levels in both diaphyseal and epiphyseal co-cultures, compared to their respective basal co-cultures. In both diaphyseal and epiphyseal co-

cultures, upon VEGF supplementation, *FLT-1* expression increased significantly in two out of three patients compared to respective monocultures (Figure 3.25, patient 1/3). However, the addition of VEGF concurrently decreased expression in diaphyseal monocultures of patient 1, thus increasing the relative difference between mono- and co-culture expression levels. In comparison, the increase in epiphyseal co-cultures with the addition of VEGF was due to an increase in the co-culture groups while epiphyseal monocultures remained unchanged upon VEGF supplementation.

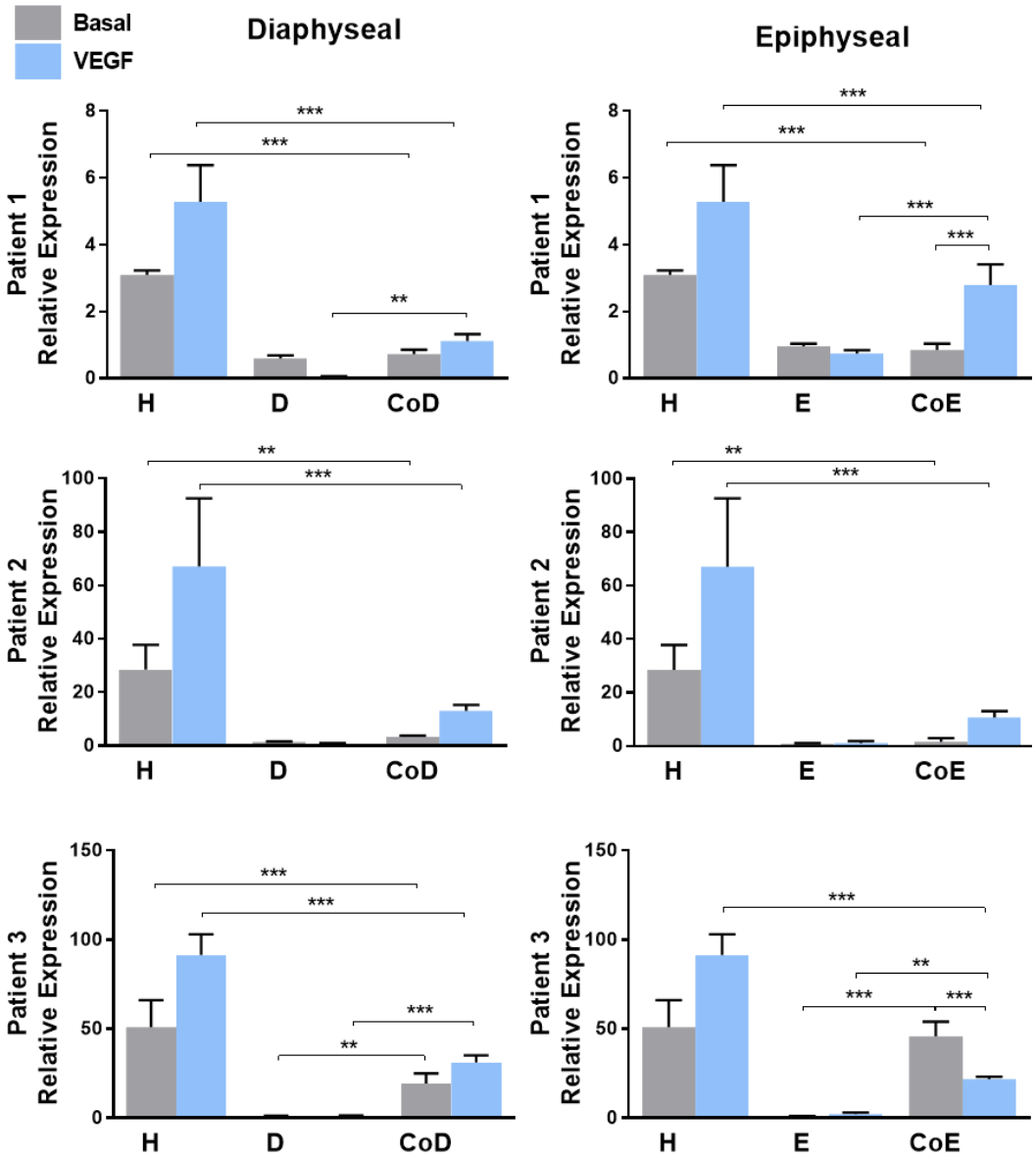

Figure 3.25. **The effect on *FLT-1*/VEGFR-1 gene expression of mono-and co-cultures supplemented with or without 50ng/ml VEGF. Graphs represent assays from 3 separate patients/experiments. Patient 1 – 3 Left**: Basal diaphyseal/HUVEC mono-/co-cultures in grey with addition of VEGF (in blue) and **Right**: Basal epiphyseal/HUVEC mono-/co-cultures (grey) with the addition of VEGF (blue). Results represent mean ± S.D; n=4 replicates; *p≤0.05, **p≤0.01, ***p≤0.001. H= HUVECs, E= epiphyseal cells, D= diaphyseal cells, CoD= diaphyseal/HUVEC co-culture, CoE= epiphyseal/HUVEC co-culture.

KDR (R2) relative expression levels of HUVEC monocultures ranged from ~70 to ~8000 in basal media (Figure 3.24 & Figure 3.26). Expression in diaphyseal and epiphyseal monocultures was negligible in all cultures. *KDR* expression in co-cultures of both diaphyseal and epiphyseal cells was substantially increased compared to their respective basal monocultures. The levels of *KDR* relative

gene expression in basal diaphyseal co-cultures increased 100-1400fold compared to diaphyseal monocultures.

Similarly gene expression in epiphyseal co-cultures between patients increased up to 2-1300fold, compared to basal epiphyseal monocultures. This was further elevated with VEGF supplementation increased *KDR* mRNA a further 2-15fold in the co-cultures, compared to respective basal co-cultures; however a 3fold diminution in expression in one epiphyseal co-culture with VEGF supplementation was observed (Figure 3.26 patient 3). Interestingly a 1.3fold reduction in KDR expression levels was observed with the addition of VEGF in the HUVEC monoculture group that demonstrated the highest expression levels in basal conditions (patient 2/3).

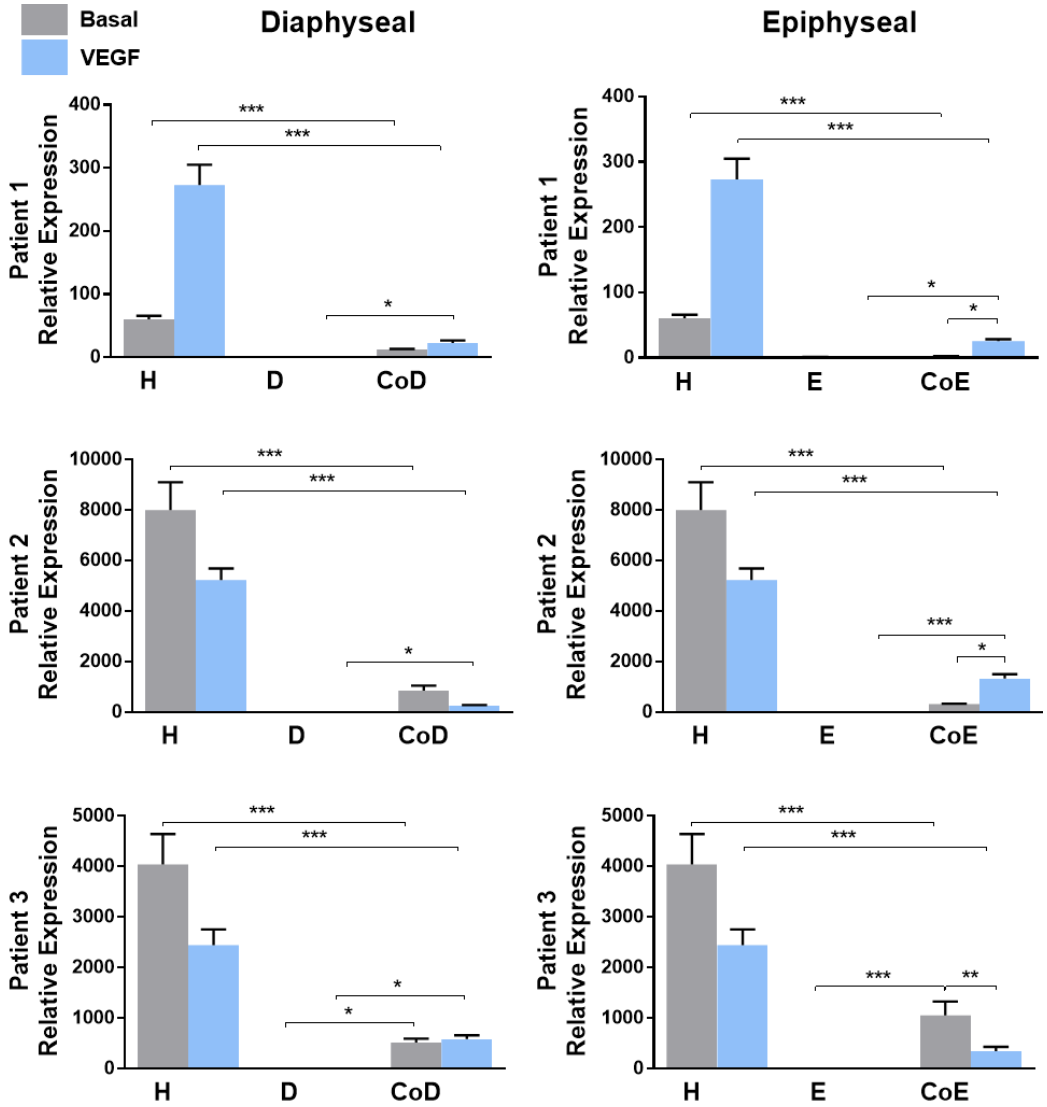

Figure 3.26. **The effect on *KDR*/VEGFR-2 gene expression of mono-and co-cultures supplemented with or without 50ng/ml VEGF. Graphs represent assays from 3 separate patients/experiments: Patient 1 – 3 Left**: Basal diaphyseal/HUVEC mono-/co-cultures in grey with addition of VEGF (in blue) and **Right**: Basal epiphyseal/HUVEC mono-/co-cultures (grey) with the addition of VEGF (blue). Results represent mean ± S.D; n=4 replicates; *p≤0.05, **p≤0.01, ***p≤0.001. H= HUVECs, E= epiphyseal cells, D= diaphyseal cells, CoD= diaphyseal/HUVEC co-culture, CoE= epiphyseal/HUVEC co-culture.

3.4.8 The effect of 100ng VEGF-165 (100ng) on *ALP* protein expression and activity in D7 mono- and co-cultures of HBMSCs/HUVECs

Following the analysis of FFDSC co-cultures with HUVECs and the effects of VEGF on osteogenic and angiogenic gene expression, the effects of adult human bone marrow stromal cells (HBMSCs) co-cultures with HUVECs, with or without VEGF supplementation, and the effects on osteogenic and angiogenic gene modulation were investigated.

Initial results with ALP culture staining demonstrated that co-cultures of adult HBMSCs with HUVECs produced enhanced ALP staining compared to counterpart monocultures. The strongest staining was observed in co-cultures following the addition of 100ng/ml VEGF compared to all other cultures. Basal HUVEC cultures demonstrated an increased proliferation with the addition of VEGF (Figure 3.27). Interestingly, in the co-cultures the cells consistently displayed a circular growth pattern and formation of thick cell bundles indicative of vessel tube-like structures, which was more pronounced with the addition of VEGF.

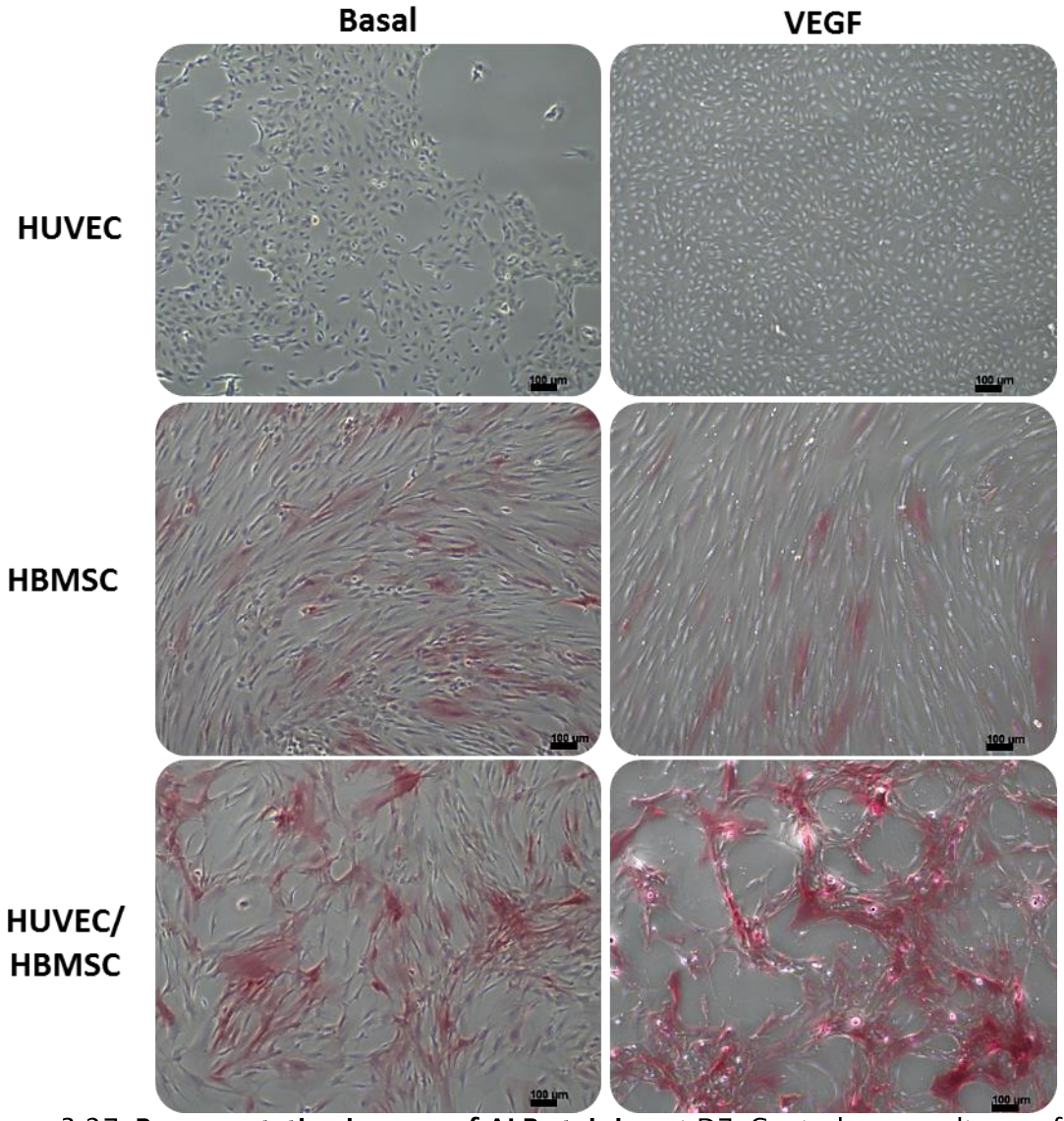

Figure 3.27. **Representative images of ALP staining** at D7. Control monocultures of HUVECs and HBMSCs; co-cultures of HBMSCs/HUVECs with and without VEGF supplementation in the cell cultures. Scale bar: 100µm

Biochemical analysis of the cultures reflected the results obtained from ALP staining of increased ALP activity in co-cultures; although this was more difficult to ascertain from the combined data graph (Figure 3.28).

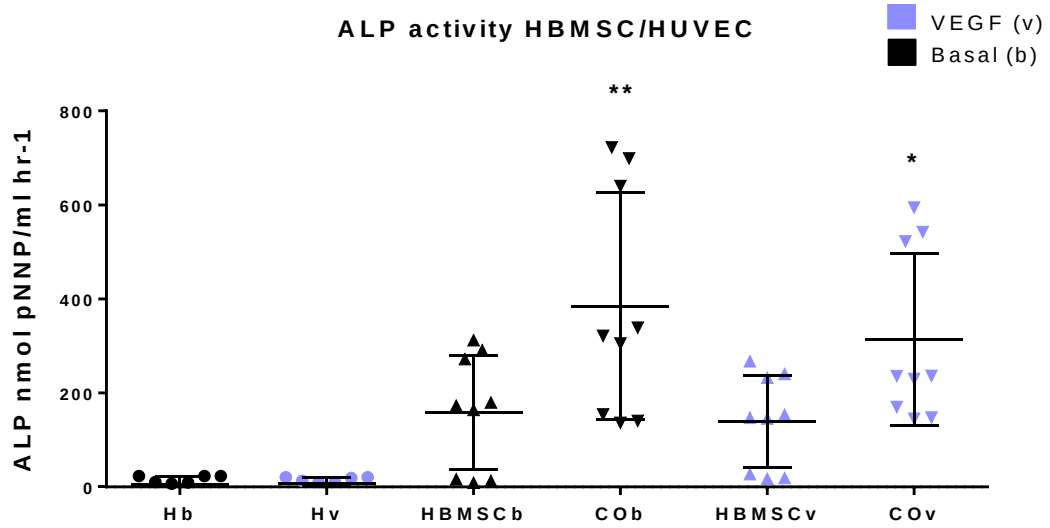

Figure 3.28. **The combined alkaline phosphatase assay data from 3 experiments**, showing overall change in levels of ALP activity of HUVECs and HBMSCs mono- vs. co-cultures in basal media and supplemented with 100ng/ml VEGF. Basal/VEGF supplemented cultures denoted with **b** and **v** (purple) respectively. Asterisks denotes significant difference between co-culture and respective skeletal monoculture. H= HUVECs, CO= co-cultures. Data presents mean ± SD, n=3 replicates; *p≤0.05, **p≤0.01, ***p≤0.001.

There was some variability in data between patients, however; this could stem from the different ages/sex of the patients and variations in cell differentiation due to *in vitro* culture (Table 2.2). A significant increase in ALP enzyme activity was observed in two out of three patient samples (patient 1/2) of the basal co-culture groups, compared to monocultures (Figure 3.29). The same level of increase in ALP activity was more or less maintained when supplemented with VEGF; however, one group that showed the highest ALP levels in basal monocultures (patient 3) compared to the other basal groups, demonstrated a marked decrease of activity upon VEGF supplementation in the co-culture. Overall, comparing the basal co-culture with the VEGF-supplemented co-culture of the same patient there was a marked decrease in ALP activity in two out of three patients (patient 1/3) and an increase in one patient (patient 2).

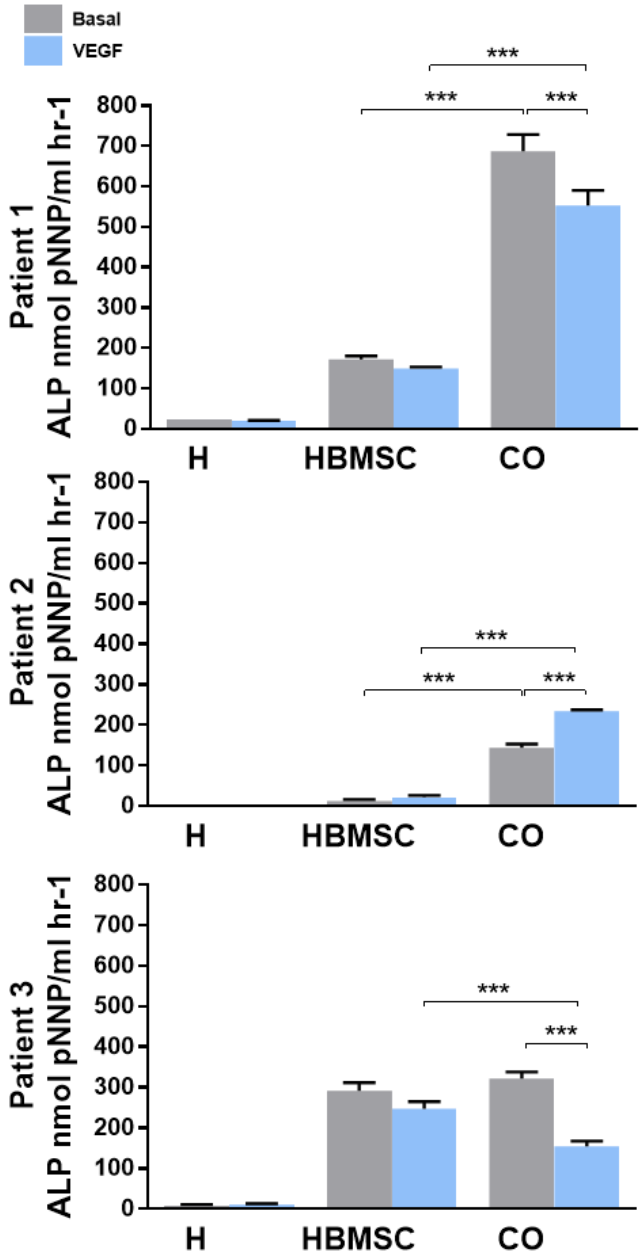

Figure 3.29. **Alkaline phosphatase activity in mono-/co-cultures**, supplemented with and without 100ng/ml VEGF. Graphs represent assays from 3 separate patients/experiments **Patient 1 – 3** in mono- and co-cultures of HUVECs (H) and HBMSCs in basal media and supplemented with 100ng/ml VEGF. Monocultures=HBMSC, HUVEC (H), Co-cultures (CO) =HBMSC/HUVEC. Results represent mean ± S.D; n=3 replicates; *p≤0.05, **p≤0.01, ***p≤0.001.

Interestingly, the ratio by which ALP activity increased between the mono- and co-cultures with and without VEGF was almost identical (Table 3.4), therefore the addition of VEGF did not have an impact on the increase in ALP over the

co-culture condition; the increase observed in the co-culture compare to their respective monocultures was of the same magnitude (Table 3.4).

Basal			
Patient	**HBMC basal**	**Co-culture basal**	**Fold increase ALP activity in co-culture (basal)**
1	172.2	687.0	**4** ↑
2	12.9	143.8	**11** ↑
3	291.6	321.9	**1** ↑
VEGF			
Patient	**HBMC (vegf)**	**Co-culture (vegf)**	**Fold in-/decrease ALP activity in co-culture (vegf)**
1	148.7	553.0	**4** ↑
2	21.4	234.0	**11** ↑
3	246.7	154.2	**2** ↓

Table 3.4. **An overview of the fold change in ALP activity** in HBMSC basal (top) and VEGF supplemented (bottom) monocultures and co-cultures (HUVEC/HBMSC). VEGF concentration 100ng/ml. Average ALP activity (measured in nmol pNNP/ml hr^{-1}) presented.

All co-cultures produced enhancement of ALP activity in basal media but one of these was not significant (Table 3.4, patient 3). All VEGF-supplemented co-cultures produced significant changes; only one of the three VEGF-supplemented co-cultures produced a significant decrease in activity, which also stemmed from patient 3 (Table 3.4).

3.4.9 Relative quantification of gene expression of osteogenic genes *ALP* and Collagen I using real-time quantitative polymerase chain reaction (qPCR) in mono- and co-cultures of HUVECs and HBMSCs supplemented with or without VEGF-165

Previous findings in this chapter (3.4.3 and 3.4.6) determined the osteogenic effect of co-culture conditions on gene expression of ALP and COL-1 and the reductive effect of the lower (50ng/ml) or higher (100ng/ml) doses of VEGF on co-cultures. In line with previous findings, the gene expression for osteogenic genes of co-cultures with adult human bone marrow stromal cells and HUVECs was performed to assess differences in expression.

Similar to previous results, a wide range of in gene expression levels of *ALP* and *COL-1* was observed between cultures, visible in the combined graphs of Figure 3.30.

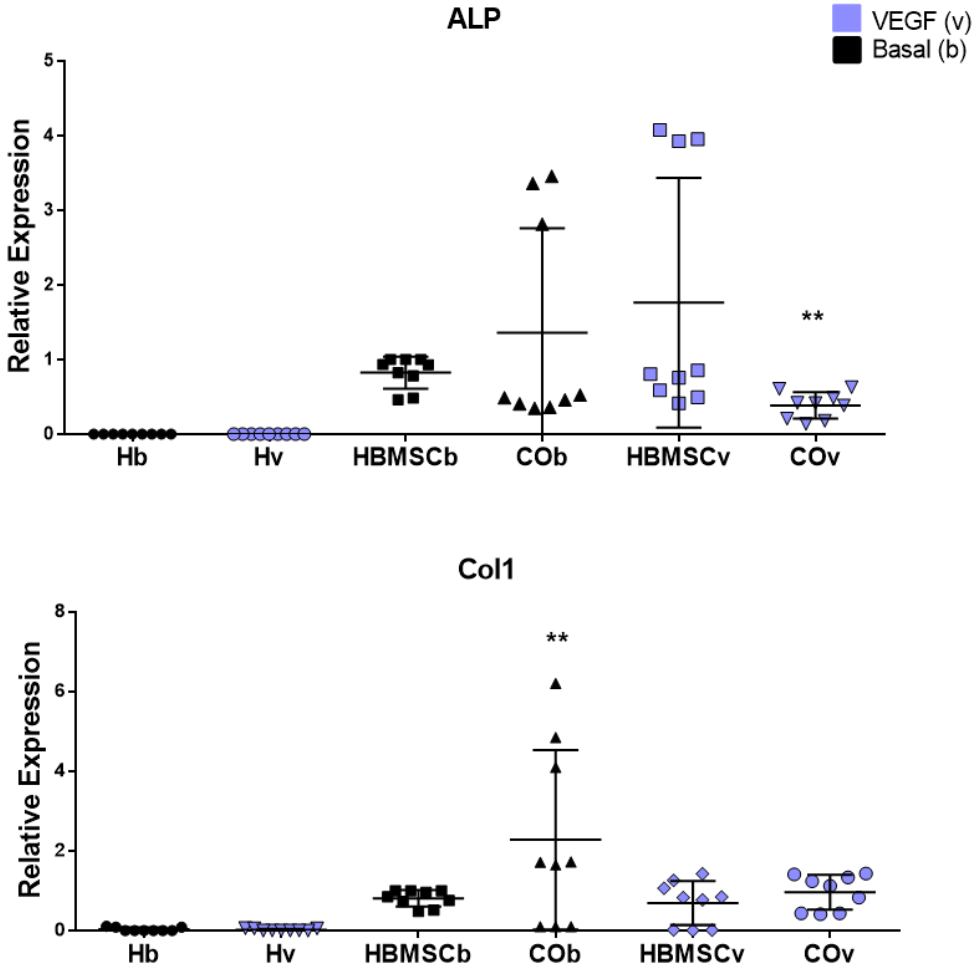

Figure 3.30. **The combined alkaline phosphatase (ALP) and Type I Collagen (COL-1) relative gene expression data from 3 experiments**, showing overall change in levels of *ALP* gene expression of HUVECs and HBMSCs mono- vs. co-cultures in basal media and supplemented with 100ng/ml VEGF. Basal/VEGF supplemented cultures denoted with **b** and **v** (purple) respectively. Asterisks denotes significant difference between co-culture and respective skeletal monoculture. H= HUVECs, CO= co-cultures. Data presents mean ± SD, n=3 replicates; *p≤0.05, **p≤0.01, ***p≤0.001.

The individual experiments produced variable results. One patient demonstrated a significant increase in *ALP* gene expression of the basal co-cultures (patient 2) that was subsequently significantly reduced with addition of VEGF; while patient 3 displayed significantly reduced *ALP* expression levels in basal and VEGF supplemented co-cultures (Figure 3.31). VEGF supplementation had a reductive effect on two co-culture groups, compared to the respective basal groups, dissimilar to the biochemical assay findings, where ALP activity was enhanced in two groups and reduced in one culture

(Figure 3.31). This, however, could be due to biochemical processes between transcription and translation and the stability of both the protein and the mRNA.

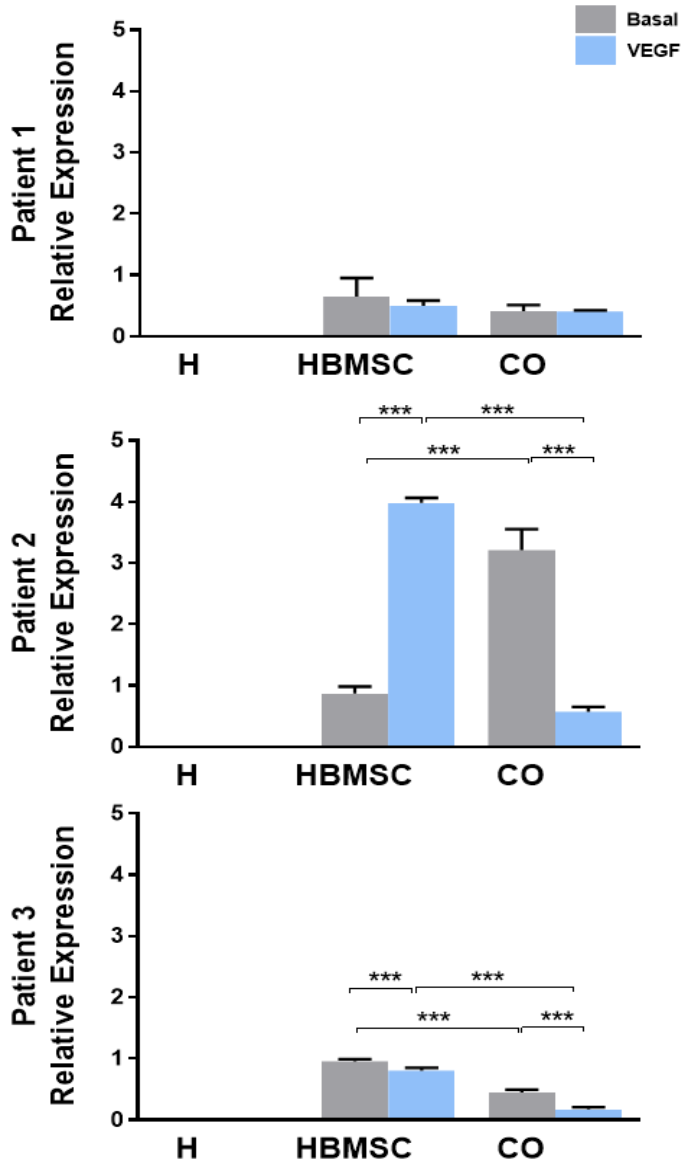

Figure 3.31. **The effect on *ALP* gene expression** of mono-and co-cultures of HUVECs and HBMSCs supplemented with or without 100ng/ml VEGF. Graphs represent data from 3 separate patients/experiments **Patient 1 – 3** in mono- and co-cultures of HUVECs (H) and HBMSCs in basal media and supplemented with 100ng/ml VEGF. Monocultures=HBMSC, HUVEC (H), Co-cultures (CO) =HB*M*SC/HUVEC. Results represent mean ± S.D; n=3 replicates; *p≤0.05, **p≤0.01, ***p≤0.001.

COL-1 gene expression equally showed variation in results, with mRNA levels being significantly elevated in two out of three basal co-cultures (Figure 3.32; patient 1/3) but significantly decreased in a further co-culture group (patient

2). The addition of VEGF decreased *COL-1* expression in two co-cultures (patient 1/3) compared to basal co-cultures. The addition of VEGF to the HBMSC monoculture of patient 2 evoked diminution of *COL-1* gene expression compared to the basal monoculture. Conversely, addition of VEGF significantly increased expression in the co-culture of the same patient (Figure 3.32 patient 2).

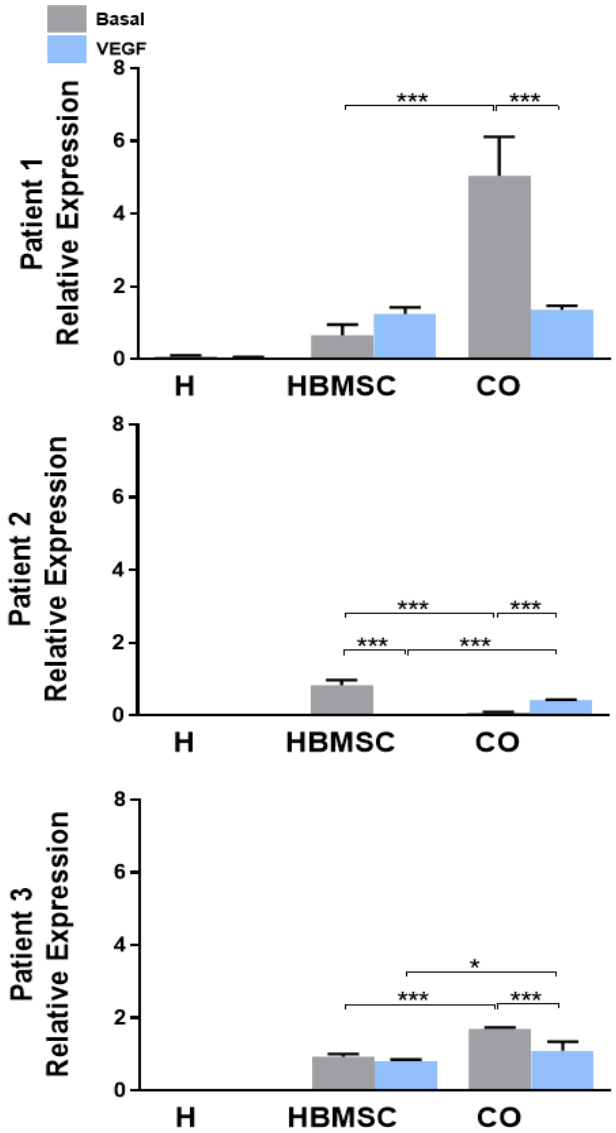

Figure 3.32 **The effect on *COL-1* gene expression** of mono-and co-cultures supplemented with or without 100ng/ml VEGF. Graphs represent data from 3 separate patients/experiments **Patient 1 – 3** in mono- and co-cultures of HUVECs (H) and HBMSCs in basal media and supplemented with 100ng/ml VEGF. Monocultures=HBMSC, HUVEC (H), Co-cultures (CO) =HBMSC/HUVEC. Results represent mean ± S.D; n=3 replicates; *p≤0.05, **p≤0.01, ***p≤0.001.

3.4.10 Relative quantification of angiogenesis-related genes during HUVEC and HBMSC mono- and co-cultures using qPCR

Following changes observed in osteogenic gene expression of HUVEC/HBMSC co-cultures, the expression of angiogenesis-related genes in mono- and co-cultures of HUVECs and HBMSCs was assessed next.

Consistent with observations earlier in this chapter (3.4.4 and 3.4.7), *vWF* and *VEGF* genes did not display significant changes in mRNA levels of the HUVEC/HBMSC mono- and co-cultures (Appendix 7.3.5-6), however similar to the results obtained in fetal cell co-cultures, significant changes in mRNA levels of VEGF receptor genes *FLT-1* (R1) and *KDR (R2)* were observed in co-cultures of HUVECs/HBMSCs (Figure 3.34).

Combined data graphs of relative gene expression (Figure 3.33) depicts the variation between the patients, concealing some of the statistically significant changes observed in the individual results (Figure 3.34 & Figure 3.35). The relative gene expression levels of the VEGF receptor genes in HUVEC monocultures were substantially elevated, compared to all other cell populations. It has to be noted that because of this, the statistically determined significance, using a multiple comparison test, suppressed some of the significant changes in gene expression, observed in skeletal monocultures relative to the co-cultures.

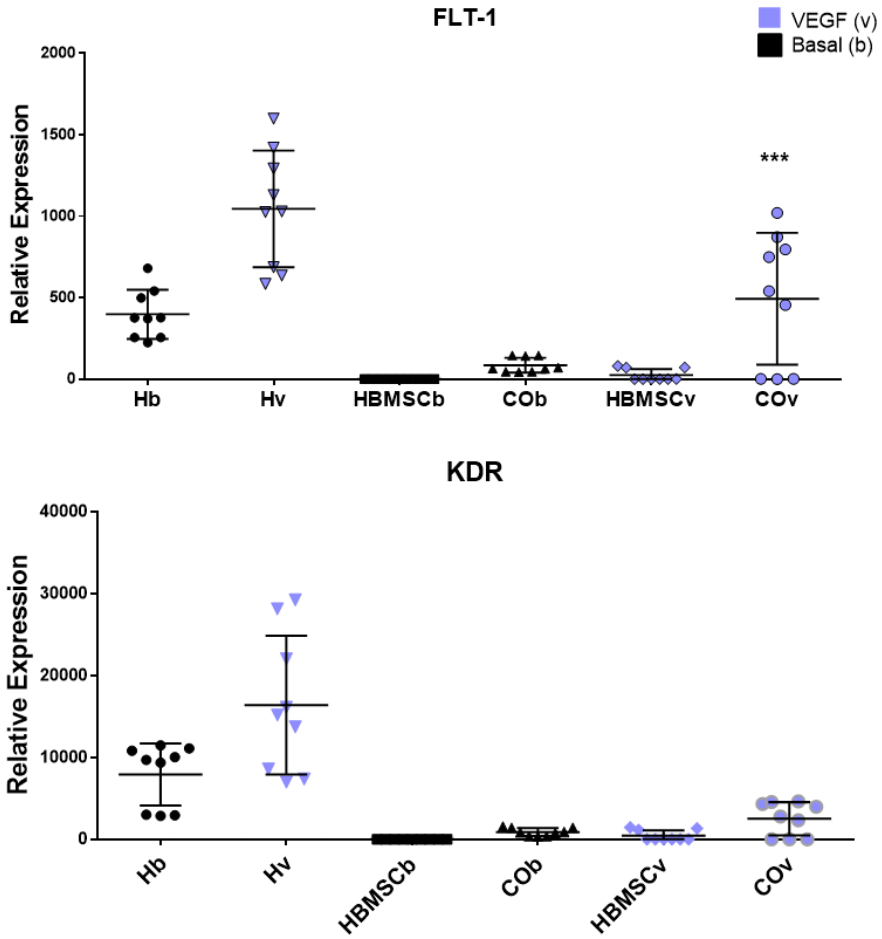

Figure 3.33. **The combined VEGF receptor 1 (FLT-1) and VEGF receptor 2 (KDR) relative gene expression data from 3 experiments**, showing overall changes in levels of gene expression in HUVEC and HBMSC mono- vs co-culture in basal media and supplemented with 100ng/ml VEGF. Basal or VEGF supplemented cultures denoted with **b** and **v** (purple) respectively. Asterisks denotes significant difference between co-culture and respective skeletal monoculture. H= HUVECs, CO= co-cultures (HUVEC/HBMSC). Data presented as mean ± SD; n=3 replicates; *p≤0.05, **p≤0.01, ***p≤0.001.

In basal monocultures, *FLT-1* gene expression was most significant in all HUVEC monocultures (Figure 3.34); *FLT-1* expression in the HBMSC monocultures was negligible but expression in co-cultures was elevated. Addition of VEGF increased *FLT-1* expression in HUVECs a further 2-3fold; and significantly elevated expression in two out of three co-culture groups (patient 1/3) with a significant reduction evident in one co-culture group (patient 2).

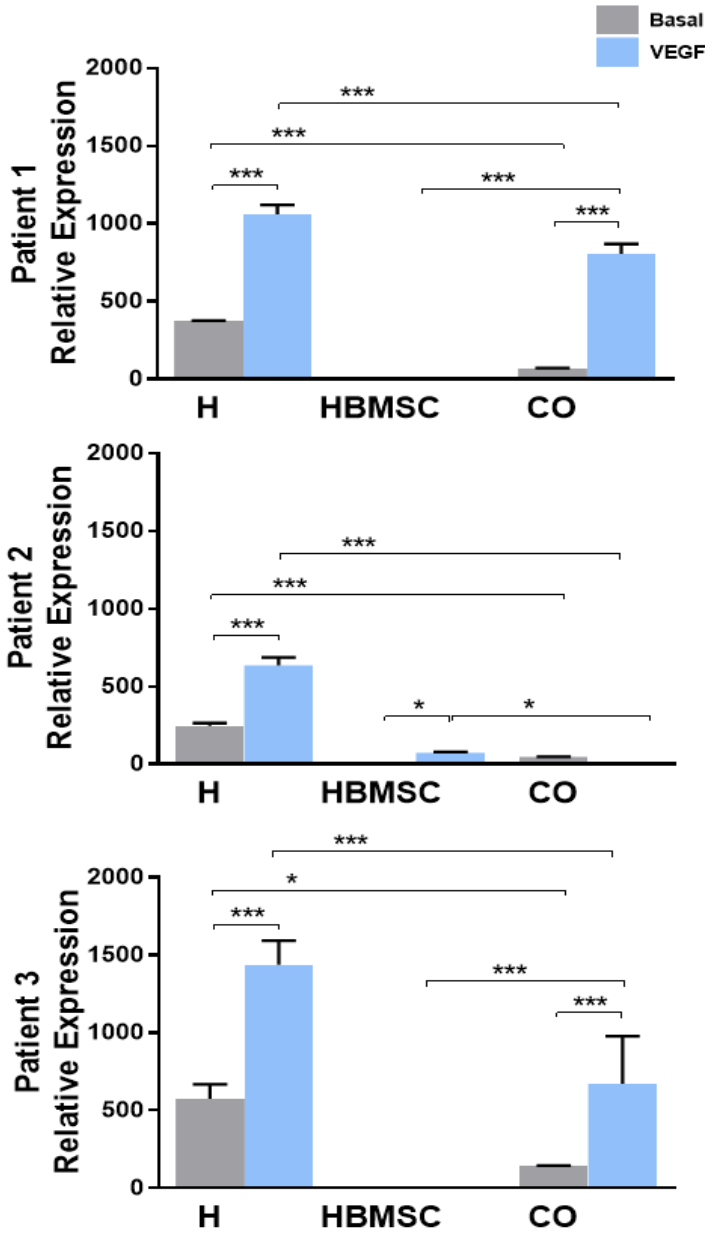

Figure 3.34. **The effect on *FLT-1*/VEGFR-1 gene expression** of mono-and co-cultures of HUVECs and HBMSCs supplemented with or without 100ng/ml VEGF. Graphs represent data from 3 separate patients/experiments **Patient 1 – 3** in mono- and co-cultures of HUVECs (H) and HBMSCs in basal media and supplemented with 100ng/ml VEGF. Monocultures=HBMSC, HUVEC (H), Co-cultures (CO) =HBMSC/HUVEC. Results represent mean ± S.D; n=3 replicates; *p≤0.05, **p≤0.01, ***p≤0.001.

KDR gene expression in basal HUVEC cultures was significantly elevated compared to all other groups, ranging from 3000-10000 (Figure 3.35). Similar to *FLT-1* expression, *KDR* gene expression levels in HBMSCs monocultures were negligibly but all basal co-cultures demonstrated increases in *KDR* mRNA. With VEGF supplementation in the HUVEC monocultures, there was a further 2-3fold

elevation in *KDR* expression levels, and a further 2-5fold increase in the co-culture groups of two patients (patient 1/3). However, a 18fold reduction of *KDR* expression was observed in the co-culture of patient 2, which was also the only group where levels of *KDR* mRNA was evident in the HBMSC monoculture, after VEGF was added.

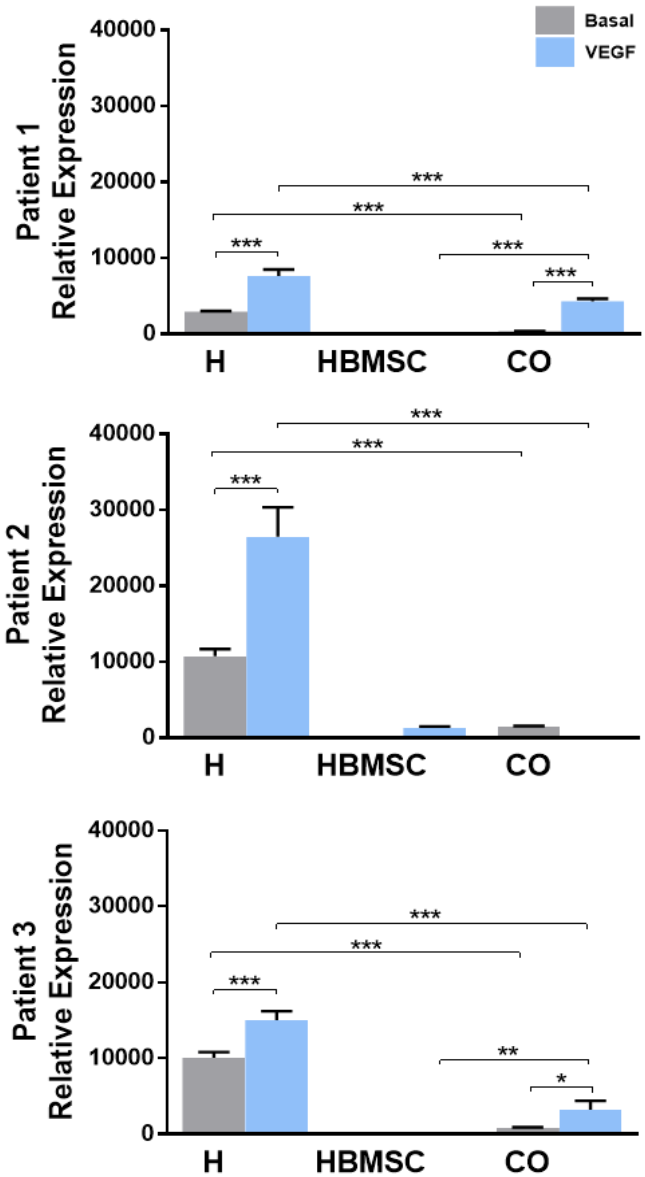

Figure 3.35. **The effect on *KDR*/VEGFR-2 gene expression** of mono-and co-cultures supplemented with or without 100ng/ml VEGF. Graphs represent data from 3 separate patients/experiments **Patient 1 – 3** in mono- and co-cultures of HUVECs (H) and HBMSCs in basal media and supplemented with 100ng/ml VEGF. Monocultures=HBMSC, HUVEC (H), Co-cultures (CO) =HBMSC/HUVEC. Results represent mean ± S.D; n=3 replicates; *p≤0.05, **p≤0.01, ***p≤0.001.

3.5 Discussion

This study has examined the combined interactive roles of human fetal diaphyseal and fetal epiphyseal cells with endothelial cells in modifying osteogenic and angiogenic responses. Furthermore, this study has compared the differentiation capacity of human adult bone marrow stromal cells (HBMSCs) when co-cultured with human endothelial cells, key cellular players in bone repair.

In essence it was hypothesised that understanding the interactive processes of the combined cell types to induce bone formation would provide novel ways to improve bone/vasculature-regeneration for translation to clinical musculoskeletal diseases

These studies have demonstrated that both human fetal femur skeletal cells and adult HBMSC co-cultured with HUVECs in the majority of patients samples examined, displayed a significant increase of the early bone marker ALP. This increase was consistently evident in basal co-cultures. VEGF supplementation frequently suppressed ALP activity and gene expression in the co-cultures of the more osteogenic-like phenotype cells, such as the fetal diaphyseal cells and the adult HBMSCs. Furthermore, these studies show supplementation with a lower dose of VEGF (50ng/ml), ALP enzyme activity was more significantly reduced. The higher dose of 100ng/ml VEGF triggered a more robust response in relative gene expression of fetal/HUVEC co-cultures compared co-cultures supplemented with 50ng/ml of VEGF; this was particularly evident in the reduced level of *ALP* mRNA in diaphyseal/HUVEC co-cultures, supplemented with the higher dose of VEGF.

Overall, the fetal epiphyseal cell populations, which typically display a more chondrogenic phenotype, demonstrated more consistent increases in ALP activity in basal co-culture but to a lesser magnitude compared to the diaphyseal cells. This was not significantly altered by the higher VEGF supplementation. The effect observed with higher and lower doses of VEGF can thus partially be ascribed to differential variations of individual cultures such

as cell phenotype, sample variation, the state of cell confluency and cell passage and variation in cell culture.

Gene expression of osteogenic markers *ALP* and *COL-1* were similarly elevated in co-culture. The addition of 100ng/ml of VEGF significantly decreased *ALP* expression in diaphyseal co-cultures; whereas supplementation with 50ng/ml (in two out of three patients) *ALP* levels triggered an inconsistent response in both diaphyseal and epiphyseal co-cultures and in one out of three, expression was decreased. Similar to the response pattern in the more osteogenic diaphyseal cell fraction, *ALP* gene expression was reduced in the adult stromal cells in response to the higher dose of VEGF. There was no consistent effect of VEGF on the skeletal monocultures, indicating that the presence of HUVECs in the co-cultures could be implicated in the effect on gene expression evidenced. These variations and somewhat unpredictable patterns in expression may also have been due to VEGF not directly acting on cells but being modulated *via* receptor action on endothelial cells and possibly the skeletal cells as reviewed by Marini et al (Marini *et al*., 2012). There were significant differences in expression of VEGF R1 and R2 in the co-culture groups; however, the gene expression of VEGF itself remained constant regardless of VEGF concentration. This may indicate a possible negative feedback mechanism maintaining VEGF levels and preventing over-induced angiogenic responses.

Given the cells isolated from the diaphyseal region of the femurs are of a more differentiated osteogenic-like phenotype than the predominant chondrogenic phenotype of the epiphyseal cells (Mirmalek-Sani *et al*., 2006; Cheung *et al*., 2014), addition of VEGF may counteract the biochemical signals present in these distinct cell populations. VEGF may induce a negative response because the system may be overstimulated by exogenous VEGF. This was observed particularly in the fetal diaphyseal/HUVEC and HBMSC/HUVEC co-cultures, where VEGF supplementation decreased *ALP* expression. It is known that within the skeletal environment, vascular cells play a fundamental role in modulating the osteogenic progression of the developing bone and in the temporal

cascade of repair mechanism following injury. Several studies have confirmed the enhanced osteogenic potential on osteoblasts in direct contact cultures with ECs (Kaigler *et al.*, 2005) (Zhang *et al.*, 2010) (Leszczynska *et al.*, 2013) (Xue *et al.*, 2009). Kaigler *et al.* also determined that ECs mediated BMP-2 signalling, which in turn enhanced BMSC osteogenic differentiation in co-culture *in vitro*. Furthermore, when co-cultured EC and BMSCs were transplanted *in vivo*, Kaigler *et al.*, observed increased bone formation. Interestingly, in line with the low expression of angiogenic genes that was observed in the current study, a significant angiogenic response was not detected (Kaigler *et al.*, 2005). More recently Leszcynska *et al.,* demonstrated that direct co-cultures of human bone-derived cells and HUVECs at varying ratios enhanced ALP activity with an up-regulation of *ALP* and *COL-1* gene expression (Leszczynska *et al.*, 2013). In a study by Zhang *et al.* 2010, it was reported that HUVEC in contact co-culture with the osteoblast-like cell line MG-63 initially stimulated cell proliferation of MG-63. The same study found significant increases in *COL-1* and *ALP* expression but these were concurrent with a decreased level of osteocalcin gene expression, a late marker of osteogenesis close to the mineralisation-stage (Zhang *et al.*, 2010).

The response of the cells in contact co-cultures of early human skeletal and endothelial cells appeared to be dependent on the differentiation state of the cells present in culture. Although the diaphyseal and epiphyseal cells are predominantly associated with osteogenic and chondrogenic phenotypes respectively, these populations are not homogenous, existing in a state of flux according to their developmental settings. This was reflected in the variability and fluctuation of expression observed in osteogenic markers *ALP* and *COL-1,* and also the lack of change in angiogenic factors vWF and VEGF across the differing patient samples within the study. It would appear that cells isolated from these femur regions, and at this stage of differentiation, are not responsive to the angiogenic stimulation of VEGF as evidenced by low levels of mRNA. Low VEGF mRNA levels may, in addition reflect a modulation *via* its cognate receptors on surrounding cells. (Marini *et al.*, 2012).

Ramasamy *et al.* (2014), postulated that bone formation is governed by a specialised angiogenic mode, implicating the Notch signalling pathway as the angiogenic pathway acting directly on osteoblasts. Disruption of Notch signalling results in impaired blood vessel formation, reduced bone formation and chondrocyte differentiation. Furthermore, Noggin (a BMP-antagonist) was able to restore these vascular and skeletal disruptions (Ramasamy *et al.*, 2014). In addition, Ramasamy and co-workers identified a subset of endothelial cells with high expression of Endomucin (Emcn) and CD31 residing in the distal arches of metaphyseal vessels of long bones, with highly expressed VEGF receptors 1, 2 and 3 residing in the bone. Hellstrom *et al.* demonstrated that distinct types of endothelial cells are involved in angiogenesis and can modulate their phenotype according to both, the stages of neovascularisation and VEGF availability. De-activation and activation of the Dll-4 (Delta-like-ligand 4) and Notch 1 pathway, respectively, was observed to switch the differential behaviour of the endothelial cells on and off resulting in a highly effective mechanism in functional and optimised blood vessel formation (Hellstrom *et al.*, 2007). As previously mentioned, the exposure and sequestration of VEGF is orchestrated mainly by VEGF receptors 1 and 2. Grellier and colleagues also observed up-regulation of *KDR* and *FLT-1* gene expression in co-cultures of human osteoprogenitors and endothelial cells. Contrary to findings in this present studies, Grellier and colleagues observed up-regulation of VEGF gene expression. Upon inhibition of *KDR* and *FLT-1*, an increase in gene expression of *ALP* and *COL-1* was shown to be abolished (Grellier *et al.*, 2009). The findings in this study demonstrated that HUVEC do not express *ALP* and *COL-1* but express both VEGF receptors abundantly whilst levels of VEGF remains constant. Therefore, any HUVEC differentiation and changes in cell phenotype would be reflected in modulatory effects on osteogenic genes and possibly VEGF receptor genes upon contact with HBMSCs and/or exogenous VEGF.

Since the vasculature does not develop in the fetal femurs until after week 10 (Nowlan *et al.*, 2007), stimulation by VEGF may be suppressed until the appropriate developmental stage is reached. VEGF receptors *FLT-1* (R1) and

KDR (R2) were strongly expressed in HUVECS, however in co-culture the range of expression levels indicated that other mechanisms modulated the levels of expression, possibly stemming from the differing function and affinity to binding VEGF of the two receptors (Waltenberger *et al.*, 1994). *FLT-1* (R1) has a soluble isoform missing the tyrosine kinase portion of the receptor and acts by binding VEGF and sequestering it (Cross *et al.*, 2003; Ferrara *et al.*, 2003). *FLT-1,* therefore exerts an inhibitory effect on VEGF signalling due to its function in restructuring and organisation of endothelial cells into blood vessels (Kappas *et al.*, 2008). *FLT-1* is also a high affinity receptor for VEGF (Wittko-Schneider *et al.*, 2013) (Koch *et al.*, 2012) (Shibuya, 2001; Ferrara *et al.*, 2003), which means that in order to exert an effect a lower expression of the receptor is required to bind VEGF. This was reflected in the lower rate of expression of *FLT-1* in the co-cultures compared to *KDR*.

VEGF mediates most of its activity through *KDR*, enhancing endothelial cell proliferation and migration and survival during blood vessel formation (Gerber *et al.*, 1999). Osteoblasts do express VEGF receptors (Tombran-Tink *et al.*, 2004) (Street *et al.*, 2009), and contact with HUVECs in co-culture may trigger the inhibition of VEGF in order to prepare the tissue for bone healing and possibly prevent bone resorption at this differential stage, which would be enhanced by VEGF (Niida *et al.*, 1999), (Street and Lenehan, 2009), (Street *et al.*, 2002). High expression levels of *KDR* (R2) and *FLT-1* (R1) in HUVEC monocultures may indicate the ECs maintaining a highly proliferative state (Sahara *et al.*, 2014), this was further increased by the addition of VEGF to the HUVECs. In contrast, HUVECs in contact with osteoblastic cells in basal media may reduce proliferation in preparation for differentiation towards mature ECs. However, the addition of VEGF switched the balance from differentiation towards proliferation, increasing VEGF receptor mRNA. Furthermore, recent work has shown the importance of endothelial cell ability to differentiate directly into skeletal cells by endothelial-mesenchymal transition (Medici *et al.*, 2012), therefore playing a subsequent role in heterotopic ossification. Moreover, it cannot be dismissed that mesenchymal skeletal progenitor cells may have the capacity to differentiate into endothelial cells (Wang *et al.*, 2013;

Wingate *et al.*, 2014) as evidenced by studies demonstrating, Rho/MRTF-A signalling pathway as a critical factor in VEGF differentiation of MSC to endothelial cells (Wang *et al.*, 2013). Reduced ALP in co-cultures upon VEGF supplementation, observed in the current study, could be an indication of the skeletal cells differentiating towards this alternative pathway.

Conclusion

The current experiments have demonstrated the intricate balances that exist in cell-to-cell interaction of different tissues. The co-culture the cell types promoted expression of early osteogenic markers and modulated *VEGF via* its cognate receptors. Furthermore, the variability in the effect of VEGF supplementation was highlighted by the down-regulation of ALP activity and the variable response observed in *COL-1* gene expression. The current studies emphasise that the environment of the originating tissue plays a crucial role in how cells respond to exogenous stimuli and will be critical when devising a co-culture or multi-factorial model for skeletal tissue regeneration. Further research is required to pinpoint the mechanisms underlying the findings obtained. These studies confirm the importance of direct cell contact as a crucial prerequisite in early osteogenesis. Further modulation of the co-culture system to deliver a facile temporal response to enable osteo- and angiogenesis and the understanding of the molecular interaction of vascular cells and associated osteoprogenitors will be crucial for future bone regenerative therapies.

In order to replicate the environment in the initial developmental patterns of bone formation and the repair mechanisms of a bone fracture, the effect of endothelial/skeletal co-cultures on the enhancement of bone formation was further examined in a 3D pellet co-culture bone defect model.

CHAPTER 4

Exploring the interactive process of 3D HBMSC and endothelial cell co-culture constructs in an osteogenic niche.

4.1 Introduction

Previous work by Mirmalek-Sani and colleagues elegantly demonstrated the multipotentiality of fetal femur-derived cells. These cells are highly proliferative and display lineage plasticity for osteogenic, chondrogenic and adipogenic differentiation (Mirmalek-Sani *et al.*, 2006). These attributes make fetal femur-derived cells a promising model to examine therapeutic strategies for skeletal regenerative studies (chapter 3.1). In related studies, El-Serafi and colleagues demonstrated that after 7-14 days of culture, developmental bone markers such as bone sialoprotein and COL-1 were expressed in pellets of fetal femur-derived osteoprogenitor and chondroprogenitor cells, in line with the developmental stage of the fetal femur. Furthermore, after 21-28 days of culture, cell pellets developed a cell-arrangement similar to the bone structure of femurs of a comparable age with an osteoid-like shell on the periphery and osteoblasts accumulating beneath the surface of the pellet. El-Serafi *et al.* further demonstrated that cells from distinct regions of the fetal femur including the epiphysis, diaphysis and hypertrophic region were capable of forming an osteoid shell, suggesting a role for the microenvironment the cells were within, being able to modulate matrix formation and lineage commitment. Thus the 3D pellet culture model offers a useful tool upon which to extend the parameters of 2D monolayer cultures to mimic the *in vivo* environment of the cells to determine the responses of a cell in a 3D *in vitro* setting (El-Serafi *et al.*, 2011).

Pellet cultures have proved to be of interest to biologists and tissue engineers, over many years, given the ability of the cells to secrete their own matrix, acting as a natural substrate and scaffold for the cells, aiding natural growth (Korff *et al.*, 1998; Akiyama *et al.*, 2006; Jaehn *et al.*, 2010; Freeman *et al.*, 2015). The aim of the current studies was to utilise previously acquired understanding from 2D co-culture studies (chapter 3) and through 3D architecture, reduce the typical limitations of 2D model systems such as spatial dynamics within cell cultures. Ultimately, the aim will be to implement this technique as a cost-effective and reliable method for *ex-vivo* tissue formation.

Previous studies (chapter 3) demonstrated FFDSCs in 2D co-culture with HUVECs displayed considerable variation in the expression of osteogenic and angiogenic genes following supplementation with VEGF-165 at 50ng and 100ng (chapter 3.4). This variability could be due in part to the developmental plasticity of FFDSC when cultured as cell monolayers.

Thus, while the use of fetal progenitor cells provides a useful tool to improve our understanding of developmental processes and interactions, the application of FFDSCs in regenerative medicine is limited by ethical and practical concerns, reviewed in (Gómez-Barrena *et al.*, 2011). To circumvent some of these issues in the current investigations, adult derived human bone marrow stem cells (HBMSCs) instead of FFDSCs were used in co-culture with HUVECs.

Ferrera *et al.* reported the enhanced capability of 3D cell structures to support continuing differentiation of osteoblasts towards the osteocyte phenotype over an extended culture period of 120 days (Ferrera *et al.*, 2002). 3D cell structures formed from pre-cultured monolayer cell sheets of human osteoblasts were cultured submerged in differentiation media (supplemented with ascorbic acid and β-glycerophosphate). 3D cell structures were analysed after 25, 31 and 48 days of culture. An array of osteogenic proteins was found to be expressed after 25 and 48 days including collagen type I, osteopontin, osteonectin, bone sialoprotein and fibronectin. Osteocalcin was detected in cell structures only at the later time point of day 48. ALP was expressed by cells at days 25 and 31 but was not detected at day 48 of culture. Furthermore, high levels of Ca incorporation were detected at day 48 of culture. Subsequent subcutaneous dorsal transplantation of cell structure into mice over a 20 day period demonstrated mineralisation of the explants in an outward progression from a sparsely cellularised core to the periphery with a multilayer of cells in a collagenous matrix invaded by host tissue (Ferrera *et al.*, 2002). In a more recent study, Freeman and colleagues observed enhanced *ALP* expression and cartilage formation in co-culture pellets of HUVECs/HBMSCs after 14 days of culture; indicating the initiation of endochondral bone formation (Freeman *et al.*, 2015). The HBMSCs were chondrogenically primed and were either cultured

alone or co-cultured with HUVECs (vascular priming). Priming of the cells, regardless of the presence of HUVECs induced cartilage formation as evidenced by production of sulphated GAG and increased *ALP* expression after 14 days, compared to an un-primed group and an osteogenic-only primed group. Interestingly, the addition of HUVECs to the co-culture significantly reduced VEGF expression by HBMSCs, indicating HUVECs negating MSCs signalling for vessel invasion (Freeman *et al.*, 2015). Furthermore, CD31 expression by HUVECs was demonstrated, together with HUVEC attachment to the cartilage template and initiation of infiltration of the cartilage by HUVECs after 1 week of culture. Crucially, rudimentary vessel formation was observed in the HUVEC/MSC co-culture pellets after 1 week (Freeman *et al.*, 2015). Goerke *et al.*, 2012, observed that co-cultures of HUVECs/HBMSCs for 1-10 days in a 1:1 ratio, supported neovascularisation. During co-cultivation, HBMSCs were induced by HUVECs to differentiate into cells with a smooth muscle/pericyte phenotype. Goerke *et al.* stipulated that in this setting, HUVECs increased smooth muscle actin expression in HBMSCs, mediated by direct cell contact and signalling via extracellular signal-regulated kinase (ERK), not by gap junction communication (Goerke *et al.*, 2012).

In the current chapter, the potential of HUVEC/HBMSCs co-culture pellets to aid bone regeneration was investigated using an organotypic embryonic chick femoral defect model (2.2.4).

4.2 Hypothesis

3D co-culture constructs of endothelial cells and HBMSCs can aid bone formation in an organotypic culture bone defect model.

4.2.1 Objective

1. To engineer 3D skeletal cell-pellet culture constructs and assess their potential to drive osteogenesis and angiogenesis using an *ex vivo* chick femur drill defect organ culture model.

To assess levels of bone formation in the chick femora, micro-CT imaging will be employed. In addition histological and immunohistochemical assessment will be performed using bone-characteristic tissue staining and antibodies indicative of osteogenesis and angiogenesis respectively.

4.3 Methods

4.3.1 3D co-culture pellets of HUVECs and HBMSCs and embryonic chick femur drill defect model.

Human bone marrow stromal cells (HBMSCs) (Table 2.3) were obtained and harvested as described in 2.2.1, and expanded to passages 1-3 in tissue culture flasks. At 80-90% confluency cell monolayers were washed with 1x PBS and incubated in Trypsin/EDTA solution to acquire a cell suspension. A total of 2.5 x 10^5 HUVECs and HBMSCs were used for monoculture pellets and 1.25 x 10^5 of each cell type HUVECs/HBMSCs for co-culture pellets (to keep pellet sizes equal). Cells were fluorescently labelled as described in chapter 2.2.7 and subsequently pelleted (2.2.5) by centrifugation in a sterile 15ml conical tube at 156g for 5min. Pellets were incubated at 37°C, 5% CO_2/balanced air under humidified conditions for 48hours.

Fertilised wild type D1, Bovans Brown chick eggs were obtained from Henry Stewart & Co., Norfolk, England. The eggs were incubated for 18 days in a Brinsea hatchmaster at 37°C in a 60% humidified atmosphere, with partial rotation programmed every hour. The eggs were opened and the chick embryo transferred to a glass petri dish and immediately culled using a schedule 1 method. Limbs were dissected from the main chick body and soft tissue removed to expose the femur. A 0.5mm metal pin was used to mark the initial drill hole in the centre of the diaphysis and a 0.9mm drill-bit was used to create a drill hole (Figure 4.1B) and as described in 2.2.9.

Cell pellets were carefully aspirated from 15ml tubes using a 1ml pipette tip and an individual pellet (Figure 4.1A) transferred to the drill defect created in the chick femurs (Figure 4.1D; Figure 4.2). Forceps were used to ease the pellet into the drill defect. Four femurs were utilised for each pellet condition i.e. HUVEC, HBMSC and HUVEC/HBMSC co-culture (CO) were transferred to an organotypic culture insert (Figure 2.3), a plastic well insert with a 30mm diameter membrane and a 0.4µm pore size (2.2.9), on which the samples were placed. The air-liquid interphase preserved the three-dimensional integrity of

the tissue, where the membrane provided a minimal amount of culture medium at the liquid/gas interface of the insert, while the tissue was exposed to air from above. Two femurs/insert were placed in each well of a 6 well plate containing 1ml/well of organotypic culture medium (Table 2.4).

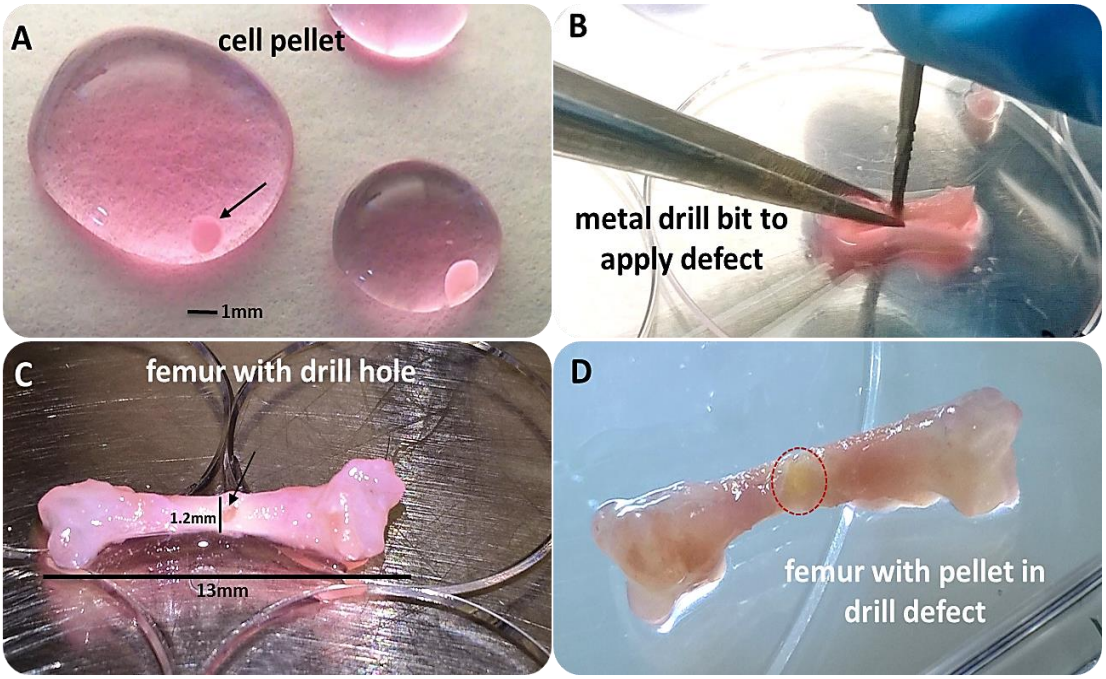

Figure 4.1. **Drill defect application and pellet implantation in E18 chick femurs**. Representative images of the preparation of E18 chick femur drill defects implanted with cell pellets for 10 day organ culture. **(A)** Cell pellets suspended in media in a petri dish prior to implantation; **(B)** Creation of drill defect using a 0.9mm metal drill bit and forceps to hold the femur in place; **(C)** Femur with applied drill defect (arrow); **(D)** Femur with pellet implanted into the drill defect (circle) prior to the 10 day organ culture period.

Femurs with created drill defect cultured in the absence of pellets served as controls. Femurs were cultured for 10 days in organotypic culture (2.2.9) with daily media changes. On day 10, the medium was aspirated, the wells were gently washed with 1x PBS and femurs were fixed in 4% PFA for at least 24 h.

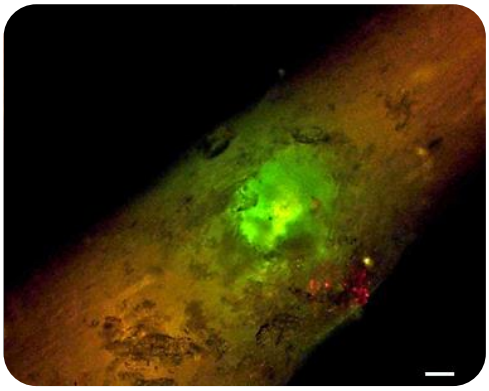

Figure 4.2. Representative fluorescent image of a cell pellet implanted E18 chick femoral defect, labelled with Vybrant™ prior to fixation at day 10 of organotypic culture. Scale bar=100μm.

4.3.2 Micro CT Analysis

Femurs were scanned prior to incubation in the organotypic culture set up, at day 0 and subsequently at day 10, using a Skyscan micro-CT machine (2.7) at a resolution of 35 microns. Each femur was contained within a sterile 0.5ml Eppendorf tube. For image analysis, CTan software (2.7) was used to set the upper and lower limits of the femur data sets (top and bottom of femur). A cross-sectional dataset of 50 image segments was applied across the region of interest (ROI), by offsetting 25 consecutive image slices either side of the centre of the defect; this was undertaken for each femur at D0 and D10. A schematic of the area comprising the volume of interest (VOI) is depicted in Figure 4.3. All datasets from D0 and D10 were analysed using the same settings (2.7). Grey scale lower and upper threshold limits were determined using Otsu averaging, a method of automatic thresholding for picture segmentation that identifies the optimal threshold for each sample. The average threshold was then normalised to a control phantom (CaHA – Calcium hydroxyapatite) (Appendix 7.4.1) with a standard density for lower (trabecular=0.25 $g.cm^{-3}$) and higher (cortical=0.75 $g.cm^{-3}$) density bone that had been scanned with the samples. The data sets of each experiment were analysed in the same batch file with the same task list. After analysis, the micro-CT data from each femur at D0 was subtracted from the D10 scan of the same femur to determine the changes in bone formation. The resulting values for change in bone volume from three separate experiments were used for

statistical analysis of variance for all femurs of the four treatment groups: HUVECs (n=12); HBMSCs (n=18) and HUVECs/HBMSCs (n=16) in comparison to no pellet control femurs (n=23). Variations in n-numbers arose due to the number of usable pellets; any remaining femurs without pellet implants were included in the control group.

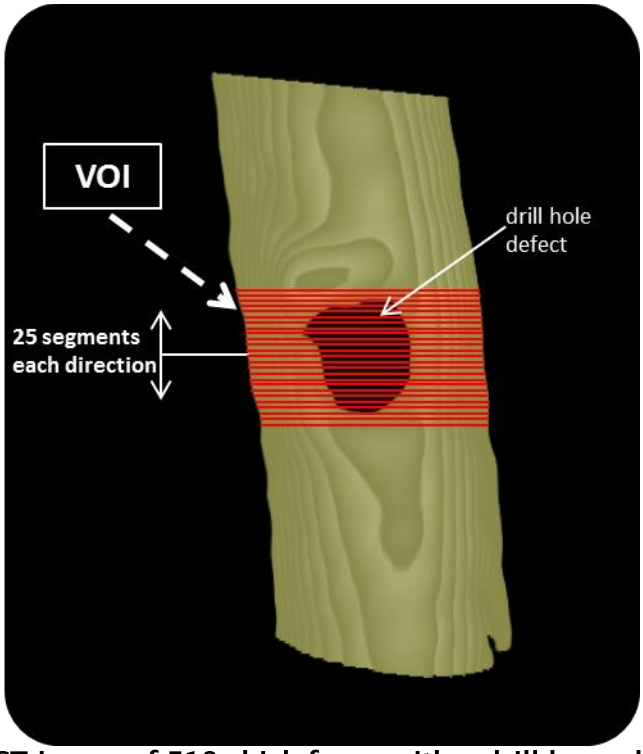

Figure 4.3. **Micro-CT image of E18 chick femurwith a drill bone defect.** Schematic of VOI (volume of interest) (dashed arrow). Up-/down arrows depict transverse segments through the bone either side of the centre of the defect (single arrow), comprising the volume of interest: 50 segments. Image created in CTvox version: 3.2.0r1294 (Bruker microCT®).

4.3.3 Histological Analysis

At the end of the organotypic culture samples and post-scanning, samples were fixed in 4% PFA for 48hrs, and subsequently processed and embedded for histological analysis as described in 2.3.1. Samples were stained for Alcian blue/Sirius red (2.3.2), von Kossa (2.3.3) and immunohistochemistry was performed using COL-1 and -2, vWF and CD31 antibodies (2.3.4) (Table 2.1).

4.3.4 Image capture

Cell pellet constructs were captured and processed using a Zeiss Axiovert 200 inverted microscope, Axiovision software version 4.7. Confocal images were kindly captured by Dr. David Johnston in the Biomedical imaging unit, Southampton General Hospital, using a confocal laser scanning platform Leica TCS SP8. Confocal images were processed using Leica Application Suite X, software version 2.0.0.14332 (Leica Microsystems).

4.3.5 Statistical analysis

Data derived from at least four replicates of 3 experiments was analysed using one-way analysis of variance (ANOVA) with Dunnett's multiple comparison posthoc test on GraphPad Prism 6 software version 6.07. *P* values ≤0.05 were considered significant. All statistical data presented as mean ± SD. Graphical representation of significance: *p≤0.05, **p≤0.01, ***p≤0.001.

4.4 Results

4.4.1 Cell Construct visualisation using fluorescent light and confocal microscopy.

The two fluorescently labelled cell types (HUVECs (red), HBMSCs (green) were clearly visible throughout the co-culture sphere (Figure 4.4), at D0 and D8, the HBMSCs were markedly visible in regions on the outside of the sphere and the HUVECs were present in distinct areas in-between the HBMSCs. At D8 of culture, the HUVECs displayed a more dominant presence throughout the outer layer of the co-culture pellet (Figure 4.4).

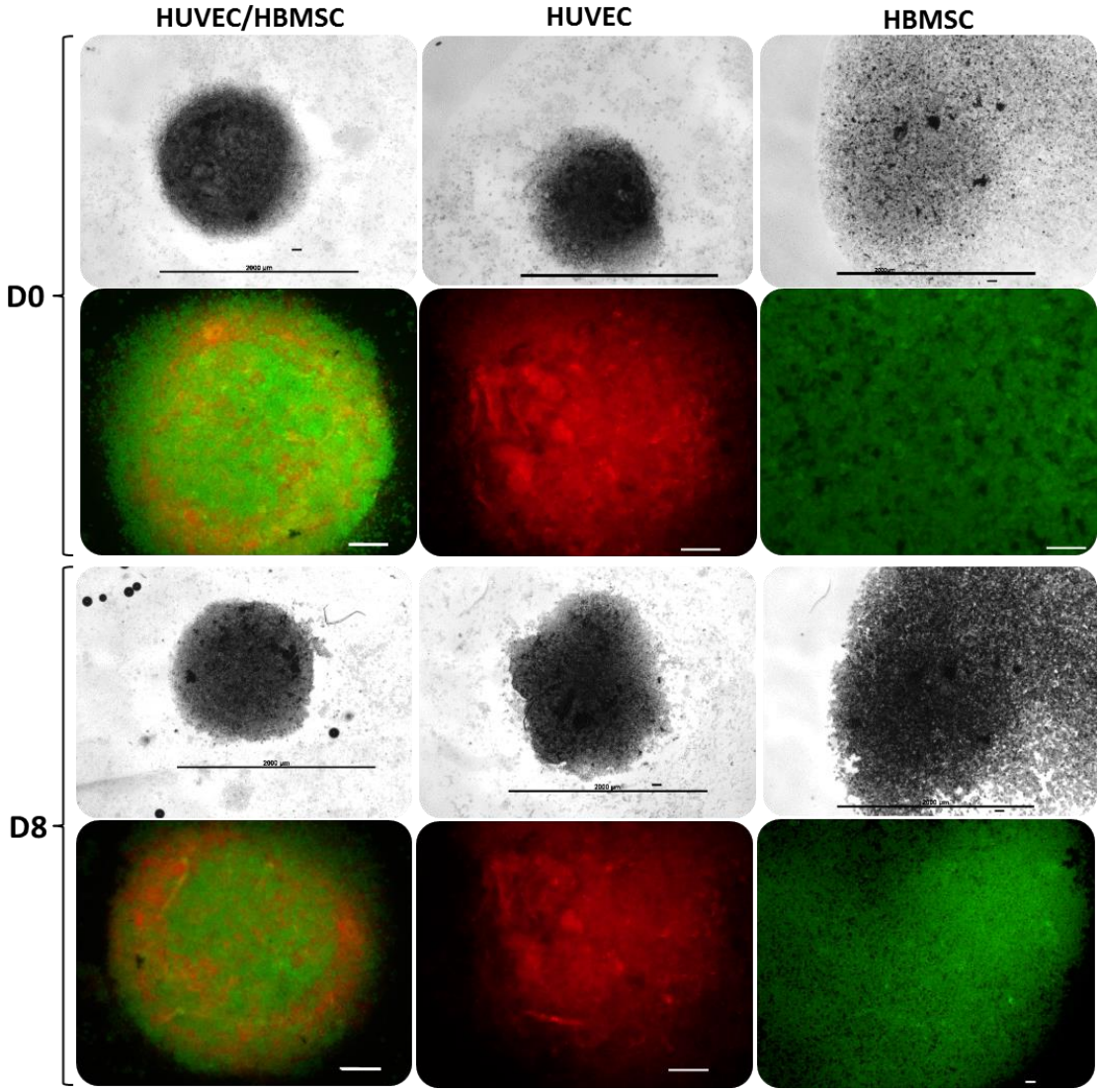

Figure 4.4. **Fluorescent and phase contrast images of cell constructs** (labelled with Vybrant™) at D0 and D8 of *in vitro* organotypic culture. HBMSCs labelled with green fluorescence (Vybrant® CFDA); HUVECs labelled with red fluorescence (Vybrant™ Dil.). The co-culture pellet (HUVEC/HBMSC) displayed a more spherical, compact shape. HBMSC pellet, atypically, was poorly formed and displayed more outgrowth of cells onto the surface. Scale bar fluorescent images: 100µm; scale bar b/w images: 2000µm.

On closer observation, confocal microscopy sequential images in Figure 4.5 (A-D) demonstrated that HBMSCs and HUVECs occupied areas of the sphere throughout the co-culture layers. HBMSCs were noted to be present in abundance at the pellet surface (A), while HUVECs were observed to emerge with increasing depth into the pellet (B-D).

Although the cell types were intermixed towards the centre of the pellet (C/D), HUVECs and HBMSCs resided within distinct compact clusters (D).

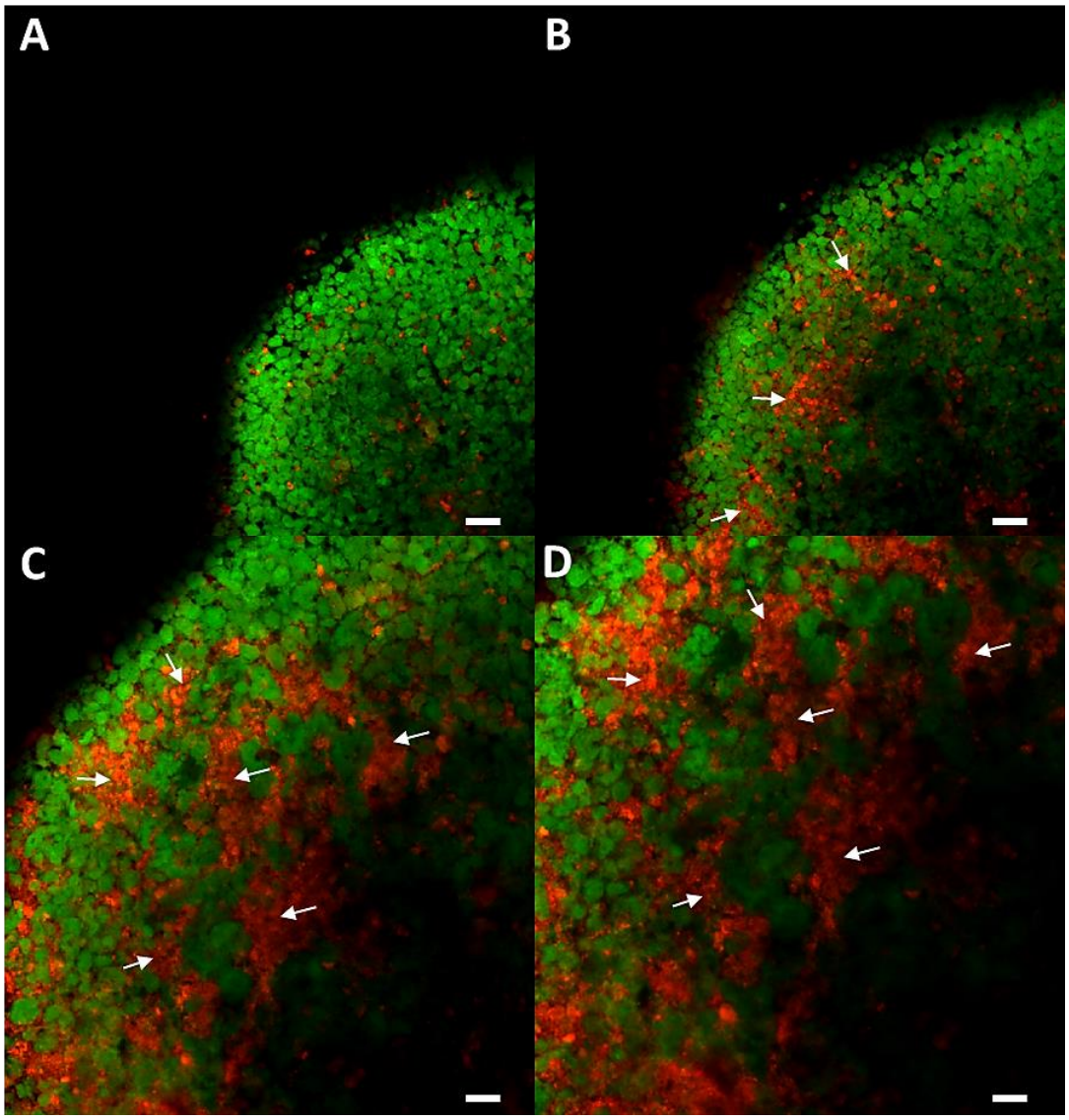

Figure 4.5. A-D. **Confocal microscopy images** of consecutive layers through a co-culture cell pellet constructs labelled with Vybrant™ Green: HBMSC, Red: HUVECs. Images showing snapshots through the cell pellet constructs at day 8 of culture from top **(A)** to bottom **(D)** with HBMSCs dominating in the outer layer **(A)** of the pellet but with increasing presence of HUVECs towards the centre of the pellet **(B-D)**; arrows depict areas of HUVEC aggregations; scale bar: 50µm.

The higher magnification images revealed the HBMSCs (green) considerably extending in length (Figure 4.6 C/D, arrows) towards neighbouring HBMSCs and forming denser cell congregations (white dashed line), while HUVECs (red) were clustered in niches in between the cell layers (Figure 4.6 A-D). There was

a notable variation in cell morphology of the HBMSCs (B, arrows), which displayed a more heterogeneous size distribution, compared to the HUVEC population.

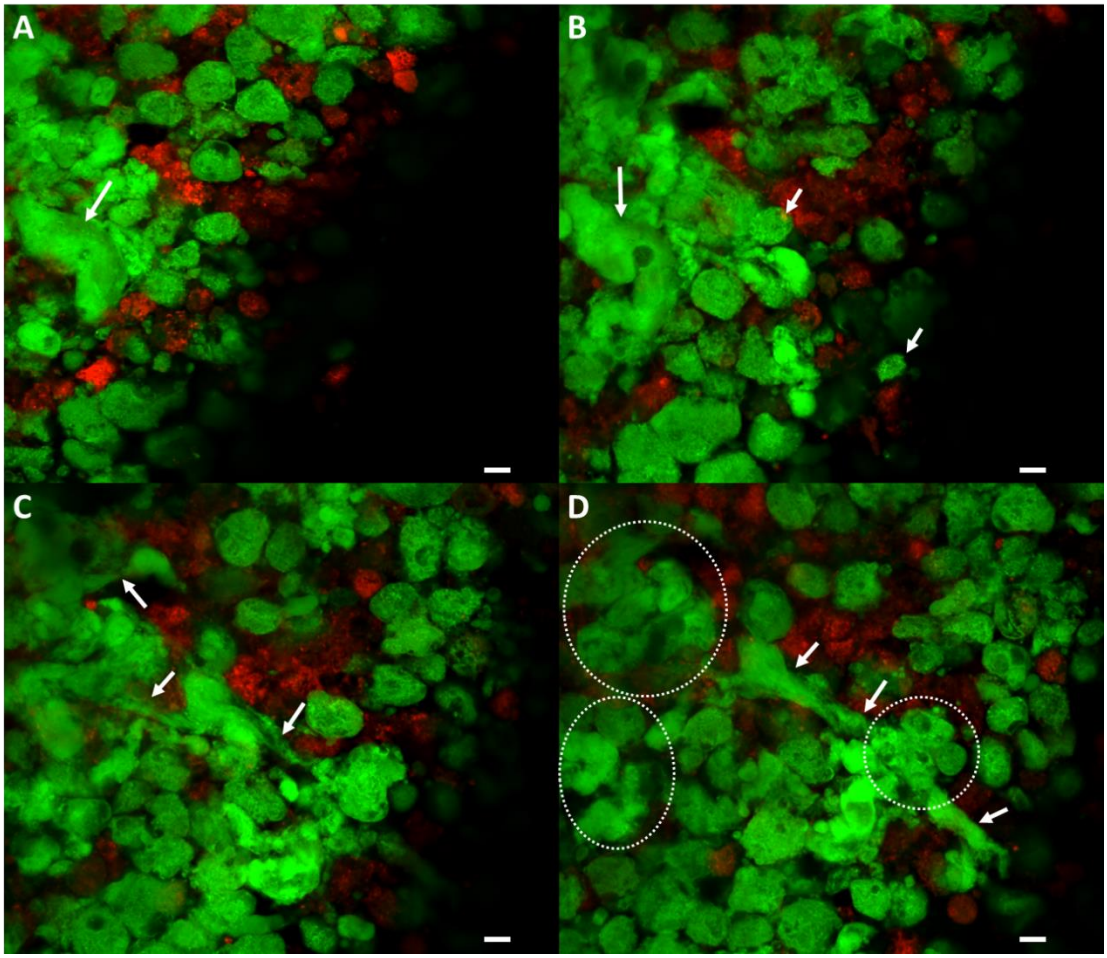

Figure 4.6. A–D. Confocal microscopy images of consecutive layers through a co-culture cell pellet constructs labelled with Vybrant™. Green: HBMSC, Red: HUVECs. Higher magnification images through the pellet, depicting snapshots of cell positions and migration within layers of the cell pellet construct at day 8 of culture; **A**/**B** variations in morphology of HBMSCs (arrows); **C**/**D** elongation of HBMSCs (arrows); **D** clusters of HBMSC aggregates (dotted lines); scale bar: 10µm.

4.4.2 Micro-CT image analysis confirms differential changes in femur bone volume and bone defect size following pellet implant

Comparative Micro-CT images of femurs at day 0 and day 10 of organ culture demonstrated a visible increase in bone density of the drill holes at day 10 (Figure 4.7). In particular HUVEC samples (B, F2, 3 and 4) and HBMSC samples

(C, F1) and in the co-culture pellet femurs (A, F1 and 2), there was a distinct visible reduction in the femur drill defects of day 10 compared to day 0.

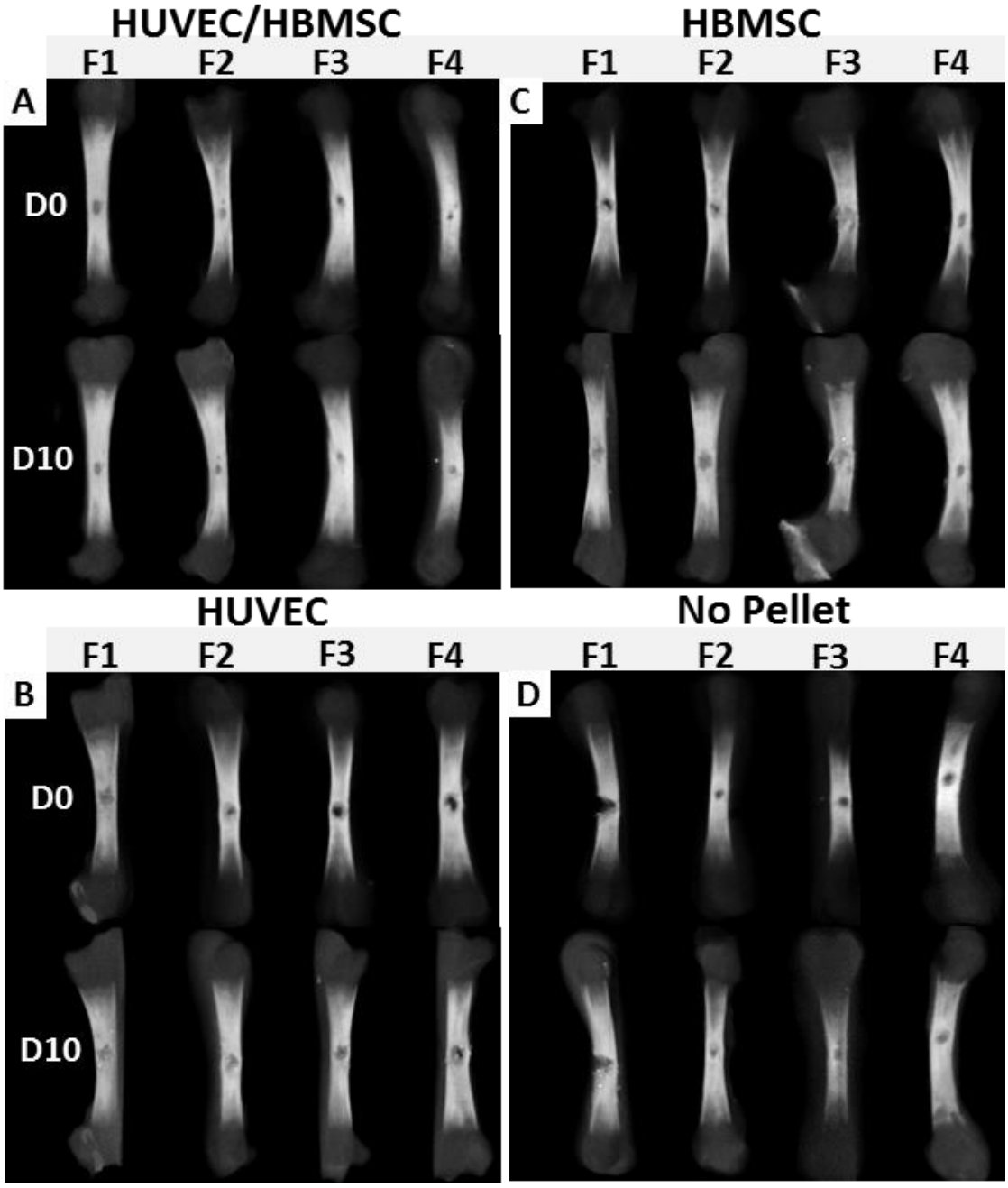

Figure 4.7. **Compararative femur defect micro-CT images at D0 and D10.** Pellet defects:**A.** Co-culture pellet (HUVECs/HBMSCs) **B.** HUVEC pellet **C.** HBMSC pellet **D.** No pellet. Femurs 1-4: F1-F4. Micro CT images created using CTvox software (Bruker) (n=4).

Figure 4.8 depicts a close up 3D image of HUVEC implanted femur B, F1. The defect size of the femur at day 10 was visibly reduced compared to the day 0 femur, with bone fragments obscuring the drill hole at D10.

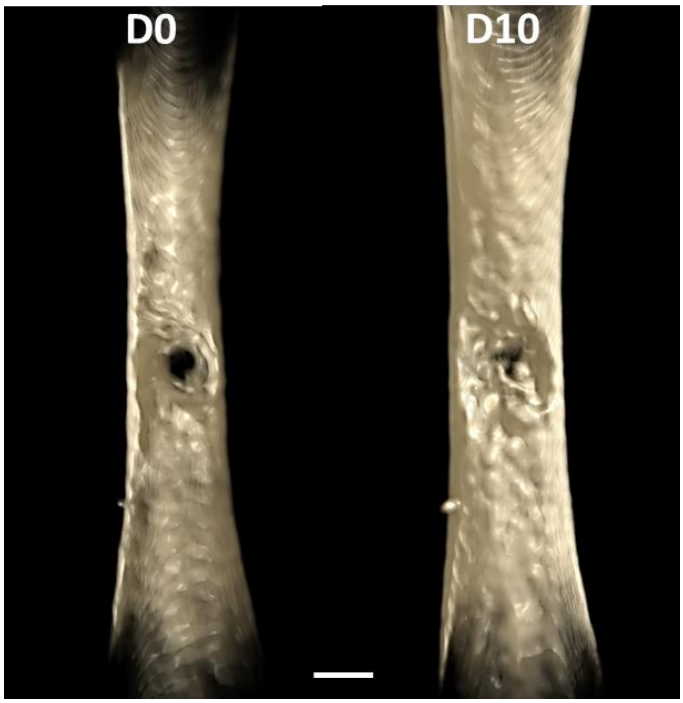

Figure 4.8. Micro-CT close-up images of femur sample with implanted HUVEC pellet (Figure 4.7B-F3) at D0 and D10 of organotypic culture depicting increased defect closure of D10 femur compared to the same femur at D0. Images created using CTvox software (Bruker). Scale bar 1mm.

Statistical analysis revealed a significant increase in bone volume (BV) and bone to tissue volume ratio (BV/TV) at D10 for all treatment groups, with the HUVEC (BV 0.42±0.21, n=12) and HBMC (BV 0.38±0.16, n=18) cell pellet treatment groups demonstrating the highest increase (Figure 4.9), compared to no pellet control femurs (BV 0.18±0.10, n=22). Note that the results for changes in BV/TV (bone volume to tissue volume ratio) depicted in the graph of Figure 4.9, demonstrated the same pattern as that of changes in BV (bone volume). The total tissue volume (TV) for each femur sample was represented by the selected volume of interest (VOI) data set (Figure 4.3), which was maintained for each sample, therefore the changes in BV/TV determined were a result of changes in BV.

Co-culture pellet implanted femurs displayed a slightly lower increase in bone volume (BV 0.32±0.17, p=18) compared to the mono-cell construct implanted femurs. The micro-CT data analysis reflected the findings of the comparative micro-CT images in Figure 4.7, with HUVEC pellet implants demonstrating the

most significant changes in bone forming parameters analysed, compared to all other treatment groups.

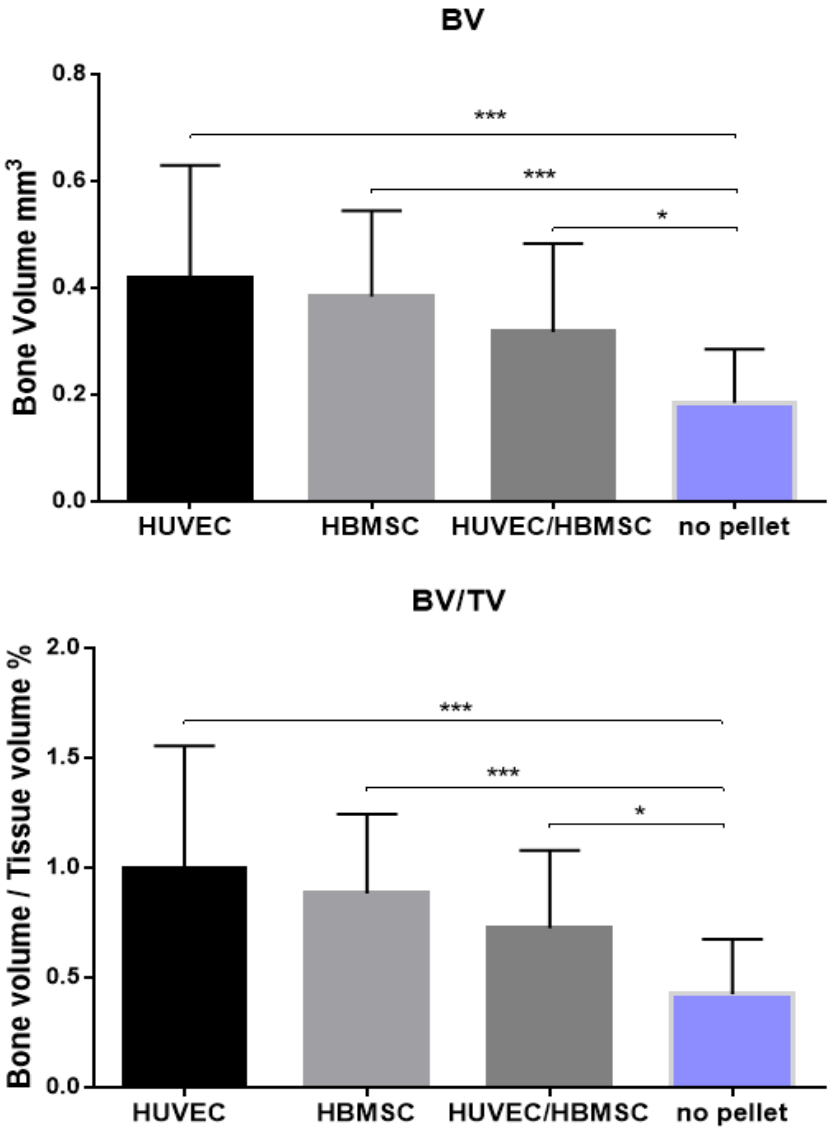

Figure 4.9. Micro CT analysis results demonstrating bone volume increase in E18 chick femurs with drill-defects with/without implanted cell pellet of three separate experiments. Bone Volume (BV) and Bone Volume to Tissue Volume ratio (BV/TV) change at D10 (normalised to D0) are shown. All treatment groups demonstrated a significant change in bone parameters over the 10 day culture period. No pellet femurs constituted controls. HUVEC pellets (n=12); HBMSC pellets (n=18); CO=co-culture pellets (n=18); no pellet (n=22). All data presented as mean ± SD. Significance set at $*p \leq 0.05$, $**p \leq 0.01$, $***p \leq 0.001$).

4.4.3 Histology

4.4.3.1 Observation of cell construct integration confirmed using Alcian blue/Sirius red staining

A/S staining revealed good integration of pellets within the drill defect of the femurs and the surrounding tissue in the majority of treatments. In contrast, negligible changes were noted in the no-pellet control femurs at day 10 (Figure 4.10).

A/S staining in the no pellet control femurs overall appeared less pronounced compared to treatment groups. There was increased collagen staining within the epiphyses (data not shown) and the diaphysis of the treatment groups compared to the controls. Noticeable thickening of the perichondrium around the defect area of the HUVEC pellet implanted femurs was observed (Figure 4.10).

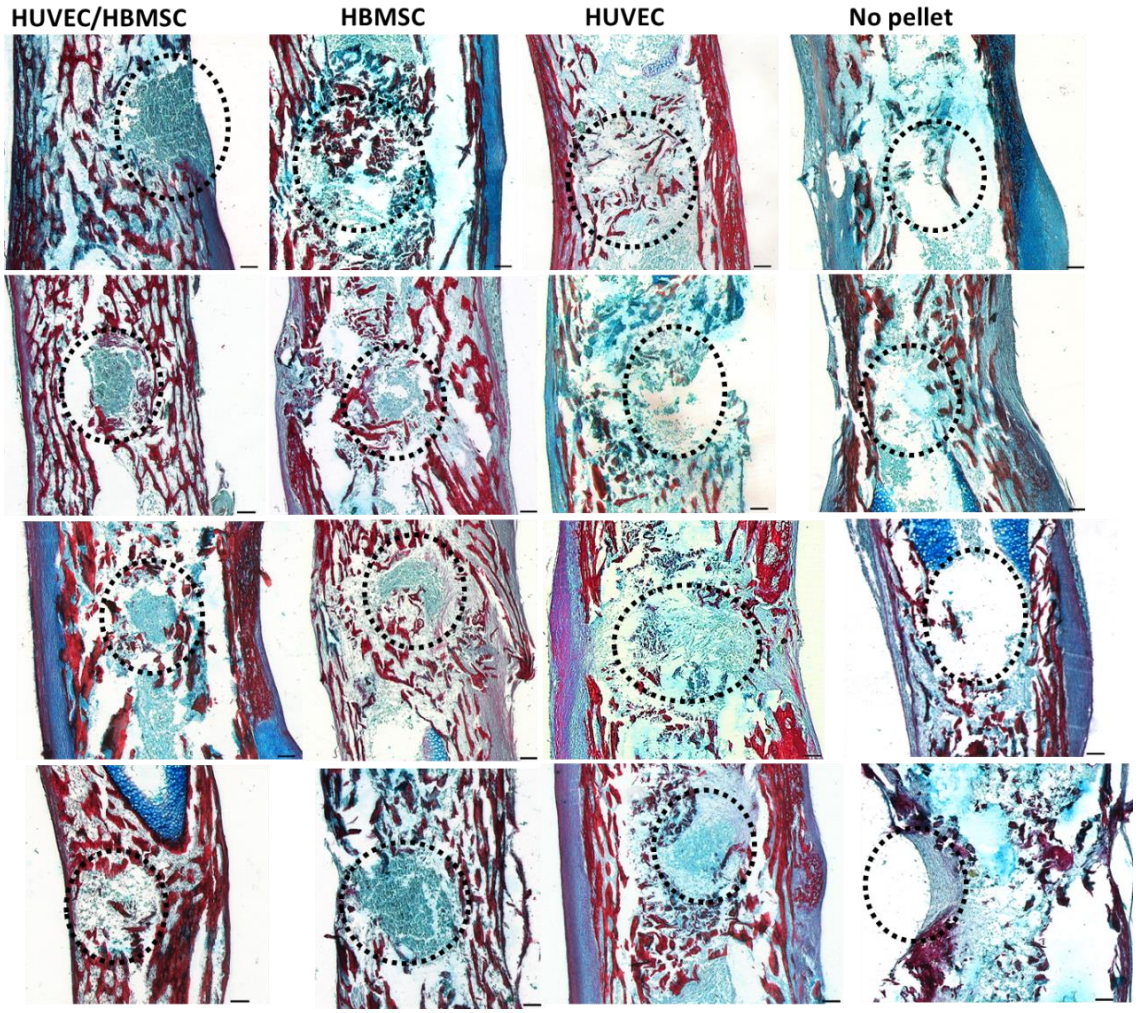

Figure 4.10. **Cell construct integration within femoral defects depicted by Alcian blue (proteoglycans) /Sirius red (collagen) staining patterns** in fetal femur defect samples. A/S stained sections of E18 chick femur pellet defects at D10 of organotypic culture. Femur drill defects containing HUVEC/HBMSC co-culture pellet; HUVEC pellet; HBMSC pellet and no pellet controls. Dotted circles depict defect area. (n=4). Scale bar: 100μm.

Within the different pellet types, there was variation in pellets retention *in situ* and in the degree of cell migration from the pellets into the surrounding tissue (dotted lines in Figure 4.11 depict pellet region). This difference was particularly evident between the co-culture and the HUVEC pellet defects (close-up images of Figure 4.11). In the co-culture pellet group, the cell pellet was predominantly compact and regions of collagen staining (red, arrows) were visible throughout the cell pellet.

In the HUVEC pellet group, the pellet was less defined, fragmented and strands of collagen fibres (arrows) appeared to surround fragments of the pellet more distinctly. Migration of cells within the interface of pellet and surrounding tissue was noted.

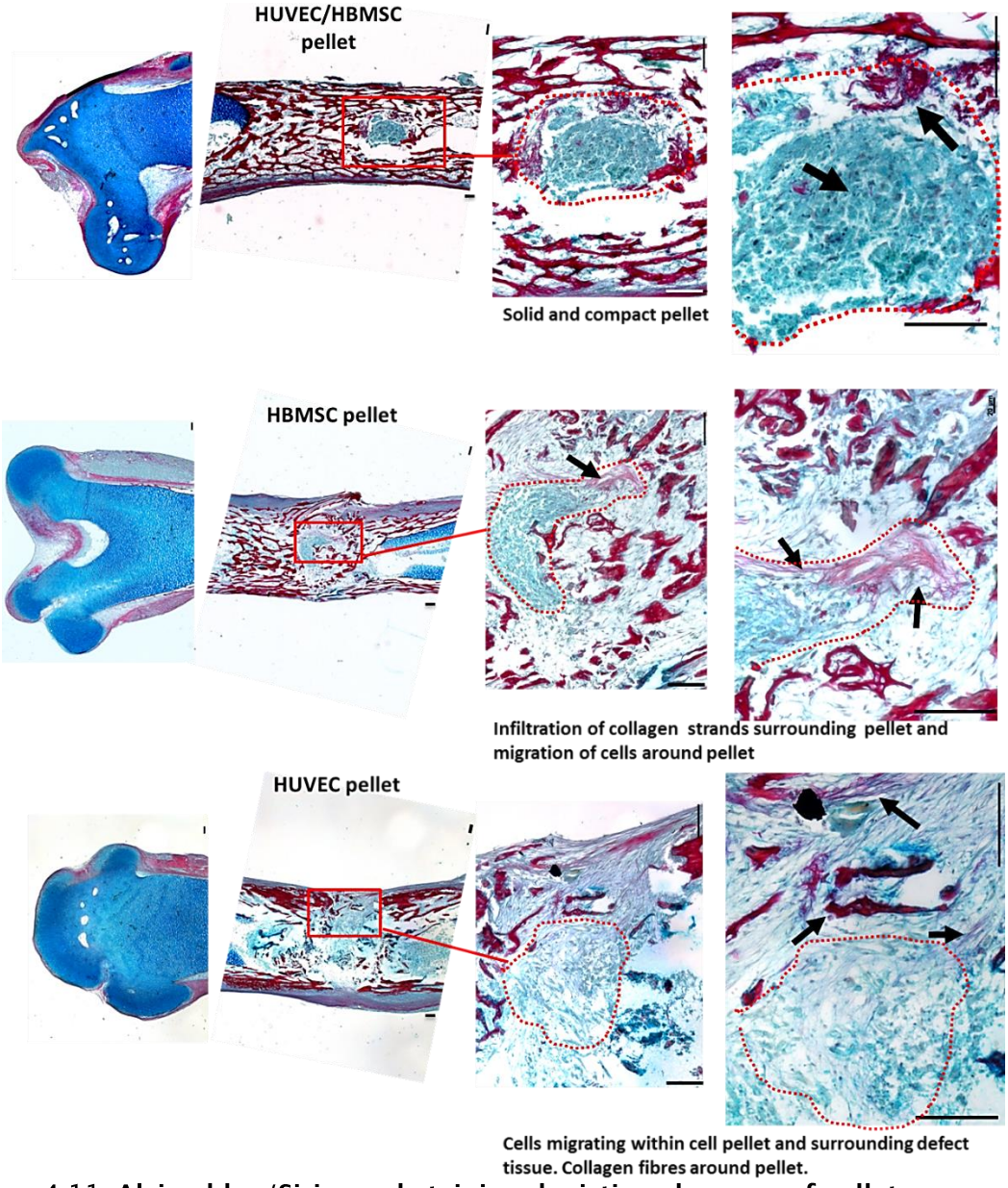

Figure 4.11. **Alcian blue/Sirius red staining depicting close-up of pellet integration.** Variation in integration of cell pellets and cell migration within defects of A/S stained E18 chick femur sections. Note compact morphology of the co-culture pellet implanted femurs compared to the less solid mono-cell pellets (dashed lines); noticeable red stained collagen fibre (arrows) extend from the HBMSC pellet to the femur trabeculae. Dotted circle depicts pellet within defect area. Scale bar: 100μm.

4.4.3.2 Enhanced Type I and Type II Collagen expression in femurs implanted with cell constructs

Control femurs (no pellet) demonstrated weak staining for type I and II collagen. Type I collagen was more strongly expressed in the bone trabeculae of pellet implanted femurs although there was no evidence of type I collagen within the pellets (Figure 4.12). Type II collagen was predominantly expressed within the co-culture (HBMSCs/HUVECs) and HBMSC pellets and within the trabeculae around the defect, whereas weaker staining was evident within the HUVEC pellets (B). In particular, the co-culture group (A) displayed robust presence of type II collagen protein within the pellet (A).

There was evidence of calcium deposition (black), evidenced by von Kossa staining in all femurs. Enhanced calcification was visible in the trabeculae of the diaphysis as would be expected, however, there was clear evidence of Calcium deposits within and around the defects implanted with HUVEC (B) and HBMSC (C) pellets, compared to no pellet controls (D), with concentric accumulations around the pellets intermixed with osteoid formation (pink). The co-culture pellets (A) displayed strong osteoid formation, with pellets firmly set within the defect. Calcium depositions were visible throughout the diaphysis.

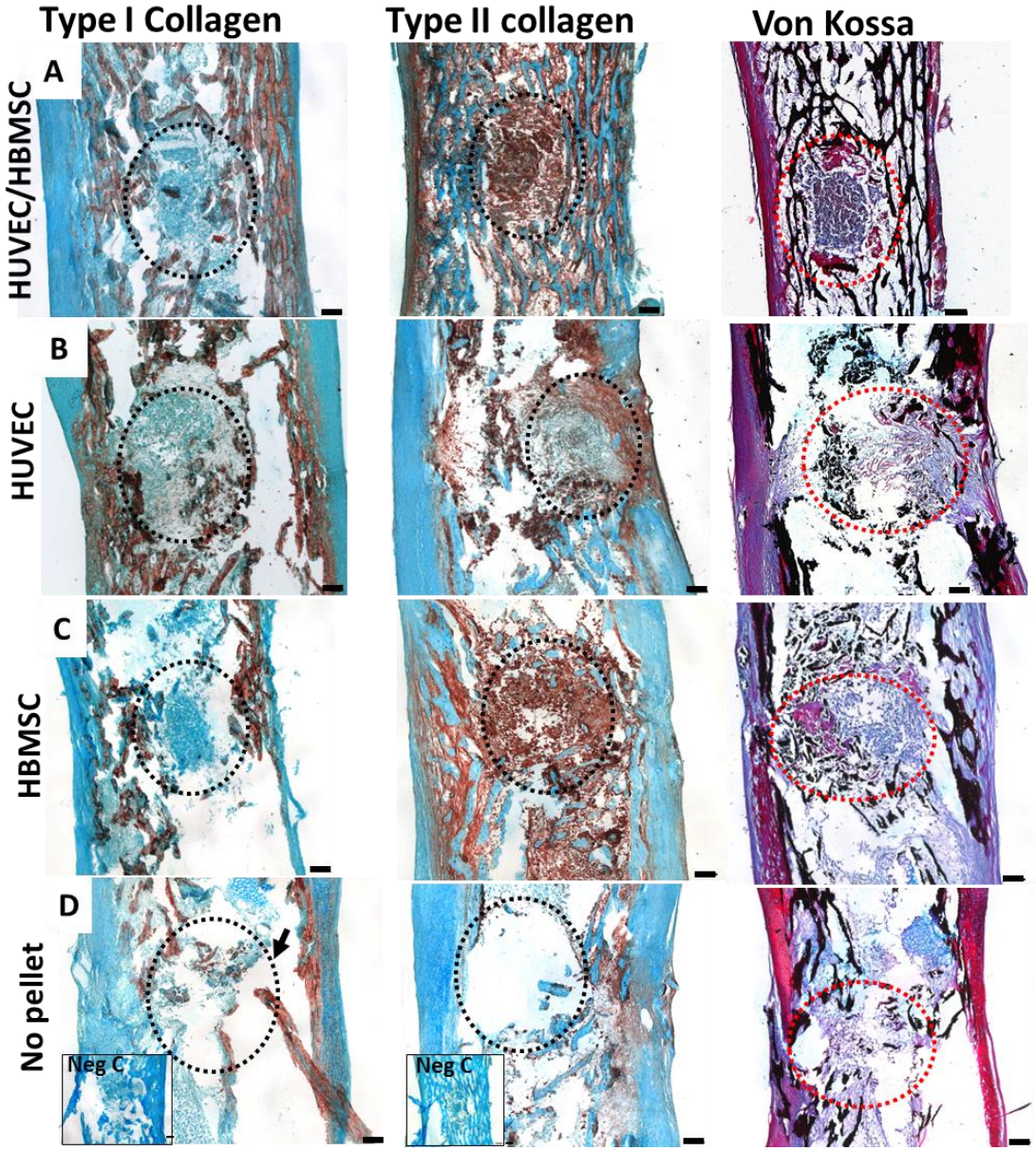

Figure 4.12. **Type I Collagen, Type II collagen immune-expression and von Kossa staining** in E18 chick femurs drill defects. Representative images of **A.** HUVEC/HBMSC co-culture pellets **B.** HUVEC pellets **C.** HBMSC pellets and **D.** No Pellet controls. Negative controls had primary antibody omitted; Calcium deposits: black; osteoid: pink. Dotted circles depict defect area. Scale bar: 100μm.

4.4.3.3 Extensive vWF expression in cell construct implanted femurs compared to controls

VWF immunohistochemistry revealed the strong presence of the VWF protein throughout pellets and defect areas, radiating into the diaphysis (Figure 4.13). The implanted HUVEC pellet displayed the strongest expression of the vWF

protein within the pellet. Expression was noted to radiate concentrically into the surrounding defect and marrow cavity (B). The co-culture femurs also showed strong vWF expression within the pellet and the remaining femur (A). However distribution was noted to be more even compared to the HUVEC group, where stronger staining was evident around the defect. HBMSC pellets (C) displayed strong staining of vWF within the pellet, although tissue around the defect was more modestly stained with presence of the protein detected in the remaining femur.

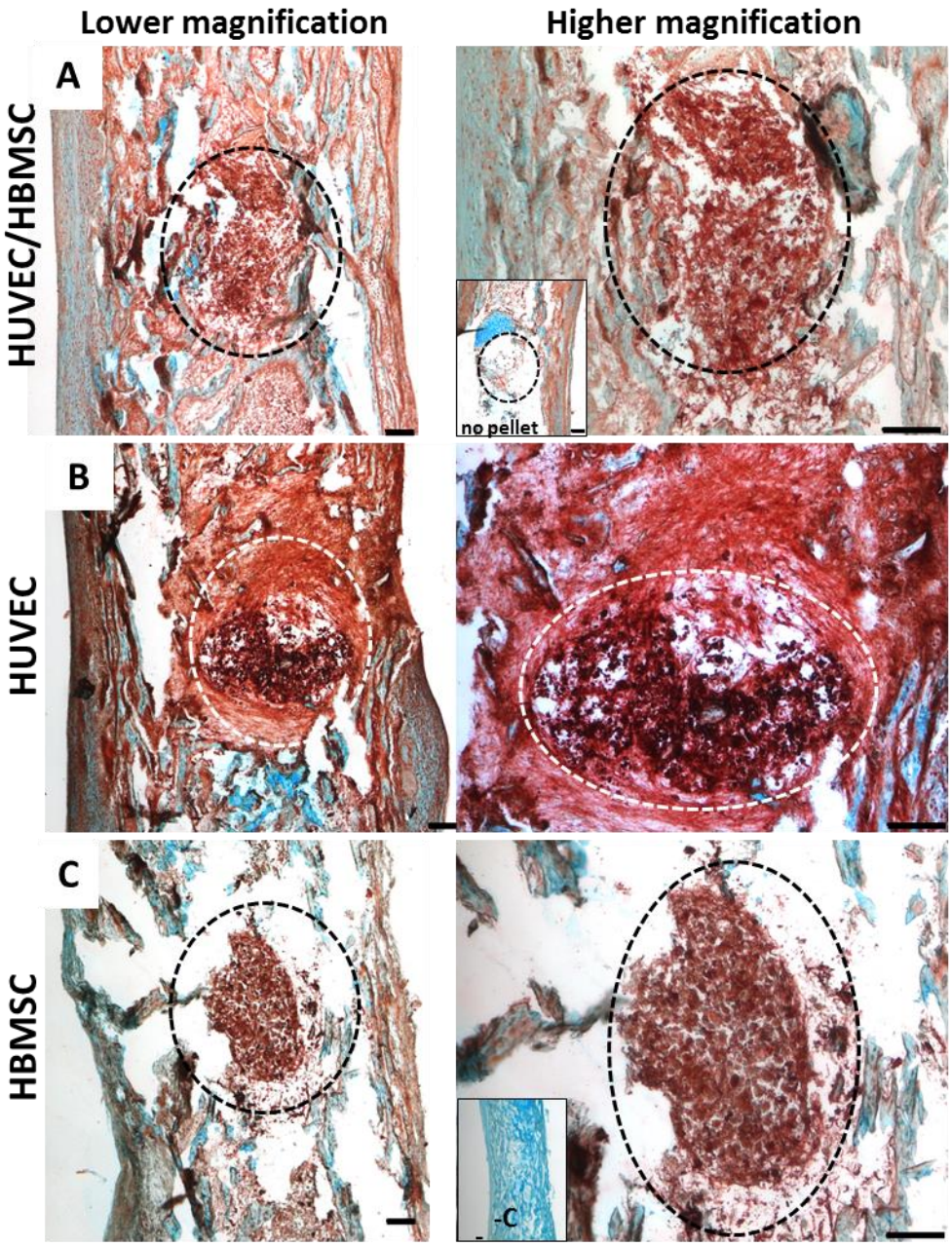

Figure 4.13. **Immunohistochemical vWF protein expression in E18 chick femur drill defects.** Representative images of femoral defects containing cell pellet implants. Defect depicted within dotted circle on the left represents higher magnification image of the same area on the right. **A.** Co-culture pellets; vWF protein present throughout the diaphysis and distinctly within the pellet; **B.** HUVEC pellets; sustained vWF presence within and around the pellet; **C**. HBMSC pellets; intense vWF staining predominant within the cell pellet; negative control had primary antibody omitted (-C) and no pellet control (with A) demonstrating unremarkable staining pattern throughout bone trabeculae. Scale bar: 100μm.

4.4.3.4 CD31 presence confirms distinct HUVEC aggregates throughout co-culture cell constructs.

CD31 expression was most evident within the HUVEC implanted femur (Figure 4.14B, arrows). CD31 expression was strongly visible as a thick band of periosteal tissue arching across the previous defect opening, suggesting migration of the endothelial cells into areas of repair within the bone (B, right). Furthermore, CD31 positive cell clusters were also visible in areas surrounding the defect of HUVEC implanted femurs.

The co-culture cell pellet (A) contained distinct elongations of robust CD31 expression (arrows), indicating cell aggregations of HUVECs within the pellet. There was evidence of CD31+ve cells in the epiphysis of the femur (A/C, right) and a structure within the cartilage reminiscent of the columnar arrangement of chondrocytes, typical of an early forming growth plate (A).

The HBMSC pellet group showed negligible CD31 expression in the defect area (C). Within the diaphyseal region, limited expression was present in the periosteum and in the marrow cavity. There was strong evidence of CD31 expression in the epiphysis, within the cartilage tissue and appearance of lumen like openings within the cartilage lined with cells positive for CD31 (C, right).

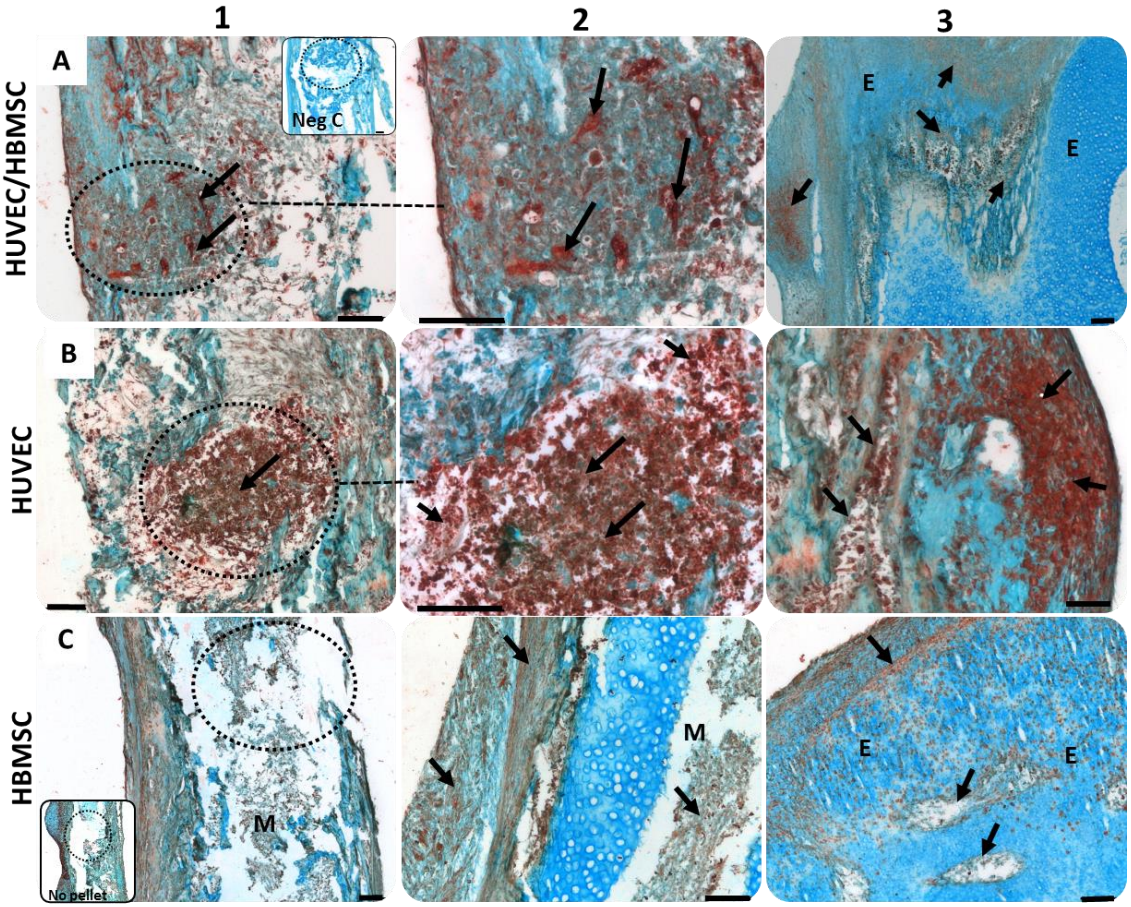

Figure 4.14 A–C. **CD31 expression in mono- and co-culture pellet/defects** Representative images of Immunohistochemistry for CD31 (PECAM-1) expression in E18 chick femoral drill defects with A–C, each row represents images of one femur for each treatment. **A.** HUVEC/HBMSC co-culture pellets **B.** HUVEC pellets and **C.** HBMSC pellets; negative control (Neg C), where the primary antibody was omitted (with **A**, left) and no pellet defects (with **C**, left). A/B 1–2 Dotted circle depicted defect area in 1 at higher magnification in 2. A3 and C3 depict CD31 positive staining within the epiphysis of femurs. B3 depicts the periosteum adjacent to the bone defect area. Circles depict defect area. Arrows depict positive staining. **E**=Epiphysis; **M**=marrow cavity. Note the dense tissue (B, right) infiltrated with CD31 positive cells, completely bridging the defect entry at the periosteum of the femur. Scale bar: 100μm.

4.5 Discussion

This study has examined the use of 3D ex-vivo organotypic femur defect cultures to emulate *in vivo* conditions to study the efficacy of the co-culture of endothelial and HBMSC constructs in these niches. Using micro-CT imaging, there was significant bone formation in an E18 chick femur drill defect model, where co-culture and monoculture pellets were used to bridge/repair a drill-hole defect. Surprisingly, the most significant increase in bone forming parameters BV and BV/TV were observed in defects implanted with HUVEC and HBMSC monoculture pellets. Although parameters for bone formation were significantly increased in all three treatment groups, contrary to expectations, the co-culture pellet model did not produce the largest increase in BV and BV/TV compared to the mono-cell pellets.

Enhanced osteogenic differentiation has previously been reported using HBMSC pellets with evidence of increased mineralisation and improved bone regeneration (Jaehn *et al.*, 2010). Equally enhanced bone regeneration has been reported following the application of chondrogenically differentiated pellets grafted into rat non-union defects, with the aim to induce endochondral ossification. The pellets showed evidence of mineralisation and the presence of hypertrophic chondrocytes after 7 and 14 days of implantation (van der Stok *et al.*, 2014). The present study surmised that the individual culture pellets were signalling to cell types residing in the bone defect to induce recruitment of cells and repair. As two major cell types were already present within the co-culture group, the activation of the surrounding tissue was not as reactive and hence, may explain why less repair was observed.

Histological staining using A/S revealed migration of cells, possibly stemming from the marrow cavity and periosteal region of the chick femur surrounding HUVEC and HBMSC mono-cell pellets within the defect. This was in contrast to the co-culture pellet group, which displayed a distinct and compact cell formation within the defect; seemingly reducing migration and integration into the surrounding bone tissue. Bone defects that contained implanted HUVEC pellets overall contained a more heterogeneous appearance with greater cell

mobility, visible around the peripheral defect tissue and invasion of cells from the chick femur appearing to migrate into the defect. In particular, vWF and CD31 protein expression was strongly associated around the defect area of HUVEC pellets compared to all other treatments, suggesting the HUVECs within the pellet, trigger the release of vWF either directly or *via* signalling molecules onto the surrounding cells/tissue. Von Kossa staining confirmed calcium deposition around and within the defect area in both the HUVEC and HBMSC implanted pellets particularly. In contrast, calcification in the co-culture pellet femurs was more evident in areas throughout the femur, although, interestingly, not at the original implant defect site.

These findings suggest that the HUVECs and HBMSCs have an important role in the migration into- and possibly the recruitment of cells from the surrounding regions of the defect area. In a co-culture pellet setting both cell types, in the first instance, interact primarily with each other, evident in the dense 'plug'-formation and lack of migration within the co-culture pellet defects. One reason for this could be the close proximity of the two cells types and that biochemical exchange and matrix formation was more localised. Thus, more resources were expended by cell-to-cell communication within pellets themselves, rather than through communication with the surrounding cells at this point. In a study by Korff *et al.*, the number of inter-endothelial cell junctional complexes was said to increase significantly in co-cultured spheroid constructs of endothelial and smooth muscle cells, visible at endothelial cell junctions (Korff *et al.*, 2001). HUVECs in contact with HBMSCs within the pellet may have equally produced increased intercellular junctions accounting for the compact structure of the pellet complex and lack of migratory activity. However, it would be interesting to see if and how these interactions change over a longer culture period and with the addition of growth factors.

Saleh *et al.* 2011, co-cultured HUVECs and MSCs over a 7 day period in a 1:1 ratio as spherical pellets and observed self-assembly of the cells into organised structures of cell-specific segregation within the sphere. HUVECs were noted to assemble at the periphery of the pellet. CD31 immunostaining of the co-culture pellets revealed distinct CD31 positive islands within the pellets

and over time, HUVECs formed substantial networks within the structure (Saleh *et al.*, 2011). Similar to these findings, the current study observed small aggregates of CD31 positive staining within the co-culture pellets, reminiscent of primitive vascular structures. When cultured osteogenically, Saleh *et al.* observed significant elevation of ALP staining. However, HUVECs also inhibited proliferation of MSCs in the co-culture pellets (Saleh *et al.*, 2011). This could explain the findings in the current study of the co-culture pellets remaining distinctly within the defect region.

Rao *et al.* devised a dual-phase, osteogenically pre-differentiated microbead-constructs of collagen/fibrin/hydroxyapatite containing HBMSCs, encompassing co-cultures of undifferentiated HBMSCs and HUVECs. Rao and colleagues observed no improvement in vascularisation and inhibition of ectopic bone formation after 4 and 8 weeks after implantation into mice, compared to controls. However the mechanisms for these observation were unclear (Rao *et al.*, 2015). Conversely, van der Stok *et al.* found that using chondrogenically differentiated MSC pellets resulted in significantly more bone formation than using undifferentiated MSCs, although this was found to be donor-dependent. The chondrogenically differentiated MSCs were said to be able to initiate endochondral bone formation in rat implants and in addition osteoclast-mediated degradation was observed (van der Stok *et al.*, 2014).

The current study suggest that the co-culture conditions within the pellet construct could have had a similar effect as priming the cells chondrogenically. This was evident by the enhanced expression of matrix protein present during endochondral bone formation and markers of angiogenesis. VWF and CD31 were enhanced in co-culture pellet defects and Col-2 protein expression was more prevalent within the pellets of the co-culture defects compared to HUVEC pellet defects, where Col-2 was more visible in the tissue surrounding the defect area. This could indicate cell interaction of HBMSCs/HUVECs encouraging endochondral bone formation, which utilises an intermediate cartilaginous step during wound healing.

As detailed in the introduction of the current chapter, Freeman and colleagues with the aim to recapitulate endochondral bone formation in cell pellets, observed strong cartilage formation of chondrogenically primed HBMSC pellets. Subsequent addition and co-culture with HUVECs produced CD31 positive cells attaching to the pellet periphery and infiltrating the cartilaginous template after 1 week of co-culture. Interestingly, when HUVECs and HBMSCs were added to the chondrogenic pellet, not HUVECs alone, rudimentary vessel formation was observed (Freeman *et al.*, 2015). Although this study was limited to the in vitro cell work, it confirms the potential and importance of cell priming by exogenous factors but importantly vascular priming and modulation by the presence of HUVECs.

In the current study, the cell pellets lay within a heterogeneous bed of bone cells within the defect. With the resultant mix of temporal signals between the implant and surrounding tissue cells were naturally primed to migrate and/or proliferate. Strong vWF expression was observed in all treatment groups, particularly in the HUVEC and co-culture pellet constructs. Endothelial cells store and secrete vWF from the Weibel-Palade bodies in response to stimuli for instance as a result of injury. Various cell type, including fibroblasts, osteoblasts and chondrocytes are able to spontaneously secrete vWF into the cytoplasm by constitutive secretory pathways (Giblin *et al.*, 2008), meaning that the protein is continuously secreted from the cells present in bone regardless of environmental factors. This mode of secretion could explain the presence of vWF in all treatment groups. However, Giblin *et al.* and colleagues found that HUVECs mainly secrete vWF through Weibel-Palade body exocytosis, triggered by stimuli, such as variations in pH level (Giblin *et al.*, 2008), which could explain the stronger presence of vWF staining observed in defects in the current study. The application of the defect and pellet to the femur may have altered pH levels of the surrounding tissue and thus triggered the release of vWF by HUVECs or/and HBMSCs.

Conclusion and future outlook

This study has demonstrated that pellets of HUVECs, HBMSCs and co-cultures of both cell types can enhance bone formation and increase expression of

osteogenic and angiogenic markers. This study has revealed an important role of endothelial cells (alone) in this *ex vivo* defect model evident in greater enhancement of bone formation by HUVECs implanted defects compared to co-culture or HBMSC implanted defects. This study has indicated that the differential in bone forming parameters may be due to a delayed interactive response by the co-culture constructs within the tissue caused by the distinct compact morphology of the pellets conveying less initial migratory cell activity; a longer culture period of this model could verify this theory. The results from the current study have highlighted the efficacy of this model as an inexpensive, high throughput ex vivo model for preliminary research. Although this model is far from being a direct test bed for clinical translation due to the size and lack of a functioning vasculature, it does provide a unique first step – bone tissue niche to understand the interactive repair mechanisms in a 3D environment.

Potential improvement of translatability could be the use of decellularised matrices as an inductive dressing. This would aid-:

a) Cell pellet containment within the defect,

b) Improved cell signal conduction and

c) Bridging of the defect areas as a cell substrate for cell proliferation and migration.

In addition, placing this model in a vascular rich bed such as the chick chorioallantoic membrane model will provide the additional interactive process of a functional vasculature.

Preliminary experiments have been conducted, using decellularised human placental vessel sleeves to cover the chick femoral defect containing the implanted cell construct (Appendix 7.5.1-4). An additional modification of the pellet implant model would be a scaling-up of the cell pellet size by fusing multiple pellets. This could be done by either manual construction or self-assembly of multiple pellets into larger tissue segments and thereby allowing

natural diffusion of the larger construct by osmosis, thus preventing tissue necrosis. Work to this end has commenced and illustrations of this are outlined in Appendix 7.4.2-7. The scaling-up of the pellet construct as described herein would equally require alterations to the defect size, therefore, to maintain consistency of results in chapter 5, the pellet size was not altered in the following investigation but the experimental alteration will be preserved for future work.

CHAPTER 5

Combining human decellularised matrices and cell construct implants to promote bone healing in an *ex vivo* organotypic bone defect model

I would like to acknowledge Dr. Karl Schneider at the Ludwig Boltzmann Institute (LBIT) for Traumatology in Vienna, Austria, who kindly provided the decellularised human placental grafts.

5.1 Introduction

In the previous chapter (4), the potential of cell-based constructs to improve bone regeneration in chick femur drill defects was demonstrated. This novel strategy illustrated the potential to supplement and improve bone regenerative strategies. However, a key limitation of the pellet-implant model was translation to a large-scale model and fixation of the implant into a large defect.

An increasingly attractive area of tissue engineering over the last decade has been the use of decellularised matrices (DMs) from a variety of tissues as biomimetic scaffolds for tissue regeneration or as whole organ transplants. Examples of decellularised tissue include lung (Balestrini *et al.*, 2015), heart (Kitahara *et al.*, 2016), vasculature (Gong *et al.*, 2016), liver (Bruinsma *et al.*, 2015; Buhler *et al.*, 2015) and adipose tissue (Haddad *et al.*, 2016).

DMs maintain the complex three-dimensional architecture and microstructure of the tissue, whilst retaining biologically active factors from the ECM, thus supporting cellular function and cell interaction as well as cell guidance, reviewed in (Hoshiba *et al.*, 2016). However, it is important to note, allo- and xenograft tissue transplants carry considerable risks to the patient such as donor site morbidity, infection, immuno-rejection as well as limitations in the amount of available donor tissue (Courtman *et al.*, 2000).

Current methods of decellularisation affect preservation of native ECM and the structural properties such as elasticity and strength, which can ultimately determine the success or failure of the graft; reviewed by (Seddon *et al.*, 2004; Crapo *et al.*, 2011). Equally, a negative outcome can be caused by incomplete decellularisation of the tissue (Spark *et al.*, 2008), contamination of graft tissue (Poornejad *et al.*, 2016) or the use of harsh chemicals and detergents during the decellularisation process; as well as extended exposure time to chemicals, as reviewed by (Hoshiba *et al.*, 2010). In order to overcome these limitations in the decellularisation process and to preserve native tissue architecture and properties, the decellularisation method employed by Schneider *et al.*, to produce the grafts for the current study utilised a customised peristaltic

perfusion system, whilst using a milder non-ionic detergent (1% Triton X-100) with a reduction of exposure time (from 48h to 24h) (Schneider *et al.*, 2016). Herein, successful cell removal was achieved by pulsatile perfusion of chemicals, demonstrated by a significant reduction in DNA content, with no evidence of cell components upon histological examination of the decellularised tissue compared to tissue treated with static perfusion (Schneider *et al.*, 2016). Furthermore, a hydroxyproline quantification assay confirmed essential collagen fibre preservation in decellularised vessel grafts, compared to non-treated tissue. However, some loss of ECM components, not atypical for the decellularisation process were reported such as partial loss of glycosaminoglycans (GAG) (30% preserved) and marginal loss in stiffness and tensile strength of the decellularised tissue (Schneider *et al.*, 2016).

Herein the current study has used human decellularised vascular matrices to serve as a protective sleeve around a bone drill defect containing a cell construct and thus shielding the defect site with the construct during repair and remodelling. This will aid to conserve the overall architectural structure of the femur and prevent rupture of the defect site. Critically, we hypothesized that factors preserved in the decellularised sleeve ECM (Schneider *et al.*, 2016) and proximity of the sleeve with the femur as well as the defect, will aid in recruiting cell invasion and tissue repair as well as protecting the defect, comparable to the application of a wound dressing. Furthermore, it would be in line with the previous study (chapter 4) to encompass the use of human allograft material benefiting from reduced immunogenicity, in combination with a stem cell based cell therapy. The native structural proteins such as collagen and GAGs (Badylak *et al.*, 2009; Schneider *et al.*, 2016), preserved within the decellularised scaffold ensure biocompatibility and constitute a suitable substrate for re-cellularisation and tissue integration within a defect, promoting cell migration (Schneider *et al.*, 2016). Equally, the factors produced by the implanted cell construct will aid in maintaining native proteins and cell/cell and cell/tissue signalling. Whilst utilising the non-cellular graft, the cellular construct has the potential to be custom designed for the defect (Appendix 7.4.2-8) and could be fixed in situ by the DM bandage.

Initially, a pilot study was performed using E18 chick femur segmental defects implanted into a rich vascular chorioallantoic membrane assay (CAM), using cell pellet constructs placed in-between the bone segments contained within the decellularised human placental sleeves (Appendix 7.5.1). A CAM assay was performed (Appendix 7.5.2) and femurs were analysed using μCT imaging (Appendix 7.5.3-4) and histological staining (Appendix 7.5.4). Initial evaluation demonstrated that the segmental setup in combination with the CAM culture revealed good integration of the sleeves with the femurs. However, the model introduced variables such as displacement of the femur segments within the sleeve, caused by movements of the chick embryo and the lack of a viable control without a sleeve. Therefore, in order to avoid aforementioned variables, an *in vitro* organotypic culture model was deemed a more suitable platform for the current study. In addition, the *ex vivo* organotypic model will build on the results of the previous studies by using the chick femur drill defect model with cell construct implants as a positive control (chapter 4), thus providing continuity from previous findings.

The current study will utilise decellularised graft obtained from non-cadaver human placentae (Schneider *et al.*, 2016). These placental vessels, from part fetal, part adult tissue origins (Tan *et al.*, 2004), were tested on femoral drill defects implanted with cell constructs and cultured organotypically for 10 days to determine the efficacy for skeletal repair.

5.2 Hypothesis

Decellularised human placental vessel sleeves enhance bone repair as a consequence of trophic factors and provision of structural support, when applied around a bone drill defect containing an implanted 3D cell construct.

5.2.1 Objective

1. To test if human placental decellularised vessels can be re-seeded with HUVECs and the ability of recellularised human placental vessels to integrate into an *in vivo* vascular bed model.

2. To examine the potential of human placental decellularised vessels to improve bone repair in a bone defect when employed as a protective sleeve around the femur.

Bone volume and structure were be assessed using micro-CT imaging and tissue architecture will be assessed by histological and immunohistochemical analysis.

5.3 Methods

Human placental decellularised blood vessels were kindly provided by Dr. Karl Schneider at the Ludwig Boltzmann Institute (LBIT) for Traumatology in Vienna, Austria prepared as previously detailed (Schneider *et al.*, 2016).

5.3.1 Human placenta harvest

Human placentas were collected by the Red Cross Hospital, Linz, Austria with approval of the Upper Austria committee and informed consent was given by donors undergoing caesarean section births. Placentas were flushed with Phosphate Buffered Saline solution (PBS) supplemented with heparin (50IU/ml) and 1% Penicillin/Streptomycin and any blood was removed from placenta vessels. Placentas were then frozen whole in PBS at -20°C prior to use (Schneider *et al.*, 2016).

5.3.1.1 Processing and decellularisation of blood vessels from the human placenta chorion.

Placentas were thawed and selected vessels of an approximate 2-3mm vessel diameter and 3-4cm length were dissected out from the chorionic plate. A surgical thread was used to tie one vessel end to a BD Venflon™ Cannula (14GA Heidelberg, Germany) (Figure 5.1) prior to a freeze thaw-step for 18 hours at -80°C and thawing in a PBS solution at room temperature (Schneider *et al.*, 2016).

Figure 5.1. Isolated placenta vessel sleeves connected to a BD Venflon™ Cannula.

5.3.1.2 Chemical decellularisation

The vessels were connected to a custom-designed recirculating perfusion system driven by a peristaltic pump (Minipuls® Evolution, Gilson Inc., Middleton, USA). Initial osmotic pressure cell lysis was achieved by perfusion of vessels for 30 minutes with a hypertonic (1.2% NaCl) and hypotonic (0.4% NaCl) saline solution at a pulsatile perfusion pressure set at a range of 60-80mmHg (8000-10670 Pa); followed by a 24 hour perfusion with 1% Triton X-100 (Sigma, Vienna, Austria) and 0.02% w/w EDTA in PBS at room temperature. Vessels were subsequently incubated overnight at 4°C in DNase I solution (200IU/ml, Roche) and washed for 3 hours with PBS (Schneider *et al.*, 2016).

5.3.1.3 Chemical sterilization

Following repeated rinsing cycles with sterile PBS the vessels were washed in 0.1% (w/v) PAA (peracetic acid) solution at pH 7.0 (Lomas *et al.*, 2003). The vessels were placed in a 50ml Falcon tube in PBS on a roller mixer (30 rpm) for 3 hours. In the final step, the vessels were repeatedly rinsed with 35ml of sterile PBS and stored at 4°C prior to use (Schneider *et al.*, 2016).

5.3.2 Recellularisation of decellularised chorionic vessel sleeves and assessing biocompatibility and integration using the chorioallantoic membrane assay (CAM)

Decellularised vessels sleeves were stored at -20°C in PBS. On the day of the experimental setup, sleeves were defrosted at room temperature, immersed in plain culture medium in a petri dish, under sterile conditions, and incubated for 3 days at 37°C. HUVECs were trypsinised, washed with 1x PBS and labelled with Cell Tracker Green™ as described in chapter 2.2.8, to confirm their presence and cell viability post re-cellularisation of the vessels. The flow diagram in Figure 5.2 gives an overview of the various stages leading up to the biocompatibility testing of the decellularised placental vessel sleeves.

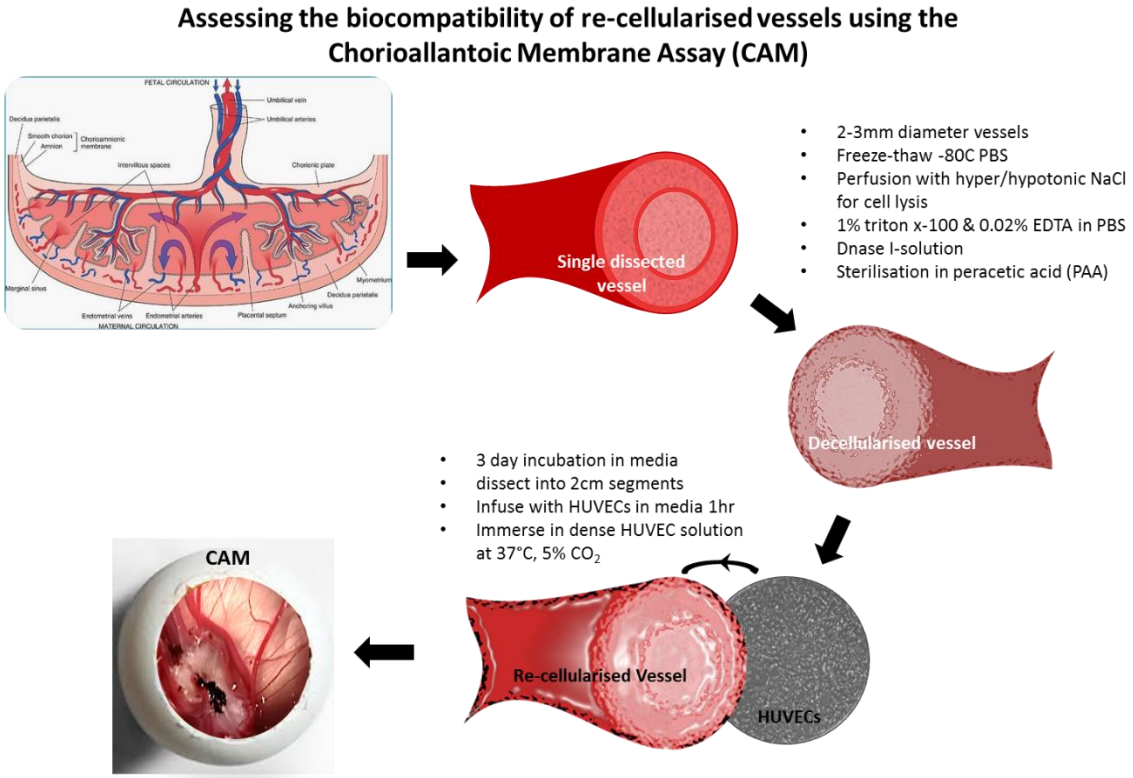

Figure 5.2 **Flow diagram of the recellularisation** process of decellularised blood vessels obtained from the human chorionic placental plate. (Image: placental chorionic plate: http://image-bros.club/c/chorionic-plate-ultrasound.html; accesses 16/02/17)

HUVECs were harvested and cultured as described in 2.2.3 and 6 x 10^6 cells were re-suspended in 5ml of endothelial cell medium (ECM) (Table 2.4). Decellularised vessel sleeves (3-4cm) isolated from the chorion of the placenta were attached to a cannula with a surgical thread (Figure 5.3A). The end of

each tube was carefully tied shut with a surgical thread. 2ml of the HUVEC suspension was taken up into a 5ml syringe and attached to the cannula (Figure 5.3B). The vessel sleeves were slowly infused with the HUVEC suspension, taking care not to apply too much pressure. The sleeves, attached to the cannula and syringe, were rested on a petri dish under sterile conditions in a class II tissue culture hood. A small volume of cell suspension was administered over the tube in order to prevent dehydration and to add to the cell exposure of the sleeves.

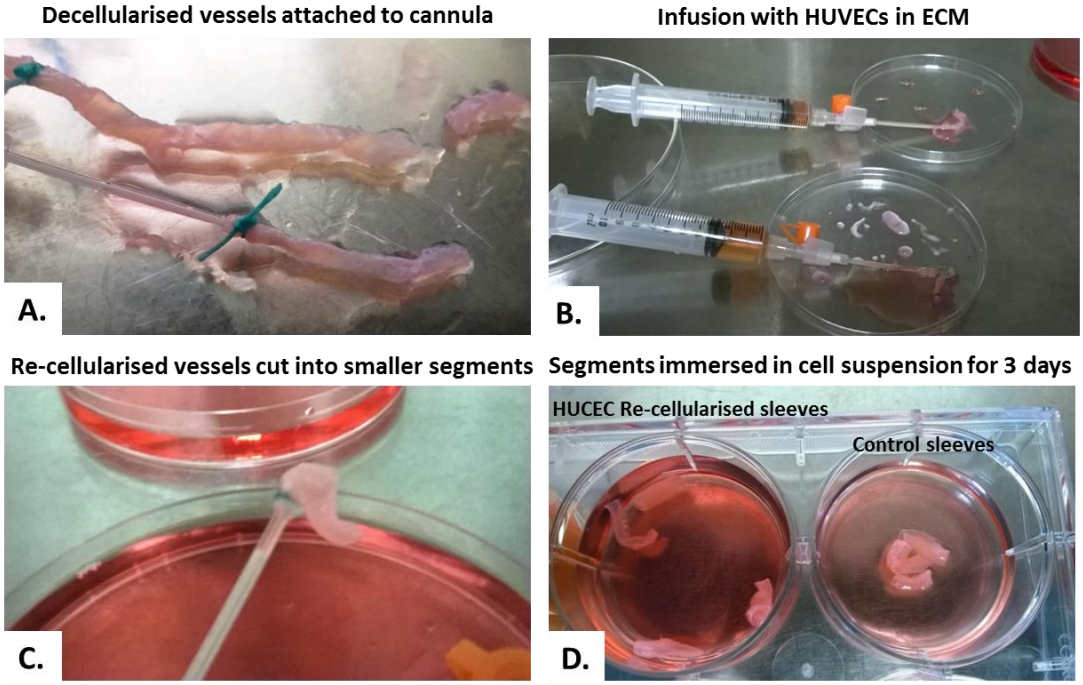

Figure 5.3 **Static re-cellularisation of acellular vessel sleeves with HUVECs. A.** Whole decellularised vessel sleeves. **B.** Syringe infusion of sleeves with concentrated HUVEC suspension for 1 hour. **C.** Section of sleeves post infusion. **D.** Further re-cellularisation of sleeves in cell suspension over 3 days.

The cell-infused sleeves were incubated for 1 hour at room temperature. The cannulae were then carefully removed from the tube by cutting the threat with a pair of small surgical scissors. The sleeves were cut into smaller segments using a scalpel and the surgical thread removed from opposite ends (Figure 5.3C). Control sleeve segments were place in the well with the cells suspension for static incubation. Sleeves with and without cells were added to a separate well with endothelial cell medium as a control (Figure 5.3D). The plate with sleeves/cells was incubated at 37°C, 5% CO_2/balanced air for 3 days.

Six E10 aged chick eggs were prepared for CAM assay by scoring the shell with a scalpel and an approximately a 3mm square opening was created in the outer shell of the egg. Three re-cellularised and three non-cellularised sleeves were implanted onto the chorioallantoic membrane inside the egg. The window was covered with a small strip of autoclave tape and labelled. Eggs were transferred to a Hatchmaster incubator and incubated for a duration of 8 days at 37°C 60% humidity (Figure 5.4) without rotation. All procedure were performed in line with ethical approval and in accordance with the Animal (Scientific Procedures) Act 1986, UK (Project License number PPL 30/2762).

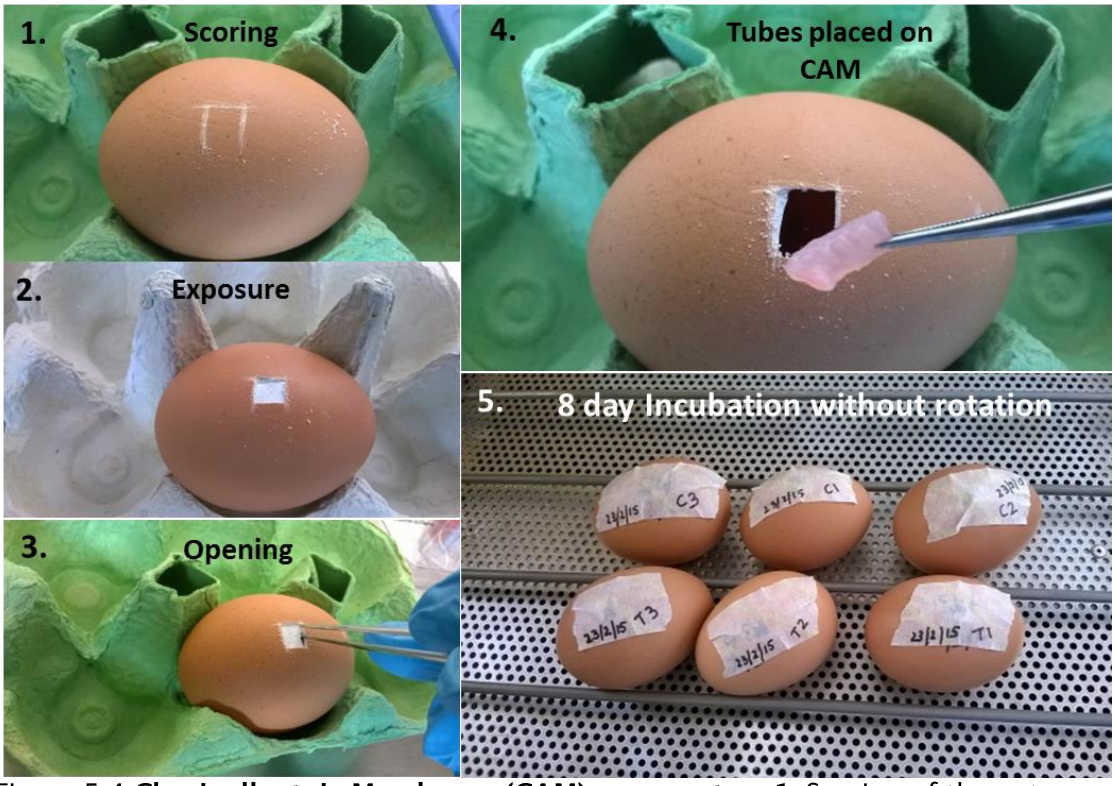

Figure 5.4 **Chorioallantoic Membrane (CAM) assay setup. 1.** Scoring of the outer egg shell. **2.** Exposure of the inner shell membrane. **3.** Opening of the window by cutting away the membrane. **4.** Insertion of the sleeve through the egg shell window onto the chorioallantoic membrane beneath. **5.** Incubation of eggs for 8 days (until E18) at 37°C under humidified conditions.

5.3.3 Decellularised matrix dressing on E18 chick femora drill defects with cell pellet implantation in organotypic culture

E18 Chick femora were dissected and drill defects created as described in chapter 02.2.9. Cell pellet constructs were prepared using HUVECs as described in chapter 2.2. There were some difficulties as the HUVEC pellet

construct did not form a fully round pellet as expected but had a flat appearance (Figure 5.5).

Figure 5.5. **An example of a flat-shaped HUVEC pellet**.

The vessel tubes were cut to an approximate length of 7mm (Figure 5.6A). For femurs containing a cell pellet implant, the construct was implanted prior to application of the sleeve. In order to apply the sleeves, the end of the diaphysis of the femur was cut using a scalpel blade to remove the epiphysis. The cut end of the femur was inserted into the lumen of the vessel sleeve using forceps under a stereo dissection microscope and the sleeve was pulled over the remaining femur, completely covering the diaphysis of the femur (Figure 5.6B). Controls constituted femurs without a sleeve and without a cell construct implant. Femurs were then transferred to an organotypic culture insert in a 6-well plate (Figure 5.6B).

During the setup of the organotypic culture, there was some considerable variation between the vessel sleeves in terms of size and thickness. The multi-layered structure of the vessel tubes made it difficult to open the lumen and insert the femur end. Once inserted, the sleeves were relatively easy to handle and maintained good elasticity when pulled over the femurs, providing a tight fit around the defect and diaphysis.

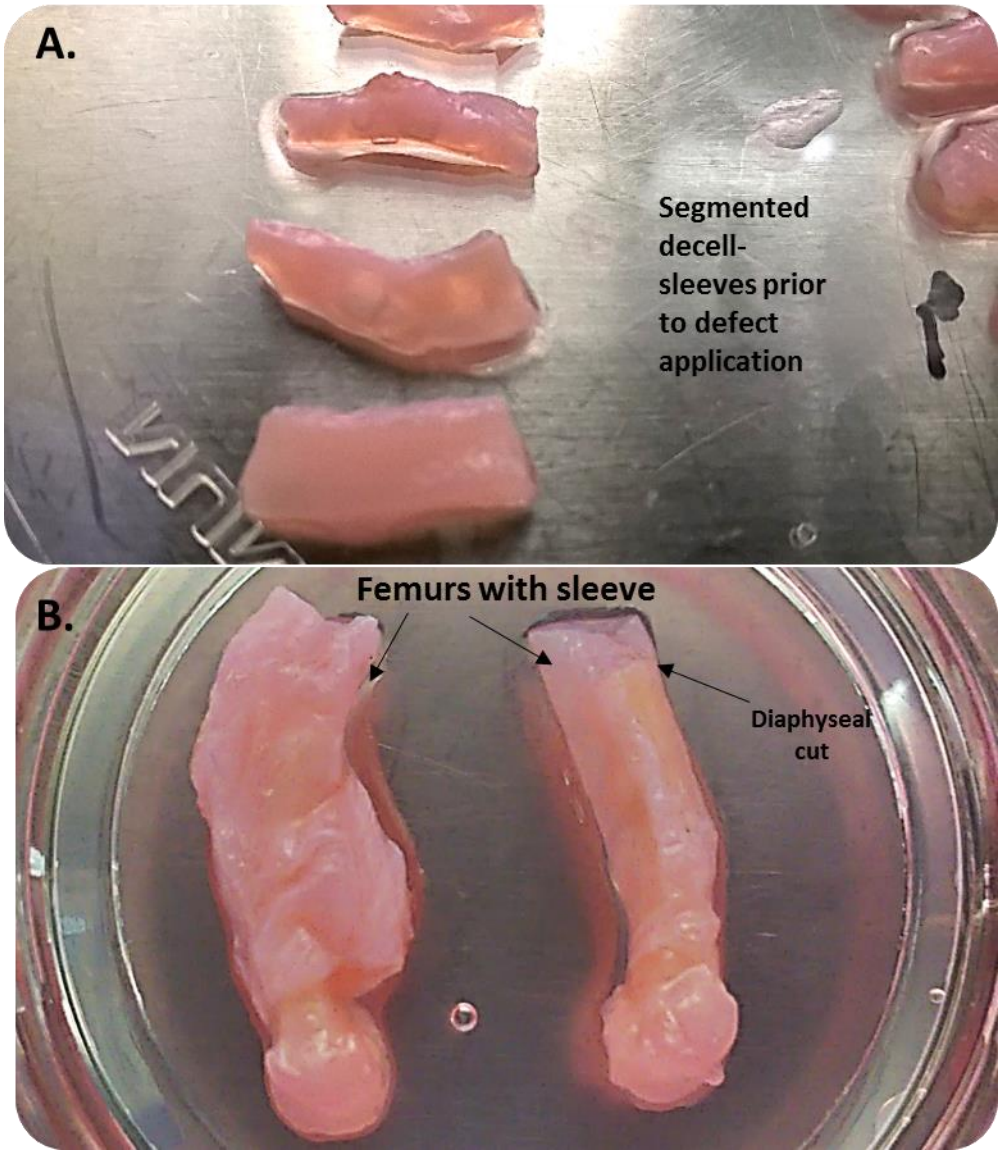

Figure 5.6 **Human placental decellularised vessel sleeves experimental setup, (A)** Segmented vessel sleeves and **(B)** Vessel sleeve surrounding the chick femoral defect with pellet implant.

5.3.4 Micro-CT Analysis

E18 chick femurs were scanned pre- and post-incubation, using the same setup and settings as described in in 2.7 and 4.3.2., as well as reconstruction of image datasets and analysis. A decellularised vessel sleeve was scanned separately. Using the CTAn software, a dataset of 160 cross-sections of the region of interest (ROI), was chosen by counting 80 cross-sections either side of the centre of the defect. Grey scale lower and upper threshold limits were determined using Otsu averaging and scans were then normalised to the vessel sleeve and the phantom control.

5.3.5 Histology

E18 chick femurs were fixed in 4% PFA for 48hrs post incubation. The samples were dehydrated and processed for paraffin embedding as described in 2.3.1. Femur sections were stained for Alcian blue/Sirius red (2.3.2) and immunohistochemistry was performed using COL-II and HIF-1α antibody (2.3.4) (Table 2.1).

5.3.6 Statistical analysis

Data derived from at least 3 replicates of 2 experiments was analysed using one-way analysis of variance (ANOVA) with Sidak's multiple comparison posthoc test and student t-test on GraphPad Prism 6 software. *P* values ≤0.05 were considered significant. Graphical representation of significance: *p≤0.05, **p≤0.01, ***p≤0.001.

5.4 Results

5.4.1 Biocompatibility and integration of decellularised and re-cellularised chorionic vessel sleeves using the chorioallantoic membrane assay (CAM).

At day 8 of the CAM assay, eggs were harvested by carefully removing the shell around the CAM window to extend the opening and to locate the sleeve (Figure 5.7). Images were taken of the integrated sleeve within the CAM; the sleeve were subsequently dissected out with a scalpel and forceps and transferred, initially to a petri dish for imaging and thereafter to a 12 well plate with 4% PFA as fixative. Controls of *in vitro* cultured sleeves were imaged and subsequently fixed in 4% PFA prior to histological processing.

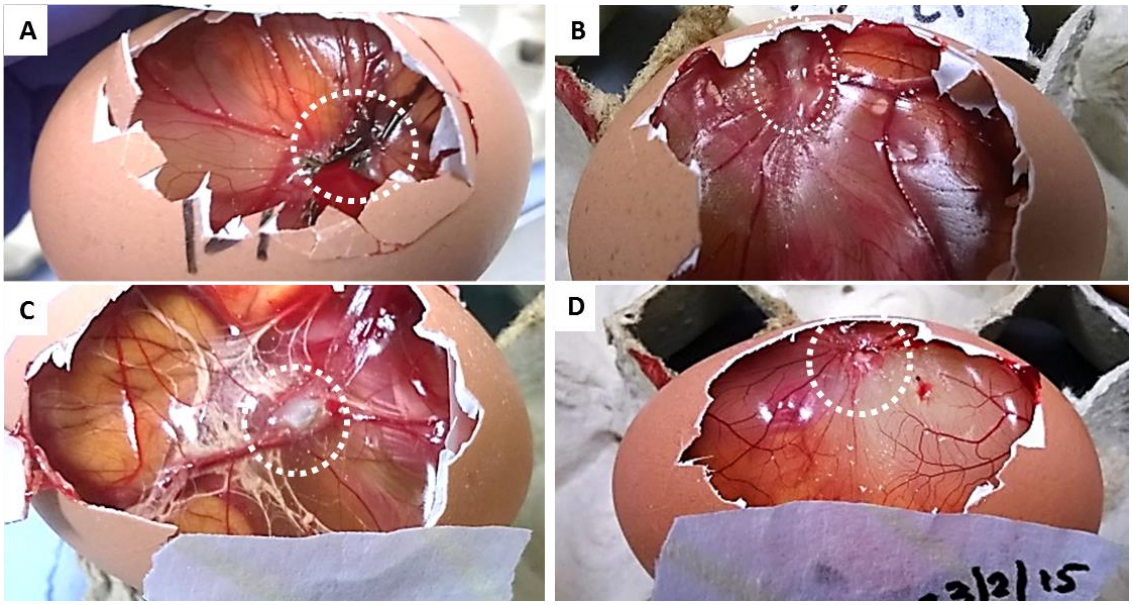

Figure 5.7. A-D. **Bio-integration CAM assay harvest at D8 incubation.** Re-cellularised vessel sleeves (A/C) and sleeves without cells (B/D) at D8 of the CAM assay showed good integration rate (70% of the sleeve samples) with the chorioallantoic membrane with visible blood vessel invasion (circle depicts location of sleeve within the membrane).

Survival rate for the CAM was 100% and CAM-integration rate was achieved by 70% of all sleeves, indicating good biocompatibility of the vessel sleeves with or without cells.

5.4.1.1 H/E staining confirmed improved integration of recellularised vessel sleeves into CAM embryonic tissue compared to controls.

H/E staining showed a distinct difference in morphological homogeneity of the decellularised sleeves post-CAM, in comparison to CAM-integrated (Figure 5.8 A-D;G,H) and non-integrated samples (Figure 5.8 E,F,I). Sleeves that were integrated showed an overall intact architecture, while non-integrated samples appeared heterogeneous with irregular fibres and ruptured architecture (Figure 5.8 E,F,I; arrows). In addition, in the integrated recellularised vessel sleeve samples (A-D), there was evidence of extensive invasion of the cellularised sleeves by chick tissue (arrows) with visible presence of blood vessels within the invading tissue, compared to non-cellularised sleeves (G-H).

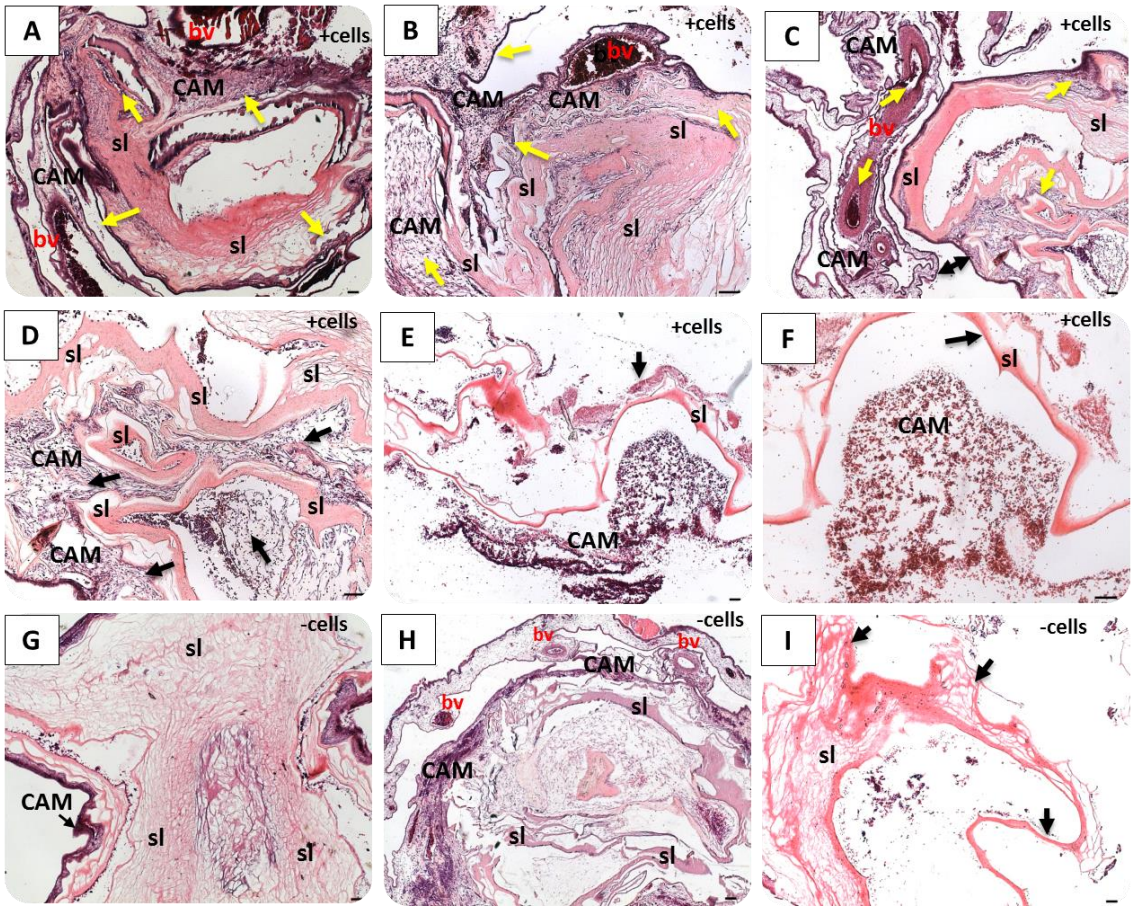

Figure 5.8 A–D. **H/E staining of tissue invasion of the decellularised vessel sleeves by the CAM** at D8 of culture with and without re-cellularisation with HUVECs. **(A–D)** integrated sleeves +cells; **(E–F)** non-integrated sleeve +cells; **(G–H)** integrated sleeves –cells; **(I)** non-integrated sleeve –cells. (Vessel) sleeve **(sl)**, (chick) blood vessel **(bv)**, chorioallantoic membrane **(CAM)**; arrows depict CAM invading tissue. Scale bar 100µm.

5.4.1.2 Fluorescent imaging revealed successful re-cellularisation of *in vitro* vessel sleeves and invasion of CAM explants with chick embryonic tissue.

Fluorescent imaging of the *in vitro* cultured control sleeves demonstrated good re-population of the vessel sleeves with CTG labelled HUVECs as well as cell survival evidenced by minimal ethidium homodimer-1 staining at day 8 of *in vitro* cultured vessel sleeves (Figure 5.9).

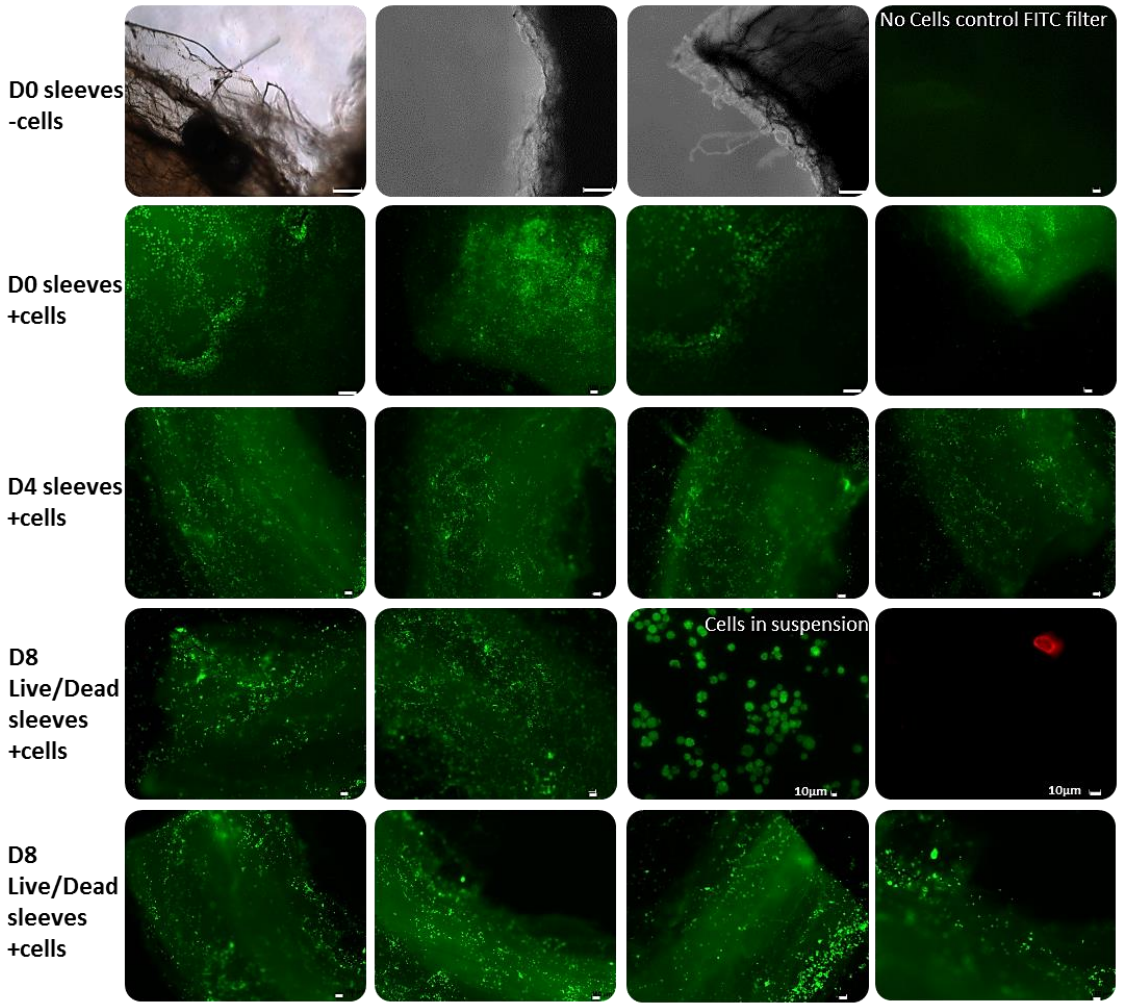

Figure 5.9 **Fluorescent images of *in vitro* re-cellularised vessel sleeves** at day (D) 0, 4 and 8 of culture; sleeves in cell suspension of ~10^6 HUVECs/ml in a 6-well tissue culture plate. Live/dead staining with Cell Tracker™ Green/ethidium homodimer-1 (red) at D8. Scale bars: 10µm (labelled) and 100µm.

Imaging of the CAM explants prior to fixation confirmed the presence of HUVECs on the human placental derived sleeves (Figure 5.10), however due to extensive invasion by the embryonic tissue and the depth of the samples, it was difficult to locate the fluorescently labelled cells on the whole explants and cell repopulation appeared reduced compared to the re-cellularised control sleeves, cultured in tissue culture plastic (Figure 5.9).

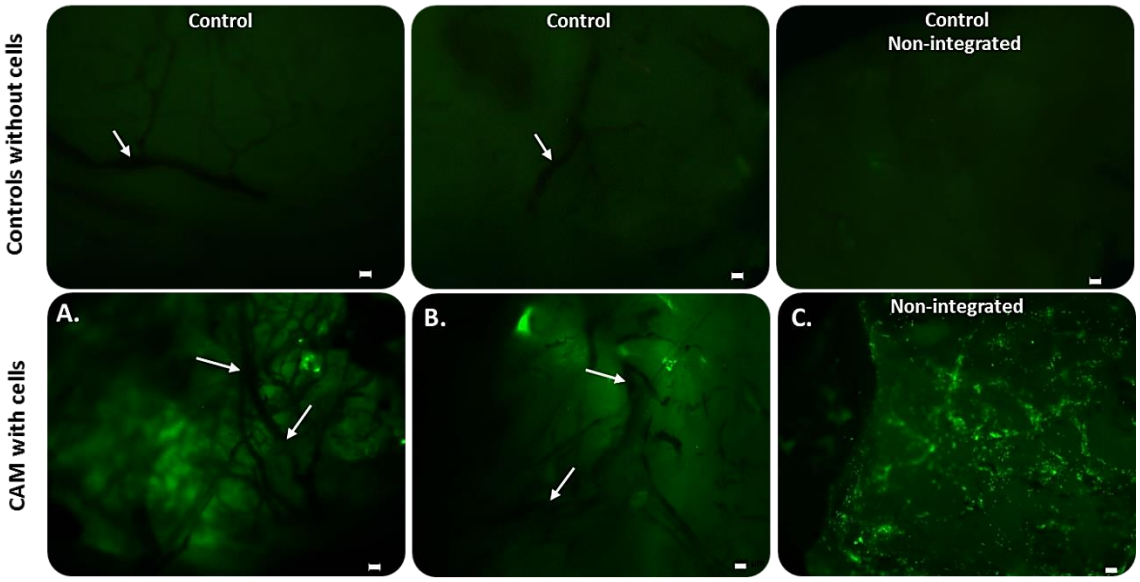

Figure 5.10 **Fluorescent images of recellularised vessel sleeves** at D8 of CAM culture assay. **Top**: Controls – CAM cultured sleeves without cells. **Bottom**: CAM explanted recellularised sleeves. A/B. CAM-integrated sleeves C. CAM non-integrated sleeves. Arrows depicts CAM blood vessels present in CAM-integrated explants. Scale bar: 100µm.

Marked blood vessel invasion from the CAM surrounding the explant sleeves was evident in the images (Figure 5.10, arrows) as previously shown by H/E staining (Figure 5.8), confirming integration and biocompatibility of the sleeves within the chick membrane. Furthermore, DAPI counterstain (Figure 5.11) revealed invasion of chick embryonic tissue in and around the vessel sleeves at day eight of CAM culture as depicted by multi-channel acquisition fluorescent imaging of CAM-sleeve paraffin sections below (Figure 5.11).

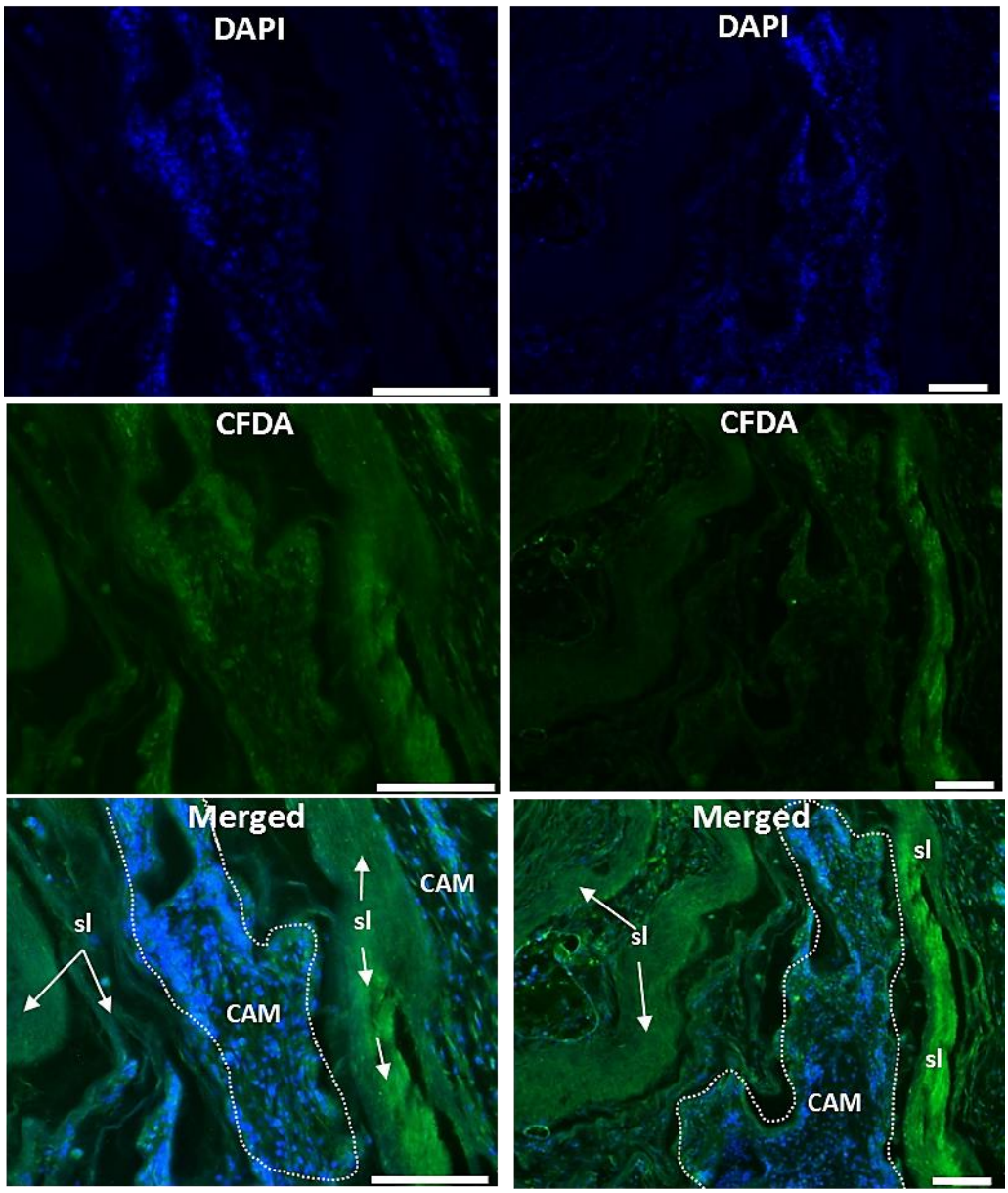

Figure 5.11. **Fluorescent imaging illustrating tissue invasion** of the recellularised sleeves by chick embryonic tissue (white dashed line); images depict CAM explants with CFDA-labelled HUVECs on paraffin embedded sections. DAPI counterstain was applied to sections post-rehydration step. Blue (DAPI) stained areas without green (CFDA) overlap represent cells stemming from the chick embryonic tissue. **sl**= sleeves, **CAM**= chorioallantoic membrane (chick embryonic tissue). Dashed line marks main area of invasion by the CAM tissue into the sleeves. Scale bar: 100µm.

5.4.2 Micro-CT analysis reveals enhanced bone volume in E18 chick femoral drill defect using decellularised vessel sleeve matrices.

Micro-CT imaging of femurs demonstrated increased closure of defects at day 10 of organotypic culture in the majority of the sleeved femurs

(NoPellet/+sleeve), where the sleeved femurs with HUVEC implant (Pellet/+sleeve) appeared to show a marginally greater defect closure at D10, compared to no pellet sample images (NoPellet/+sleeve) (Figure 5.12). There were negligible differences in the visible appearance of the defect at D0 and D10 of femurs without sleeves and without cell pellets (NoPellet/-sleeve) in the micro-CT images in Figure 5.12. These samples appeared to show the least closure of the defect at D10 compared to the defect size at D0. In comparison, femurs without a human placental derived sleeve but with a cell implant exhibited a visible difference between defects at D0 and D10 (+pellet/-sleeve) (Figure 5.12).

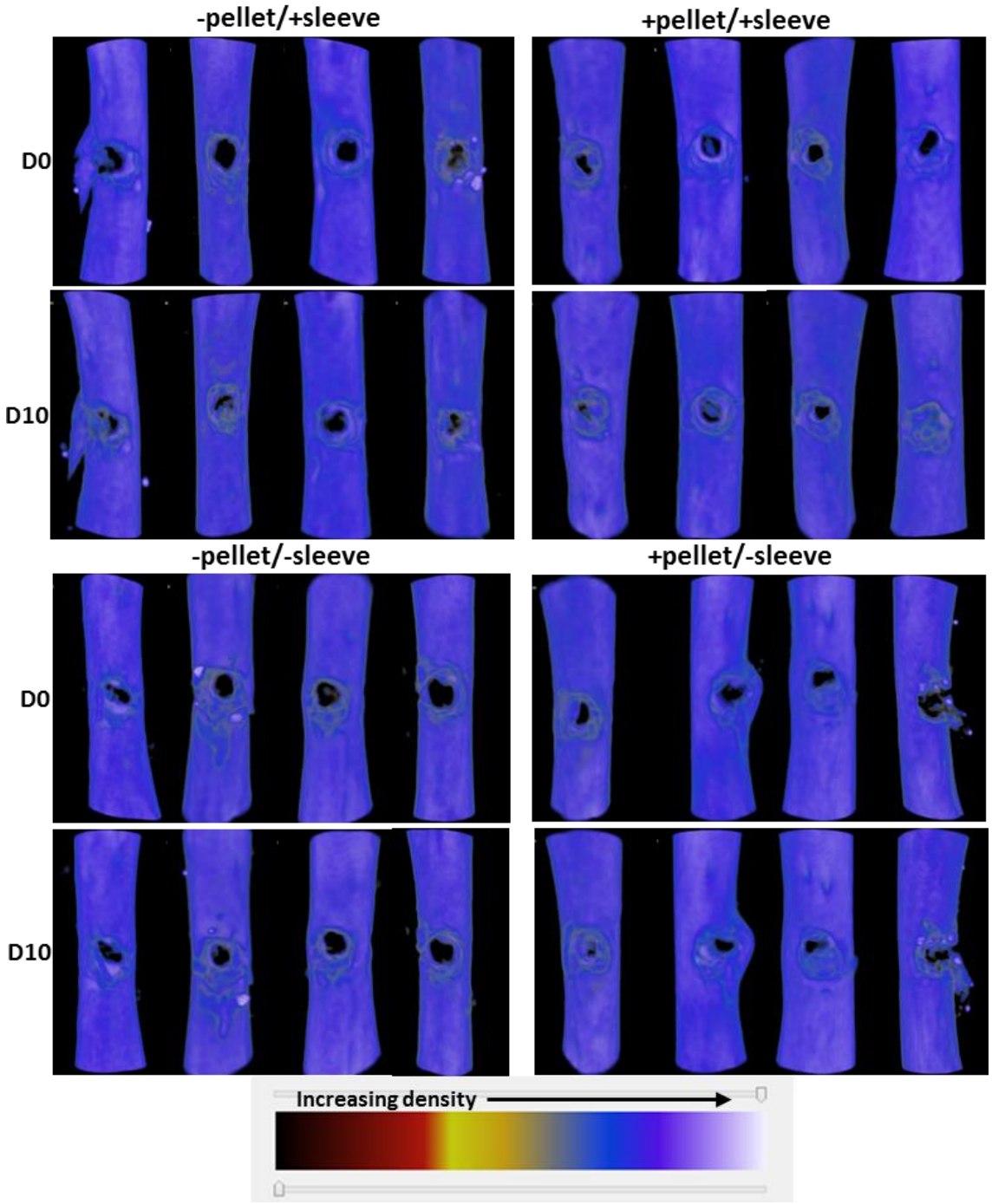

Figure 5.12. **Micro-CT 3D images of E18 chick femurs drill defects** pre- (D0) and post- (D10) organotypic culture with human placental vessel sleeve (+); without sleeve (-); on left: femurs without HUVEC pellet implants +/- sleeve; on right: femurs with HUVEC pellet implant +/- sleeve. Below the images: colour spectrum palette corresponding to tissue densities. Images created in CTvox software. (Bruker, Kontich, Belgium)

5.4.2.1 Decellularised human placental sleeves enhance bone formation.

Quantitative analysis of bone histomorphometry from micro-CT imaging revealed statistically significant increases in bone volume and bone/tissue ratio of sleeved femurs, independent of the cell implant when compared to controls without the sleeves. Sleeved femurs maintained in the absence of cell pellet constructs demonstrated an increase in bone volume of 0.52±0.19 (n=11). This increase was comparable to that observed in pellet implanted femurs contained within human placental derived sleeves (BV 0.52±0.28, n=9); this was in contrast to the bone volume increase in control femurs without a sleeve: -sleeve/-pellet (BV -0.05±0.15) and -sleeve/+pellet (-0.08±0.06).

No significant differences in bone volume of cell construct implanted femurs without sleeve, compared to the no pellet controls were observed. As a consequence of sleeve addition, the binarised data threshold set in order to avoid false positives equally may have restricted detection of more subtle changes in bone volume.

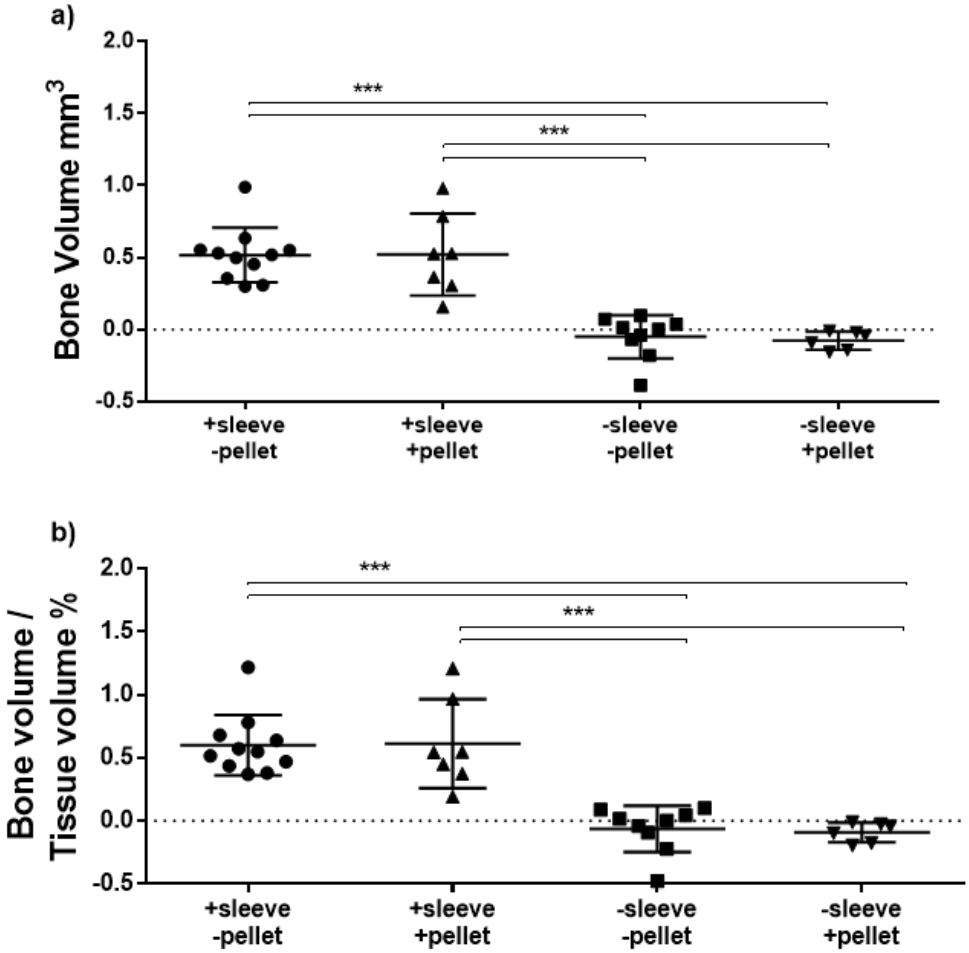

Figure 5.13 **Increase in Bone Volume of E18 chick femurs over the 10 day culture period** following culture +/- human placental sleeves and +/- pellet.**a)** bone volume (BV), **b)** bone volume/tissue volume (BV/TV). Increase in BV was obtained by normalising D10 to D0 scan results. Statistically significance was derived using ANOVA with posthoc Sidak's test. + sleeve/-pellet (n=11), +sleeve/+pellet (n=7), -sleeve/-pellet (n=9), -sleeve/+pellet (n=6). Data presented as mean ± SD. Significance set at *$p \leq 0.05$, **$p \leq 0.01$, ***$p \leq 0.001$).

Re-grouping of all femurs with decellularised human placental vessel sleeves and comparison against those without a sleeve (Figure 5.14), demonstrated a significant increase in bone volume (BV 0.52±0.22) and bone to tissue ratio (BV/TV 0.61±0.28) of the sleeved samples at D10, reinforcing the results of bone forming parameters observed between the treatment groups in Figure 5.13 above.

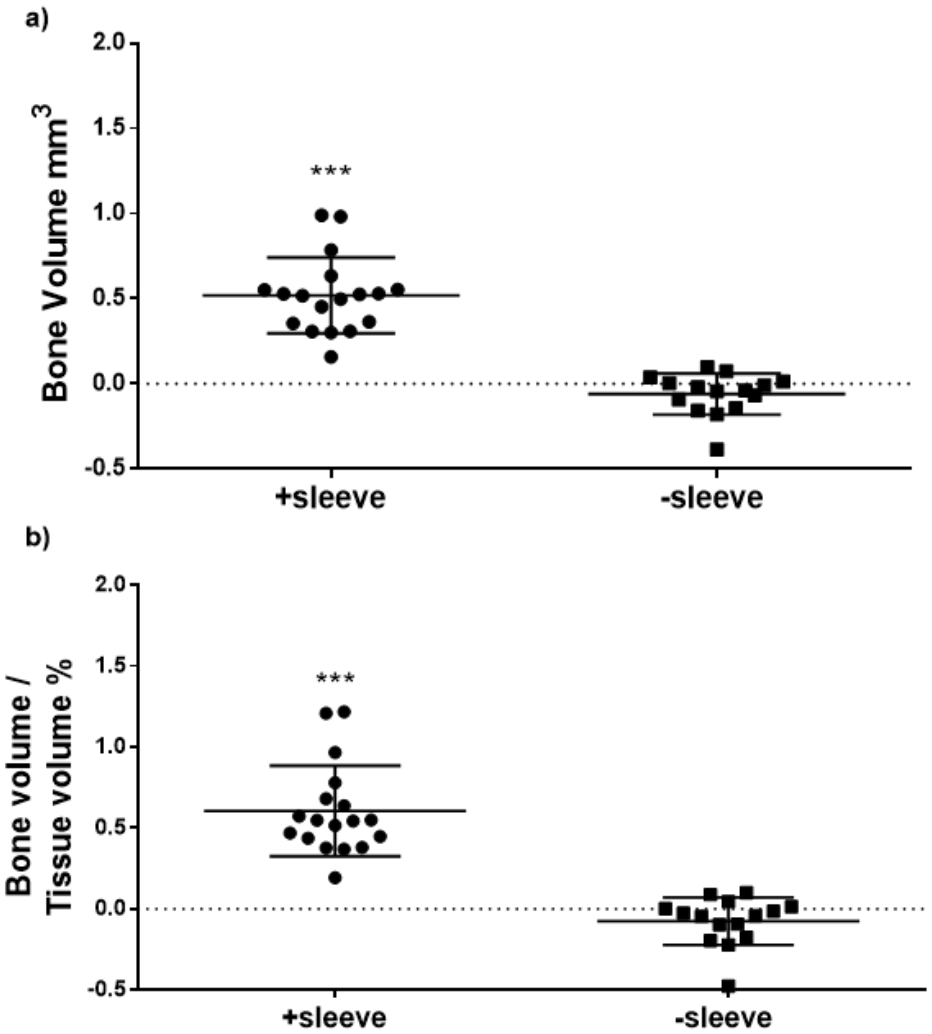

Figure 5.14 **Increase in Bone Volume of E18 chick femurs over the 10 day culture period** following culture with and without human placental sleeves; **a)** Bone volume (BV), **b)** Bone volume/tissue volume (BV/TV). The change in BV was obtained by normalising D10 to D0 scan results. Statistically significance was derived using student t-test with samples grouped according to presence and absence of human placental sleeve. +sleeve (n=18) and -sleeve (n=15). Data presented as mean ± SD. Significance set at *$p \leq 0.05$, **$p \leq 0.01$, ***$p \leq 0.001$

5.4.3 Histology demonstrates integration of placental decellularised vessel graft with bone periosteum and conservation of bone architecture within the graft bandage

Histological examination, using H/E staining, confirmed the successful integration of the vessel sleeves into the CAM with visible vascularisation around the sleeve segments compared to non-integrated sleeves (Figure 5.8). A/S staining showed integration of the periosteal tissue into the collagen fibres of the sleeves. The femur architecture was preserved within the sleeve

preventing rupture of the defect and fragmentation of the trabeculae (Figure 5.15).

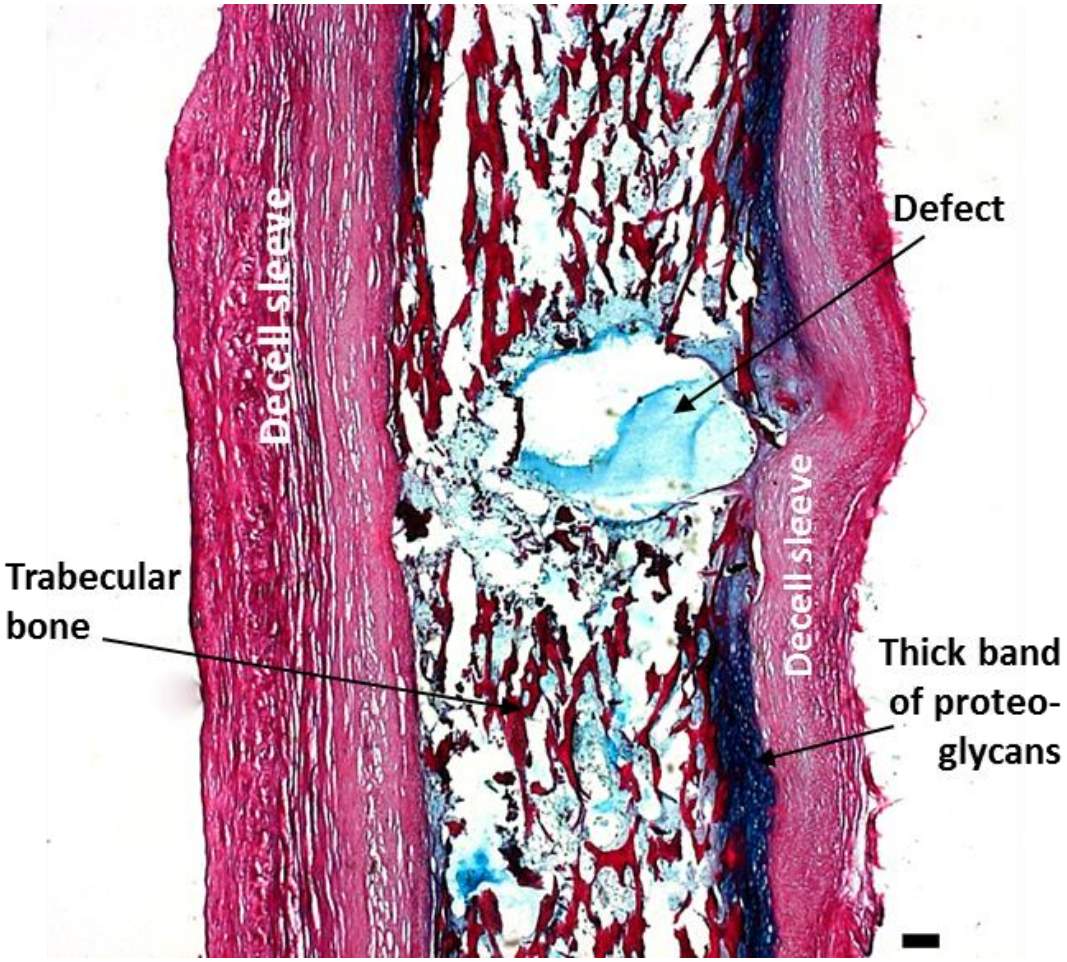

Figure 5.15. **A/S staining of E18 femur with sleeve, without pellet.** Tight integration of femur within sleeve was visible and appearance of proteoglycans (blue) at the sleeve/periosteum boundary was evident. Collagen staining (red) was visible throughout the well preserved bone trabeculae and the fibres of the sleeve. Scale bar: 100μm.

At a higher magnification in Figure 5.16A, a robust band of proteoglycans can be observed between the femur periosteum and inner edge of the sleeve; the presence of a cartilaginous phenotype was confirmed by COL-2 immunostaining **(B)** throughout the Alcian blue **(A)** stained region (Figure 5.16).

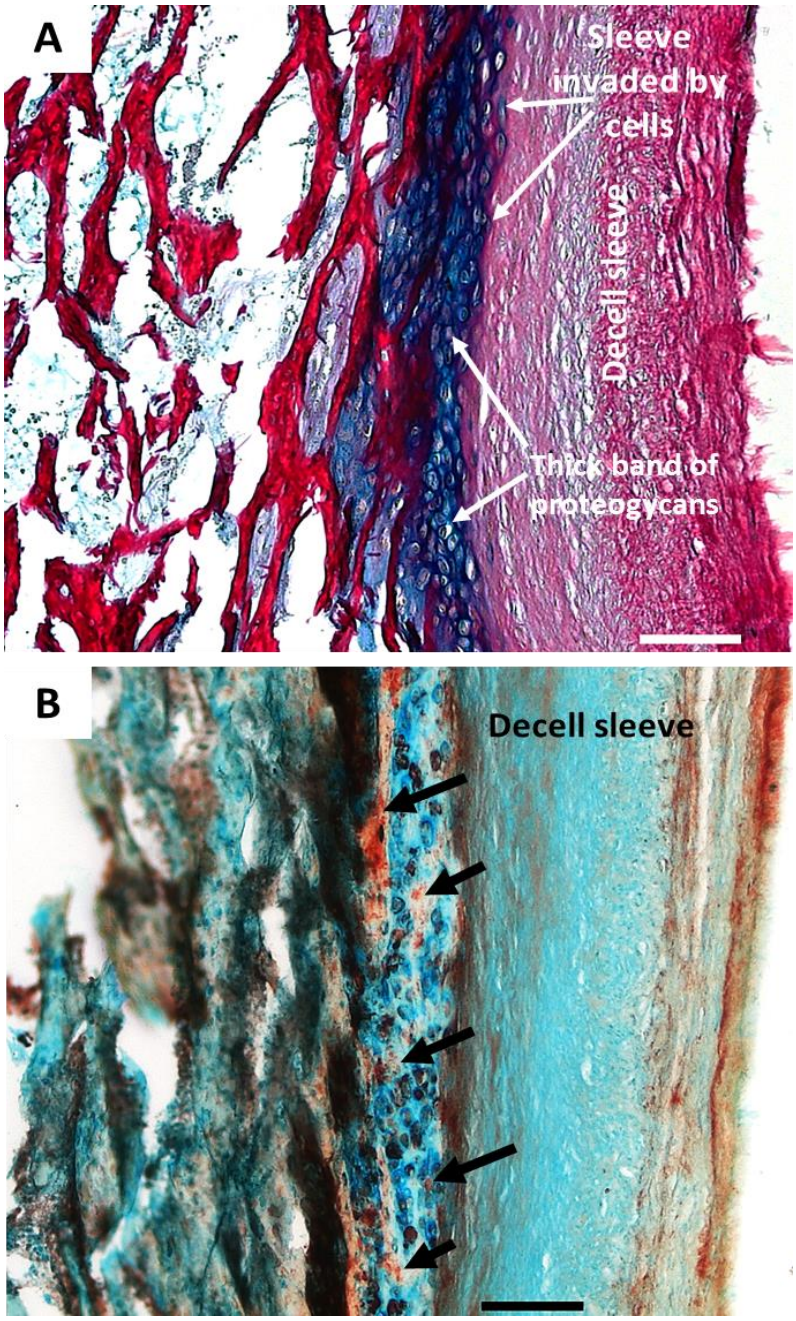

Figure 5.16 **Cartilaginous tissue formation depicted with A/S and COL-2 staining** **A.** A/S staining and **B.** COL-2 Immunohistochemistry on E18 femur with placental decellularised sleeve at D10 of organotypic culture. **A.** A thick band of proteoglycans stained with Alcian blue, extending into the sleeve at the sleeve/periosteum boundary, **B.** Arrows depict areas of COL-2 positive staining within the thick band of proteoglycans lying between the sleeve and the periosteal bone. Scale bar: 100μm.

Comparison of the femurs (Figure 5.17) with the added vessel sleeves (b) against those without a sleeve (a) demonstrated an improved preservation of overall architecture of the femurs, particularly around the defect area. Although a drill defect was still clearly visible in some of the no-pellet femurs with the sleeve, a larger area of the defects was obscured by tissue with a less

ruptured appearance (Figure 5.17b). The difference between pellet implanted positive control femurs maintained with or without the vessel sleeve was less marked (c).

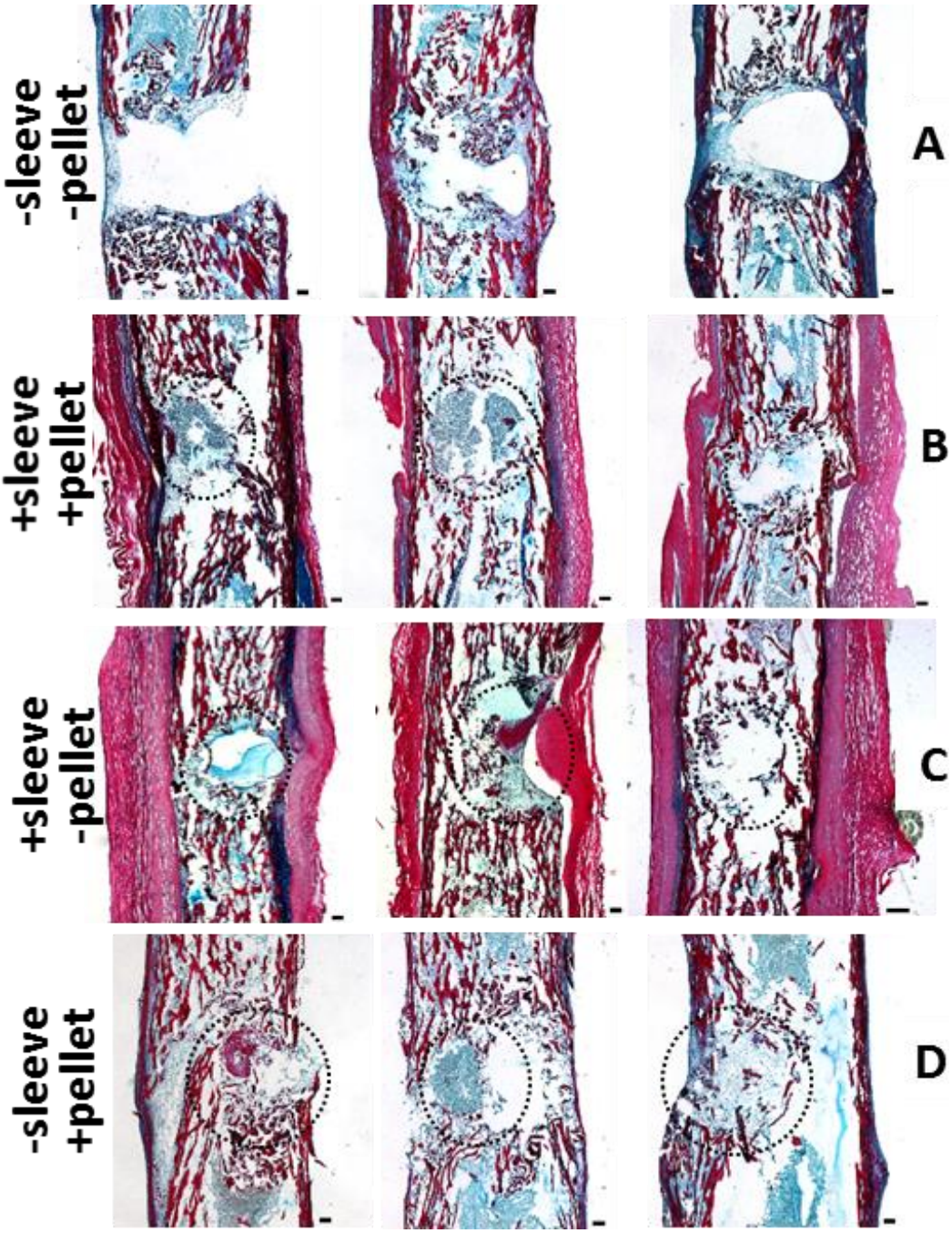

Figure 5.17. **Representative images depicting A/S staining of E18 femurs at D10** of organotypic cultures with and without decellularised human placental vessel sleeves; a) negative control femurs without sleeves or pellet (–sleeve/–pellet) B. Femurs with sleeves and with pellet implant (+sleeve/+pellet), C. Femurs with sleeve and without pellet (+sleeve/–pellet), D. positive control, without sleeve and with pellet implants (–sleeve/+pellet). The negative control femurs (A) demonstrated a large empty defect area, with negligible tissue visible within the defect compared to sleeved femurs (B/C), with tissue visibly obscuring part of the defect. Note strong presence of collagen (red) and visible proteoglycan (blue) band in between sleeve and femur (B/(C). Positive control femurs (D) demonstrated presence of the pellet within the defect. Dotted Circles depict defect area. Scale bar: 100µm.

HIF-1α immunostaining indicated distinct areas of associated hypoxic regions in the femurs, particularly around the defect region both, in femurs with (Figure 5.18B) or without a vascular sleeve (Figure 5.18A). HIF-1α positive cells were more strongly associated with cell aggregates fringing defects of sleeved femurs (Figure 5.18B).

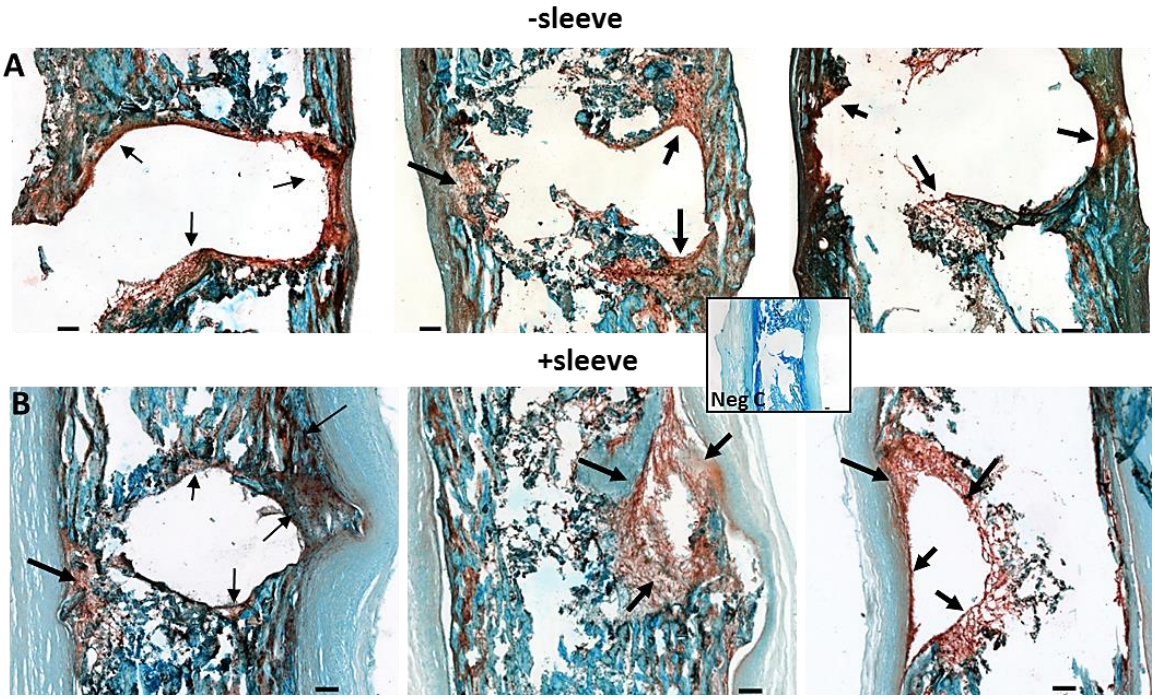

Figure 5.18. **Immunohistological detection of HIF-1α protein** within A. Control femurs without human placental vessel sleeve (-sleeve) and B. Femurs with human placental vessel sleeve (+sleeve) at D10 of organotypic culture. HIF-1α antigen was prominent at the margins of the defects (arrows) of sleeved femurs and present but less prominent around defects of unsleeved femurs. Additional presence of HIF-1α protein was detected within trabeculae of femurs adjacent to the defect and at the sleeve/femur interface (arrows). Scale bar: 100μm.

Furthermore, HIF-1α expression was more prominent in regions between the vascular sleeve and the periosteal region of the femur (Figure 5.19). Additionally, HIF-1α presence was observed throughout areas of the cut end of the diaphysis of sleeved femurs (Figure 5.19A/B, arrows). Regions of cartilaginous tissue and part of the marrow cavity were infiltrated with HIF-1α protein and along sleeve/femur periosteal interface (A/B and C arrows). Interestingly, COL-2 expression was observed to be co-localised with the HIF-1α stained regions (Figure 5.20)

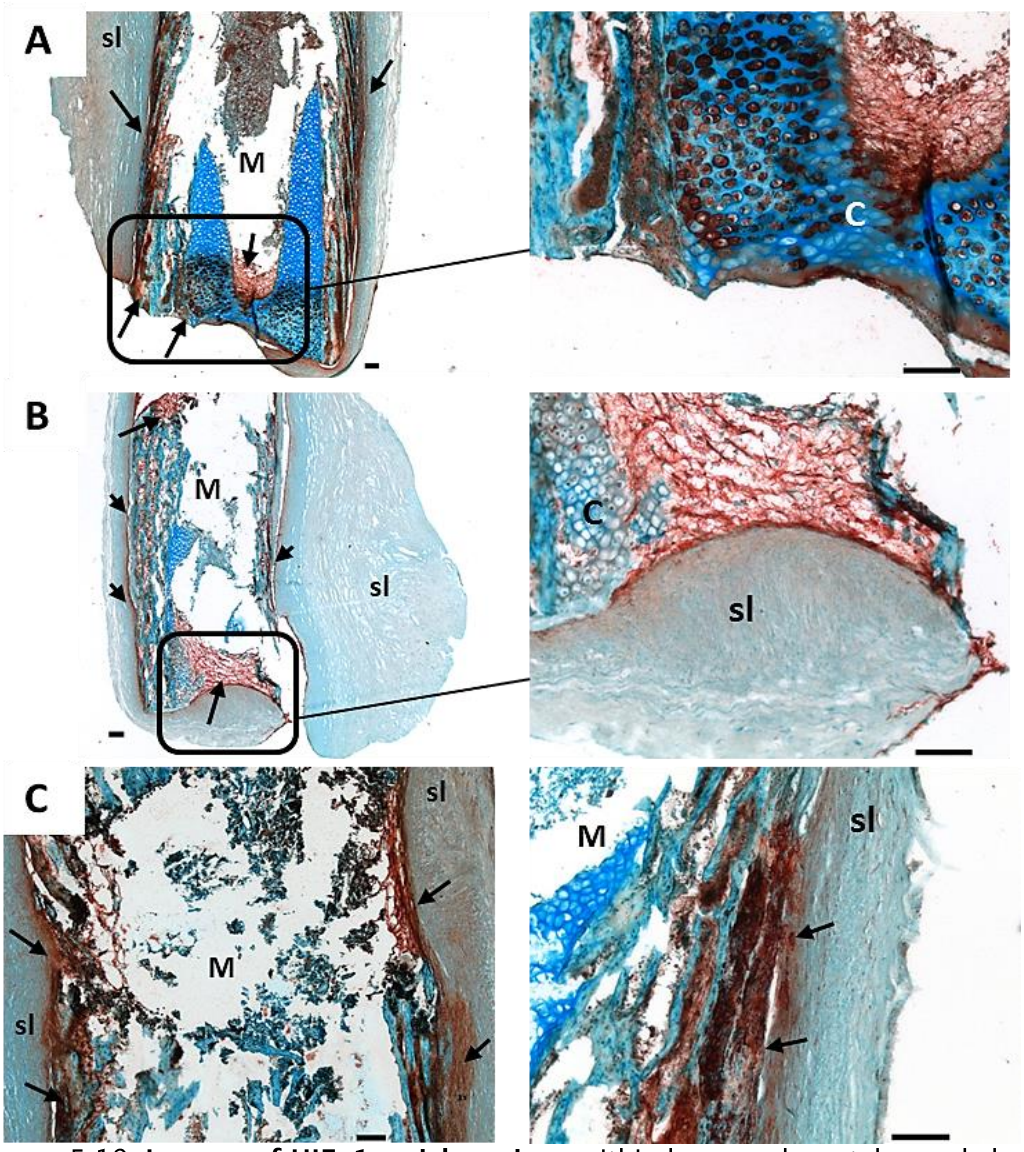

Figure 5.19. **Images of HIF-1α-rich regions** within human placental vessel sleeve contained femurs, **A**/**B** Apical cut ends of femurs contained within human placental derived sleeves (higher magnification images on right), **C** HIF-1α stained regions between the sleeve and the periosteum of two femurs. Note prominent expression within the advancing cartilage of the cut end (A, higher magnification) and fibre-like staining pattern between the sleeve covered cut end and adjacent cartilage (B, higher magnification). M= marrow cavity; C= cartilage; sl= sleeve. Arrows depict areas of marked HIF-1α positive staining. Scale bar: 100μm.

Control femurs typically demonstrated a large hollow defect area with some evidence of COL-2 immunostaining around the defect area and throughout parts of the bone trabeculae. The human placental vessel sleeve showed COL-2 positive staining typically at the inner margin of the sleeve adjacent to the periosteal region. This was followed by a COL-2 negative region of the sleeve towards the sleeve mid-region and then a stronger COL-2 positive stained outer region of the sleeve. COL-2 was evident around the defect margins of

control femurs omitting the sleeve and pellet and there was some COL-2 positive staining within the trabecular bone of the diaphysis. There were areas of abundant COL-2 staining along the sleeve/periosteum boundary in all sleeved femurs. This staining pattern was indicative of the HIF-1α positive areas in Figure 5.19C above.

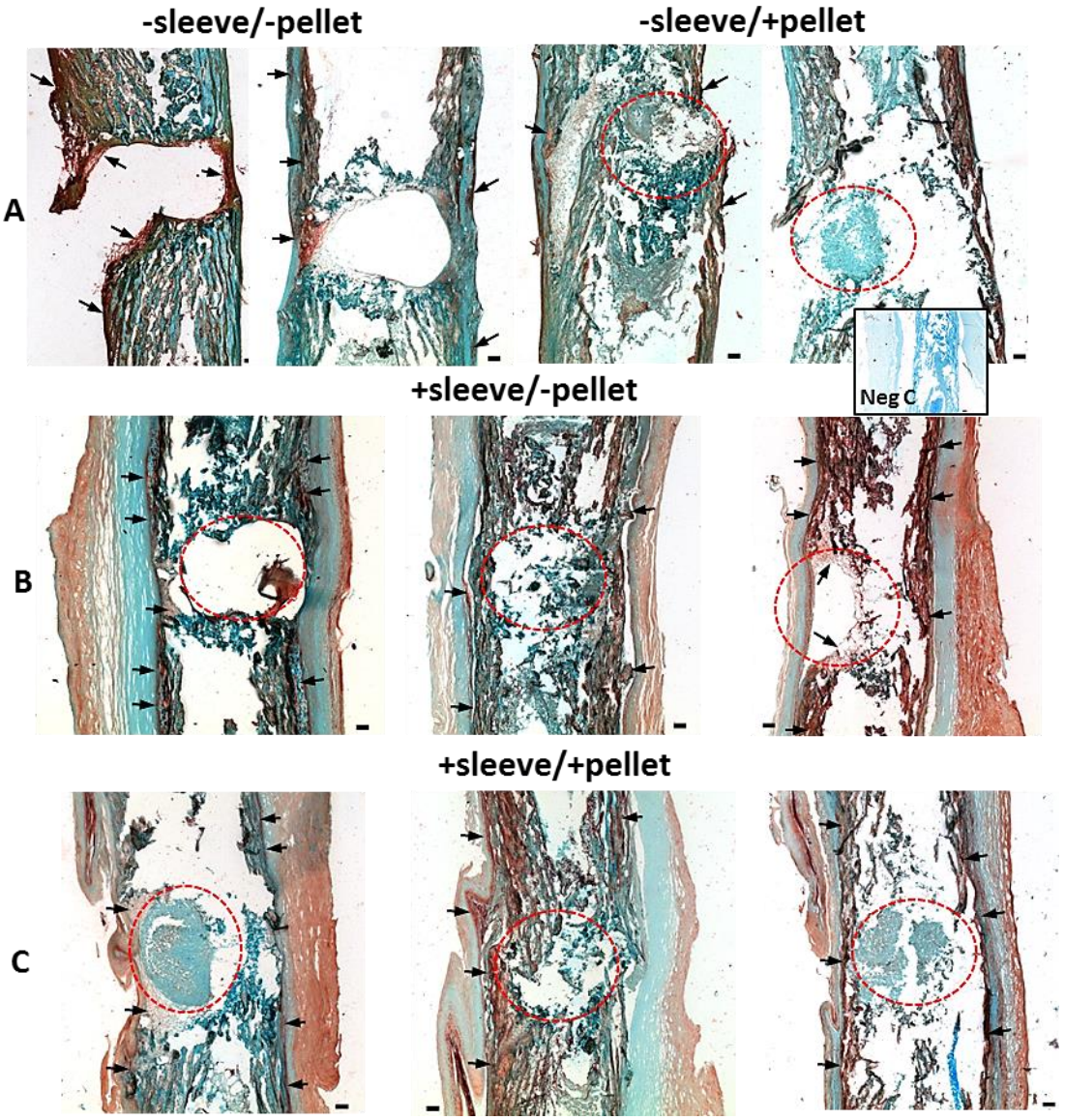

Figure 5.20. **COL-2 positive staining** of D10 femurs sections with and without human placental vessel sleeves. **A.** Control femurs without vessel sleeves with and without pellet implants (-sleeve/±pellet), **B.** Sleeved femurs without a pellet (+sleeve/-pellet), **C.** sleeved femurs with pellet (+sleeve/+pellet). COL-2 staining was evident within the margins of the defect in some of the control femurs. COL-2 was distinctly expressed along the sleeve/periosteum interface (arrows). Circles depict defect area. Scale bar: 100μm.

5.5 Discussion

Decellularised matrices (DMs) offer a useful substitute for biomimetic scaffolds in tissue engineering, reviewed in (Pashneh-Tala *et al.*, 2016). Desirable properties of DMs comprises the ability to preserve essential components of the native ECM and the architecture of the tissue (Badylak *et al.*, 2009). Typically decellularised matrices are used in applications replacing the same tissue type. In the case of the vasculature this line of therapeutic intervention has produced varied results in clinical applications (Olausson *et al.*, 2012). Heterotypic tissue application of vascular decellularised graft in particular could prove useful for application in bone fractures to encourage cell invasion by host tissue, integration and remodelling, stimulated by vascular chemotactic factors contained within decellularised ECM.

In this study, the small-diameter (<4mm) decellularised blood vessel grafts from the human placenta chorion (Schneider *et al.*, 2016), were utilised as a support sleeve surrounding cell pellet constructs within a precision drill defect of (E18) embryonic chick femora. The aim was to assess biocompatibility and suitability for bone regeneration application of the vessel matrices in this setting and the potential to aid bone formation as a source of growth factors and scaffold for cell migration and proliferation, and furthermore, to shield the defect, with or without implanted cells constructs from any disruption or dislodgement. The current study has demonstrated the successfully re-cellularisation of the vessels with allogenic cells (HUVEC), with good cell viability as indicated by Live/Dead staining. It was established that the decellularised vessel graphs demonstrated good biocompatibility (100% survival) and integration (70% integration) in a CAM assay over an 8 day incubation period. This was further confirmed by histological assessment using tissue and antibody staining, revealing invasion of the vessel sleeves by chick embryonic tissue with a well-maintained morphology (CAM integrated sleeves) of the vessel sleeves compared to non-CAM-integrated sleeves.

Previously, re-cellularisation of decellularised human liver scaffolds with human hepatic cell lines demonstrated excellent viability, migration and proliferation of the cells as well as good biocompatibility, subcutaneously tested in immune competent mice over 21 days (Mazza *et al.*, 2015). In studies

comprising a short-term mouse (14 days) and long-term porcine (6 months) model using decellularised human dermis scaffolds for wound healing, Bannash *et al.* 2007, observed successful integration of the dermis with reduced wound contraction and reduced myofibroblast formation compared to the control group grafted with epithelial cells (Bannasch *et al.*, 2007).

Decellularised placental tissue has been reported as a promising candidate for tissue engineering applications to generate an adipose tissue-substitute following lumpectomy surgery (Flynn *et al.*, 2006). Given the fetal-maternal origin of the placenta and its function in immune tolerance during pregnancy, placental tissue offers significant potential in appropriate clinical regenerative applications (Caruso *et al.*, 2012). Placental tissue is typically more readily available than other graft tissue, such as saphenous vein or internal thoracic artery grafts involving invasive harvest (Pashneh-Tala *et al.*, 2016). Placental tissue is rich in human ECM and can be readily harvested, whilst highlighting a more favourable source of non-cadaver human allograft material (Flynn *et al.*, 2006; Schneider *et al.*, 2016).

In this study, Micro CT 3D imaging revealed a visible reduction of the defect area in femurs covered with the sleeves compared to non-sleeved controls over the 10 day organotypic culture period. Subsequent analysis of bone forming parameters confirmed a significant increase in Bone Volume in sleeved treatment groups compared to femurs without placental vessel sleeves. Interestingly, the addition of the cell pellet construct had no additive effect on the repair of the bone defect as revealed by micro-CT analysis. However, the micro-CT images of the pellet implanted femurs indicated a reduction in the defect at day 10, compared to day 0. Thus it can be inferred the shielding effect of the sleeve surrounding the defect, provided an environment conducive to bone healing. Dislodged bone fragments in and around the defect as a result of the initial drill defect application were maintained in situ by the sleeve and may have contributed to the healing process and to homeostatic cell signalling via cells within the fragments. Preservation of the defect area by the sleeve may contribute to secreted factors being more readily contained within the bandage, rather than dissipating out into the surrounding culture medium.

Evaluation of bone forming parameters at the lower resolution of 35µm, to ensure minimum exposure of the cells to radiation, and the global thresholding somewhat limited the micro-CT analysis. This resulted in negative values of bone volume in the negative controls and the positive construct-implanted controls, contrary to data shown in chapter 4 of increased bone volume in pellet implanted femurs. Additionally, 3D imaging depicting a partial closure of the defect in the cell implanted non-sleeved femur samples, indicated bone healing was occurring within the femurs. Increased scanning resolution of micro-CT certainly would improve image quality and thresholding for future experiments but has to be carefully weighed against possible damage caused to the embryonic tissue by longer radiation exposure times. A cofounding factor for the results in the bone volume parameter of the positive and negative control groups could be the stated problems experienced during the HUVEC pellet setup. The altered shape and lack of cohesion of the pellet had an effect on the fixation within the defect. This alteration may have impacted on the cell interaction of the implant with the femoral tissue.

Histological analysis demonstrated extensive collagen expression and significant integration of the decellularised sleeves with the bone collar (Figure 5.15). Cell invasion of the sleeves, possibly from the periosteum, was observed at the sleeve/bone interface with visible proteoglycan formation between the sleeves and the periosteal bone detected by A/S staining and co-located with COL-2.

Interestingly, the expression pattern of HIF-1α within the femurs/sleeve often coincided with COL-2 expression, where COL-2 is an essential cartilage matrix protein and believed to be induced by HIF-1α (Duval *et al.*, 2009). Duval *et al.*, 2009, reported loss of chondrogenic markers aggrecan and COL-2 post expansion of chondrocytes for autologous implantation and subsequent hypoxia induced re-differentiation of COL-2. HIF-1α was identified in preventing dedifferentiation of cartilage and manipulation of HIF-1α via hypoxia could induce re-differentiation of cartilage cells (Duval *et al.*, 2009). Similarly, cultured chondrocyte expression of GAG, aggrecan and COL-2 were observed to be increased by hypoxia (2-5% oxygen) (Duval *et al.*, 2009; Lu *et al.*, 2013) which could indicate that the sleeve/bone integration induced regions of reduced oxygen levels between the femur and sleeve boundaries

thus triggering a secondary healing mechanism involving the HIF-1α pathway and COL-2 production. Furthermore, HIF-1α has previously been shown to induce VEGF gene expression during fracture repair and co-expression of HIF-1α and VEGF has been demonstrated in fracture callus samples of rat femora (Komatsu *et al.*, 2004). The band of cartilage located within the sleeved femurs in this study, therefore, could represent a temporary matrix to connect the sleeve with the bone. Thus, it was tempting to speculate this could represent the formation of a soft callus connecting two fracture ends during endochondral bone healing (Carano, 2003).

The application of decellularised vessel matrices for bone regeneration has received scant attention to date as bone reconstructive surgery frequently uses demineralised bone grafts, either synthetic or from autograft tissue, while decellularised matrices are increasingly used in reconstructive surgery of frequently occurring tendon injuries (Ning *et al.*, 2012; Pan *et al.*, 2015). The dense structure of bone and tendons, however, can make the decellularisation process problematic and prolonged chemical treatment can affect their specific mechanical properties (Anisimova *et al.*, 2015), thus application of a soft decellularised matrix of vascular origin poses a novel alternative.

Conclusions and future outlook

The current model provides a novel approach to critical aspects of bone repair, such as defect fixation, tissue preservation and growth factor homeostasis as well as demonstrating a dual application of (a cell based) scaffold and decellularised sleeve dressing, acting as a periosteal dressing to aid bone healing. Long-term studies are required for this model to recapitulate the bone healing process further and to observe callus remodelling in line with endochondral bone formation. Initial expansion of the organotypic culture of the current model from 10 days to 20 days, prior to an *in vivo* application, could greatly enhance results in bone formation already observed in the current study. In addition, implantation into the CAM model could give insight into the sleeve repair properties of bone defects with the added presence of a functional vasculature.

In summary, the current 3D vascular sleeve/cell construct bone defect model has demonstrated extensive integration of decellularised vessel grafts with bone healing characteristic factors as well as denoting a significant increase in bone parameters. Sleeved femurs demonstrated higher levels of bone formation compared to non-sleeved samples, regardless of the presence or absence of pellet constructs. This does not preclude application of the cell construct in this model as reported in chapter 4; rather the current results indicate shortcoming in the analysis, which can be overcome in refining future studies. Such studies could include:

- Extending the culture period of organotypic culture.
- Using pellet constructed shapes as demonstrated in (Appendix 7.4.2-7) to up-scale the experimental setup.
- Increasing the defect size within the decellularised vessel sleeve and scaling up the pellet construct within the defect as mentioned above.
- Increasing micro-CT scanning resolution to 18µm to improve bone forming parameter analysis of subtle changes of newly regenerated bone.

The current model has indicated the potential of decellularised human placental vessel grafts to augment bone healing. Furthermore, in combination with cell pellets in particular, the migratory activity of HIF-1α positive cells was observed. Further investigations are required to elucidate the mechanisms involved and to explore the potential of this model for bone or indeed cartilage regeneration in tissue engineering.

Chapter 6

Final discussion

6.1 Conclusions

This thesis has explored the inter-relationship of endothelial and skeletal cells within the bone niche and reciprocal involvement of these cell types in the process of bone healing. To this end, cell-based strategies were employed to demonstrate that endothelial cells in combined culture with fetal or adult skeletal cells, potentiate osteogenic and angiogenic differentiation by modulating the expression of early bone markers ALP and COL-1 as well as VEGF receptor genes. Further investigation established the osteogenic effect of skeletal and endothelial cell constructs in a bone drill defect organ culture that further underpinned HUVEC potential for bone healing within this niche by producing the highest levels of bone forming parameters. A final investigation comprising the application of periosteal sleeves in combination with endothelial/skeletal cell constructs established further an improved bone defect healing over non-sleeved treatments.

Cell based tissue engineering offers an exciting approach to regenerate tissue in the absence of exogenous, naturally or synthetically engineered biomaterials, thus reducing the potential of rejection, ensuring functionality and preventing the build-up of residue toxins (Fishbach *et al.*, 2017). Although, the continuous development of smart biomaterials is currently extending the boundaries of regenerative medicine, the application of a cell based approach offers unique characteristics that remain superior to the plethora of biomaterials in use in regenerative medicine today. In essence, cells display significant adaptation potential and can sense their surrounding environment and respond to a multitude of subsequent cues.

Cells are able to modulate migration and proliferation or activate/inactivate regulatory processes (Fishbach *et al.*, 2017). Furthermore, cells have the ability to interact selectively to specific signals and with specific tissues; reviewed by (Fishbach *et al.*, 2017). While much of the experimental work in tissue engineering is undertaken on single cell types *in vitro*, the cells in tissue/organs are typically exposed to and interact with a number of distinct cell phenotypes to modulate tissue and organ function. In regenerative medicine the interactive processes of multiple cell types is now starting to be

harnessed as a potential therapeutic strategy. Cell co-culture models involve extracting, expanding and then re-combining the cells present in a particular tissue *in vivo*. Co-cultures, in particular three-dimensional constructs, can mimic the microenvironment by producing native ECM and thus generating factors that stimulate the biochemical communication of the cells present. Co-culture models, however, do rely on an intricate balance and temporal cascade of molecules that determine cell differentiation and the complex pathways that affect the interaction of various cell types (Kaigler *et al.*, 2005). Indeed, homeostasis of the tissue of interest is constantly being monitored and maintained by cells, through autocrine and paracrine actions. 2D monolayer co-cultures lack the three dimensionality of cell migration, differentiation, mechanical stimulation and subsequent interaction with the surrounding tissue. In this culture setting, the cell system responds differently to exogenous factors in comparison to cells within a 3D co-culture environment and system. Thus, typically, a 2D co-culture will only provide a snapshot of the cell interaction but 2D co-culture can demonstrate a useful initial indicator of functional interaction of the cells of interest. Three-dimensional co-culture constructs in contrast, offer an approach to mimic, in part, the natural tissue by being multi-layered thus increasing contact area and proximity of the cells to each other as well as mechanical forces and enabling three- dimensional growth.

Bone is a multicellular, highly vascularised organ that is able to grow and self-repair under normal conditions (Einhorn, 2005). The cells involved within maintenance of bone homeostasis can be viewed as a classical dynamic co-culture system where the predominant players, osteoclasts, osteoblasts and osteocytes (each displaying distinct phenotypes) coordinate to respond to the functional needs of the body. As early as the process of embryogenesis, the combination of skeletal progenitor cells, together with the developing vasculature gives rise to the complex structure of bone and, critically, throughout the duration of life, the vasculature has a central role in the maintenance of skeletal integrity. Thus, during endochondral fracture healing a number of the developmental bone forming processes are recapitulated. In

order to gain an insight into the bone forming potential of the cell assembly in embryonic development, it was necessary to recapitulate the osteogenic and angiogenic potential within the cellular structure of embryonic bone.

Chapter 3: Interaction of skeletal and vascular cell lineages and the influence on respective functionalities when cultured together.

This chapter examined the hypothesis that *vascular and skeletal progenitor cells cooperatively enhance markers of bone formation when maintained and combined in contact-culture.*

The specific aim of the work in chapter 3 was to define the functional interaction between human endothelial and fetal or adult stromal cells. The initial objective was achieved by demonstrating how the contact co-culture of human fetal and adult skeletal cells in combination with human endothelial cells stimulated osteogenic and angiogenic inductive pathways, as assessed by enzyme activity assay and gene expression analysis. ALP and COL-1 typically, were significantly enhanced in co-cultures, indicating increased bone-inductive processes being activated such as phosphate production and collagen fibre synthesis, both central in bone formation. A similar pattern of osteogenic effects on co-cultures was observed between adult skeletal and fetal skeletal cultures in combination with HUVECs. Along with the hypothesis stated, HUVECs were shown to be a key driver in this setting as the increase in osteogenic inductive markers was observed in the co-cultures, whilst HUVECs failed to express the key osteogenic markers examined. The osteogenic effect of HUVECs on ALP expression was correlated to ALP expression in the basal skeletal cultures for both fetal and adult lineages. Skeletal progenitors demonstrated enhanced osteogenic differentiation following co-culture with HUVECs. Conversely, HUVECs demonstrated raised gene expression of VEGF receptors, KDR and FLT-1, which were significantly upregulated in the co-cultures, but demonstrated negligible expression in HBMSC monocultures. Furthermore, in line with objective 2, to investigate the effect of VEGF on co-cultures of fetal or adult skeletal cells with HUVECs, it was established that VEGF supplementation at different concentrations reduced ALP in osteogenic cells and enhanced VEGF receptor gene expression in co-cultures. These results highlighted the importance of the temporal coordination of osteogenic

and angiogenic factors and associated processes during bone differentiation and formation. Therefore, the hypothesis set out in chapter 3 that vascular and skeletal progenitor cells cooperatively enhance markers of bone formation in co-culture, was proven.

To further evaluate the osteo- or angiogenic effect of endothelial and skeletal cell co-cultures, an extension of the culture model from a more simplistic 2D system to one more closely resembling 3D *in vivo* cell behaviour was undertaken. HBMSC/HUVEC constructs were employed as an implant in a chick femoral drill defect to explore the interactive cell processes during bone healing.

Chapter 4: Engineering 3D endothelial and skeletal cell constructs and exploring the osteogenic potential within a bone defect.

In chapter 4, the hypothesis that 3D co-culture constructs of HUVECs and HBMSCs can aid bone formation in an organotypic culture bone defect model, was examined.

The interaction of skeletal and vascular cells in a three dimensional bone setting to drive osteogenesis was explored, specifically the capacity of cell pellet constructs to improve healing in bone defects. To this end, a drill defect in the mid diaphysis of an embryonic chick bone was employed to encompass the spherical co-culture cell construct. This model removed the need for invasive fracture fixation that could damage the marrow cavity, which, together with the periosteum and the surrounding soft tissue provide sources of skeletal progenitor cells (Gerstenfeld *et al.*, 2003) that could interact with the implanted cell pellets and accelerate bone healing.

Micro CT analysis revealed that treatment groups containing pellets consistently displayed a significant increase in bone volume, compared to empty defect controls. Surprisingly, the constructs of vascular cells (HUVECs) demonstrated the highest increase in bone volume compared to HBMSCs or the co-culture constructs. The differences observed in the cell construct integration of HUVECs within the femoral defects revealed that HUVEC implants displayed a less dense and more heterogeneous morphology compared to the

more compacted, less tissue-interactive co-culture constructs. Within the HUVEC constructs, increased cell activity was observed, evidenced by enhanced cell migration, collagen fibre formation, as well as cell invasion into and around the defect region. It is likely that HUVECs provide cell-signalling molecules through cell-to-cell contact or paracrine/autocrine exchange with the surrounding cells/tissue to mobilise angio- or osseo-conducive biochemical signalling, resulting in enhanced bone formation. This was further confirmed with immunological staining by the presence of key proteins indicative of bone matrix formation such as COL-1 and particularly COL-2 as well as inductive mediation of angiogenesis by HUVEC expression of CD31 and vWF. CD31 positive HUVECs were observed forming small aggregates within the co-culture pellets, suggestive of vessel tube formation, together with the migration of HUVECs, infiltrating adjacent areas of the defect.

These results confirmed that co-culture constructs have the potential to drive bone formation and angiogenesis during the healing process and further suggested a central role of HUVEC pellets, in particular, in the bone forming process evidenced by enhanced bone volume increases. The cell co-culture construct defect model produced promising results proving the hypothesis set out in chapter.

Interestingly though, HUVECs and HBMSCs alone exceeded the co-culture constructs in their capacity to regenerate bone in this organotypic model. Increased cell-tissue migratory activity in the HUVEC implanted defects observable with A/S staining and lack of migratory cell activity of the compacted co-culture pellet may indicate this differential in bone formation, caused by an initial slower response to healing. However, it has to be considered that the co-culture implanted defects still produced a significant change in bone volume. The central role of endothelial and skeletal cooperation and co-dependence in cell migration and recruitment was demonstrated in an ectopic bone-forming model by Tasso and co-workers, 2010 identifying an endogenously recruited cell population from a mouse implanted MSC/bioscaffold construct after 7 and 11 days of implantation. The recruited cell populations were enriched with CD31+ endothelial progenitors at day 7 and with CD146+ pericyte-like enriched cells at day 11. The authors did not observe this population enrichment with scaffolds without MSCs. Tasso

and colleagues indicated that the pericyte-like cell population was dependent on the initial CD31+ cell population, which was equally recruited by factors released from the initial scaffold-seeded MSCs (Tasso *et al.*, 2010). These observations further demonstrate the importance of the signalling cascade between the various cells present in and around the defect area.

Additional to this, the need to develop systems that can recapitulate human tissue formation is driven by increasing ethical concerns of animal use, the lack of tissue accessibility and variability in animal biology and the need for high throughput models. To this end, the cell organoid is superior in serving as a platform for testing compounds, and for regenerative therapies whilst reducing invasive animal work. To scale up the current model to be employed for future *in vivo* testing, an obvious limitation was the lack of a functional blood supply and a lack of scalability for a larger model. Thus, prior to any animal work it would be prudent to refine the current model in order to implement the cell based construct with a suitable matrix that is able to integrate into a larger defect. Models for tissue replacement and regeneration in cardiovascular or orthopaedic surgery routinely use synthetic tissue grafts/scaffolds engineered from polymers seeded with autologous bone marrow cells. (Shin'oka *et al.*, 2005). However, these techniques are often prone to lack of integration due to post-operative complications such as thrombosis, aneurism or calcification of the graft. Similarly, the preferred treatment to regenerate the bone and vasculature following damage caused by fractures, or disease, are autograft material. Limited availability of autograft material and donor site damage are a major restriction of these techniques (Cheng *et al.*, 2014). With the refinement of tissue decellularisation processes of the past years, decellularised vascular grafts are a promising alternative to meet the demand for non-thrombogenic arterial conduits, which would be equally essential for re-vascularising of tissue surrounding bone to avoid necrosis, in orthopaedics. Thus, in the following chapter adaptation of the current model to cross-integrate the pellet construct defect model with a human derived decellularised vascular matrix was explored (Papadimitropoulos *et al.*, 2015).

Chapter 5: The effect on bone formation of using human placental decellularised blood vessel matrices and implanted cell constructs in an ex vivo organotypic bone defect model.

Chapter 5 examined the hypothesis that decellularised human placental vessel sleeves enhance bone repair as a consequence of trophic factors and provision of structural support, when applied around a bone drill defect containing an implanted 3D cell construct.

In order to combine the benefit of tissue proxies with a natural addition of structure and ECM, decellularised blood vessel matrices were used to augment cell implant fixation and improve containment within the defect area. The aim was to improve bone healing of a chick femoral defect and to improve scalability of the cell construct model for larger defect application for future translational use. Objective 1 of chapter 5 comprised testing of human placental decellularised vessels by reseeding with HUVECs and bio-integration testing of grafts in a vascular bed. This objective was confirmed where good biocompatibility of the human tissue derived sleeves in the CAM assay was established and successful recellularisation of the vessel sleeves was demonstrated. Following on from these experiments, in the organotypic bone defect culture model, micro-CT imaging demonstrated superior bone healing activity in sleeved femoral defects compared to unsleeved samples; confirming objective 2, to examine the potential of human placental decellularised vessels to aid bone repair when employed as a protective sleeve around the femoral defect.

Cell based constructs and decellularised vessel tubes demonstrated comparable levels of enhanced bone formation over controls in the organotypic chick femoral model. Interestingly, under the specific methods of analysis it was not possible to show an additive positive effect in the combined results. This could have been improved by adapting and refining the cell construct size and the femoral defect to better accommodate the contribution to the bone healing process added by the construct implant within the CT analysis parameters.

Decellularised matrices have been mainly produced from a number of species including mouse (Anghelescu *et al*., 2015), porcine (Dimitrievska *et al*., 2015),

and rat (Katsimpoulas *et al.*, 2015). However, few studies have tested decellularised vessel grafts in a regenerative capacity in *in vivo* or clinical scenarios (Pellegata *et al.*, 2015) (Olausson *et al.*, 2012); furthermore, very little data has been established regarding the efficacy of whole decellularised organ transplantation (Kitahara 2016), indicating that this research field is still at an early stage within the clinical setting. Kitahara et al. sacrificed 12 pigs to test transplantation of whole decellularised and recellularised pig hearts into 3 or more recipient pigs. Due to the physiological experimental modifications to the blood flow, the experiment was not designed suitable for clinical application. Transplants were harvested after 3 days with arterial occlusion by thrombi evident and massive inflammatory cell invasion into the atria observed histologically (Kitahara *et al.*, 2016). Transplantations were deemed successful evidenced by coronary artery angiography detecting presence of contrast medium within the cardiac chambers (but not the coronary artery); however, no indication to the post-operative condition of the pigs were reported or whether consciousness of the animals was regained, post-transplantation. *In vivo* transplants are often short term and, indeed concerns may be raised over ethical reservations towards the transplantation prior to extensive refinement of the technique in smaller animal studies or proficient suitability of large animal models for clinical application.

In order to avoid haemorrhaging and occlusion of blood vessel and alternative to fusing existing vasculature, pre-vascularisation of the graft could be beneficial. In an attempt to encourage vasculature into a recellularised tissue engineered scaffolds, Shandalov *et al.*, 2015, reported the use of an engineered muscle flap to reconstruct a mouse abdominal soft tissue defect. A polymer scaffold was pre-cultured with an array of cells and temporarily implanted near the femoral blood supply of the animal. The construct was subsequently transferred as an autologous axial flap into a deep abdominal wall mouse defect. The muscle flap showed extensive integration, vascularisation and strength after one week of implantation (Shandalov *et al.*, 2014; Shandalov *et al.*, 2015).

Indeed, to integrate a functional vasculature, the decellularised vessel sleeves in combination with cell constructs, as demonstrated in chapter 5, could be

pre-vascularised to encourage blood vessels into the existing ECM of the sleeve. This approach would also retain the cell construct in situ with the surrounding vasculature invading the sleeve accompanied by cells and factors from the surrogate vessels, possibly pre-differentiating the cell constructs within the sleeve. If cultured over an extended period the sleeve/organoid could demonstrate more advanced soft callus characteristics, subsequent to protein expression (COL-1, COL-2, CD31 and vWF) observed after the 10 day organotypic culture of the pellet construct implanted femurs in chapter 4 and the sleeved femur defects assessed in chapter 5 (COL-2, HIF1-α, proteoglycans). A pre-differentiated, pre-vascularised organoid could in the future serve as a callus substitute within a bone lesion initiating blood vessel invasion and hence aiding the regeneration of the bone defect.

Future work

The current studies have demonstrated the potential of skeletal and endothelial cell combinations to stimulate early osteo and angio-inductive processes in bone defects. In addition of decellularised human vessel sleeves, a source of trophic factors and bone structural support have been demonstrated to improve bone healing.

A number of explorative areas remain to be addressed to establish whether these models will stand as a high throughput, preliminary *ex vivo* model for bone defect applications or indeed, whether this model or part of it can be up-scaled for *in vivo* studies and/or clinical translation:

The defect and pellet construct size used for implantation into the femurs need to reflect the application area of the human placental vessel sleeve around the bone to improve evaluation of results. The sleeve covers most of the diaphysis of the bone and a suitably sized defect and cell construct needs to be applied proportionately to the area covered by the sleeve. This will improve results of the bone forming parameters reflecting the combined effect of the sleeve/cell application during the healing process.

Possible alteration of the bone defect type/size, implementing, for example, a wedge defect into which pellet constructs or pellet customised shapes could be

employed, thus accommodating a larger tissue assembly. In addition, further *in vitro* cell co-culture combinations, such as different cell types (e.g. chondrocytes and endothelial cells) (Freeman *et al.*, 2015) and cell ratios within constructs could be investigated and optimised together with protein expression profiles to assess the pattern of differentiation and viability of the constructs.

With results of enhanced bone formation already observed within 10 days in the current organotypic models of chapter 4 and 5, an increase in the culture period would be essential to assess changes occurring further during the later phases of endochondral bone healing encompassing callus maturation and remodelling (van der Stok *et al.*, 2014). This could demonstrate bone healing, against a timeline more comparable to the natural healing process; and indeed indicate, whether the current pellet/vascular ECM sleeve/construct model could enable healing of a non-union fractures over the longer culture period (Ferrera *et al.*, 2002). Therefore, an increased culture period from 10 days to at least 21 days could inform whether bone formation occurred within the defects of the current model.

To investigate the vascular regenerative potential of the pellet constructs/decellularised vessel sleeve model further, testing of the effect of hypoxic and hyperoxic conditions would be beneficial in view of the observed HIF-1α expression patterns demonstrated in chapter 5. During hypoxic conditions, HIF-1α transcription factor is known to stimulate blood vessel formation via VEGF gene expression (Schipani *et al.*, 2008). Conversely, hyperoxia has been shown to accelerate fracture healing demonstrating larger callus formation, increased osteoblast proliferation and enhanced COL-1 and ALP gene expression, in a mouse model following exposure of the mice to high oxygen levels (Kawada *et al.*, 2013).

Exploring the spatiotemporal release of growth factors within the organotypic cultures would be beneficial to highlight areas for improvement of the cell based implantation method. The current *ex vivo* model was based on the omission of exogenously added factors and thus relied on the femoral tissue in combination with the cell constructs and the decellularised vessel sleeves to

provide the necessary growth factors (environment) for bone repair. Contrary to demonstrating variability in the effect of VEGF supplementation of *in vitro* co-cultures, addition of VEGF (100ng/ml) previously demonstrated an increase in bone forming parameters in an organotypic chick femur culture (Inglis *et al.*, 2016). To gain an insight into the spectrum of osteo- and angiogenic action on the bone healing process in the current model, temporal addition of growth factors such as VEGF and BMP-2 to femurs under organotypic culture with pellet construct and umbilical vessel sleeve would be beneficial.

Furthermore, it would be valuable to assess the potential of this model for vascularisation as well as bone healing by implementation into the chorioallantoic membrane culture (CAM) model or a small in vivo study, such as the mouse subcutaneous implantation model (Walser *et al.*, 2013). This would aid in assessing whether a pre-vascularisation of the sleeve/construct implant would have a regenerative potential.

Future outlook

This project has demonstrated the use of human cell based therapy in combination with a novel human decellularised matrix to successfully improve bone tissue healing in an organ culture model that is inexpensive and has a high throughput capability. The translation from reliable *in vitro* to *in vivo* testing requires further refinement and a tighter control on directing cell migration, proliferation and differentiation. In order to produce the optimal tissue replacement, the tissue must be integrated with the central control mechanism to engineer desired cell behaviour. Further refinement of functional control of the current cell construct/sleeve model could be achieved, for instance by implementing temporal release of growth factors using loaded vectors, such as nanoparticles within hydrogel coating (Rao *et al.*, 2015), contained within the decellularised sleeve.

Regenerative research today strives to reduce large animal models and replace them with less invasive *ex vivo* high turnover models while translating these into clinically applied therapies that are relatively easy and quick to produce and cost effective (Tang *et al.*, 2016; Fishbach *et al.*, 2017). For future therapies, the source of tissue material used for replacement surgery needs to

be balanced against functional necessity and health consequences for the donor. Placental tissue is readily available with reduced immunogenicity and negligible trauma when removed from the donor. Placental tissue contains vital ECM factors, which depending on use may avoid the addition of costly exogenous factors (Pashneh-Tala *et al.*, 2016).

3D printing is a vastly progressing technology that has recently shown great promise in tissue engineering applications by combining cell/tissue and biomaterials for tissue regeneration. Recent improvements in hydrogel/thermo-polymer composition by reducing shear stress, strain and improving thermo-sensitivity, together with enhanced mechanical integrity of printed constructs may prove critical for bioprinting technology development (Abbadessa *et al.*, 2016). Future advances in 3D printing technologies may eventually reach a stage for bio-printing perfect replica body parts, organs, or customised tissue scaffolds containing the optimal balance of biochemicals and cellular components (Kang *et al.*, 2016). However, all avenues, be it cell based or tissue engineered, will eventually complete a picture from which to select only a few of the most effective, practicable and self-sufficient therapies.

The current studies have established a novel combination of natural components for regenerative therapies by demonstrating the potential of endothelial cells in driving bone formation by:

a) Determining the expression of markers associated with osteogenesis and angiogenesis using 2D co-cultures of human endothelial and skeletal cells;

b) Demonstrating that cell-based co-culture constructs of endothelial and skeletal cells in a bone defect are able to enhance bone healing without exogenous factors, when cultured organotypically and

c) Integrating decellularised matrices as a periosteal support sleeve for structural support and enhanced bone healing to the overall bone architecture in a bone defect cell construct model.

The knowledge gained in this study will be of value to the research community, in particular researchers investigating tissue regeneration using stem cells,

organoids and biomimetic scaffolds. Furthermore, the potential of cell based co-culture constructs in combination with biomimetic scaffolds to enhance bone formation is relevant for tissue engineering and clinical applications of bone and vascular regeneration.

Appendices

7.1 Appendix chapter 2: Methods

The table below lists fetal foot length, in cm, with the corresponding age of the foetus, in days post-conception. The age of fetal tissue used for fetal co-cultures experiments and sequential fetal femur staining in chapter 3 was described using this chart.

Human foetal tissue age	
Foot Length	Days post-conception
3.5	51
3.75	52
4	53
4.5	54
5	55
5.5	56
6	59
6.5	61
7	63
7.5	65
8	68
8.5	70
9	72
9.5	73
10	77

Table 7.1 **Human fetal tissue age, determined by foot length (Lutterodt *et al.*, 2009).**

7.2 Appendix chapter 3: The effect on *vWF* and *VEGF* relative gene expression of endothelial/skeletal mono- and co-cultures with and without VEGF-165 supplementation

Additional gene expression data: following analysis of osteogenic gene expression produced by endothelial/skeletal mono- and co-cultures, the angiogenic potential of the cell cultures with and without VEGF supplementation was assessed by analysing v*WF* and *VEGF* relative gene expression. However, repeated relative gene expression analysis of vWF and VEGF with or without VEGF (50ng or 100ng/ml) produced no significant changes in expression levels, thus the related graphs were included in the appendix of chapter 3.

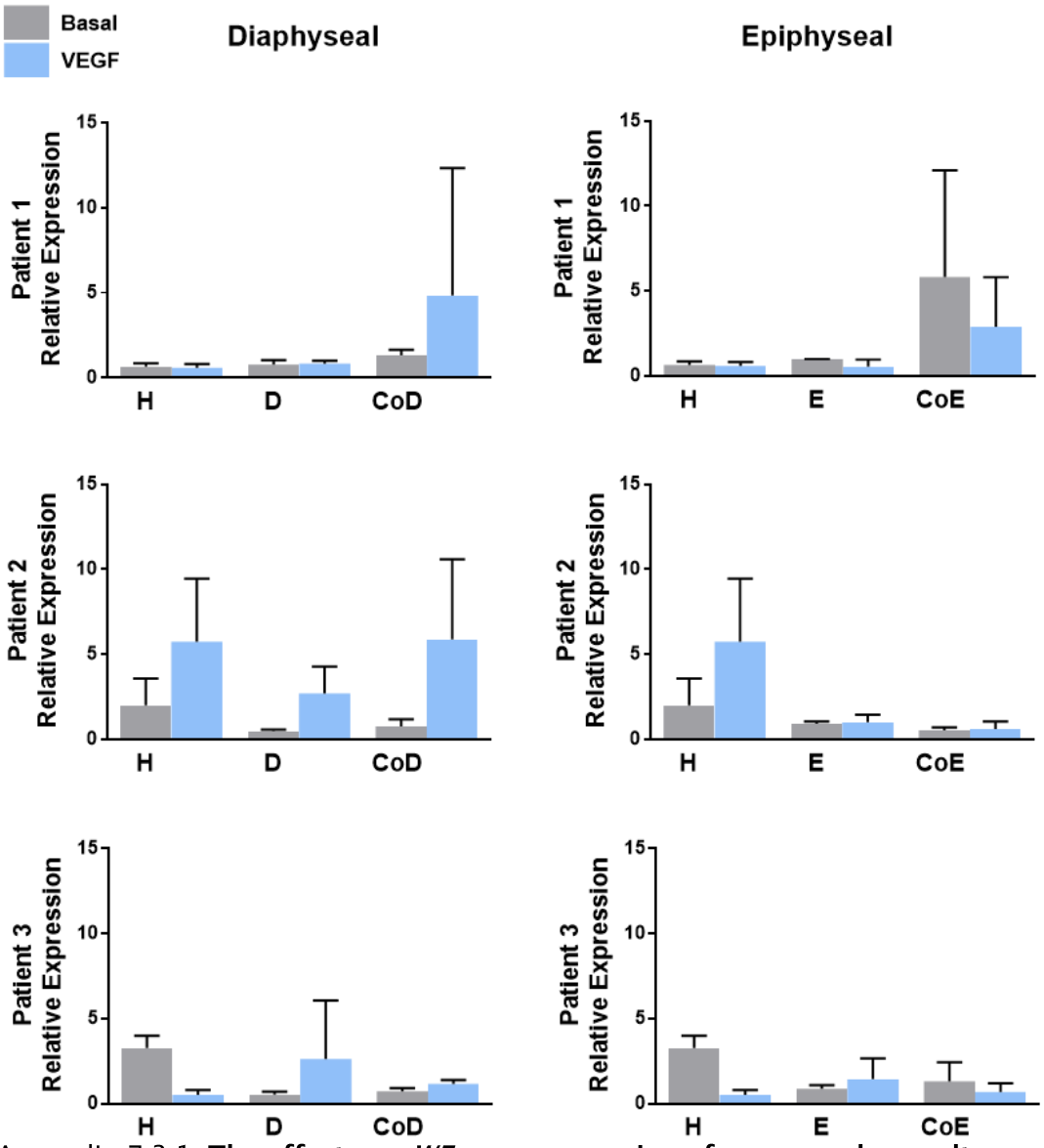

Appendix 7.3.1. **The effect on *vWF* gene expression of mono-and co-cultures supplemented with or without 100ng/ml VEGF**. Graphs represent assays from 3 separate patients/experiments **Patient 1 – 3 Left**: Basal diaphyseal/HUVEC mono-/co-cultures in grey with/without addition of VEGF (in blue) and **Right**: Basal epiphyseal/HUVEC mono-/co-cultures (grey) with/without the addition of VEGF (blue). Results represent mean ± S.D; n=4 replicates; *p≤0.05, **p≤0.01, ***p≤0.001. H= HUVECs, E= epiphyseal cells, D= diaphyseal cells, CoD= diaphyseal/HUVEC co-culture, CoE= epiphyseal/HUVEC co-culture.

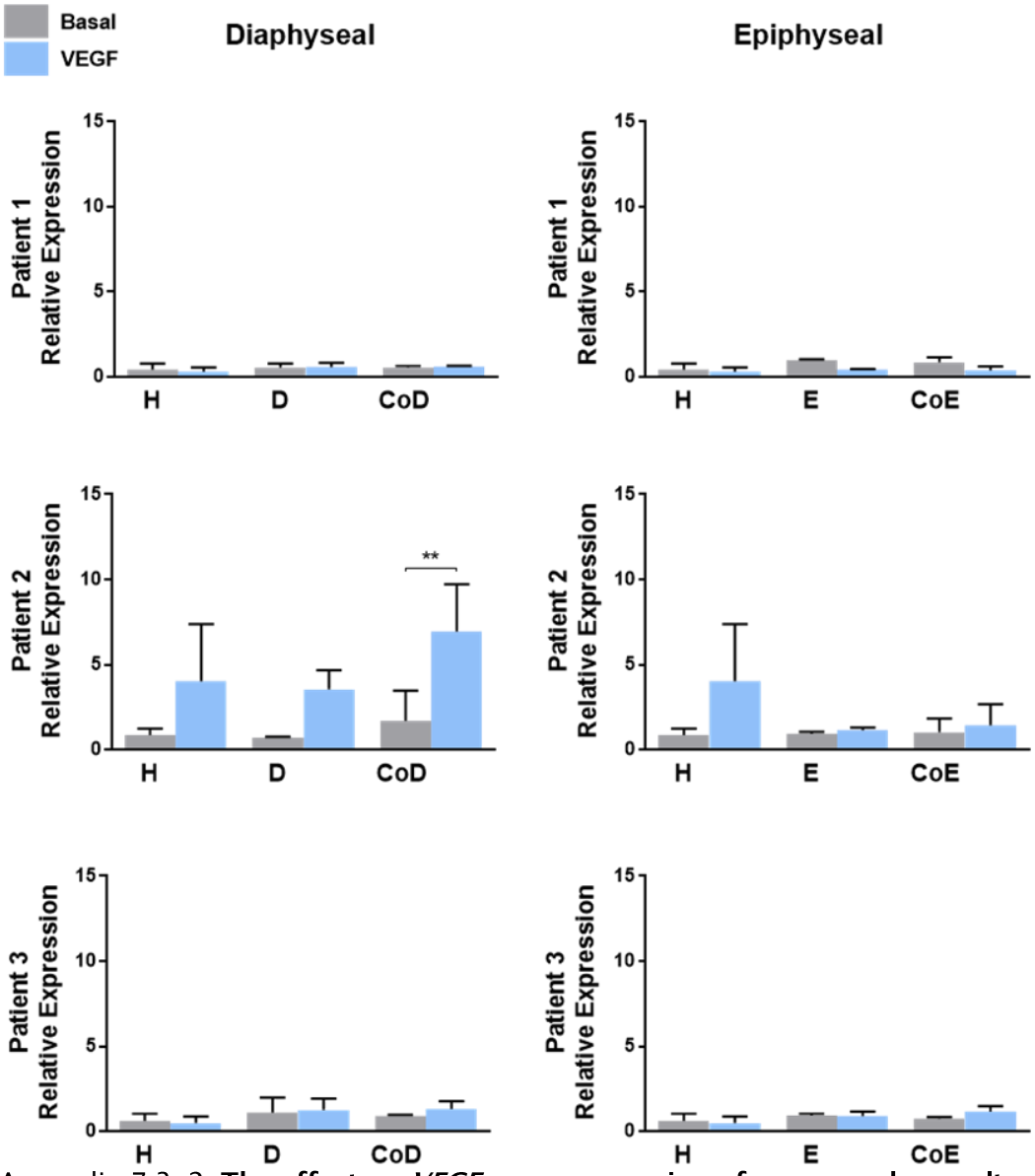

Appendix 7.3. 2. **The effect on *VEGF* gene expression of mono-and co-cultures supplemented with or without 100ng/ml VEGF.** Graphs represent assays from 3 separate patients/experiments **Patient 1 – 3 Left**: Basal diaphyseal/HUVEC mono-/co-cultures in grey with/without addition of VEGF (in blue) and **Right**: Basal epiphyseal/HUVEC mono-/co-cultures (grey) with/without the addition of VEGF (blue). Results represent mean ± S.D; n=4 replicates; *p≤0.05, **p≤0.01, ***p≤0.001. H= HUVECs, E= epiphyseal cells, D= diaphyseal cells, CoD= diaphyseal/HUVEC co-culture, CoE= epiphyseal/HUVEC co-culture.

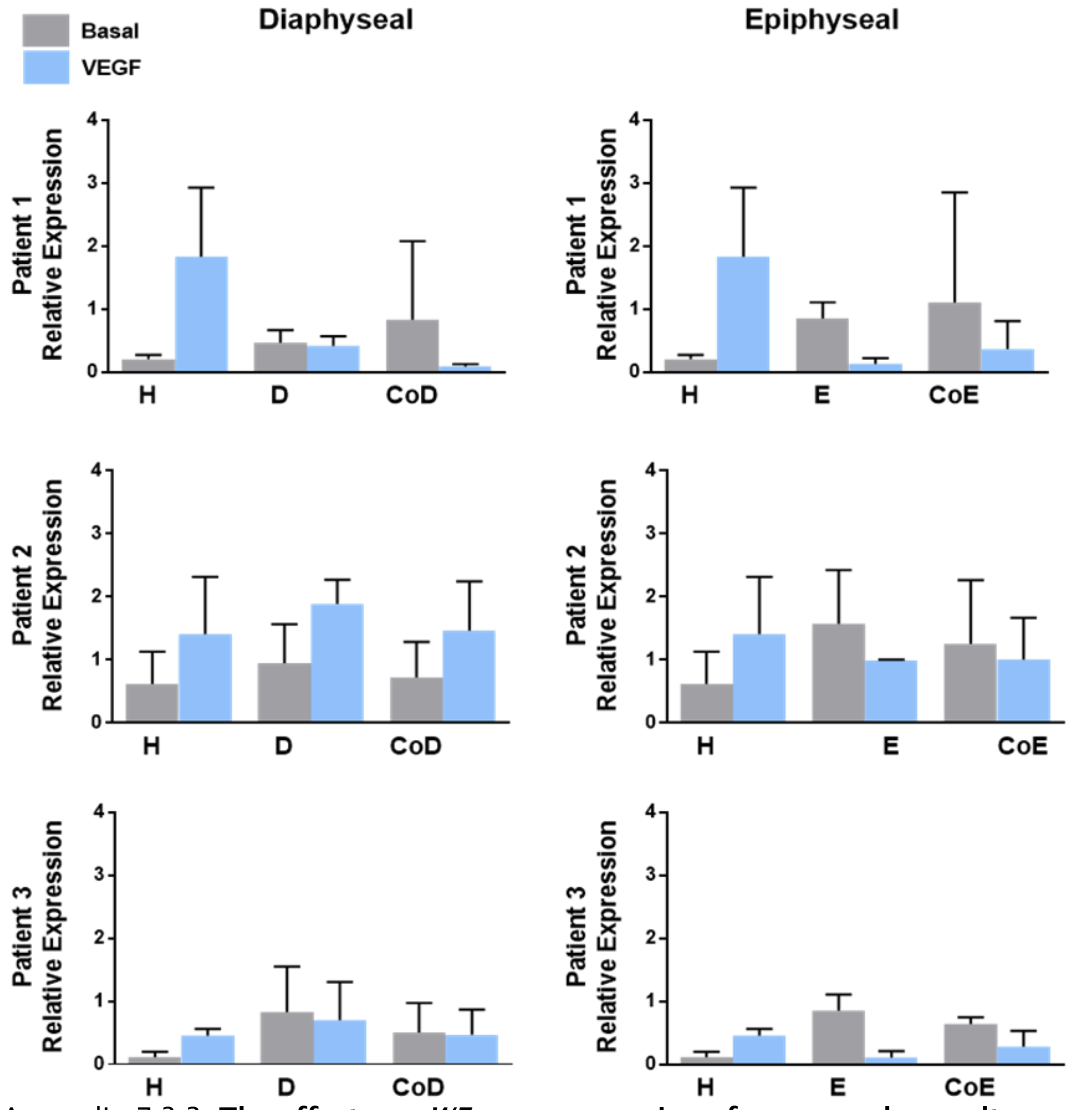

Appendix 7.3.3. **The effect on *vWF* gene expression of mono-and co-cultures supplemented with or without 50ng/ml VEGF.** Graphs represent assays from 3 separate patients/experiments **Patient 1 – 3 Left**: Basal diaphyseal/HUVEC mono-/co-cultures in grey with/without addition of VEGF (in blue) and **Right**: Basal epiphyseal/HUVEC mono-/co-cultures (grey) with/without the addition of VEGF (blue). Results represent mean ± S.D; n=4 replicates; *p≤0.05, **p≤0.01, ***p≤0.001. H= HUVECs, E= epiphyseal cells, D= diaphyseal cells, CoD= diaphyseal/HUVEC co-culture, CoE= epiphyseal/HUVEC co-culture.

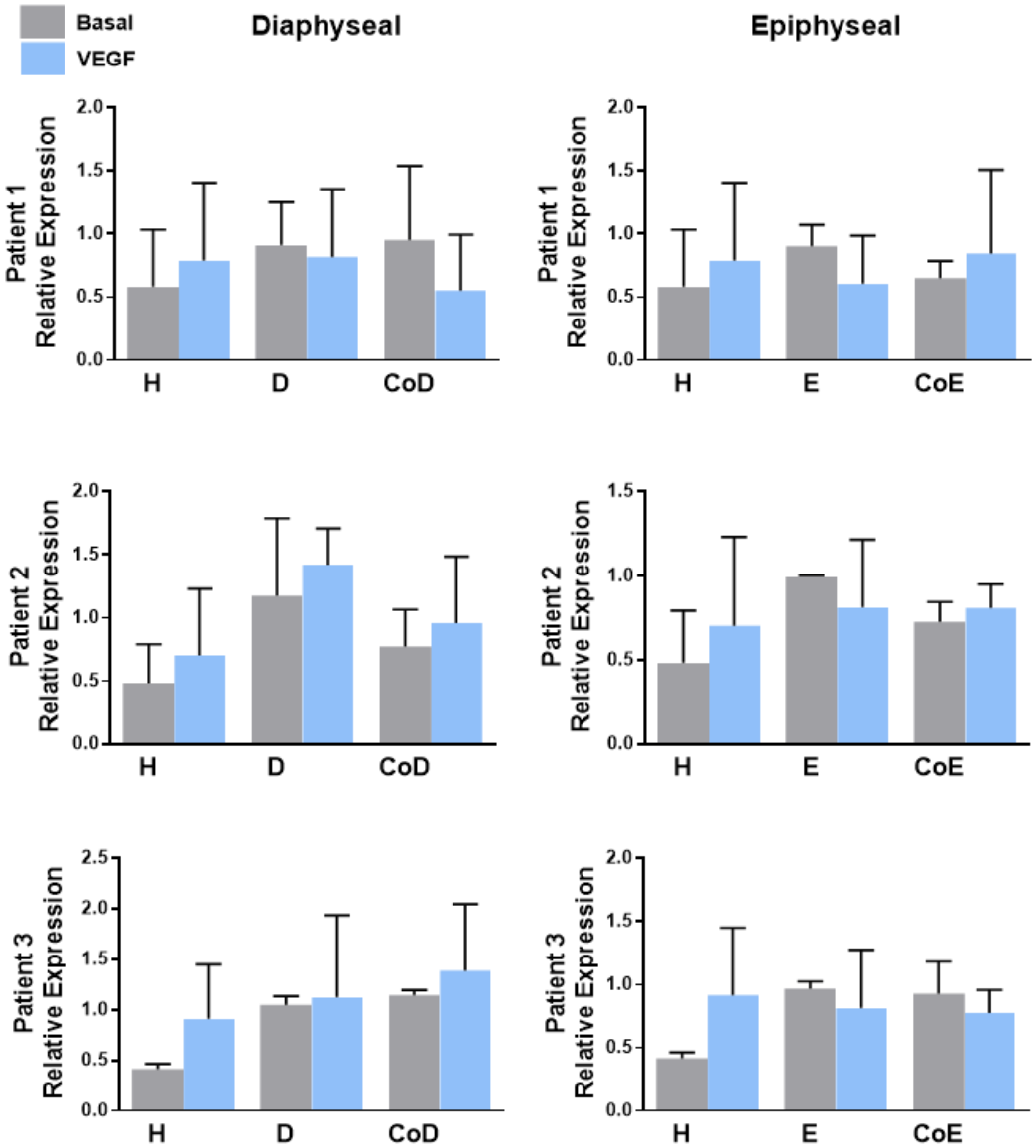

Appendix 7.3.4. **The effect on *VEGF* gene expression of mono-and co-cultures supplemented with or without 50ng/ml VEGF**. Graphs represent assays from 3 separate patients/experiments **Patient 1 – 3 Left**: Basal diaphyseal/HUVEC mono-/co-cultures in grey with/without addition of VEGF (in blue) and **Right**: Basal epiphyseal/HUVEC mono-/co-cultures (grey) with/without the addition of VEGF (blue). Results represent mean ± S.D; n=4 replicates; *p≤0.05, **p≤0.01, ***p≤0.001. H= HUVECs, E= epiphyseal cells, D= diaphyseal cells, CoD= diaphyseal/HUVEC co-culture, CoE= epiphyseal/HUVEC co-culture.

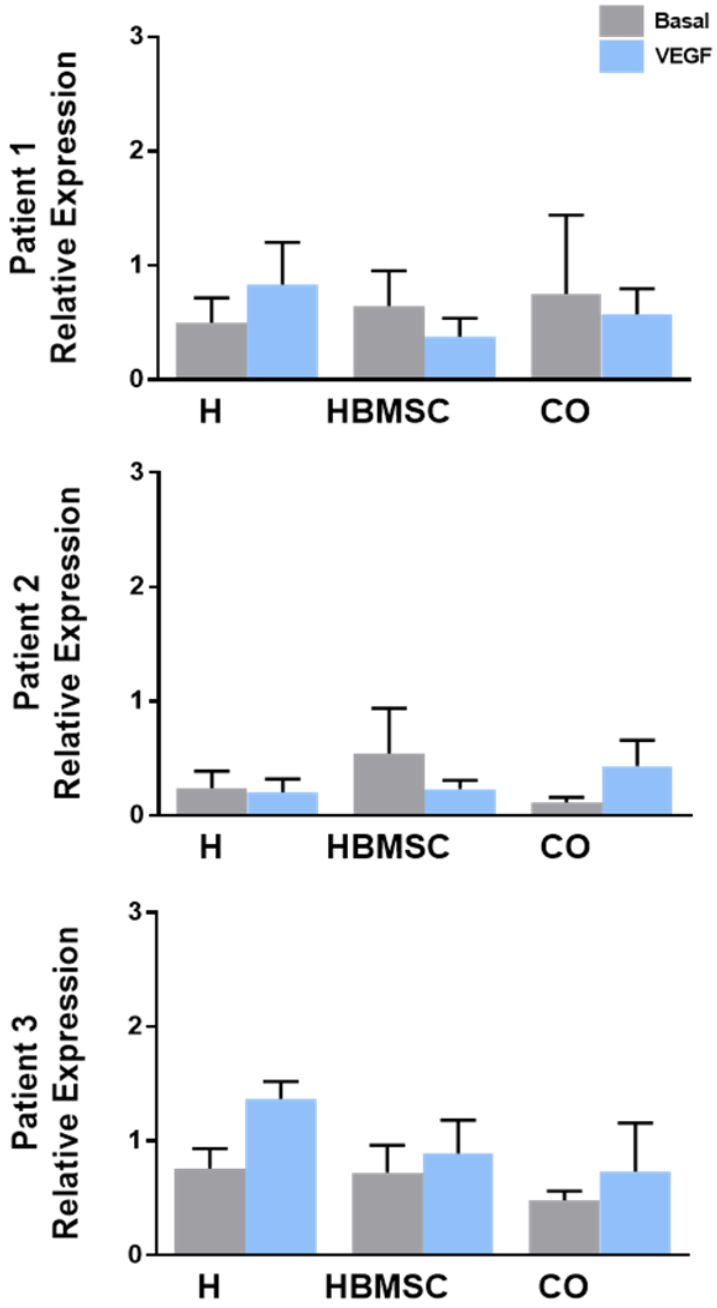

Appendix 7.3.5. **The effect on *vWF* gene expression of mono-and co-cultures of HUVEC and HBMSC supplemented with or without 100ng/ml VEGF**. Graphs represent assays from 3 separate patients/experiments **Patient 1 – 3** in mono- and co-cultures of HUVEC (H) and HBMSC in basal media and supplemented with 100ng/ml VEGF. Monocultures=HBMSC, HUVEC (H), Co-cultures (CO) =HBMSC/HUVEC. Results represent mean ± S.D; n=3 replicates; *p≤0.05, **p≤0.01, ***p≤0.001.

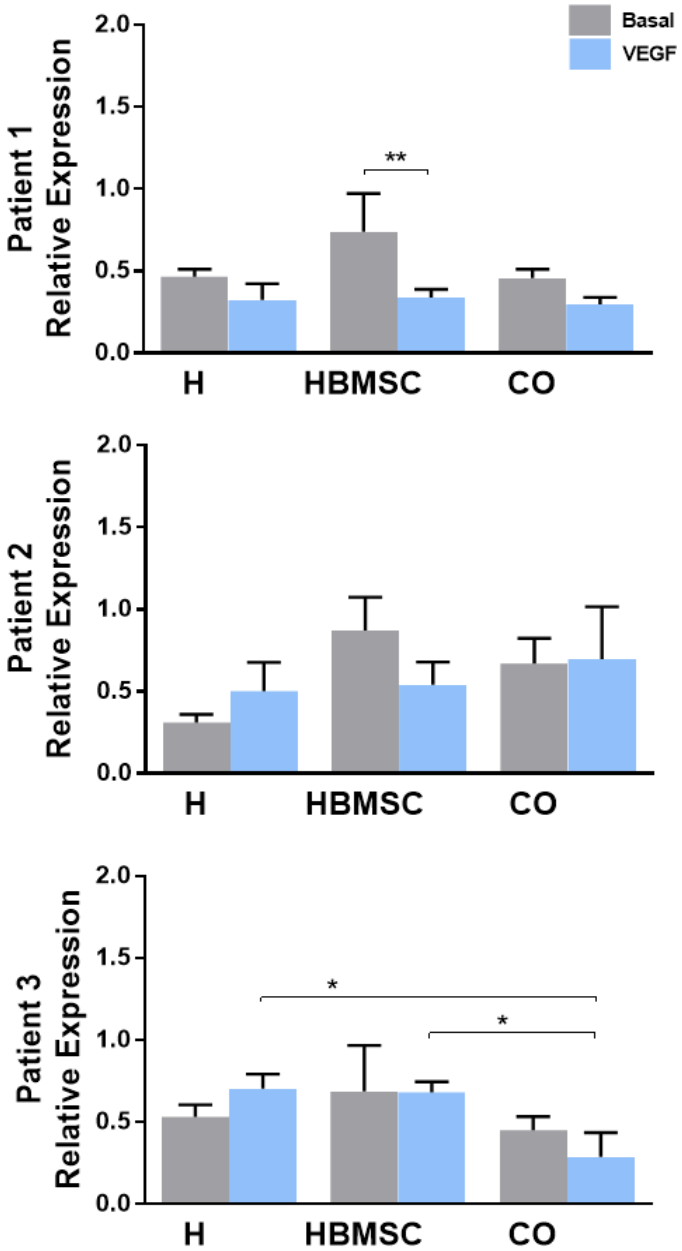

Appendix 7.3.6. **The effect on *VEGF* gene expression in mono-and co-cultures of HUVEC and HBMSC supplemented with or without 100ng/ml VEGF**. Graphs represent assays from 3 separate patients/experiments **Patient 1 – 3** in mono- and co-cultures of HUVEC (H) and HBMSC in basal media and supplemented with 100ng/ml VEGF. Monocultures=HBMSC, HUVEC (H), Co-cultures (CO) =HBMSC/HUVEC. Results represent mean ± S.D; n=3 replicates; *p≤0.05, **p≤0.01, ***p≤0.001.

7.3 Appendix chapter 4: Organotypic culture custom shaped cell pellet constructs.

Micro-CT images of hydroxyapatite phantoms used in chapter 4 in order to calibrate micro-CT data analysis of pre- and post-culture scans of chick femurs, following a 10 day organotypic culture period.

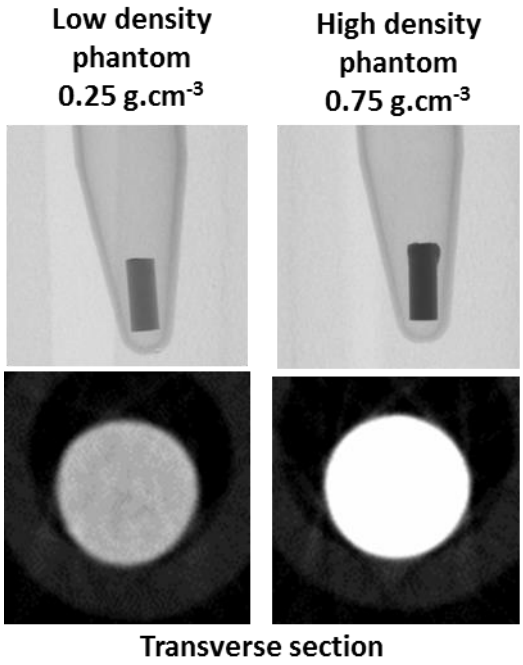

Appendix 7.4.1. **Micro-CT images of Ca Hydroxyapatite phantoms**used to calibrate the experimental micro-CT data.

Additional imaging: variations of cell pellet assemblies to create increased cell-based tissue implant-size for future chick bone defect applications. Multiple cell pellet assemblies were cultured organotypically over various culture periods to assess overall morphology, cell viability and osteogenic/chondrogenic protein expression of the assemblies at different time points.

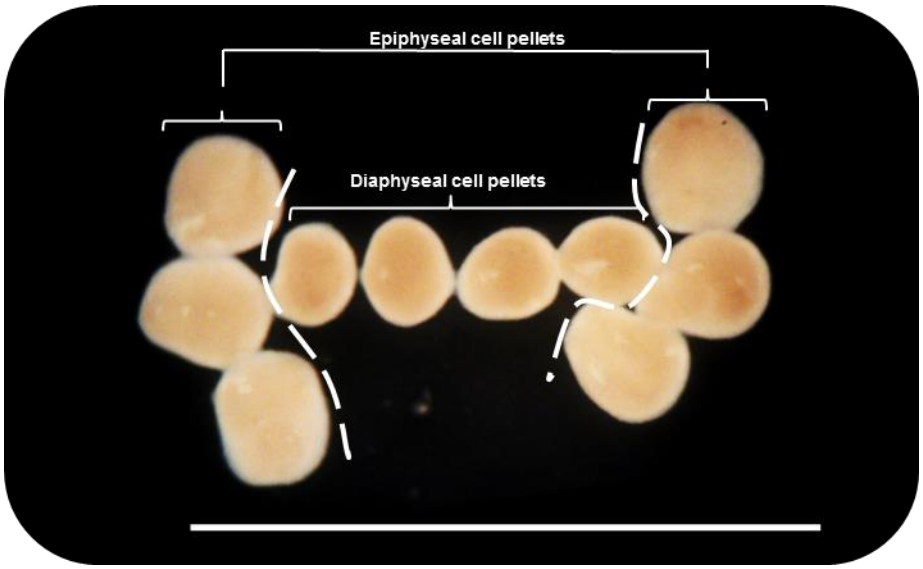

Appendix 7.4.2. Organotypic culture custom shaped cell pellet constructs ($1x10^5$ cells/pellet). Day 0 setup of a human fetal diaphyseal/epiphyseal pellet construct in the shape of a femur, comprising the diaphysis made up of 4 diaphyseal cell pellets and the epiphyses made up of 3 epiphyseal cell pellets each. Pellet constructs were cultured organotypically in basal TCM for 28 days. Scale bar 3500µm.

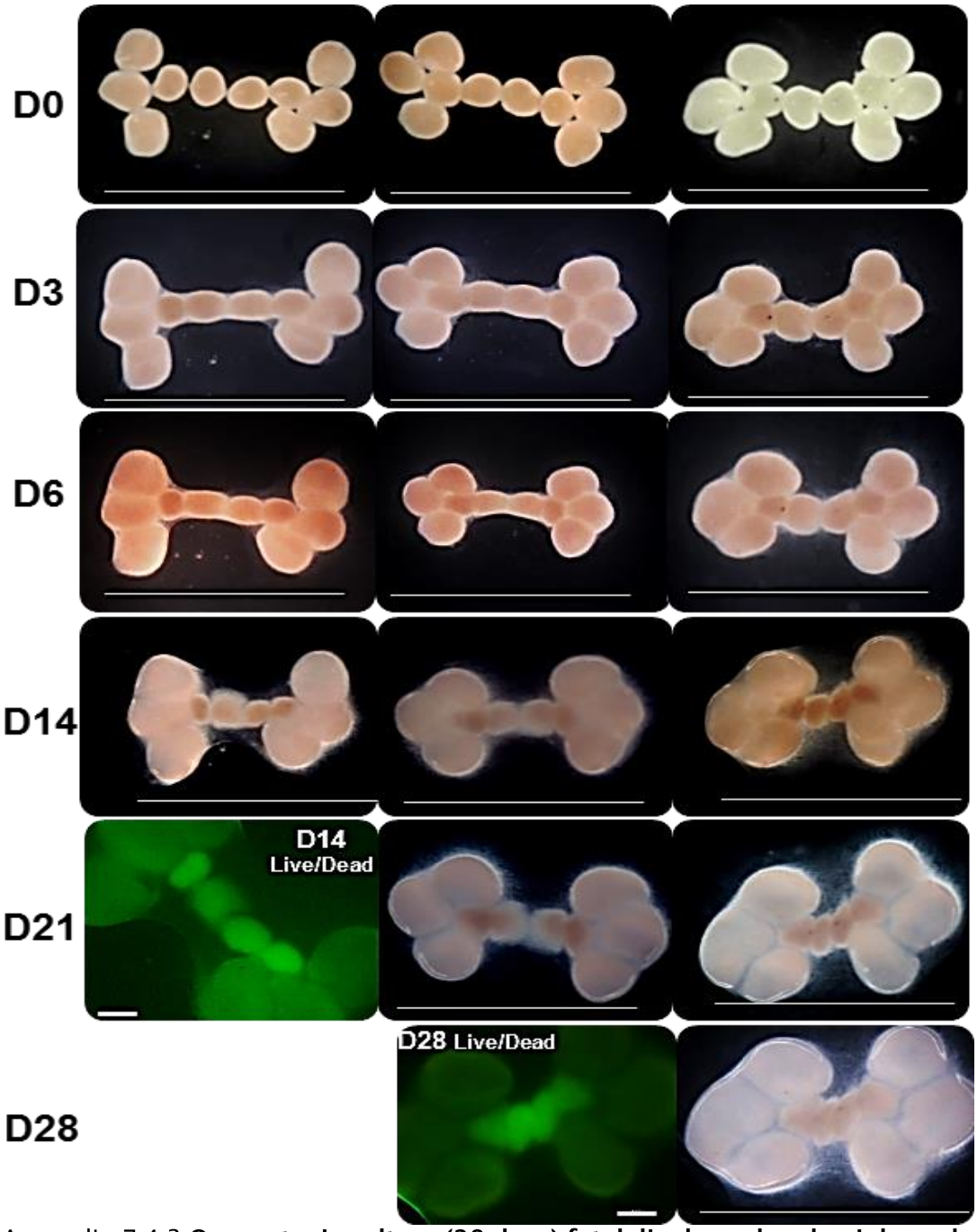

Appendix 7.4.3.**Organotypic culture (28 days) fetal diaphyseal and epiphyseal femur cell pellets arranged in distinct 'femur-shape' constructs** (10^5cells/pellet) over a 28 day organotypic culture period. At day 0, pellets were assembled in a distinct femur-like pattern on an organotypic culture insert. Live/dead staining using CTG™ and ethidium homodimer staining of pellet constructs at day 14 and day 28 of organotypic culture. No cytotoxicity was detected using live/dead staining. Note increasingly dark/dense appearance of diaphyseal cell pellet constructs, with higher fluorescence expression compared to the epiphyseal pellets, over the culture period; particularly between days 14-28. Also of note is the increased pellet morphology of the epiphyseal pellets over the culture period. Scale bar: 3000μm, fluorescent images: 400μm.

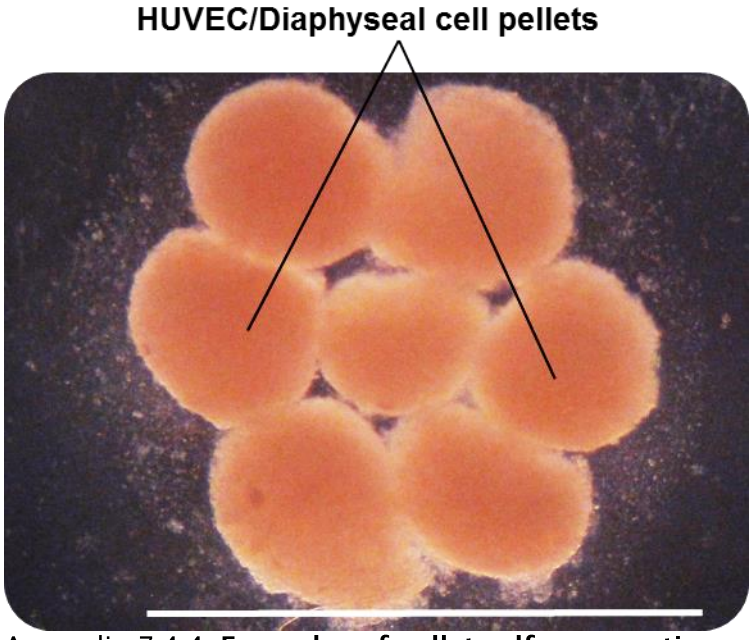

Appendix 7.4.4. **Examples of pellet self-aggregation assembly of co-culture cell pellet constructs.** D0 setup of human fetal diaphyseal/HUVEC co-culture pellet construct over a 21 day organotypic culture period. Initially, one pellet was placed on the membrane of an organotypic culture insert; subsequent pellets were placed adjacent to the initial pellet and allowed to self-aggregate into a sphere-like shape, cultured organotypically. Scale bar 3000µm.

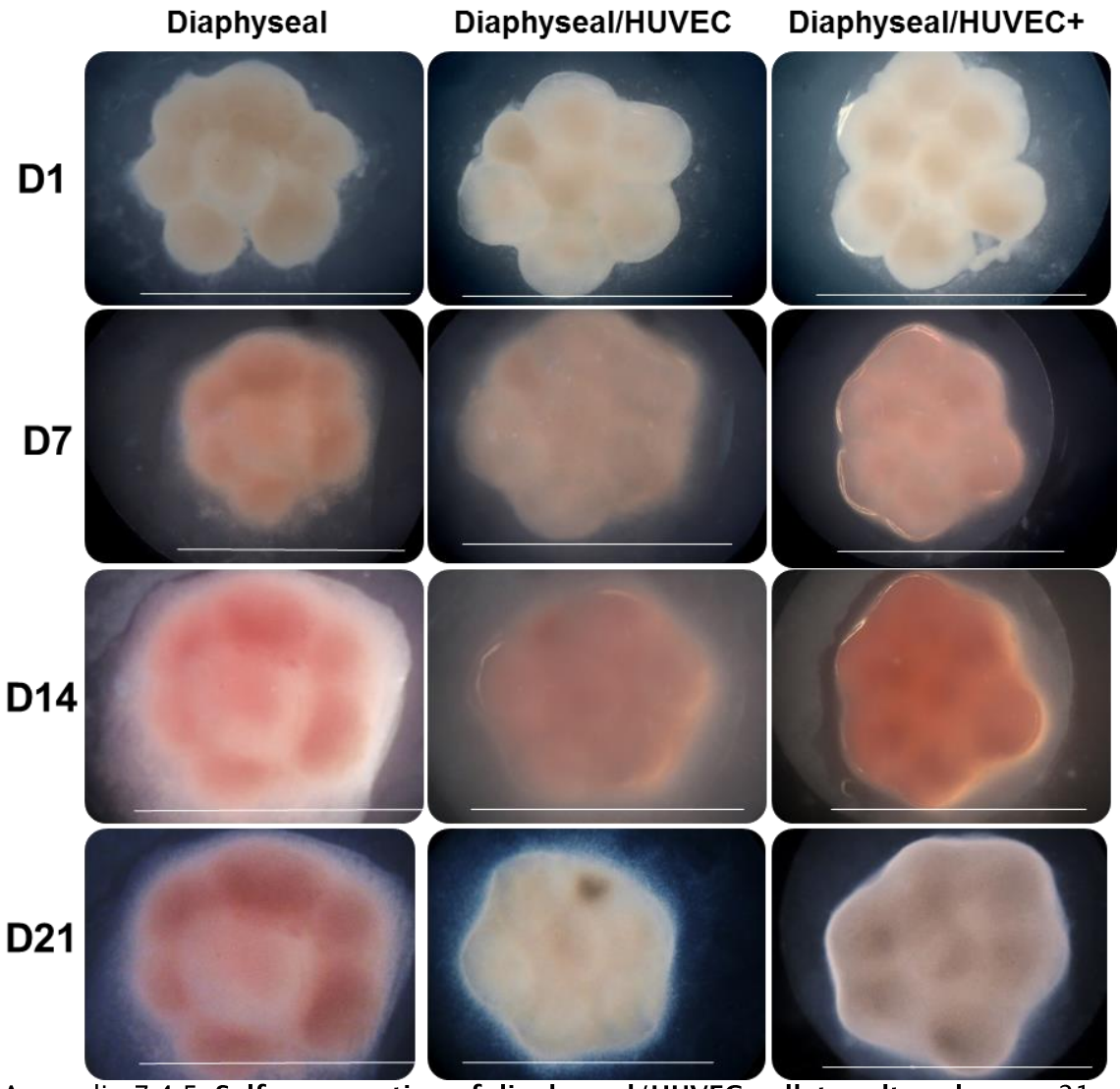

Appendix 7.4.5. **Self-aggregation of diaphyseal/HUVEC pellets cultured** over a 21 day organotypic culture period. Self-aggregation of pellet shapes using $1x10^5$ cells for **diaphyseal** mono-cell pellets and **diaphyseal/HUVEC** co-culture pellets ($1x10^5$/pellet, 1:1 ratio); **diaphyseal/HUVECs (+)** = twice the amount of HUVECs were used ($2x10^5$ cells/pellet, 1:2 ratio). Pellet shapes were cultured organotypically over 21 days. The shapes maintained a consistent morphology over the culture period. Scale bar 3000μm.

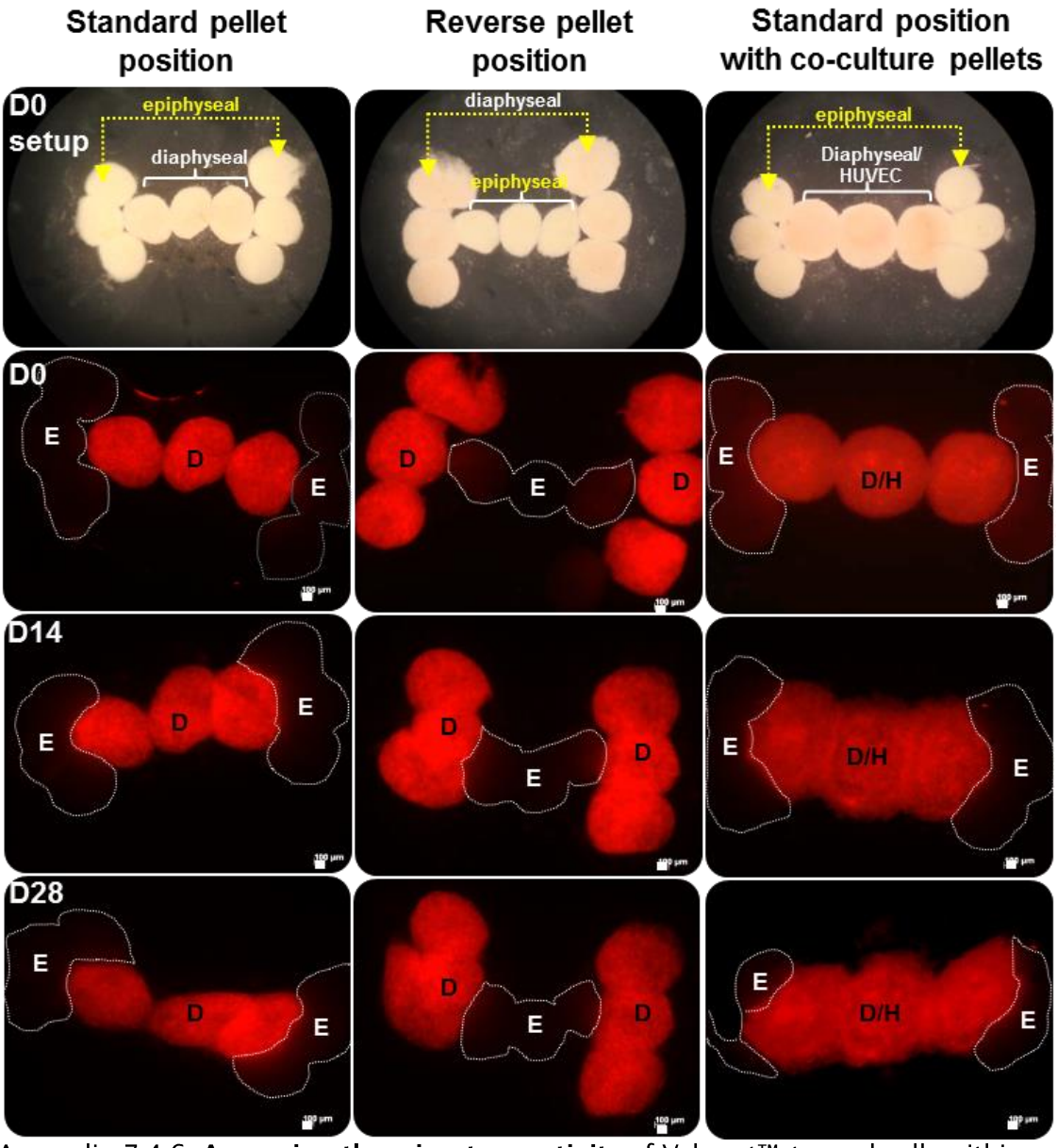

Appendix 7.4.6. **Assessing the migratory activity** of Vybrant™-tagged cells within cell pellet constructs over 28 days of organotypic culture. D= diaphyseal cell pellets; D/H= diaphyseal/HUVEC pellets; E= epiphyseal cell pellets (white dotted outline). Fluorescent imaging of human fetal diaphyseal cells tagged with Vybrant™ DiI (red). Epiphyseal or HUVECs were not tagged. Brightfield images (top row): D0 setup of mono-cell pellets comprising ($1x10^5$ cells/pellet) epiphyseal and diaphyseal cells arranged in femur-shape; 3 diaphyseal cell pellets formed the diaphysis; 3 epiphyseal cell pellets each formed the epiphysis. Middle image column: reversed pellet positions: diaphyseal cell pellets positioned at the epiphysis; epiphyseal cell pellets (outline) positioned at the diaphysis of the femur shape. Right image column: standard epiphyseal cell pellet position; diaphyseal/HUVEC co-culture pellets ($2x10^5$ cells/pellet) at the diaphysis position. Negligible migration of cells between pellet types of the standard shape or the reversed shape were observed by fluorescent cells relocating of diaphyseal cells. Fusion of the pellets can be observed albeit cells overall remaining within the distinct positions; scale bar: 100µm.

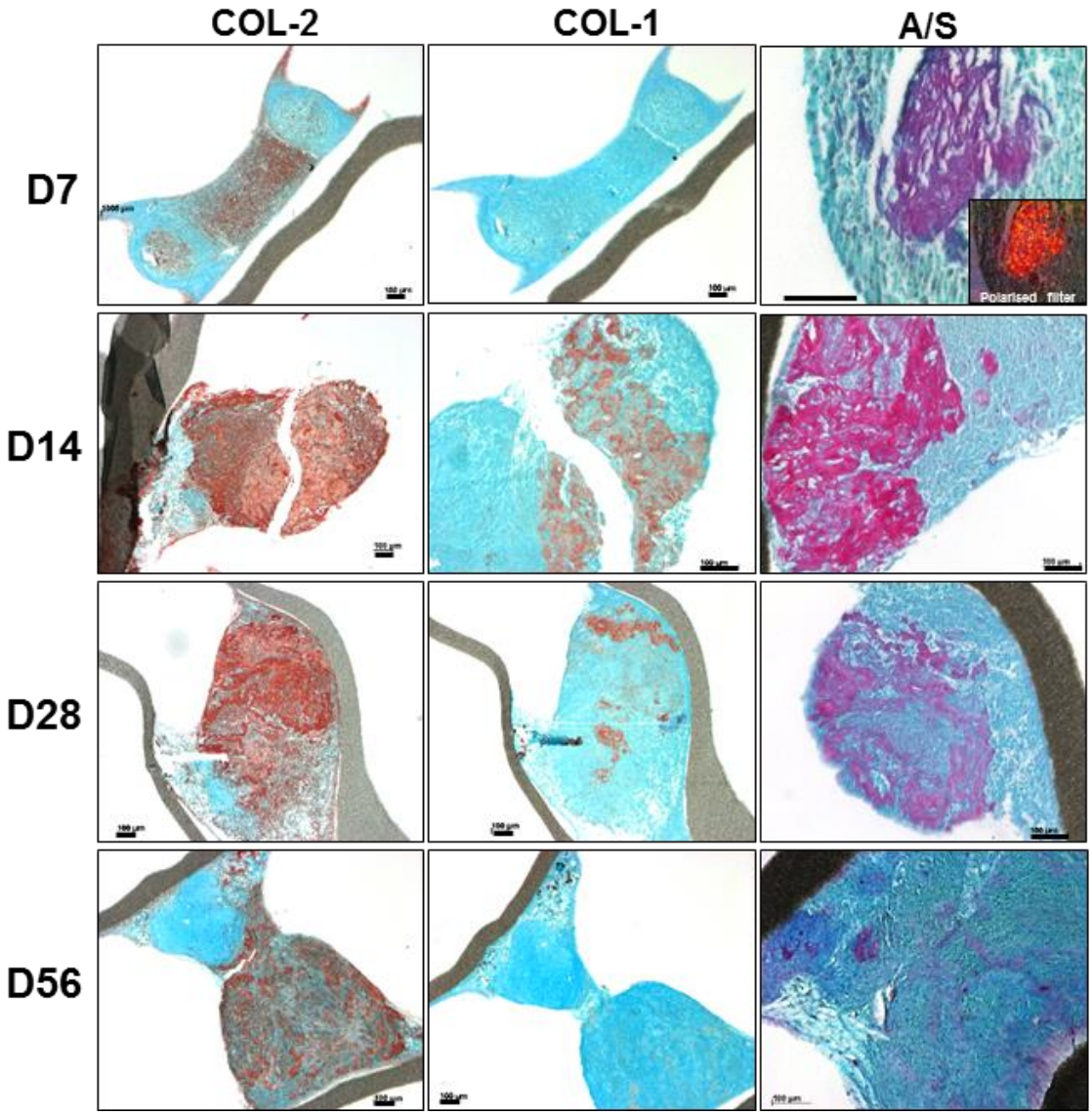

Appendix 7.4.7. **Selected images of pellet-shapes** depicting COL-1 and COL-2 protein expression and Alcian blue/Sirius red tissue staining at various time points of organotypic culture (7-56days). Additionally, an image was taken using a polarised filter for visual presence of collagen fibres within the collagen stained area (red) of the adjacent A/S image. The culture method used for growing pellets (attached to a membrane of a well insert) and subsequent histological processing (contraction due to dehydration), posed a challenge in obtaining intact sections of the entire pellet shapes. COL-2 was strongly evident at the various time points, while COL-1 demonstrated negligible expression at the earliest and latest time points, day 7 and 56. COL-1 protein expression was more distinct in areas of the pellet, while overall less dominant compared to COL-2. COL-2 was strongly expressed throughout the pellet-shapes. Scale bar: 100µm

7.4 Appendix chapter 5: Assessment of decellularised human placental vascular sleeves to aid pellet implanted segmental fracture repair.

Pilot study of chick femoral segmental defects contained within human placental vascular sleeves and cell pellet implants to assess fracture repair in an 8 day chick chorioallantoic membrane culture. Chick femur segments were in inserted into the placental sleeve, holding a cell pellet between opposing segments. After the 8 day culture period, good integration of the placental vessel sleeve with the femur periosteum was evident, however, the culture method, together with the segmental defect, caused considerable displacement of the bone segments within the sleeves; therefore, it was not possible to verify bone forming parameters using micro-CT imaging.

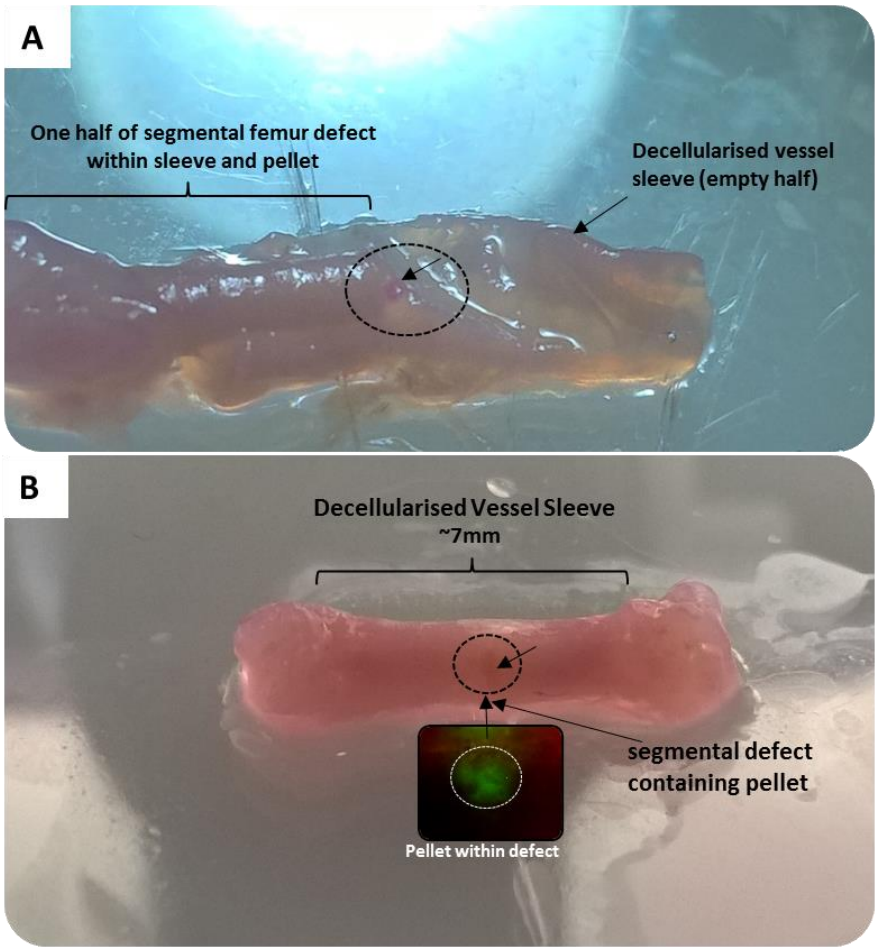

- decellularised human placental vessel tubes were cut into ~7mm sleeves.
- a segmental defect was applied to E18 femur by cutting through the mid-diaphysis using a scalpel blade.
- A vessel sleeve was pulled over one half of the femur segmental defect covering the diaphysis.
- Using a 1ml pipette tip, the pellet was placed at the distal end of the femur segment within the decell sleeve.
- the second segment of the femur was inserted into the opposing end of the vessel sleeve.

Appendix 7.5.1. **Assessment of a decellularised placental vessel sleeve** to aid pellet implanted segmental fracture repair. Decellularised human placental vessel sleeves were applied as a dressing around a chick segmental femoral defect containing a pellet construct. This construct was implanted onto the embryonic chick chorioallantoic membrane and cultured over 8 days. **A**. One femur segment was inserted into the vessel sleeve; the cell pellet was placed at the cut end of the inserted femur segment (circle); **B**. The opposite femur segment was inserted from the opposite sleeve-end so that the pellet was wedged in between the opposing femur segments. Circles depict pellets.

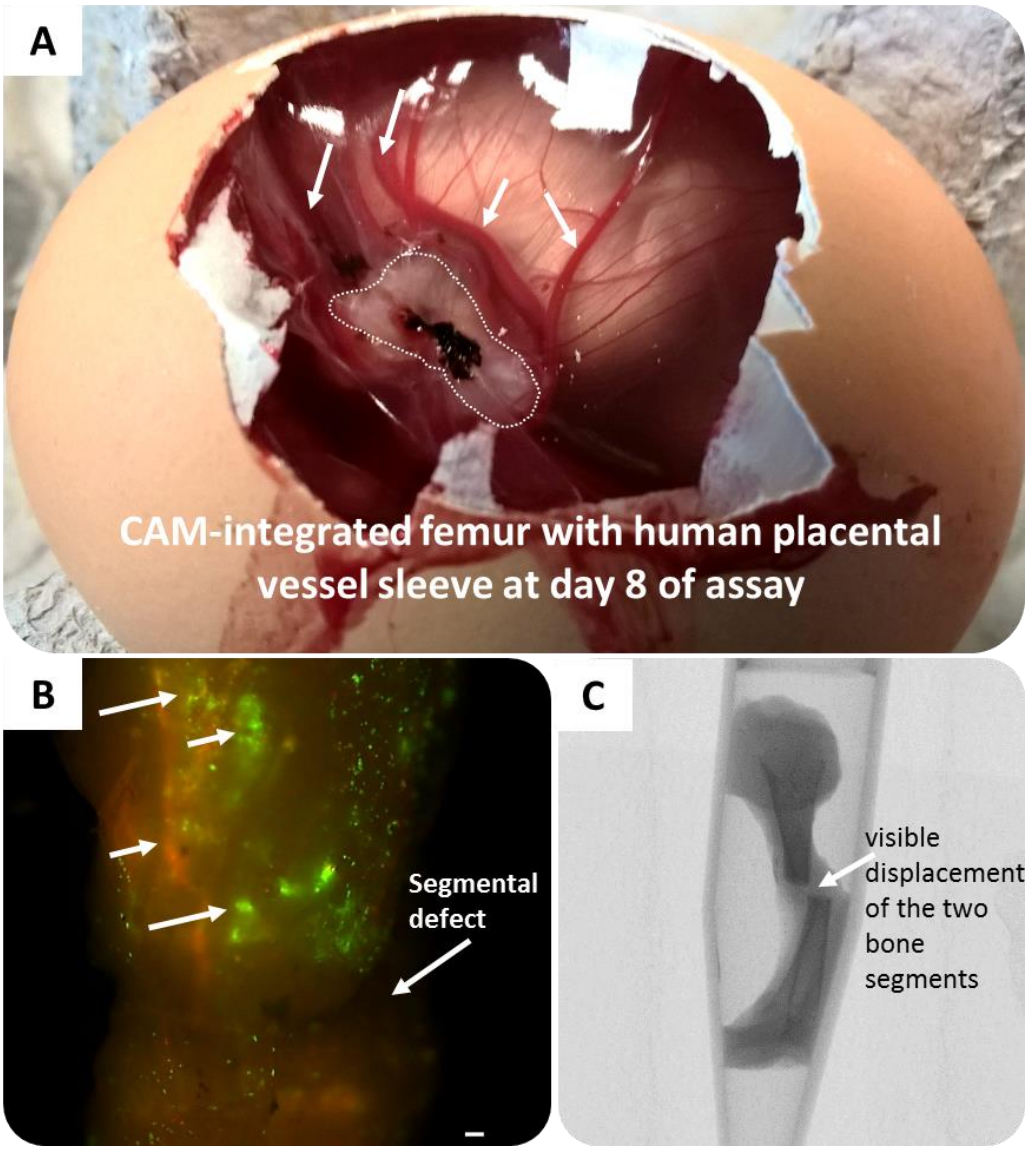

Appendix 7.5.2. **Post-CAM images** of the same femur with segmental defect and co-culture pellet implant. **A.** CAM explant harvest at D8 with CAM implanted E18 femur; sleeved femur was well integrated into the CAM (dotted line); abundant blood vessel invasion by the chick embryonic tissue was visible (arrows). **B.** Image of Vybrant™-fluorescently labelled cell pellet fragments, (HUVEC=red; HBMSC=green) (arrows) within the sleeve of the same femur explant; segmental defect region marked with arrow on right. **C.** Micro-CT image of the same femur with visible displacement of the femur segments within the sleeve. Scale bar: 100μm

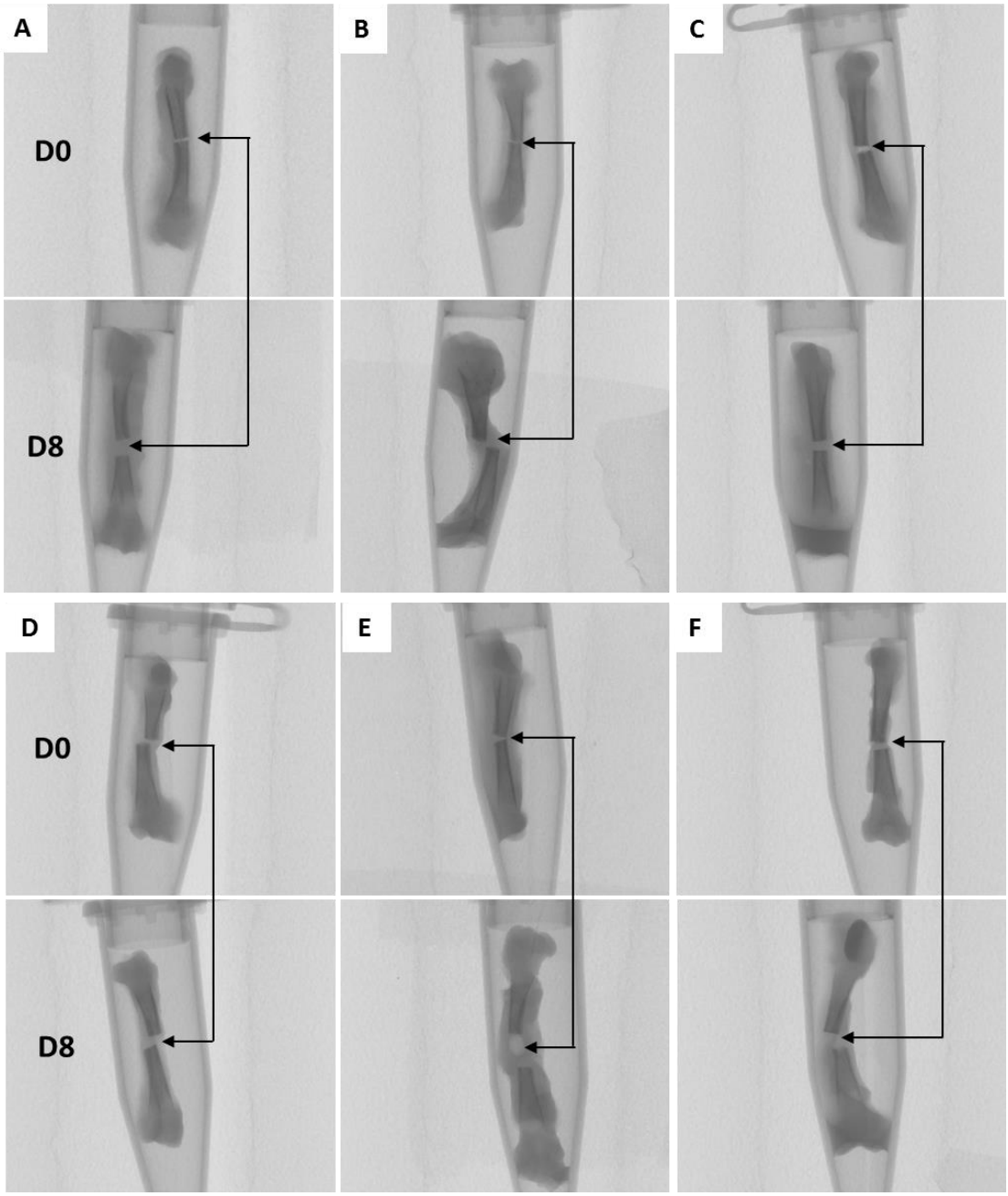

Appendix 7.5.3. A-F. **Comparative pre- and post-CAM micro-CT** scanned images of CAM cultured segmental chick femoral defects with added sleeves/cell pellets. Displacement of femoral segments within sleeves were observed between day 0 and day 8 of culture (double arrows), caused by movement of the chick embryo during the CAM culture and lack of femur/sleeve fixation.

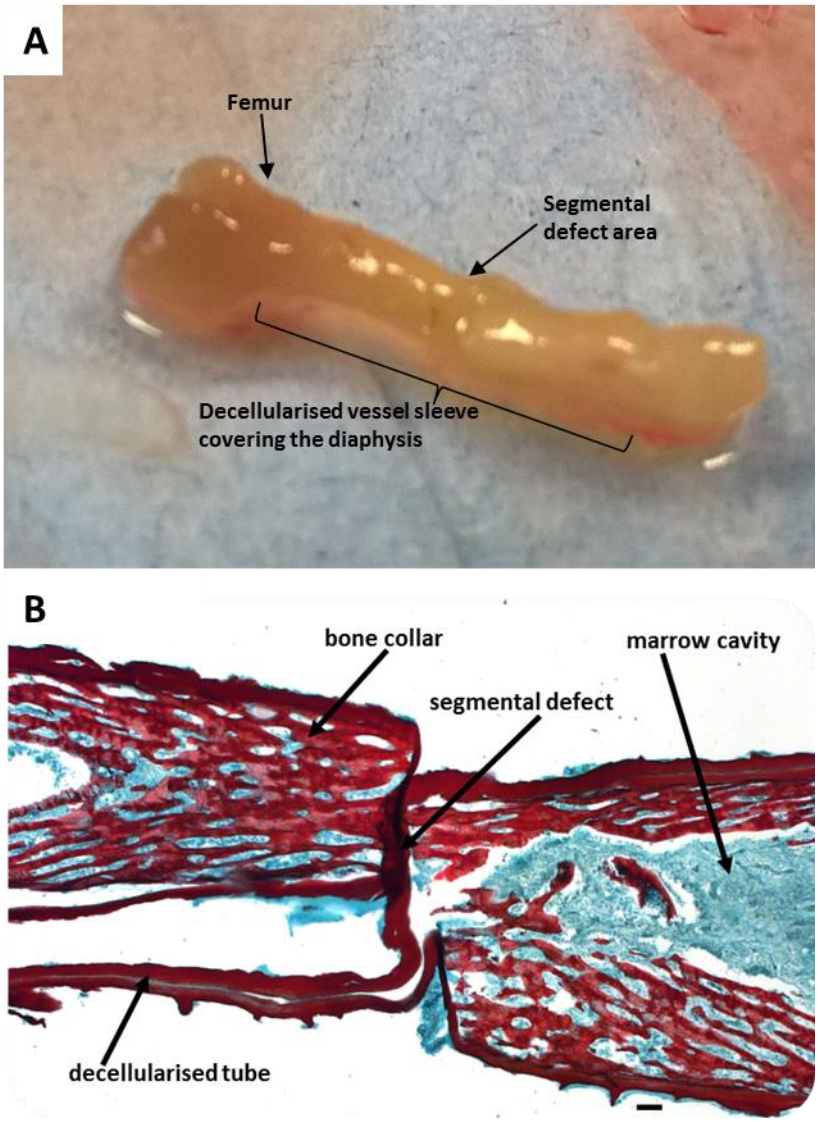

Appendix 7.5.4. **Post-CAM chick femur explant and histological tissue section of the same femur at day 8. A.** Chick femur explant post-CAM with segmental defect (arrow); the vessel sleeve encompassing the diaphysis (label) is difficult to identify. **B.** A/S staining on CAM cultured (8 days) segmental defect/pellet implanted E18 femurs. Some displacement of the femur segments was observed. Decellularised sleeves were well integrated with the bone collar, forming a tight connected sleeve around the bone. Presence of collagen (red) within bone trabeculae and proteoglycans in the marrow cavity were evident by A/S staining. Scale bar 100μm

Glossary

2D	two dimensional
3D	three dimensional
Allograft	tissue from one donor/patient to another
Angio-	related to blood vessels
Angioblast	developing blood vessel cell
Angiogenic	of vascular origin
Angiogenesis	development of blood vessels
Autograft	tissue from the same donor/patient
De-novo	from new
Centrifugation	spinning of cells to obtain a cell pellet
Chondro-	relating to cartilage
Chondrocyte	mature cartilage cell
Chondroblast	immature cartilage cell
Chondrogenesis	formation of cartilage cells/tissue
Endothelial-	related to vessels
Endothelium	layer of cells making forming vessels
Ex vivo	outside of the body
Haemangioblast	developing blood/blood-vessel cell
In situ	within its place
In vitro	within the laboratory
In vivo	within a patient/animal

Glossary

Lacuna	cell pit
Organotypic	organ-like
Osteo-	relating to bone
Osteoblast	developing bone cell
Osteoclast	bone remodelling cell
Osteocyte	mature bone cell
Osteogenesis	formation of bone cells/tissue
Passage	splitting of cultured cell populations
Pericyte	contractile cells around blood vessel cells
Phenotype	physical appearance/expression of distinct markers by cells
Plasticity	differentiation from one cell type to another
Vasculo-	related to blood vessels
Vasculogenesis	de novo blood vessel formation

Bibliography

1 Abbadessa, A., M. M. Blokzijl, et al. (2016). "A thermo-responsive and photo-polymerizable chondroitin sulfate-based hydrogel for 3D printing applications." *Carbohydr Polym* **149**: 163-174.
2 Akiyama, M., H. Nonomura, et al. (2006). "Periosteal cell pellet culture system: a new technique for bone engineering." *Cell Transplant* **15**(6): 521-532.
3 Alphonsus, C. S. and R. N. Rodseth (2014). "The endothelial glycocalyx: a review of the vascular barrier." *Anaesthesia* **69**(7): 777-784.
4 Andrae, J., R. Gallini, et al. (2008). "Role of platelet-derived growth factors in physiology and medicine." *Genes Dev* **22**(10): 1276-1312.
5 Anghelescu, M., J. R. Tonniges, et al. (2015). "Vascular Mechanics in Decellularized Aortas and Coronary Resistance Microvessels in Type 2 Diabetic db/db Mice." *Ann Biomed Eng* **43**(11): 2760-2770.
6 Anisimova, N. Y., M. V. Kiselevsky, et al. (2015). "Fabrication method, structure, mechanical, and biological properties of decellularized extracellular matrix for replacement of wide bone tissue defects." *J Mech Behav Biomed Mater* **49**: 255-268.
7 Armitage, W. J., M. N. Jones, et al. (2014). "The suitability of corneas stored by organ culture for penetrating keratoplasty and influence of donor and recipient factors on 5-year graft survival." *Invest Ophthalmol Vis Sci* **55**(2): 784-791.
8 Badylak, S. F., D. O. Freytes, et al. (2009). "Extracellular matrix as a biological scaffold material: Structure and function." *Acta Biomaterialia* **5**(1): 1-13.
9 Balestrini, J. L., A. L. Gard, et al. (2015). "Production of decellularized porcine lung scaffolds for use in tissue engineering." *Integr Biol (Camb)* **7**(12): 1598-1610.
10 Bannasch, H., G. B. Stark, et al. (2007). "Decellularized dermis in combination with cultivated keratinocytes in a short- and long-term animal experimental investigation." *J Eur Acad Dermatol Venereol* **22**(1): 41-49.
11 Barnes, G. L., P. J. Kostenuik, et al. (1999). "Growth factor regulation of fracture repair." *J Bone Miner Res* **14**(11): 1805-1815.
12 Boos, A. M., J. S. Loew, et al. (2012). "Engineering axially vascularized bone in the sheep arteriovenous-loop model." *J Tissue Eng Regen Med*.
13 Bosker, B. H., H. B. Ettema, et al. (2012). "High incidence of pseudotumour formation after large-diameter metal-on-metal total hip replacement: a prospective cohort study." *J Bone Joint Surg Br* **94**(6): 755-761.
14 Brandenburger, M., J. Wenzel, et al. (2012). "Organotypic slice culture from human adult ventricular myocardium." *Cardiovasc Res* **93**(1): 50-59.
15 Brandi, M. L. and P. Collin-Osdoby (2006). "Perspective - Vascular Biology and the Skeleton." *Journal of Bone and Mineral Research* **21**(2): 183-192.
16 Brindle, N. P., P. Saharinen, et al. (2006). "Signaling and functions of angiopoietin-1 in vascular protection." *Circ Res* **98**(8): 1014-1023.
17 Bruinsma, B. G., Y. Kim, et al. (2015). "Layer-by-layer heparinization of decellularized liver matrices to reduce thrombogenicity of tissue engineered grafts." *J Clin Transl Res* **1**(1): 1-17.

18 Bruns, I., R. P. Cadeddu, et al. (2012). "Multiple myeloma-related deregulation of bone marrow-derived CD34(+) hematopoietic stem and progenitor cells." *Blood* **120**(13): 2620-2630.
19 Buchwald, P. (2009). "FEM-based oxygen consumption and cell viability models for avascular pancreatic islets." *Theor Biol Med Model* **6**: 5.
20 Buckwalter, J. A., M. J. Glimcher, et al. (1995). "Bone Biology." *J Bone Joint Surg Am* **77-A**(8).
21 Buhler, N. E., K. Schulze-Osthoff, et al. (2015). "Controlled processing of a full-sized porcine liver to a decellularized matrix in 24 h." *J Biosci Bioeng* **119**(5): 609-613.
22 Burri, P. H. and V. Djonov (2002). "Intussusceptive angiogenesis--the alternative to capillary sprouting." *Molecular Aspects of Medicine* **23**(6, Supplement): 1-27.
23 Caetano-Lopes, J., H. Canhao, et al. (2007). "Osteoblasts and bone formation." *Acta Reum Port* **32**: 103-110.
24 Carano, R. A. (2003). "Angiogenesis and bone repair." *Drugs Discovery Today* **8**(21): 980-989.
25 Cardus, A., S. Panizo, et al. (2009). "1,25-Dihydroxyvitamin D3 regulates VEGF production through a vitamin D response element in the VEGF promoter." *Atherosclerosis* **204**(1): 85-89.
26 Carmeliet, P. and R. K. Jain (2000). "Angiogenesis in cancer and other diseases." *Nature* **407**(6801): 249-257.
27 Carmeliet, P. and R. K. Jain (2011). "Molecular mechanisms and clinical applications of angiogenesis." *Nature* **473**(7347): 298-307.
28 Caruso, M., M. Evangelista, et al. (2012). "Human term placental cells: phenotype, properties and new avenues in regenerative medicine." *Int J Mol Cell Med* **1**(2): 64-74.
29 Ceradini, D. J. and G. C. Gurtner (2005). "Homing to hypoxia: HIF-1 as a mediator of progenitor cell recruitment to injured tissue." *Trends Cardiovasc Med* **15**(2): 57-63.
30 Chadwick, E. J., D. P. Yang, et al. (2015). "A Brain Tumor/Organotypic Slice Co-culture System for Studying Tumor Microenvironment and Targeted Drug Therapies." *J Vis Exp*(105).
31 Chan, B., H. T. Yuan, et al. (2008). "Receptor tyrosine kinase Tie-1 overexpression in endothelial cells upregulates adhesion molecules." *Biochem Biophys Res Commun* **371**(3): 475-479.
32 Chan, K. L. and C. C. Mok (2012). "Glucocorticoid-induced avascular bone necrosis: diagnosis and management." *Open Orthop J* **6**: 449-457.
33 Chen, D., W. Tian, et al. (2012). "Osteoblast-specific transcription factor Osterix (Osx) and HIF-1alpha cooperatively regulate gene expression of vascular endothelial growth factor (VEGF)." *Biochem Biophys Res Commun* **424**(1): 176-181.
34 Chen, J. D., Q. F. Yu, et al. (2012). "Preparation and biocompatibility of nanohybrid scaffolds by in situ homogeneous formation of nano hydroxyapatite from biopolymer polyelectrolyte complex for bone repair applications." *Colloids and Surfaces B-Biointerfaces* **93**: 100-107.
35 Cheng, C. W., L. D. Solorio, et al. (2014). "Decellularized tissue and cell-derived extracellular matrices as scaffolds for orthopaedic tissue engineering." *Biotechnol Adv* **32**(2): 462-484.

36 Cheung, K. S., N. Sposito, et al. (2014). "MicroRNA-146a Regulates Human Foetal Femur Derived Skeletal Stem Cell Differentiation by Down-Regulating SMAD2 and SMAD3." *PLoS One* **9**(6): e98063.
37 Chung, A. S. and N. Ferrara (2011). "Developmental and pathological angiogenesis." *Annu Rev Cell Dev Biol* **27**: 563-584.
38 Clarke, B. (2008). "Normal Bone Anatomy and Physiology." *Clinical Journal of the American Society of Nephrology : CJASN* **3**(Suppl 3): S131-S139.
39 Cleaver, O. and D. A. Melton (2003). "Endothelial signaling during development." *Nat Med* **9**(6): 661-668.
40 Cohen Jr, M. M. (2006). "The new bone biology: Pathologic, molecular, and clinical correlates." *American Journal of Medical Genetics Part A* **140A**(23): 2646-2706.
41 Colnot, C. (2005). "Cellular and molecular interactions regulating skeletogenesis." *J Cell Biochem* **95**(4): 688-697.
42 Coultas, L., K. Chawengsaksophak, et al. (2005). "Endothelial cells and VEGF in vascular development." *Nature* **438**(7070): 937-945.
43 Courtman, D. W., B. F. Errett, et al. (2000). "The role of crosslinking in modification of the immune response elicited against xenogenic vascular acellular matrices." *Journal of Biomedical Materials Research Part A* **55**(4): 576-586.
44 Crapo, P. M., T. W. Gilbert, et al. (2011). "An overview of tissue and whole organ decellularization processes." *Biomaterials* **32**(12): 3233-3243.
45 Crisan, M., S. Yap, et al. (2008). "A perivascular origin for mesenchymal stem cells in multiple human organs." *Cell Stem Cell* **3**(3): 301-313.
46 Cross, M. J., J. Dixelius, et al. (2003). "VEGF-receptor signal transduction." *Trends in Biochemical Sciences* **28**(9): 488-494.
47 Danilevicius, C. F., J. B. Lopes, et al. (2007). "Bone metabolism and vascular calcification." *Braz J Med Biol Res* **40**(4): 435-442.
48 Dawson, J. I., J. M. Kanczler, et al. (2011). "Clay gels for the delivery of regenerative microenvironments." *Adv Mater* **23**(29): 3304-3308.
49 Dawson, J. I., D. A. Wahl, et al. (2008). "Development of specific collagen scaffolds to support the osteogenic and chondrogenic differentiation of human bone marrow stromal cells." *Biomaterials* **29**(21): 3105-3116.
50 Deckers, M. M., R. L. van Bezooijen, et al. (2002). "Bone morphogenetic proteins stimulate angiogenesis through osteoblast-derived vascular endothelial growth factor A." *Endocrinology* **143**(4): 1545-1553.
51 DeLise, A. M., L. Fischer, et al. (2000). "Cellular interactions and signaling in cartilage development." *Osteoarthritis Cartilage* **8**(5): 309-334.
52 Dery, M. A., M. D. Michaud, et al. (2005). "Hypoxia-inducible factor 1: regulation by hypoxic and non-hypoxic activators." *Int J Biochem Cell Biol* **37**(3): 535-540.
53 Dessau, W., H. von der Mark, et al. (1980). "Changes in the patterns of collagens and fibronectin during limb-bud chondrogenesis." *J Embryol Exp Morphol* **57**: 51-60.
54 Dimitrievska, S., C. Cai, et al. (2015). "Click-coated, heparinized, decellularized vascular grafts." *Acta Biomater* **13**: 177-187.
55 Ding, W. G., Z. X. Wei, et al. (2011). "Reduced local blood supply to the tibial metaphysis is associated with ovariectomy-induced osteoporosis in mice." *Connect Tissue Res* **52**(1): 25-29.

56 Donahue, H. J. (2000). "Gap junctions and biophysical regulation of bone cell differentiation." *Bone* **26**(5): 417-422.
57 Dong, Q. S., H. T. Shang, et al. (2012). "Prefabrication of axial vascularized tissue engineering coral bone by an arteriovenous loop: A better model." *Materials Science & Engineering C-Materials for Biological Applications* **32**(6): 1536-1541.
58 Drake, C. J., J. E. Hungerford, et al. (1998). "Morphogenesis of the first blood vessels." *Ann N Y Acad Sci* **857**: 155-179.
59 Ducy, P., R. Zhang, et al. (1997). "Osf2/Cbfa1: a transcriptional activator of osteoblast differentiation." *Cell* **89**(5): 747-754.
60 Duval, E., S. Leclercq, et al. (2009). "Hypoxia-inducible factor 1alpha inhibits the fibroblast-like markers type I and type III collagen during hypoxia-induced chondrocyte redifferentiation." *Arthritis Rheum* **60**(10): 3038-3048.
61 Einhorn, T. A. (2005). "The science of fracture healing." *J Orthop Trauma* **19**(10 Suppl): S4-6.
62 El-Serafi, A. T., D. I. Wilson, et al. (2011). "Developmental plasticity of human foetal femur-derived cells in pellet culture: self assembly of an osteoid shell around a cartilaginous core." *Eur Cell Mater* **21**: 558-567.
63 Farhadi, J., C. Jaquiery, et al. (2005). "Differentiation-dependent up-regulation of BMP-2, TGF-beta 1, and VEGF expression by FGF-2 in human bone marrow stromal cells." *Plastic and Reconstructive Surgery* **116**(5): 1379-1386.
64 Fell, H. B. and R. Robison (1929). "The growth, development and phosphatase activity of embryonic avian femora and limb-buds cultivated in vitro." *Biochem J* **23**(4): 767-784 765.
65 Ferrara, N. (2001). "Role of vascular endothelial growth factor in regulation of physiological angiogenesis." *Am J Physiol Cell Physiol* **280**(6): C1358-1366.
66 Ferrara, N. (2004). "Vascular endothelial growth factor: basic science and clinical progress." *Endocr Rev* **25**(4): 581-611.
67 Ferrara, N., H.-P. Gerber, et al. (2003). "The biology of Vascular Endothelial Growth Factor." *Nature Medicine* **9**(6): 669-676.
68 Ferrara, N. and R. S. Kerbel (2005). "Angiogenesis as a therapeutic target." *Nature* **438**(7070): 967-974.
69 Ferrera, D., S. Poggi, et al. (2002). "Three-dimensional cultures of normal human osteoblasts: proliferation and differentiation potential in vitro and upon ectopic implantation in nude mice." *Bone* **30**(5): 718-725.
70 Fishbach, M. A., J. A. Bluestone, et al. (2017). "Cell-Based Therapeutics: The Next Pillar of Medicine." *Science Translational Medicine* **5**(170): 1-7.
71 Florencio-Silva, R., G. R. Sasso, et al. (2015). "Biology of Bone Tissue: Structure, Function, and Factors That Influence Bone Cells." *Biomed Res Int* **2015**: 421746.
72 Flynn, L., J. L. Semple, et al. (2006). "Decellularized placental matrices for adipose tissue engineering." *J Biomed Mater Res A* **79**(2): 359-369.
73 Folkman, J. (1971). "Tumor Angiogenesis: Therapeutic Implications." *New England Journal of Medicine* **285**(21): 1182-1186.
74 Freeman, F. E., M. G. Haugh, et al. (2015). "An in vitro bone tissue regeneration strategy combining chondrogenic and vascular priming enhances the mineralization potential of mesenchymal stem cells in vitro while also allowing for vessel formation." *Tissue Eng Part A* **21**(7-8): 1320-1332.

75 Gale, N. W. and G. D. Yancopoulos (1999). "Growth factors acting via endothelial cell-specific receptor tyrosine kinases: VEGFs, angiopoietins, and ephrins in vascular development." *Genes Dev* **13**(9): 1055-1066.
76 Garlanda, C. and E. Dejana (1997). "Heterogeneity of Endothelial Cells." *Arteriosclerosis, Thrombosis, and Vascular Biology* **17**: 1193-1202.
77 Garlanda, C. and E. Dejana (1997). "Heterogeneity of endothelial cells - Specific markers." *Arteriosclerosis Thrombosis and Vascular Biology* **17**(7): 1193-1202.
78 Gerber, H.-P. and N. Ferrara (2000). "Angiogenesis & Bone Growth." *Trends Cardiovasc Med*(10): 223-228.
79 Gerber, H.-P., T. H. Vu, et al. (1999). "VEGF couples hypertrophic cartilage remodeling, ossification and angiogenesis during endochondral bone formation." *Nature America* **5**(6): 623-628.
80 Gerstenfeld, L. C., D. M. Cullinane, et al. (2003). "Fracture healing as a post-natal developmental process: molecular, spatial, and temporal aspects of its regulation." *J Cell Biochem* **88**(5): 873-884.
81 Giannoudis, P. V., H. Dinopoulos, et al. (2005). "Bone substitutes: An update." *Injury-International Journal of the Care of the Injured* **36**: 20-27.
82 Giblin, J. P., L. J. Hewlett, et al. (2008). "Basal secretion of von Willebrand factor from human endothelial cells." *Blood* **112**(4): 957-964.
83 Glowacki, J. (1998). "Angiogenesis in fracture repair." *Clin Orthop Relat Res*(355 Suppl): S82-89.
84 Goerke, S. M., J. Plaha, et al. (2012). "Human Endothelial Progenitor Cells Induce Extracellular Signal-Regulated Kinase-Dependent Differentiation of Mesenchymal Stem Cells into Smooth Muscle Cells upon Cocultivation." *Tissue Engineering Part A* **18**(23-24): 2395-2405.
85 Gómez-Barrena, E., P. Rosset, et al. (2011). "Bone regeneration: stem cell therapies and clinical studies in orthopaedics and traumatology." *Journal of Cellular and Molecular Medicine* **15**(6): 1266-1286.
86 Gong, W., D. Lei, et al. (2016). "Hybrid small-diameter vascular grafts: Anti-expansion effect of electrospun poly epsilon-caprolactone on heparin-coated decellularized matrices." *Biomaterials* **76**: 359-370.
87 Goriainov, V., R. Cook, et al. (2014). "Bone and metal: an orthopaedic perspective on osseointegration of metals." *Acta Biomater* **10**(10): 4043-4057.
88 Grellier, M., N. Ferreira-Tojais, et al. (2009). "Role of vascular endothelial growth factor in the communication between human osteoprogenitors and endothelial cells." *J Cell Biochem* **106**(3): 390-398.
89 Guillotin, B., R. Bareille, et al. (2008). "Interaction between human umbilical vein endothelial cells and human osteoprogenitors triggers pleiotropic effect that may support osteoblastic function." *Bone* **42**(6): 1080-1091.
90 Gushi, A., M. Tanaka, et al. (2008). "The 3G5 antigen is expressed in dermal mast cells but not pericytes." *J Cutan Pathol* **35**(3): 278-284.
91 Haddad, S. M., E. Omidi, et al. (2016). "Comparative biomechanical study of using decellularized human adipose tissues for post-mastectomy and post-lumpectomy breast reconstruction." *J Mech Behav Biomed Mater* **57**: 235-245.
92 Hall, A. P., F. R. Westwood, et al. (2006). "Review of the effects of anti-angiogenic compounds on the epiphyseal growth plate." *Toxicol Pathol* **34**(2): 131-147.
93 Hellstrom, M., L.-K. Phng, et al. (2007). "VEGF and Notch Signaling The Yin and Yang of Angiogenic Sprouting." *Nature* **445**(7129): 776-780.

94 Henstock, J. R., M. Rotherham, et al. (2013). "Cyclic hydrostatic pressure stimulates enhanced bone development in the foetal chick femur in vitro." *Bone* **53**(2): 468-477.
95 Hernigou, P. (2015). "Bone transplantation and tissue engineering. Part II: bone graft and osteogenesis in the seventeenth, eighteenth and nineteenth centuries (Duhamel, Haller, Ollier and MacEwen)." *International Orthopaedics* **39**(1): 193-204.
96 Hickman, J. A., R. Graeser, et al. (2014). "Three-dimensional models of cancer for pharmacology and cancer cell biology: capturing tumor complexity in vitro/ex vivo." *Biotechnol J* **9**(9): 1115-1128.
97 Hidaka, C. and M. B. Goldring (2008). "Regulatory Mechanisms of Chondrogenesis and Implications for Understanding Articular Cartilage Homesostasis." *Curr Rheum Rev* **4**(3): 1-12.
98 Hoffmann, W., S. Feliciano, et al. (2015). "Novel perfused compression bioreactor system as an in vitro model to investigate fracture healing." *Frontiers in Bioengineering and Biotechnology* **3**.
99 Hofmann, F., R. Blasche, et al. (2015). "A co-culture system with an organotypic lung slice and an immortal alveolar macrophage cell line to quantify silica-induced inflammation." *PLoS One* **10**(1): e0117056.
100 Horner, A., S. Bord, et al. (2001). "Tie2 Ligands Angiopoietin-1 and Angiopoietin-2 Are Coexpressed With Vascular Endothelial Cell Growth Factor in Growing Human Bone." *Bone* **28**(1): 65-71.
101 Hoshiba, T., G. Chen, et al. (2016). "Decellularized Extracellular Matrix as an In Vitro Model to Study the Comprehensive Roles of the ECM in Stem Cell Differentiation." *Stem Cells Int* **2016**: 6397820.
102 Hoshiba, T., H. Lu, et al. (2010). "Decellularized matrices for tissue engineering." *Expert Opin Biol Ther* **10**(12): 1717-1728.
103 Hulsart-Billstrom, G., J. I. Dawson, et al. (2016). "A surprisingly poor correlation between in vitro and in vivo testing of biomaterials for bone regeneration: results of a multicentre analysis." *Eur Cell Mater* **31**: 312-322.
104 Inglis, S., D. Christensen, et al. (2016). "Human endothelial and foetal femur-derived stem cell co-cultures modulate osteogenesis and angiogenesis." *Stem Cell Res Ther* **7**(13): 1-16.
105 Jaehn, K., R. G. Richards, et al. (2010). "Pellet Culture Model for Human Primary Osteoblasts." *European Cells and Materials* **20**: 149-161.
106 Jaffe, E. A., R. L. Nachman, et al. (1973). "Culture of human endothelial cells derived from umbilical veins. Identification by morphologic and immunologic criteria." *J Clin Invest* **52**(11): 2745-2756.
107 Jain, R. K. (2003). "Molecular regulation of vessel maturation." *Nat Med* **9**(6): 685-693.
108 Kaigler, D., P. H. Krebsbach, et al. (2005). "Endothelial cell modulation of bone marrow tromal cell osteogenic potential." *FASEB J*.
109 Kaigler, D., P. H. Krebsbach, et al. (2005). "Endothelial cell modulation of bone marrow stromal cell osteogenic potential." *FASEB J* **19**(6): 665-667.
110 Kanczler, J. M. and R. O. Oreffo (2008). "Osteogenesis and angiogenesis: the potential for engineering bone." *Eur Cell Mater* **15**: 100-114.
111 Kanczler, J. M., E. L. Smith, et al. (2012). "A novel approach for studying the temporal modulation of embryonic skeletal development using organotypic bone cultures and microcomputed tomography." *Tissue Eng Part C Methods* **18**(10): 747-760.

112 Kang, H. W., S. J. Lee, et al. (2016). "A 3D bioprinting system to produce human-scale tissue constructs with structural integrity." *Nat Biotechnol* **34**(3): 312-319.
113 Kappas, N. C., G. Zeng, et al. (2008). "The VEGF receptor Flt-1 spatially modulates Flk-1 signaling and blood vessel branching." *J Cell Biol* **181**(5): 847-858.
114 Kasama, T., T. Isozaki, et al. (2007). "Expression of angiopoietin-1 in osteoblasts and its inhibition by tumor necrosis factor-alpha and interferon-gamma." *Transl Res* **149**(5): 265-273.
115 Kashiwagi, A., E. Schipani, et al. (2010). "Targeted deletion of Capn4 in cells of the chondrocyte lineage impairs chondrocyte proliferation and differentiation." *Mol Cell Biol* **30**(11): 2799-2810.
116 Katsimpoulas, M., L. Morticelli, et al. (2015). "Investigation of the biomechanical integrity of decellularized rat abdominal aorta." *Transplant Proc* **47**(4): 1228-1233.
117 Kawada, S., E. Wada, et al. (2013). "Hyperbaric Hyperoxia Accelerates Fracture Healing in Mice." *PLOS ONE* **8**(8): e72603.
118 Kilkenny, C., W. Browne, et al. (2010). "Animal research: reporting in vivo experiments: the ARRIVE guidelines." *Br J Pharmacol* **160**(7): 1577-1579.
119 Kim, K. S., J. Y. Park, et al. (2010). "Regulation of Weibel-Palade body exocytosis by alpha-synuclein in endothelial cells." *J Biol Chem* **285**(28): 21416-21425.
120 Kini, U. and B. N. Nandeesh (2012). "Physiology of Bone Formation, Remodeling, and Metabolism." 29-57.
121 Kitahara, H., H. Yagi, et al. (2016). "Heterotopic transplantation of a decellularized and recellularized whole porcine heart." *Interact Cardiovasc Thorac Surg* **22**(5): 571-579.
122 Koch, S. and L. Claesson-Welsh (2012). "Signal transduction by vascular endothelial growth factor receptors." *Cold Spring Harb Perspect Med* **2**(7): a006502.
123 Kolarova, H., B. Ambruzova, et al. (2014). "Modulation of endothelial glycocalyx structure under inflammatory conditions." *Mediators Inflamm* **2014**: 694312.
124 Komatsu, D. E. and M. Hadjiargyrou (2004). "Activation of the transcription factor HIF-1 and its target genes, VEGF, HO-1, iNOS, during fracture repair." *Bone* **34**(4): 680-688.
125 Korff, T. and H. G. Augustin (1998). "Integration of Endothelial Cells in Multicellular Spheroids Prevents Apoptosis and Induces Differentiation." *The Rockefeller University Press* **143**(5): 1341-1352.
126 Korff, T., S. Kimmina, et al. (2001). "Blood vessel maturation in a 3-dimensional spheroidal coculture model: direct contact with smooth muscle cells regulates endothelial cell quiescence and abrogates VEGF responsiveness." *FASEB J* **15**(2): 447-457.
127 Lambert, C., M. Mathy-Hartert, et al. (2012). "Characterization of synovial angiogenesis in osteoarthritis patients and its modulation by chondroitin sulfate." *Arthritis Res Ther* **14**(2): R58.
128 Lawson, N. D., N. Scheer, et al. (2001). "Notch signaling is required for arterial-venous differentiation during embryonic vascular development." *Development* **128**(19): 3675-3683.

129 Leach, J. K., D. Kaigler, et al. (2006). "Coating of VEGF-releasing scaffolds with bioactive glass for angiogenesis and bone regeneration." *Biomaterials* **27**(17): 3249-3255.
130 Leng, T., J. M. Miller, et al. (2004). "The chick chorioallantoic membrane as a model tissue for surgical retinal research and simulation." *The journal of retinal and vitreous disease* **24**(3).
131 Leszczynska, J., B. Zyzynska-Granica, et al. (2013). "Contribution of endothelial cells to human bone-derived cells expansion in coculture." *Tissue Eng Part A* **19**(3-4): 393-402.
132 Leung, D. W., G. Cachianes, et al. (1989). "Vascular endothelial growth factor is a secreted angiogenic mitogen." *Science* **246**(4935): 1306-1309.
133 Liebermann, J. R., A. Daluiski, et al. (2002). "The role of growth factors in the repair of bone." *J Bone Joint Surg* **84-A**(6): 1032-1044.
134 Liu, Y., A. D. Berendsen, et al. (2012). "Intracellular VEGF regulates the balance between osteoblast and adipocyte differentiation." *J Clin Invest* **122**(9): 3101-3113.
135 Liu, Z. H., J. S. Xu, et al. (2002). "Coordination of chondrogenesis and osteogenesis by fibroblast growth factor 18." *Genes & Development* **16**(7): 859-869.
136 Lomas, R. J., J. E. Cruse-Sawyer, et al. (2003). "Assessment of the biological properties of human split skin allografts disinfected with peracetic acid and preserved in glycerol." *Burns* **29**(6): 515-525.
137 Lopatina, E. V., A. V. Kipenko, et al. (2015). "Organotypic tissue culture investigation of homocysteine thiolactone cardiotoxic effect." *Acta Physiol Hung* **102**(2): 137-142.
138 Lovett, M., K. Lee, et al. (2009). "Vascularization strategies for tissue engineering." *Tissue Eng Part B Rev* **15**(3): 353-370.
139 Lu, C., N. Saless, et al. (2013). "The role of oxygen during fracture healing." *Bone* **52**(1): 220-229.
140 Lu, C., Z. Xing, et al. (2010). "Recombinant human bone morphogenetic protein-7 enhances fracture healing in an ischemic environment." *J Orthop Res* **28**(5): 687-696.
141 Lutterodt, M. C., M. Rosendahl, et al. (2009). "Age determination enhanced by embryonic foot bud and foot plate measurements in relation to Carnegie stages, and the influence of maternal cigarette smoking." *Hum Reprod* **24**(8): 1825-1833.
142 Mackie, E. J., Y. A. Ahmed, et al. (2008). "Endochondral ossification: how cartilage is converted into bone in the developing skeleton." *Int J Biochem Cell Biol* **40**(1): 46-62.
143 Marini, M., E. Sarchielli, et al. (2012). "Expression and localization of VEGF receptors in human fetal skeletal tissues." *Histology and Histopathology* **27**.
144 Marsell, R. and T. A. Einhorn (2011). "The biology of fracture healing." *Int J Injury* **42**(6): 551-555.
145 Mazza, G., K. Rombouts, et al. (2015). "Decellularized human liver as a natural 3D-scaffold for liver bioengineering and transplantation." *Sci Rep* **5**: 13079.
146 Medici, D. and B. R. Olsen (2012). "The role of endothelial-mesenchymal transition in heterotopic ossification." *J Bone Miner Res* **27**(8): 1619-1622.
147 Mendes, L. F., R. P. Pirraco, et al. (2012). "Perivascular-Like Cells Contribute to the Stability of the Vascular Network of Osteogenic Tissue Formed from Cell Sheet-Based Constructs." *PLoS One* **7**(7): e41051.

148 Mi, M., S. Shi, et al. (2012). "TIMP2 deficient mice develop accelerated osteoarthritis via promotion of angiogenesis upon destabilization of the medial meniscus." *Biochem Biophys Res Commun* **423**(2): 366-372.
149 Minina, E., C. Kreschel, et al. (2002). "Interaction of FGF, Ihh/Pthlh, and BMP signaling integrates chondrocyte proliferation and hypertrophic differentiation." *Dev Cell* **3**(3): 439-449.
150 Mirmalek-Sani, S.-H., R. S. Tare, et al. (2006). "Characterization and Multipotentiality of Human Fetal Femur-Derived Cells: Implications for Skeletal Tissue Regeneration." *Stem Cells* **24**(4): 1042-1053.
151 Mogensen, C., B. Bergner, et al. (2011). "Isolation and functional characterization of pericytes derived from hamster skeletal muscle." *Acta Physiol (Oxf)* **201**(4): 413-426.
152 Mountziaris, P. M. and A. G. Mikos (2008). "Modulation of the inflammatory response for enhanced bone tissue regeneration." *Tissue Eng Part B Rev* **14**(2): 179-186.
153 Murphy, S. V. and A. Atala (2014). "3D bioprinting of tissues and organs." *Nat Biotechnol* **32**(8): 773-785.
154 Nguyen, L. H., N. Annabi, et al. (2012). "Vascularized bone tissue engineering: approaches for potential improvement." *Tissue Eng Part B Rev* **18**(5): 363-382.
155 NHFD (2016). "National Hip Fracture Database (NHFD) annual report 2016."
156 Nickerson, C. A., E. G. Richter, et al. (2007). "Studying host-pathogen interactions in 3-D: organotypic models for infectious disease and drug development." *J Neuroimmune Pharmacol* **2**(1): 26-31.
157 Niida, S., M. Kaku, et al. (1999). "Vascular endothelial growth factor can substitute for macrophage colony-stimulating factor in the support of osteoclastic bone resorption." *J Exp Med* **190**(2): 293-298.
158 Ning, L. J., Y. Zhang, et al. (2012). "Preparation and characterization of decellularized tendon slices for tendon tissue engineering." *J Biomed Mater Res A* **100**(6): 1448-1456.
159 Nowak-Sliwinska, P., T. Segura, et al. (2014). "The chicken chorioallantoic membrane model in biology, medicine and bioengineering." *Angiogenesis* **17**(4): 779-804.
160 Nowlan, N. C., P. Murphy, et al. (2007). "Mechanobiology of embryonic limb development." *Ann N Y Acad Sci* **1101**: 389-411.
161 O'Sullivan, C., A. Schubart, et al. (2016). "The dual S1PR1/S1PR5 drug BAF312 (Siponimod) attenuates demyelination in organotypic slice cultures." *J Neuroinflammation* **13**(1): 31.
162 Ohba, S., F. Yano, et al. (2009). "Tissue engineering of bone and cartilage." *IBMS BoneKEy* **6**(11): 405-419.
163 Olausson, M., P. B. Patil, et al. (2012). "Transplantation of an allogeneic vein bioengineered with autologous stem cells: a proof-of-concept study." *The Lancet* **380**(9838): 230-237.
164 Oliver, G. (2004). "Lymphatic vasculature development." *Nat Rev Immunol* **4**(1): 35-45.
165 Olsson, A. K., A. Dimberg, et al. (2006). "VEGF receptor signalling - in control of vascular function." *Nat Rev Mol Cell Biol* **7**(5): 359-371.

166 Oreffo, R. O., F. C. Driessens, et al. (1998). "Growth and differentiation of human bone marrow osteoprogenitors on novel calcium phosphate cements." *Biomaterials* **19**(20): 1845-1854.
167 Ornitz, D. M. and N. Itoh (2001). "Fibroblast growth factors." *Genome Biol* **2**(3): REVIEWS3005.3001-3011.
168 Ortega, N., D. J. Behonick, et al. (2004). "Matrix remodeling during endochondral ossification." *Trends Cell Biol* **14**(2): 86-93.
169 Ortega, N., K. Wang, et al. (2010). "Complementary interplay between matrix metalloproteinase-9, vascular endothelial growth factor and osteoclast function drives endochondral bone formation." *Dis Model Mech* **3**(3-4): 224-235.
170 Pajevic, P. D. (2009). "Regulation of bone resorption and mineral homeostasis by osteocytes." *IBMS BoneKEy* **6**(2): 63-70.
171 Pan, J., G. M. Liu, et al. (2015). "Rotator cuff repair using a decellularized tendon slices graft: an in vivo study in a rabbit model." *Knee Surg Sports Traumatol Arthrosc* **23**(5): 1524-1535.
172 Papadimitropoulos, A., C. Scotti, et al. (2015). "Engineered decellularized matrices to instruct bone regeneration processes." *Bone* **70**: 66-72.
173 Pashneh-Tala, S., S. MacNeil, et al. (2016). "The Tissue-Engineered Vascular Graft—Past, Present, and Future." *Tissue Engineering. Part B, Reviews* **22**(1): 68-100.
174 Patan, S. (2000). "Vasculogenesis and angiogenesis as mechanisms of vascular network formation growth and development." *Journal of Neuro-Oncology* **50**: 1-15.
175 Patan, S., B. Haenni, et al. (1996). "Implementation of Intussusceptive Microvascular Growth in the Chicken Chorioallantoic Membrane (CAM): 1. Pillar Formation by Folding of the Capillary Wall." *Microvascular Research* **51**(1): 80-98.
176 Pellegata, A. F., T. Dominioni, et al. (2015). "Arterial Decellularized Scaffolds Produced Using an Innovative Automatic System." *Cells Tissues Organs* **200**(6): 363-373.
177 Pérez-Campo, F. M., A. Santurtún, et al. (2016). "Osterix and RUNX2 are Transcriptional Regulators of Sclerostin in Human Bone." *Calcified Tissue International* **99**(3): 302-309.
178 Petersen, W., M. Tsokos, et al. (2002). "Expression of VEGF121 and VEGF165 in hypertrophic chondrocytes of the human growth plate and epiphyseal cartilage." *J Anat* **201**(2): 153-157.
179 Pinto, S., H. J. Stark, et al. (2015). "3D Organotypic Co-culture Model Supporting Medullary Thymic Epithelial Cell Proliferation, Differentiation and Promiscuous Gene Expression." *J Vis Exp*(101): e52614.
180 Poornejad, N., J. J. Nielsen, et al. (2016). "Comparison of four decontamination treatments on porcine renal decellularized extracellular matrix structure, composition, and support of human renal cortical tubular epithelium cells." *J Biomater Appl* **30**(8): 1154-1167.
181 Ramasamy, S. K., A. P. Kusumbe, et al. (2014). "Endothelial Notch activity promotes angiogenesis and osteogenesis in bone." *Nature* **507**(7492): 376-380.
182 Rao, R. R., M. L. Vigen, et al. (2015). "Dual-phase osteogenic and vasculogenic engineered tissue for bone formation." *Tissue Eng Part A* **21**(3-4): 530-540.

183 Reitsma, S., D. W. Slaaf, et al. (2007). "The endothelial glycocalyx: composition, functions, and visualization." *Pflugers Arch* **454**(3): 345-359.
184 Ren, B., S. Yu, et al. (2015). "Invasion and anti-invasion research of glioma cells in an improved model of organotypic brain slice culture." *Tumori* **101**(4): 390-397.
185 Reumann, M. K., T. Nair, et al. (2010). "Production of VEGF receptor 1 and 2 mRNA and protein during endochondral bone repair is differential and healing phase specific." *J Appl Physiol (1985)* **109**(6): 1930-1938.
186 Ribatti, D. (2008). "The chick embryo chorioallantoic membrane in the study of tumor angiogenesis." *Romanian Journal of Morphology and Embryology* **49**(2): 131-135.
187 Ribatti, D. (2011). "From the discovery of vascular endothelial growth factor to the introduction of avastin in clinical trials - an interview with Napoleone Ferrara by Domenico Ribatti." *Int J Dev Biol* **55**(4-5): 383-388.
188 Risau, W. (1997). "Mechanisms of angiogenesis." *Nature* **386**(6626): 671-674.
189 Roach, H. I. (1990). "Long-Term organ culture of embryonic chick femora: A system for investigating bone and cartilage formation at an intermediate level of organisation." *Journal of Bone and Mineral Research* **5**(1): 85-100.
190 Rozen, N., T. Bick, et al. (2009). "Transplanted blood-derived endothelial progenitor cells (EPC) enhance bridging of sheep tibia critical size defects." *Bone* **45**(5): 918-924.
191 Rui, Z., X. Li, et al. (2012). "GIT1Y321 phosphorylation is required for ERK1/2- and PDGF-dependent VEGF secretion from osteoblasts to promote angiogenesis and bone healing." *Int J Mol Med* **30**(4): 819-825.
192 Sahara, M., E. M. Hansson, et al. (2014). "Manipulation of a VEGF-Notch signaling circuit drives formation of functional vascular endothelial progenitors from human pluripotent stem cells." *Cell Res* **24**(7): 1-22.
193 Saleh, F. A., M. Whyte, et al. (2011). "Effects of Endothelial Cells on Human Mesenchymal Stem Cell Activity in a Three-Dimensional in vitro Model." *European Cells and Materials* **22**: 242-257.
194 Schipani, E. and T. L. Clemens (2008). "Hypoxia and the hypoxia-inducible factors in the skeleton." *IBMS BoneKEy* **5**(8): 275-284.
195 Schipani, E., C. Maes, et al. (2009). "Regulation of osteogenesis-angiogenesis coupling by HIFs and VEGF." *J Bone Miner Res* **24**(8): 1347-1353.
196 Schipani, E., H. E. Ryan, et al. (2001). "Hypoxia in cartilage: HIF-1alpha is essential for chondrocyte growth arrest and survival." *Genes Dev* **15**(21): 2865-2876.
197 Schneider, K. H., P. Aigner, et al. (2016). "Decellularized human placenta chorion matrix as a favorable source of small-diameter vascular grafts." *Acta Biomater* **29**: 125-134.
198 Schuppli, C. A. and D. Fraser (2005). "The interpretation and application of the three Rs by animal ethics committee members." *Altern Lab Anim* **33**(5): 487-500.
199 Seddon, A. M., P. Curnow, et al. (2004). "Membrane proteins, lipids and detergents: not just a soap opera." *Biochim Biophys Acta* **1666**(1-2): 105-117.
200 Shafiee, A. and A. Atala (2016). "Printing Technologies for Medical Applications." *Trends Mol Med* **22**(3): 254-265.

201 Shamir, E. R. and A. J. Ewald (2014). "Three-dimensional organotypic culture: experimental models of mammalian biology and disease." *Nat Rev Mol Cell Biol* **15**(10): 647-664.
202 Shandalov, Y., D. Egozi, et al. (2015). "A method for constructing vascularized muscle flap." *Methods* **84**: 70-75.
203 Shandalov, Y., D. Egozi, et al. (2014). "An engineered muscle flap for reconstruction of large soft tissue defects." *PNAS* **111**(16).
204 Shibuya, M. (2001). "Structure and dual function of vascular endothelial growth factor receptor-1 (Flt-1)." *Int J Biochem Cell Biol* **33**(4): 409-420.
205 Shin'oka, T., G. Matsumura, et al. (2005). "Midterm clinical result of tissue-engineered vascular autografts seeded with autologous bone marrow cells." *The Journal of Thoracic and Cardiovascular Surgery* **129**(6): 1330-1338.
206 Shinbrot, E., K. G. Peters, et al. (1994). "Expression of the platelet-derived growth factor beta receptor during organogenesis and tissue differentiation in the mouse embryo." *Dev Dyn* **199**(3): 169-175.
207 Simmons, P. J. and B. Torok-Storb (1991). "Identification of stromal cell precursors in human bone marrow by a novel monoclonal antibody, STRO-1." *Blood* **78**(1): 55-62.
208 Singh, S., B. M. Wu, et al. (2012). "Delivery of VEGF using collagen-coated polycaprolactone scaffolds stimulates angiogenesis." *J Biomed Mater Res A* **100**(3): 720-727.
209 Smith, A. J., P. Dieppe, et al. (2012). "Risk of cancer in first seven years after metal-on-metal hip replacement compared with other bearings and general population: linkage study between the National Joint Registry of England and Wales and hospital episode statistics." *BMJ* **344**: e2383.
210 Smith, E. L., J. M. Kanczler, et al. (2014). "Evaluation of skeletal tissue repair, Part 1: Assessment of novel growth-factor-releasing hydrogels in an ex vivo chick femur defect model." *Acta Biomater* **10**(10): 4186-4196.
211 Smith, E. L., J. M. Kanczler, et al. (2014). "Evaluation of skeletal tissue repair, Part 2: Enhancement of skeletal tissue repair through dual-growth-factor-releasing hydrogels within an ex vivo chick femur defect model." *Acta Biomater* **10**(10): 4197-4205.
212 Smith, E. L., H. Rashidi, et al. (2015). "The effects of 1alpha, 25-dihydroxyvitamin D3 and transforming growth factor-beta3 on bone development in an ex vivo organotypic culture system of embryonic chick femora." *PLoS One* **10**(4): e0121653.
213 Smith, J. O., R. O. Oreffo, et al. (2003). "Changes in the antiangiogenic properties of articular cartilage in osteoarthritis." *J Orthop Sci* **8**(6): 849-857.
214 Spark, J. I., S. Yeluri, et al. (2008). "Incomplete cellular depopulation may explain the high failure rate of bovine ureteric grafts." *Br J Surg* **95**(5): 582-585.
215 Stannard, J. T., K. Edamura, et al. (2016). "Development of a whole organ culture model for intervertebral disc disease." *Journal of Orthopaedic Translation* **5**: 1-8.
216 Stoppini, L., P. A. Buchs, et al. (1991). "A simple method for organotypic cultures of nervous tissue." *J Neurosci Methods* **37**(2): 173-182.
217 Stratton, S., N. B. Shelke, et al. (2016). "Bioactive polymeric scaffolds for tissue engineering." *Bioactive Materials* **1**(2): 93-108.

218 Street, J., M. Bao, et al. (2002). "Vascular endothelial growth factor stimulates bone repair by promoting angiogenesis and bone turnover." *Proc Natl Acad Sci U S A* **99**(15): 9656-9661.
219 Street, J. and B. Lenehan (2009). "Vascular endothelial growth factor regulates osteoblast survival - evidence for an autocrine feedback mechanism." *J Orthop Surg Res* **4**(19): 1-13.
220 Sugiyama, T., H. Kohara, et al. (2006). "Maintenance of the hematopoietic stem cell pool by CXCL12-CXCR4 chemokine signaling in bone marrow stromal cell niches." *Immunity* **25**(6): 977-988.
221 Summerlee, A. J. S. (2013). "Bone formation & development." *Book*.
222 Sumpio, B. E., J. T. Riley, et al. (2002). "Cells in focus: endothelial cell." *Journal of Biochemistry & Cell Biology* **34**: 1508-1512.
223 Suzuki, T., T. Miyamoto, et al. (2007). "Osteoblast-specific Angiopoietin 1 overexpression increases bone mass." *Biochem Biophys Res Commun* **362**(4): 1019-1025.
224 Takahash, K., C. M. Shanahan, et al. (1991). "Fracture healing of chick femurs in tissue culture." *Acta Orthop Scand* **62**(4): 352-355.
225 Tammela, T., B. Enholm, et al. (2005). "The biology of vascular endothelial growth factors." *Cardiovasc Res* **65**(3): 550-563.
226 Tan, P. H., C. Chan, et al. (2004). "Phenotypic and functional differences between human saphenous vein (HSVEC) and umbilical vein (HUVEC) endothelial cells." *Atherosclerosis* **173**(2): 171-183.
227 Tang, D., R. S. Tare, et al. (2016). "Biofabrication of bone tissue: approaches, challenges and translation for bone regeneration." *Biomaterials* **83**: 363-382.
228 Tang, W. J., F. Yang, et al. (2012). "Transcriptional Regulation of Vascular Endothelial Growth Factor (VEGF) by Osteoblast-specific Transcription Factor Osterix (Osx) in Osteoblasts." *Journal of Biological Chemistry* **287**(3): 1671-1678.
229 Tang, Y., X. Wu, et al. (2009). "TGF-beta1-induced migration of bone mesenchymal stem cells couples bone resorption with formation." *Nat Med* **15**(7): 757-765.
230 Tasso, R., F. Fais, et al. (2010). "The recruitment of two consecutive and different waves of host stem/progenitor cells during the development of tissue-engineered bone in a murine model." *Biomaterials* **31**(8): 2121-2129.
231 Tennant, M. and J. K. McGeachie (1991). "PLATELET-DERIVED GROWTH FACTOR AND ITS ROLE IN ATHEROGENESIS: A BRIEF REVIEW." *Australian and New Zealand Journal of Surgery* **61**(7): 482-488.
232 Tombran-Tink, J. and C. J. Barnstable (2004). "Osteoblasts and osteoclasts express PEDF, VEGF-A isoforms, and VEGF receptors: possible mediators of angiogenesis and matrix remodeling in the bone." *Biochem Biophys Res Commun* **316**(2): 573-579.
233 Trueta, J. (1963). "The role of the vessels in osteogenesis." *J Bone Joint Surg Br* **45B**(2): 402-418.
234 Tseng, S. S., M. A. Lee, et al. (2008). "Nonunions and the potential of stem cells in fracture-healing." *J Bone Joint Surg Am* **90 Suppl 1**: 92-98.
235 Tsigkou, O., I. Pomerantseva, et al. (2010). "Engineered vascularized bone grafts." *Proc Natl Acad Sci U S A* **107**(8): 3311-3316.
236 Ucuzian, A. A. and H. P. Greisler (2007). "In vitro models of angiogenesis." *World J Surg* **31**(4): 654-663.

237 Vaira, V., G. Fedele, et al. (2010). "Preclinical model of organotypic culture for pharmacodynamic profiling of human tumors." *Proc Natl Acad Sci U S A* **107**(18): 8352-8356.
238 van der Stok, J., M. K. E. Kooler, et al. (2014). "Chondrogenically differentiated mesenchymal stromal cell pellets stimulate endochondral bone regeneration in critical-sized bone defects." *european Cells and Materials* **27**: 137-148.
239 van Hinsbergh, V. W. M. (2012). "Endothelium—role in regulation of coagulation and inflammation." *Seminars in Immunopathology* **34**(1): 93-106.
240 Villars, F., L. Bordenave, et al. (2000). "Effect of human endothelial cells on human bone marrow stromal cell phenotype: role of VEGF?" *J Cell Biochem* **79**(4): 672-685.
241 Villars, F., B. Guillotin, et al. (2002). "Effect of HUVEC on human osteoprogenitor cell differentiation needs heterotypic gap junction communication." *Am J Physiol Cell Physiol* **282**(4): C775-785.
242 von Haller, A. (1763). Experimentorum de Ossium Formatione. http://books.google.com, Digitized by Google.
243 Wallis, G. A. (1996). "Bone growth: coordinating chondrocyte differentiation." *Curr Biol* **6**(12): 1577-1580.
244 Walser, R. and W. Metzger (2013). "Generation of co-culture spheroids as vascularisation units for bone tissue engineering." *European Cells and Materials* **26**: 222-223.
245 Waltenberger, J., L. Claesson-Welsh, et al. (1994). "Different signal transduction properties of KDR and Flt1, two receptors for vascular endothelial growth factor." *J Biol Chem* **269**(43): 26988-26995.
246 Wan, J., K. H. Li, et al. (2012). "Could nonunion tissue be transformed capable of bone formation by negative pressure: a new alternative to treat bone nonunion?" *Med Hypotheses* **78**(4): 417-419.
247 Wang, N., R. Zhang, et al. (2013). "Vascular endothelial growth factor stimulates endothelial differentiation from mesenchymal stem cells via Rho/myocardin-related transcription factor--a signaling pathway." *Int J Biochem Cell Biol* **45**(7): 1447-1456.
248 Wang, Q. Y., J. Dai, et al. (2012). "Osteochondral angiogenesis in rat mandibular condyles with osteoarthritis-like changes." *Arch Oral Biol* **57**(6): 620-629.
249 Wang, Y., C. Wan, et al. (2007). "The hypoxia-inducible factor alpha pathway couples angiogenesis to osteogenesis during skeletal development." *J Clin Invest* **117**(6): 1616-1626.
250 Wang, Y., C. Wan, et al. (2007). "Oxygen sensing and osteogenesis." *Ann N Y Acad Sci* **1117**: 1-11.
251 Warnke, P. H. (2006). "Repair of a human face by allotransplantation." *Lancet* **368**(9531): 181-183.
252 Warnke, P. H., I. N. Springer, et al. (2004). "Growth and transplantation of a custom vascularised bone graft in a man." *Lancet* **364**(9436): 766-770.
253 White, A. and G. Wallis (2001). "Endochondral ossification: A delicate Balance between Growth and Mineralisation." *Current Biology* **11**(15): R589-R591.
254 Wingate, K., M. Floren, et al. (2014). "Synergism of Matrix Stiffness and Vascular Endothelial Growth Factor on Mesenchymal Stem Cells for Vascular Endothelial Regeneration." *Tissue Eng Part A* **20**(17): 2503-2512.

255 Wittko-Schneider, I. M., F. T. Schneider, et al. (2013). "Brain homeostasis: VEGF receptor 1 and 2-two unequal brothers in mind." *Cell Mol Life Sci* **70**(10): 1705-1725.
256 Xue, Y., Z. Xing, et al. (2013). "Co-culture of human bone marrow stromal cells with endothelial cells alters gene expression profiles." *Int J Artif Organs* **36**(9): 650-662.
257 Xue, Y., Z. Xing, et al. (2009). "Endothelial cells influence the osteogenic potential of bone marrow stromal cells." *Biomed Eng Online* **8**(34): 1-9.
258 Yancopoulos, G. D., S. Davis, et al. (2000). "Vascular-specific growth factors and blood vessel formation." *Nature* **407**: 242-248.
259 Yang, Y. Q., Y. Y. Tan, et al. (2012). "The role of vascular endothelial growth factor in ossification." *Int J Oral Sci* **4**(2): 64-68.
260 Yasuda, H., K. Yano, et al. (2012). "Repair of critical long bone defects using frozen bone allografts coated with an rhBMP-2-retaining paste." *J Orthop Sci* **17**(3): 299-307.
261 Yau, J. W., H. Teoh, et al. (2015). "Endothelial cell control of thrombosis." *BMC Cardiovascular Disorders* **15**: 130.
262 Yildiz, C., A. Cetin, et al. (2013). "Anti-angiogenic effects of diltiazem, Imatinib, and Bevacizumab in the CAM Assay." *Int J Scient and Res Pub* **3**(8): 2250-3153.
263 Yuan, H., H. Fernandes, et al. (2010). "Osteoinductive ceramics as a synthetic alternative to autologous bone grafting." *Proc Natl Acad Sci U S A* **107**(31): 13614-13619.
264 Zhang, Y., A. Schedle, et al. (2010). "The proliferation and differentiation of osteoblasts in co-culture with human umbilical vein endothelial cells: An improved analysis using fluorescence-activated cell sorting." *Cell Mol Biol Lett* **15**(4): 517-529.
265 Zonari, A., S. Novikoff, et al. (2012). "Endothelial Differentiation of Human Stem Cells Seeded onto Electrospun Polyhydroxybutyrate/Polyhydroxybutyrate-Co-Hydroxyvalerate Fiber Mesh." *PLoS One* **7**(4).
266 Zustiak, S. P., Y. Wei, et al. (2012). "Protein-Hydrogel Interactions in Tissue Engineering: Mechanisms and Applications." *Tissue Eng Part B Rev* **19**(2): 1-12.